COLLECTED PAPERS

ON

COHERENT OPTO-ELECTRONICS

Volume 5

August 1989—July 1990

Associate Professor

Motoichi OHTSU

TOKYO INSTITUTE OF TECHNOLOGY

THE GRADUATE SCHOOL AT NAGATSUTA

4259 Nagatsuta, Midori-ku, Yokohama,

Kanagawa 227, JAPAN

各位殿

拝啓　時下ますますご清祥のこととお慶び申し上げます。
さて、このたび、前回に引き続きまして、最近の私どもの発表論文をまとめましたので、ここにお送り致します。よろしくご査収下されば幸いです。
いずれも未熟な論文ばかりですので、ご意見、ご批評をお待ちしております。
今後ともご指導ご鞭撻のほどお願い申し上げます。

敬具

平成２年８月

東京工業大学　総合理工学研究科

大津　元一

PREFACE

This is a research review on coherent opto-electronics by Assoc. Prof. M. Ohtsu, Tokyo Institute of Technology. It contains copies of technical papers published during August 1989 - July 1990, and is composed of three parts, which correspond to research fields of M. Ohtsu. They are [I] IMPROVEMENT IN COHERENCE OF LASERS, [II] APPLICATION TO ATOMIC CLOCKS, and [III] APPLICATION TO THE PHOTON SCANNING TUNNELING MICROSCOPE.

The linewidth of a semiconductor laser has been reduced to narrower than 1 kHz, and is approaching to 1 Hz level. By using this high-quality laser, M. Ohtsu is carrying out several novel researches on quantum optics. Their results will be published in the forthcoming volume of the collected papers.

Back numbers of the collected papers are still available on your request.

MEMBERS

Associate Professor

Motoichi OHTSU (Dr. Eng.)

Research Associate

Ken'ichi NAKAGAWA (Dr. Sci.)

Graduate Students (Doctor Candidates)

Hiroyuki FURUTA (M. Eng.)

Chul Ho SHIN (M. Eng.)

Hideo KUSUZAWA (M. Eng.)

Shudong JIANG (M. Eng.)

Morihiro KOUGORI (M. Eng.) (1990.4 -)

Graduate Students (Master Course)

Eiji IKEGAMI (B. Eng.)[a] (- 1990.3)

Isao KOSHIISI (B. Eng.)[b] (- 1990.3)

Hiromasa SUZUKI (B. Eng.)

Mitsuhiro TESHIMA (B. Eng.)

Naoyuki TOMITA (B. Eng.)

Yasumasa KIKUNAGA (B. Eng.) (1990.4 -)

Yoshihiko FUJIE (B. Eng.) (1990.4 -)

Keiji YAMAMOTO (B. Eng.) (1990.4 -)

Undergraduate Students

Akihiko KIYOHARA[c] (- 1990.3)

Yoshinari AWAJI (1990.4 -)

Hideo OCHI (1990.4 -)

Kazunobu YAMADA (1990.4 -)

Yasunori TODA (1990.4 -)

Kouji TAKADA (1990.4 -)

Yukitaka SHIMIZU (1990.4 -)

Research Students

Toru IMAI[d]

Jun KAWAKAMI[e]

Togar PANGARIBUAN[f]

Visiting Scientists

Weizhi WANG[g)]

Tadanori SENO[h)]

Naoto KITABAYASI[i)]

Secretary

Yuko YABE

a) Presently with Nomura Sogo Kenkyusyo Co. Ltd.

b) Presently with Shin-nittetsu Co. Ltd.

c) Presently with Graduate School, Tokyo Institute of Technology

d) Permanent affiliation : Tokyo Aircraft Instrument Co. Ltd., Tokyo Japan

e) Permanent affiliation : NIKON Co. Ltd., Kanagawa, Japan

f) Permanent affiliation : Graduate School, University of Indonesia, Jakarta, Indonesia

g) Permanent affiliation : Optical Engineering Department, Zhejiang University, Zhejiang, P.R. China

h) Permanent affiliation : Central Research Laboratory, Asahi Glass Co. Ltd., Kanawaga, Japan

i) Permanent affiliation : Research Laboratory, Nihon Musen Co. Ltd., Saitama, Japan

LIST OF PAPERS

[I] IMPROVEMENTS IN COHERENCE OF LASERS

(a) Journal Papers

[1] H. Furuta and M. Ohtsu, "Evaluations of frequency shift and stability in rubidium vapor stabilized semiconductor lasers", Appl. Opt., Vol.28, No.17 (1989) pp.3737-3743

[pp.1 - 7]

[2] K. Kuboki and M. Ohtsu, "A Synthesized Method to Improve Coherence in Semiconductor Lasers by Electrical Feedback", IEEE J. Quantum Electron., Vol.25, No.10 (1989) pp.2084-2090

[pp.8 - 14]

[3] T. Ikegami, S. Ohshima and M. Ohtsu, "Frequency Stabilization of Laser Diodes to the Cs-D_2 Line with the Zeeman Modulation Method", Jpn. J. Appl. Phys., Vol.28, No.10 (1989) pp.L1839-L1841

[pp.15 - 17]

[4] M. Ohtsu and K. Nakagawa, "Frequency Control of Semiconductor lasers and Its Applications", Oyo-Buturi (J. Jpn. Soc. Appl. Phys.), Vol.58, No.10 (1989) pp.1428-1444 (Review paper, in Japanese)

[pp.18 - 34]

[5] M. Ohtsu, M. Murata and M. Kourogi, "FM Noise Reduction and Subkilohertz Linewidth of an AlGaAs Laser by Negative Electrical Feedback", IEEE J. Quantum Electron., Vol.26, No.2 (1990) pp.231-241

[pp.35 - 45]

[6] C.-H. Shin, M. Teshima, M. Ohtsu, T. Imai, J. Yoshida and K. Nishide, "FM Characteristics and Compact Modules for Coherent Semiconductor Lasers Coupled to an External Cavity", IEEE Photonics Technol. Lett., Vol.2, No.3 (1990) pp.167-169

[pp.46 - 48]

[7] C.-H. Shin and M. Ohtsu, "Heterodyne Optical Phase-Locked Loop by Confocal Fabry-Perot Cavity Coupled AlGaAs Lasers", IEEE Photonics Technol. Lett., Vol.2, No.4 (1990) pp.297-300

[pp.49 - 52]

[8] M. Ohtsu, C.-H. Shin, H. Kusuzawa, M. Kourogi and H. Suzuki, "Frequency and Phase Controls of Semiconductor Lasers", Trans. Institute of Electronics, Information and Commun. Eng., Vol.J73-C-I, No.5 (1990) pp.277-285 (Invited paper, in Japanese)

[pp.53 - 61]

(b) International Conferences

[1] K. Nakawaga and M. Ohtsu, "Laser frequency stabilization with applications to atomic frequency standards", Fourth European Frequency and Time Forum (EFTF90), March 1990, Neuchatel, Switzerland, FS-04-1 (Invited)

[pp.62 - 73]

[2] M. Ohtsu, K. Nakagawa, C.-H. Shin, H. Kusuzawa, M.Kourogi and H. Suzuki, "Progress toward a 1 PHz hypercoherent optical sweep generator by semiconductor lasers", Proceedings of the Conference on Lasers and Electro-Optics (CLEO'90), May 1990, Anaheim, CME5 (Invited)

[pp.74 - 75]

[3] H. Kusuzawa, E. Ikegami, H. Furuta, K. Nakagawa and M. Ohtsu, "Proposal of a Semiconductor Laser Diode Based Peta Hertz Class Coherent Optical Sweep Generator", Third Optoelectronics Conference, July 1990, Makuhari Messe, Japan, 12D2-1

[pp.76 - 77]

[4] C.-H. Shin and M. Ohtsu, "Optical Phase-Locking Experiments by Confocal Fabry-Perot Cavity Coupled Semiconductor Lasers", Third Optoelectronics Conference, July 1990, Makuhari Messe, Japan, 12C3-3

[pp.78 - 79]

[II] APPLICATION TO ATOMIC CLOCKS

(a) Journal Papers

[1] M. Hashimoto and M. Ohtsu, "Modulation transfer and optical Stark effect in a rubidium atomic clock pumped by a semiconductor laser", J. Opt. Soc. Am. B, Vol.6, No.10 (1989) pp.1777-1789

[pp.80 - 92]

[2] M. Hashimoto and M. Ohtsu, "A Novel Method to Compensate for the Effect of Light Shift in a Rubidium Atomic Clock Pumped by a Semiconductor Laser", IEE Trans. Instrum. Meas., Vol.39, No.3 (1990) pp.458-462

[pp.93 - 97]

(b) International Conferences

[1] H. Furuta, K. Nakagawa and M. Ohtsu, "DIODE LASER-PUMPED Rb-ATOMIC CLOCK AS A NOVEL PRIMARY FREQUENCY STANDARD", Proceedings of the Conference on Precision Electromagnetic Measurements (CPEM'90), June 1990, Ottawa, Canada, pp.428-429

[pp.98 - 99]

[III] APPLICATION TO PHOTON SCANNING TUNNELING MICROSCOPE

(b) International Conferences

[1] M. Ohtsu, K. Nakagawa, S. Jiang and N. Tomita, "Super-Resolution Photon Scanning Tunneling Microscope", Third Optoelectronics Conference, July 1990, Makuhari, Japan, 12D1-1

[pp.100 - 101]

[2] S. Jiang, N. Tomita, K. Nakagawa and M. Ohtsu, "Proposal of super-sensitive reflection-mode phase-locked photon scanning tunneling microscope by diode lasers", Third Optoelectronics Conference, July 1990, Makuhari, Japan, 12D1-3

[pp.102 - 103]

[IV] AWARD

[1] A Best Paper Award : "Proposal of a Semiconductor Laser Diode Based Peta Hertz Class Coherent Optical Sweep Generator" by H. Kusuzawa, E. Ikegami, H. Furuta, K. Nakagawa and M. Ohtsu, presented at The Third Optoelectronics Conference, July 1990, Makuhari Messe, Japan, paper No.12D2-1

Reprinted from Applied Optics

Evaluations of frequency shift and stability in rubidium vapor stabilized semiconductor lasers

Hiroyuki Furuta and Motoichi Ohtsu

Laser frequencies were stabilized to the linear and saturated absorption spectral lines(LAS, SAS) in ^{87}Rb vapors which were filled into two kinds of glass cell: cell A (^{87}Rb vapor only) and cell B (^{87}Rb vapor and buffer gases). The frequency shifts induced by the change of laser power density were -5 MHz/(mW/cm^2) and -10 MHz/(mW/cm^2) for cells A and B, respectively, when LAS was used. A frequency shift of -0.8 MHz/K was observed for cell B, which underwent a temperature change. However, such a temperature-induced shift was not observed for cell A. The highest frequency stability was 7.7×10^{-11} at a 70-s integration time.

I. Introduction

Frequency stabilization of semiconductor lasers has been carried out by several authors.[1–6] Using these frequency stabilized lasers, several applications to optical sensing and optical measurements have been proposed.[7] In these applications, characteristics of frequency shift (or accuracy) are as important as those of frequency stability in achieving accurate coherent light sources. (Definitions of frequency accuracy and stability are given in Appendix I.)

Furthermore, these frequency-stabilized semiconductor lasers can be employed in the field of microwave frequency standards. For example, highly stable rubidium (^{87}Rb) atomic clocks of 6.8-GHz microwave frequency have been used for microwave communication systems, global positioning systems (GPS),[8] and so on. To improve the performance of these ^{87}Rb atomic clocks, a technique of coherent optical pumping by a stabilized semiconductor laser has been proposed.[9,10] By the precise investigation of a light-induced microwave frequency shift (light shift) in these clocks, it has been found that a quantitative evaluation of the frequency accuracy of the laser is necessary.[11] However, such quantitative evaluations on the frequency accuracy and shift of a stabilized semiconductor laser have not yet been reported.

In recent work on the water-vapor-stabilized semiconductor laser, the laser frequency shift was evaluated as a function of the temperature of a water–vapor cell.[12] In Ref. 12, the laser frequency shift and stability were evaluated by measuring the error signals from the frequency discriminator. However, because error signals obtained by such a method would include the effect of laser intensity fluctuations, accurate evaluations of frequency shift and stability could become difficult. For accurate evaluations, a heterodyning technique should be employed to measure directly the frequency fluctuations.

For these reasons, frequency shift and stability of semiconductor lasers were quantitatively evaluated in the present work by monitoring the beat frequency between two lasers independently stabilized to the ^{87}Rb D_2 line ($5S_{1/2}\,F = 1 - 5P_{3/2}$). The experimental setup is described in Sec. II. In Sec. III, experimental results of the frequency shift and stability of stabilized lasers are presented. In Sec. IV, the results are summarized.

II. Experimental Setup

Figures 1(a) and (b) show two types of experimental setup for frequency stabilization of semiconductor lasers: linear absorption spectroscopy and saturated absorption spectroscopy, respectively. The semiconductor lasers(LDs) used here were CSP-type AlGaAs lasers(Hitachi HL7802E) operated at the 780.0-nm wavelength. Mounted on thermoelectrically cooled heat sinks, their temperature fluctuations were reduced to 1 mK in vacuum chambers. The laser frequency changes due to changes in ambient temperature and dc injection current were -30 GHz/K and -3 GHz/mA, respectively. The rubidium(Rb) gas cells used were made of cylindrical glass tubes, whose diameter and length were 30 and 35 mm, respectively. Two kinds of Rb gas cell were used; one was filled with rubidium 87(^{87}Rb) vapor only (gass cell A), and the other with ^{87}Rb vapor and buffer gases ($Ar/N_2 = 1.65$, total pressure = 43 Torr—gas cell B). Gas cell A was used to investigate the property of the ^{87}Rb vapor itself. Since gas cell B has been popularly used for

The authors are with Tokyo Institute of Technology, Graduate School at Nagatsuta, 4259 Nagatsuta, Midori-ku, Yokohoma 227, Japan.

Received 20 October 1988.
0003-6935/89/173737-07$02.00/0.

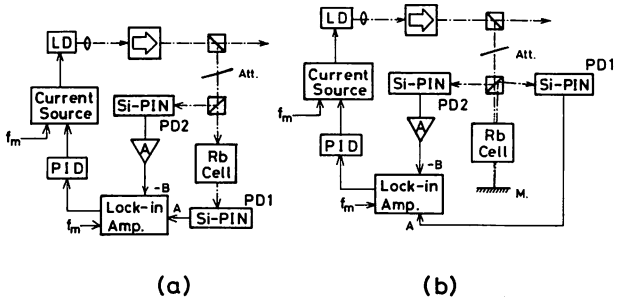

Fig. 1. Experimental setup for the frequency stabilization of a semiconductor laser. To obtain the frequency disciminator, the injection current was modulated at the modulation frequency f_m = 2kHz, and a lock-in amplifier was used to obtain the first derivative of the spectral lineshape in ^{87}Rb vapor. (a) Setup for linear absorption spectroscopy. (b) Setup for saturated absorption spectroscopy.

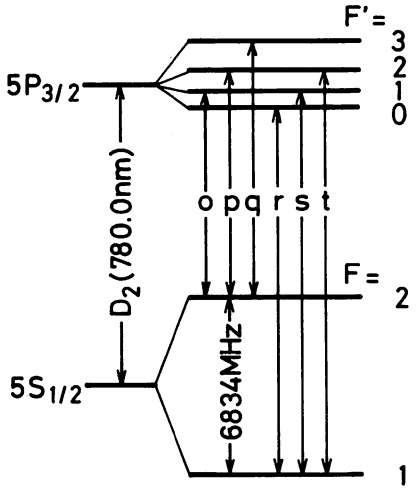

Fig. 2. Energy levels of the ^{87}Rb atom. The quantum numbers F and F' represent the total angular momenta for the hyperfine levels in the ground state $5S_{1/2}$ and in the excited state $5P_{3/2}$, respectively. In this paper, the transitions from the hyperfine level of $F = 2$ in $5S_{1/2}$ to the levels of $F' = 1$, 2, and 3 in $5P_{3/2}$ are referred to o, p, and q, and those from the level of $F = 1$ in $5S_{1/2}$ to the levels of $F' = 0$, 1, and 2 in $5P_{3/2}$ to r, s, and t, respectively.

^{87}Rb atomic clocks, it was also used to obtain the basic data for use in optical pumping of the ^{87}Rb atomic clock in future. Temperatures of these gas cells were thermoelectrically controlled.

The energy levels of a ^{87}Rb atom ($5S_{1/2}$—$5P_{3/2}$) are shown by Fig. 2. In this figure, the quantum numbers F and F' represent the total angular momenta for the hyperfine levels in the ground state $5S_{1/2}$ and in the excited state $5P_{3/2}$, respectively. In this paper, the transitions from the hyperfine level of $F = 2$ in $5S_{1/2}$ to the levels of $F' = 1$, 2, and 3 in $5P_{3/2}$ are referred to o, p and q, and those from the level of $F = 1$ in $5S_{1/2}$ to the levels of $F' = 0$, 1 and 2 in $5P_{3/2}$ to r, s and t, respectively.

The laser frequency was modulated by modulating the injection current at a frequency of f_m = 2 kHz with an amplitude of i_m = 10–50 μA_{p-p}. The output signal

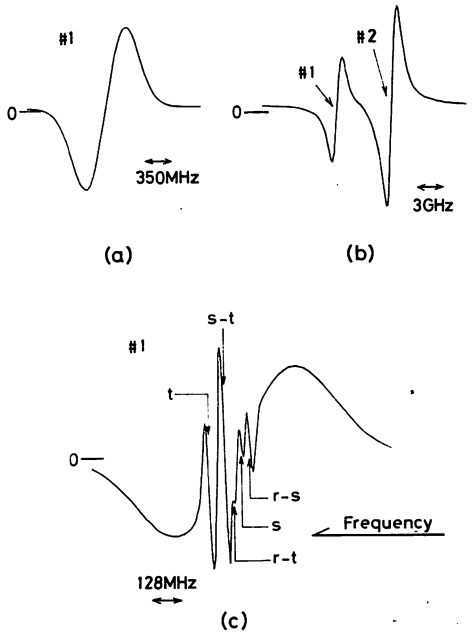

Fig. 3. First derivative of the linear absorption spectral line (LAS) obtained by sweeping the injection current of the laser: (a) gas cell A; (b) gas cell B. The injection current was modulated at a frequency of f_m = 2 kHz with the amplitude of i_m = 50 μA_{p-p}. (c) The first derivative of the saturated absorption spectral line (SAS) obtained for gas cell A: at a frequency of f_m = 2 kHz and i_m = 10 μA_{p-p}. The spectral profiles #1 and #2 in these figures correspond to the transitions from the level of $F = 1$(r, s, and t in Fig. 2) and $F = 2$(o, p, and q in Fig. 2), respectively. The symbols s—t, r—t, and r—s represent the crossover resonances between a hyperfine level($F = 1$) in $5S_{1/2}$ and two hyperfine levels in $5P_{3/2}$.

from the photodetector PD1 was synchronously demodulated by a lock-in amplifier. The output signal from the lock-in amplifier corresponds to the first derivative of the Rb spectral lineshape, which was used as a frequency discriminator for frequency stabilization. Figures 3(a) and (b) show such a first derivative of the linear absorption spectral line (LAS) obtained by using gas cells A and B, respectively, for which the experimental setup of Fig. 1(a) was used. Figure 3(c) shows the first derivative of the saturated absorption spectral line (SAS) obtained by using gas cell A, of which the experimental setup is shown by Fig. 1(b). The spectral profiles #1 and #2 in these figures correspond to the transitions from the level of $F = 1$ (r, s, and t in Fig. 2) and $F = 2$ (o, p, and q in Fig. 2), respectively. In Figs. 3(a) and (b), the hyperfine transitions r, s, and t were not resolved, because of Doppler broadening and pressure broadening by the buffer gases. In Fig. 3(c), two hyperfine transitions (s and t) and three other transitions (s—t, r—t, and r—s) were observed. These represent three transitions of the crossover resonances between a hyperfine level ($F = 1$) in the ground state and two hyperfine levels in the excited state.

By using the first derivative of the spectral profile #1 in Fig. 3 ($5S_{1/2}$ $F = 1$—$5P_{3/2}$) as a frequency discriminator, the laser frequency was locked to its zero crossing point by controlling the injection current. To

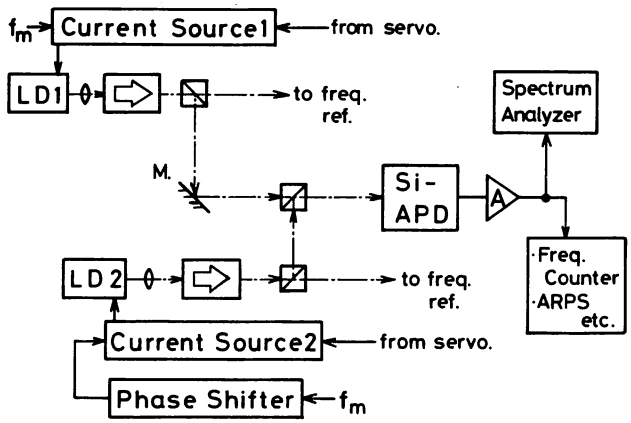

Fig. 4. Experimental setup for the measurements of frequency shift and stability. Here, ARPS represents the Allan variance real-time processing system[14].

compensate for the effect of laser intensity fluctuations, the intensity fluctuations were monitored by a photodetector PD2, and its output signal was sent to the differential input terminal of the lock-in amplifier, as indicated in Fig. 1.

Characteristics of laser frequency shift were investigated by varying two parameters: 1) the laser power density (P_L) incident on the Rb cell, and 2) temperature of Rb cell (T_{Rb}).

Figure 4 shows the experimental setup used for measurement of the frequency shift and stability of lasers. The frequencies of the test laser (LD1) and the reference laser (LD2) were independently stabilized. The frequency shift Δf of LD1 due to the change of P_L or T_{Rb} was ascertained by measuring the change of the beat frequency between the two lasers. The frequency of LD2 was stabilized to the center frequency of the LAS in gas cell A. The values of P_L and T_{Rb} for LD2 were set at 1.6 mW/cm^2 and 303 K, respectively. To estimate the frequency stability of the laser, the Allan variance[13] of the beat frequency fluctuations was measured by the Allan variance real-time processing system (ARPS).[14] The value of the Allan variance of the beat frequency fluctuations corresponds to twice that of the frequency fluctuations of each laser if the frequency stability of the two independent lasers are assumed to be equal.

The field spectral profile of the beat signal was broadened and contained several FM sidebands, which were induced by independent modulation of the injection currents of the two lasers. These FM sidebands would induce the error for the measurement of beat frequency fluctuations. A phase shifter was used to reduce this error by synchronizing the modulation of the injection currents of the two lasers.

III. Experimental Results and Discussions

A. Frequency Shift of Semiconductor Lasers

Figure 5 shows the frequency shift Δf of the test laser LD1 when its frequency was locked to the zero crossing point of the LAS of gas cell A. In this figure, the

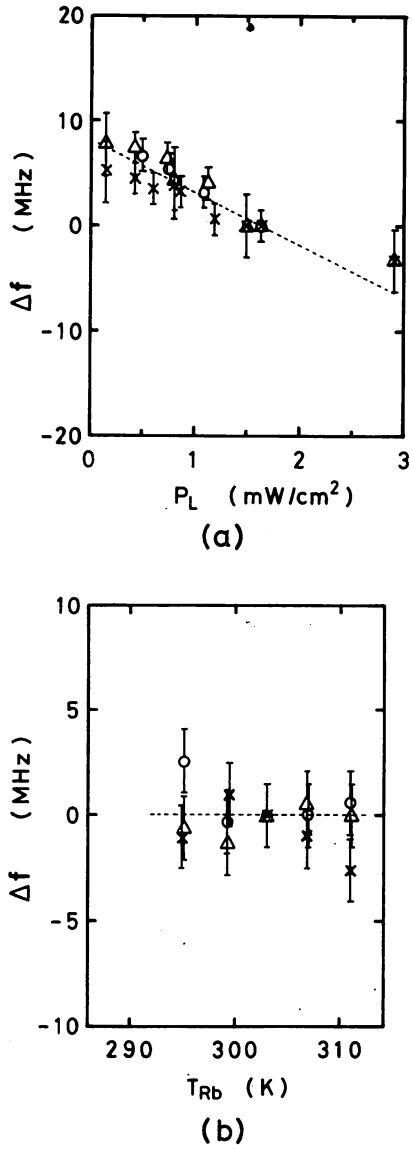

Fig. 5. Frequency shift Δf of a semiconductor laser when the laser was locked to the LAS line center (F = 1) of gas cell A: (a) as a function of P_L at T_{Rb} = 303 K; (b) as a function of T_{Rb} at P_L = 1.6 mW/cm^2. The reference (Δf = 0) was the beat frequency at T_{Rb} = 303 K and P_L = 1.6 mW/cm^2. Here O, Δ, and × represent the results for the modulation amplitude i_m = 10, 20 and 50 μA_{p-p}, respectively.

reference was the beat frequency when the frequency of LD1 was locked to P_L = 1.6 mW/cm^2 and T_{Rb} = 303 K, i.e., at which Δf = 0. The values of Δf were plotted as a function of P_L at T_{Rb} = 303 K, and as a function of T_{Rb} at P_L = 1.6 mW/cm^2, in Figs. 5(a) and (b), respectively. It is clearly seen in Fig. 5(a) that Δf decreases by increasing P_L, and this power-induced shift $d(\Delta f)/dP_L$ was estimated to −5 MHz/(mW/cm^2). Figure 5(b) shows that Δf was almost independent of T_{Rb}.

Figure 6 shows the frequency shift Δf of LD1 when its frequency was locked to the zero crossing of the LAS of gas cell B. In this figure, the reference was the beat frequency when the frequency of LD1 was locked to P_L = 1.6 mW/cm^2 and T_{Rb} = 333 K. Figures 6(a) and (b) represent the dependence of Δf on P_L at T_{Rb} = 333 K

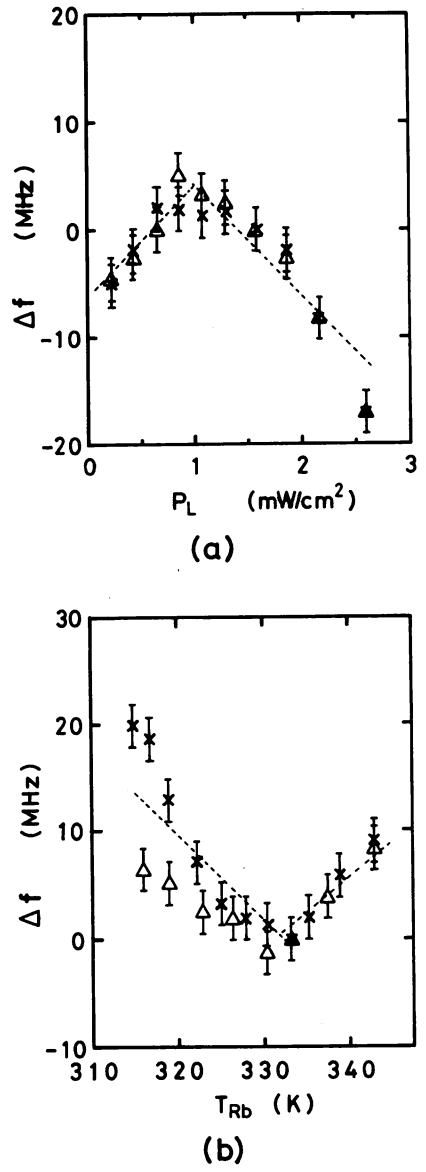

Fig. 6. Frequency shift Δf of a semiconductor laser when the laser was locked to the LAS line center ($F = 1$) of gas cell B: (a) as a function of P_L at $T_{Rb} = 333$ K; (b) as a function of T_{Rb} at $P_L = 1.6$ mW/cm^2. The reference($\Delta f = 0$) was the beat frequency at $T_{Rb} = 333$ K and $P_L = 1.6$ mW/cm^2. Here Δ and $\times$ represent the results for the modulation amplitude $i_m = 20$ and 50 μA_{p-p}, respectively.

and on T_{Rb} at $P_L = 1.6$ mW/cm^2, respectively. As seen in Fig. 6(a), Δf increased at the rate of +10MHz/(mW/cm^2) for $P_L \leqq 1$ mW/cm^2. For $P_L \geqq 1$ mW/cm^2, the value of Δf decreased at a rate of -10 MHz/(mW/cm^2). Figure 6(b) shows that the value of $d(\Delta f)/dT_{Rb}$ was -0.8 MHz/K for 315 K $\leqq T_{Rb} \leqq$ 330 K, and +0.6 MHz/K for 330 K $\leqq T_{Rb} \leqq$ 345 K. The negative value of $d(\Delta f)/dT_{Rb}$ for 315 K $\leqq T_{Rb} \leqq$ 330 K can be explained as follows: the profile of the buffer-gas-broadened linear absorption spectral lineshape can be expressed as

$$I(\nu) = I_1(\nu) + I_2(\nu), \tag{1}$$

where $I_1(\nu)$ and $I_2(\nu)$ represent the spectral profiles of the transition from the $F = 1$ and 2 levels of the ground state, respectively. Spectral profiles #1 and #2 in Fig. 3(b) correspond to $I_1(\nu)$ and $I_2(\nu)$, respectively. Since the spectral profile $I_1(\nu)$ is composed of the Lorentzian profiles of the hyperfine transition components r, s, and t, it can be expressed as

$$I_1(\nu) = I_1 \sum_{i=1}^{3} \frac{p_i \gamma_1^2}{(\nu - \nu_i)^2 + \gamma_1^2}, \tag{2}$$

where p_i and $\nu_i (i = 1\text{–}3)$ represent the relative transition probability and center frequency of the components r, s, and t, respectively. The values of these constants, used for the present calculations, are given in Appendix II. The spectral linewidth γ_1 was assumed to have the same value for these three components. The spectral profile $I_2(\nu)$ is composed of the hyperfine transition components o, p, and q, which is expressed as

$$I_2(\nu) = I_2 \sum_{i=4}^{6} \frac{p_i \gamma_2^2}{(\nu - \nu_i)^2 + \gamma_2^2}. \tag{3}$$

The quantities p_i, ν_i and γ_2 are defined in a similar way for Eq. (2). Since the laser frequency was locked to one of the frequencies of the spectral peak of $I(\nu)$, this peak frequency should be estimated. For this estimation, Eq. (1) was least-square-fitted to the spectral profile measured at several values of T_{Rb} by adjusting the values of I_1, I_2, γ_1, and γ_2. The values of these parameters used for this fitting are shown in Fig. 7(a) as a function of T_{Rb}, where it can be seen that the values of these parameters increased with increasing T_{Rb}. The increase of I_1 and I_2 resulted from the increase of Rb pressure. Those of γ_1 and γ_2 resulted from the increase of collisions between Rb atoms and buffer gases. These increases can induce the change in the characteristics of the overlap between the spectral profiles $I_1(\nu)$ and $I_2(\nu)$, by which the peak frequency shifts of the spectral lineshape and locked laser frequency shifts can also be induced. Using the estimated values of these parameters, the peak frequencies of the spectral lineshapes #1 and #2 were estimated from Eqs. (1)–(3). The relationship between T_{Rb} and the estimated peak frequency of the spectral lineshape #1 is shown by Fig. 7(b). This figure corresponds to Fig. 6(b). It can be seen that the characteristics of the frequency shifts in Figs. 6(b) and 7(b) agree with each other for 315 K $\leqq T_{Rb} \leqq$ 330 K. From this agreement, it can be concluded that the cause of the negative value of $d(\Delta f)/dT_{Rb}$ is the change in the characteristics of the overlap of the Lorentzian lineshapes of the absorption spectral profile.

The cause of the positive value of $d(\Delta f)/dT_{Rb}$ for 330 K $\leqq T_{Rb} \leqq$ 345 K can be assumed to be the increase of buffer-gas-pressure induced by the increase of T_{Rb}. However, detailed studies have not yet been made.

Figures 8(a) and (b) show the dependence of the frequency shift Δf of LD1 on P_L at $T_{Rb} = 303$ K and on T_{Rb} at $P_L = 2.6$ mW/cm^2, respectively, where the LD1 frequency was locked to each zero crossing point of the

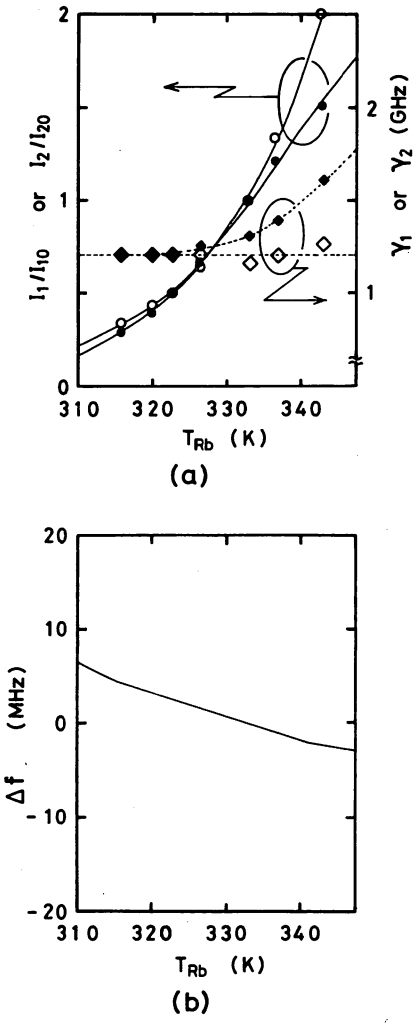

Fig. 7. (a) Values of I_1, I_2, γ_1, and γ_2 used for the least-square-fitting, given as a function of T_{Rb} of gas cell B at $P_L = 1.6$ mW/cm^2. In this figure, I_1 and I_2 were normalized to the values at $T_{Rb} = 333$ K. The values of I_1 and I_2 at $T_{Rb} = 333$ K were expressed as I_{10} and I_{20}, respectively. The measured value of I_{20}/I_{10} was 2.15. Open(○, ◇) and solid(●, ◆) correspond to the spectral profiles #1 and #2 in Fig. 3(b), respectively. (b) Estimated results of frequency shift Δf as a function of T_{Rb}, using the values of (a) and Eqs. (1)–(3). The reference ($\Delta f = 0$) was the estimated frequency at $T_{Rb} = 333$ K.

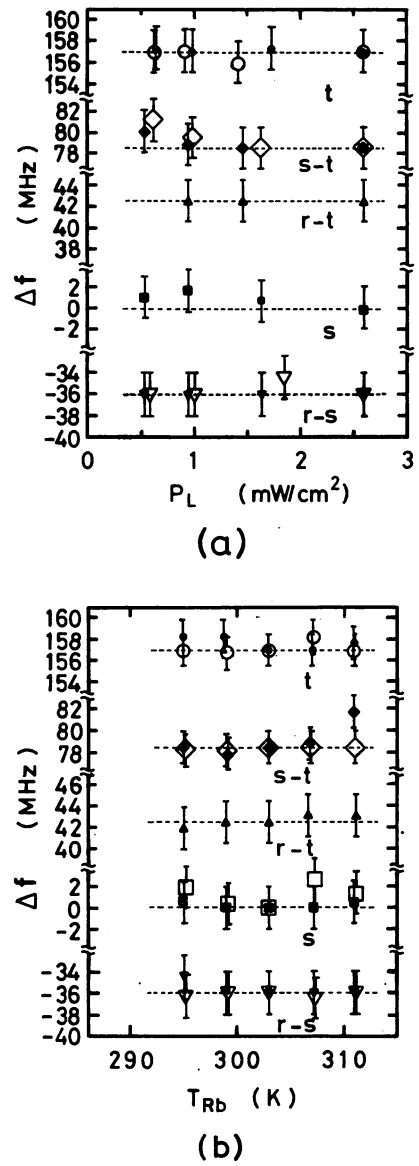

Fig. 8. Frequency shift Δf of a semiconductor laser when the laser was locked to the SAS line centers [$F = 1$: t, r—t, s—t, s, and r—s in Fig. 3(c)] of gas cell A: (a) as a function of P_L at $T_{Rb} = 303$ K; (b) as a function of T_{Rb} at $P_L = 2.6$ mW/cm^2. The reference ($\Delta f = 0$) was the beat frequency when the frequency of the test laser was locked to the component s when $T_{Rb} = 303$ K and $P_L = 2.6$ mW/cm^2. Solid(●, ◆, ▲, ■, ▼) and open(○, ◇, △, □, ▽) represent the results for the modulation amplitude $i_m = 10$ and 20 μA_{p-p}, respectively.

SAS of gas cell A[t, s—t, r—t, s, and r—s in Fig. 3(c)]. In these figures, the reference was the beat frequency when the frequency of LD1 was locked to the zero crossing point of the spectral component s when $P_L = 2.6$ mW/cm^2 and $T_{Rb} = 303$ K. The frequency separations of spectral components t, s—t, r—t, s, and r—s agreed with the theoretical values shown in Fig. 10 of Ref. 15. It can be seen from Figs. 8(a) and (b) that the SAS in gas cell A did not induce any frequency shifts.

In comparison with the magnitude of the temperature-induced shift of 3 MHz/K for water vapor,[12] those of the shifts in Figs. 5(b), 6(b), and 8(b) were smaller. It can be concluded from these measurements that ^{87}Rb vapor is more stable than water vapor when it is used as the frequency reference of the semiconductor laser for frequency stabilization.

B. Frequency Stability of Semiconductor Lasers

Figure 9 shows the square root of the Allan variance $\sigma^2(\tau)$ of the residual beat frequency fluctuations of semiconductor lasers. Here, $\sigma^2(\tau)$ was normalized to the optical center frequency of a laser. Curve A represents the result of a free running laser. Curves B, C, and D represent the results of frequency stabilization using the first derivatives of the LAS of gas cell A, the LAS of gas cell B, and the SAS of gas cell A, respectively.

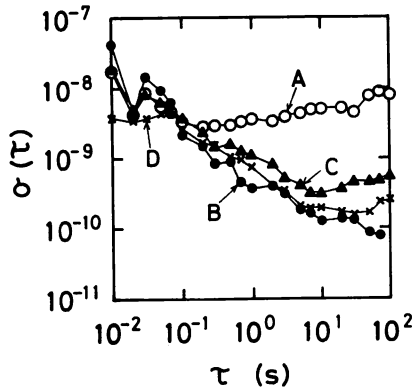

Fig. 9. Square root of the Allan variance $\sigma^2(\tau)$ for the residual beat frequency fluctuations of semiconductor lasers. The value of $\sigma^2(\tau)$ was normalized to the optical frequency of a laser. A: Result of the free running lasers. B: Result of frequency stabilization by using the first derivative of the LAS of gas cell A. C: Result of frequency stabilization by using the first derivative LAS of gas cell B. D: Result of frequency stabilization by using the first derivative of SAS of gas cell A.

In these measurements, the laser frequencies were locked by setting the time constant of the feedback loop of 0.1 s, which was mainly determined by the time constant of a low pass filter in the lock-in amplifier.

The minimum of $\sigma(\tau)$ is seen on curve B, which is 7.7×10^{-11} at integration time τ of 70 s. This value was ~1/100 times that of the free running laser (curve A), from which the improvement in frequency stability was confirmed. On curves C and D, improvements of frequency stability were also seen and the minima on these curves were 3.0×10^{-10} (at τ = 10 s) and 1.5×10^{-10} (at τ = 30 s), respectively. These frequency stability values were almost the same as or higher than those of lasers whose frequency was stabilized to the third derivative of the SAS of ^{87}Rb D_1 line.[16]

IV. Summary

Frequency shift and stability of semiconductor lasers were evaluated by monitoring the beat frequency between two lasers whose frequencies were stabilized independently to ^{87}Rb D_2 line ($5S_{1/2}F = 1 - 5P_{3/2}$). Evaluations were carried out using the linear absorption spectral line (LAS) and the saturated absorption spectral line (SAS) for two kinds of Rb gas cell: cell A(^{87}Rb only) and cell B[^{87}Rb and buffer gases (Ar/N_2 = 1.65, total pressure = 43 Torr)]. Laser frequency shifts depending on the laser power (P_L) and the temperature of the Rb cell (T_{Rb}) were investigated.

The frequencies of the lasers locked to the LAS of cells A and B were shifted by P_L. The coefficients of these shifts were −5 MHz/(mW/cm^2) and −10 MHz/(mW/cm^2), respectively. A frequency shift by the variation of T_{Rb} was observed for $315\ K \leqq T_{Rb} \leqq 330\ K$, when the laser frequency was stabilized to the LAS of gas cell B. Its coefficient was −0.8 MHz/K. This temperature-induced shift was attributed to the change of the characteristics of the overlap of the buffer-gas-broadened absorption spectral profile. However, this temperature-induced frequency shift was not observed when the laser frequencies were locked to both LAS and SAS for gas cell A.

The square root of the Allan variance of the beat frequency fluctuations was measured to evaluate the frequency stability. The minimum values were

7.7×10^{-11} (at τ = 70 s); LAS, gas cell A
1.5×10^{-10} (at τ = 30 s); SAS, gas cell A
3.0×10^{-10} (at τ = 10 s); LAS, gas cell B.

The authors would like to thank Y. Teramachi of University of Industrial Technology, S. Kano of IBM Japan, Ltd., and M. Hashimoto of their institute for their valuable discussions. They also wish to thank to K. Chiba and H. Sumiyoshi of Fujitsu, Ltd. for their support for the experiments.

Appendix I

Definitions of frequency stability and accuracy of quantum oscillators, i.e., semiconductor lasers, follow those of Refs. 17 and 18, and are summarized as follows:

Stability: A sequence of N readings of a particular oscillator frequency in a particular adjustment, against a comparison oscillator assumed temporally constant, will show fluctuations. The standard deviation of these observations is often called the stability.[17]

Accuracy: Accuracy means fractional uncertainty in determining an atomic transition frequency of the free atom and is expressed by 3σ limits for statistically determined frequencies.[18]

Appendix II

The values of p_i (i = 1–6), i.e., the relative transition probabilities of the hyperfine transitions (o–t) in absorption spectroscopy were calculated from a textbook[19] and obtained as follows:

$p_1 = 1/36$ (component r),
$p_2 = 5/72$ (component s),
$p_3 = 5/72$ (component t),
$p_4 = 1/120$ (component o),
$p_5 = 3/72$ (component p),
$p_6 = 7/60$ (component q).

The frequency separations between the spectral components (o–t) can be calculated by the formula given in Ref. 20. For this calculation, the values of the magnetic dipole constants and the electric quadrupole constants in hyperfine structures of ^{87}Rb given also in Ref. 20 were used. As a result of this calculation, the center frequencies ν_i(i = 1–6; $i \neq 2$) with respect to ν_2(component s) can be expressed as:

$\nu_1 = \nu_2 - 72$ MHz,
$\nu_3 = \nu_2 + 157$ MHz,
$\nu_4 = \nu_2 - 6834$ MHz,
$\nu_5 = \nu_2 - 6677$ MHz,
$\nu_6 = \nu_2 - 6410$ MHz,

References

1. J. L. Picque and S. Roizen, "Frequency-Controlled CW Tunable GaAs Laser," Appl. Phys. Lett., **27,** 340–342 (1975).
2. H. Tsuchida, S. Sanpei, M. Ohtsu, and T. Tako, "Frequency Stability Measurement of Feedback Stabilized AlGaAs DH Laser," Jpn. J. Appl. Phys., **19,** L721–L724 (1980).
3. T. Okoshi and K. Kikuchi, "Frequency Stabilization of Semiconductor Lasers for Heterodyne-Type Optical Communication Systems," Electron. Lett., **16,** 179–181 (1980).
4. T. Yabuzaki, A. Ibaragi, H. Hori, M. Kitano, and T. Ogawa, "Frequency-Locking of a GaAlAs Laser to a Doppler-Free Spectrum of Cs-D_2 Line," Jpn. J. Appl. Phys., **20,** L451–L454 (1981).
5. H. Tsuchida, M. Ohtsu, T. Tako, N. Kuramochi and N. Oura, "Frequency Stabilization of AlGaAs Semiconductor Laser Based on the ^{85}Rb-D_2 Line," Jpn. J. Appl. Phys., **21,** L561–L563 (1982).
6. C. J. Nielsen and G. Jacobsen, "Frequency Stabilization of Singlemode Semiconductor Lasers at 830 nm and 1.3 μm," J. Opt. Commun., **4,** 122–125 (1983).
7. M. Ohtsu and T. Tako, "Coherence in Semiconductor Lasers," in *Progress in Optics XXV*, E. Wolf, Ed. (Elsevier Science, Amsterdam, 1988) pp. 191–278.
8. T. Shiomi, "Highly Precise Positioning System Using GPS," (in Japanese) J. IEICE Jpn., **70,** 521–523 (1987).
9. L. L. Lewis and M. Feldman, "Optical Pumping by Lasers in Atomic Frequency Standards," in *Proceedings, Thirty-Fifth Annual Symposium on Frequency Control, Fort Monmouth, NJ* (1981) pp. 612–624.
10. M. Hashimoto and M. Ohtsu, "Experiments on a Semiconductor Laser Pumped Rubidium Atomic Clock," IEEE J. Quantum Electron., **QE-23,** 446–451 (1987).
11. M. Hashimoto, M. Ohtsu, and H. Furuta, "Ultra-Sensitive Frequency Discrimination in a Diode Laser Pumped ^{87}Rb Atomic Clock," in *Proceedings, Forty-First Annual Symposium on Frequency Control*, Philadelphia, PA (1987), pp. 25–35.
12. V. Pevtschin and S. Ezekiel, "Investigation of Absolute Stability of Water-Vapor-Stabilized Semiconductor Laser," Opt. Lett., **12,** 172–174 (1987).
13. D. W. Allan, "Statistics of Atomic Frequency Standards," Proc. IEEE, **54,** 221–230 (1966).
14. I. Siio, M. Ohtsu and T. Tako, "Development of the Allan Variance Real-Time Processor," (in Japanese) Trans. IECE Jpn., **J64-C,** 204–208 (1981).
15. M. Ohtsu, M. Hashimoto, and H. Ozawa, "A Highly Stabilized Semiconductor Laser and Its Application to Optically Pumped Rb Atomic Clock," in *Proceedings, Thirty-Ninth Annual Symposium on Frequency Control*, Philadelphia, PA (1985), pp. 43–53.
16. G. P. Barwood, P. Gill and W. R. C. Rowley, "Laser Diode Frequency Stabilization to Doppler-Free Rubidium Spectra," Electron. Lett. **24,** 769–770 (1988).
17. R. E. Beehler, R. C. Mockler, and J. M. Richardson, "Cesium Beam Atomic Time and Frequency Standards," Metrologia, **1,** 114–131 (1965).
18. R. E. Beehler and D. J. Glaze, "The Performance and Capability of Cesium Beam Standards at the National Bureau of Standards," IEEE Trans. Instrum. Meas., **IM-15,** 48–55 (1966).
19. A. R. Edmonds, *Angular Momentum in Quantum Mechanics* (Princeton U.P., Princeton, 1968).
20. E. Arimondo, M. Inguscio and P. Violino, "Experimental Determinations of the Hyperfine Structure in the Alkali Atoms," Rev. Mod. Phys., **49,** 31–75 (1977).

A Synthesized Method to Improve Coherence in Semiconductor Lasers by Electrical Feedback

K. KUBOKI AND MOTOICHI OHTSU, MEMBER, IEEE

Abstract—**A synthesized method to improve coherence in semiconductor lasers by negative electrical feedback was proposed for stabilization of the center frequency of the field spectrum, linewidth reduction of the field spectrum, frequency tracking to another highly coherent laser, and stable and wide-band frequency sweep. An experiment for center frequency stabilization of the master laser showed that the magnitude of frequency fluctuations was reduced to 50 kHz at the integration time $\tau = 3$ s. The linewidth of the master laser was reduced to 100 kHz, which was 1/50 times that of the free-running laser. It was confirmed that the value of this linewidth was narrower than that determined by the magnitude of spontaneous emission of the free-running laser. Under these conditions of frequency control for the master laser, the frequency of the slave laser was controlled in order that the phase of the heterodyne signal between the master and the slave lasers could be locked to that of the stable microwave synthesizer. As a result of this control, residual frequency fluctuations of the heterodyne signal were reduced as low as 0.6 Hz at $\tau = 1000$ s. It was confirmed from this result that the slave laser frequency tracked accurately to the master laser frequency. Furthermore, the frequency of the slave laser could be continuously swept in a stable manner by sweeping the frequency of the microwave synthesizer while maintaining the condition of this frequency tracking. The total range of the continuous frequency sweep of the slave laser was 64.3 GHz.**

I. Introduction

PERFORMANCES of semiconductor lasers have been improved in recent years so that the semiconductor lasers can be used for a variety of applications such as measurements, communications, and so on. However, further improvements of their coherence are required for passive ring cavity-type fiber gyroscopes [1], optically pumped rubidium and cesium atomic clocks [2], coherent optical communication systems [3], and so on. It can be deduced from well-developed techniques for microwave oscillators [4] and gas lasers [5] that at least four objectives should be simultaneously achieved to improve coherence of semiconductor lasers. They are 1) stabilization of center frequency of the field spectrum, 2) linewidth reduction of the field spectrum, 3) frequency tracking to another highly coherent laser, and 4) stable and wide-band frequency sweep. These have been studied separately. For example, optical feedback has been employed for objective 1), and injection locking phenomena have been utilized for objectives 3) and 4). However, optical feedback technique had several problems, including the deterministic instabilities which depended on the phase of the reflected light, the decrease of the direct frequency modulation index, and so on. The injection locking technique also had the problem that the locking range depended on the powers of the two lasers. To overcome these difficulties, the authors have proposed a technique using negative electrical feedback to control the injection current [6]. The authors have also proposed a system which can realize the above-mentioned four objectives simultaneously by the electrical feedback technique, and have reported the results of the preliminary experiments for 1), 3), and 4) [7]. In the present work, further improvements of the performance of the system are reported to realize the four objectives simultaneously.

Manuscript received November 14, 1988; revised April 13, 1989. This work was supported in part by a Grant-in-Aid for Scientific Research from the Ministry of Education, Science and Culture of Japan.

The authors are with the Graduate School at Nagatsuta, Tokyo Institute of Technology, 4259 Nagatsuta, Midori-ku, Yokohama, Kanagawa 227, Japan.

IEEE Log Number 8930146.

II. Experimental Setup

Fig. 1 shows an experimental setup. AlGaAs lasers (CSP-type, Hitachi, HL8312E) of 0.83 μm wavelength were used as the master and slave lasers. Temperatures of their heat sinks were controlled by two peltier elements to reduce their temperature fluctuations as low as 2 mK for more than 3 h. Temperatures of the heat sinks of the master and the slave lasers were fixed to 294 and 295 K, respectively. At those temperatures, the threshold currents I_{th} of these lasers were 55 and 56 mA, respectively.

As the first step, experiments for center frequency stabilization and linewidth reduction of the field spectrum for the master laser were carried out. A detailed experimental setup for the master laser is shown in Fig. 2. Blocks (a) and (b) of Fig. 2 represent the feedback loops for center frequency stabilization and for linewidth reduction, respectively.

A linear part of a slope of resonance curve of the light reflected from a Fabry–Perot interferometer was used as a frequency reference for center frequency stabilization. The Fabry–Perot interferometer used for frequency reference was made of a cylindrical rod of fused silica with dielectric multilayer films coated on both ends, and had a free spectral range of 3.45 GHz with reflectivities of 90 percent. An additional master laser was prepared, which was stabilized by using the same Fabry–Perot interferometer mentioned above, to estimate frequency stability of the master laser quantitatively. The Allan variance $\sigma^2_{yM}(\tau)$ [8] of residual frequency fluctuations of the heterodyne signal between the two master lasers was measured, as will be shown later.

0018-9197/89/1000-2084$01.00 © 1989 IEEE

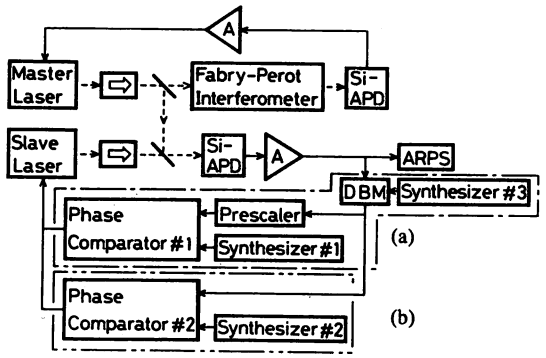

Fig. 1. Experimental setup. (a) Slow feedback loop of the frequency tracking. (b) Fast feedback loop of the frequency tracking. Phase comparator #1: a wide dynamic range digital phase comparator. Phase comparator #2: a wide-band analogue phase comparator. DBM: Double balanced mixer. ARPS: the Allan variance real-time processing system. The division rate M of the prescaler was fixed within the range of $3 \leqq M \leqq 2000$.

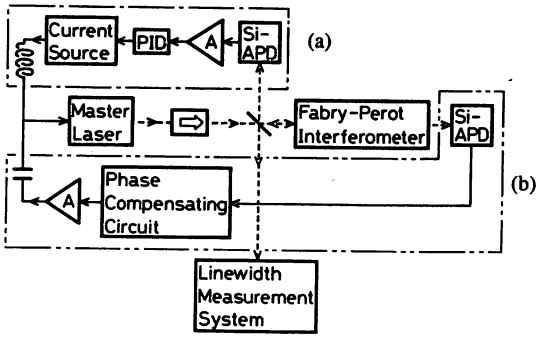

Fig. 2. Experimental setup for the master laser. (a) Feedback loop for stabilization of center frequency of the field spectrum. (b) Feedback loop for linewidth reduction of the field spectrum.

The Allan variance real-time processing system (ARPS) [9], whose preliminary setup has been developed by the authors, was improved to be able to measure for the integration time of $1\ \mu s \leqq \tau \leqq 1000$ s. The factor which fixed the shortest measurable integration time to $1\ \mu s$ is as follows. The heterodyne-type frequency locked loop realized in the second step of the present study had a bandwidth wider than 1 MHz. For comparison between the Allan variance of the residual frequency fluctuations of the heterodyne signal under free-running conditions and that under feedback conditions, the shortest measurable integration time had to be at least $1\ \mu s$. A block diagram of the improved ARPS is shown in Fig. 3. In the improved ARPS, the frequency of the input signal was counted by TTL counters at every integration time τ. Then, the counted data were stored in the memory without any dead time in measurement. When the number of the data reached a preset sample number $N\ (=100)$, they were transferred to a personal computer. After the Allan variance was calculated from these data by the computer, a relation between τ and the square root of the Allan variance was plotted on a X–Y plotter. The shortest measurable integration time was extended by using an external memory in the improved ARPS. By this improvement, the measurement time of the Allan variance was reduced to

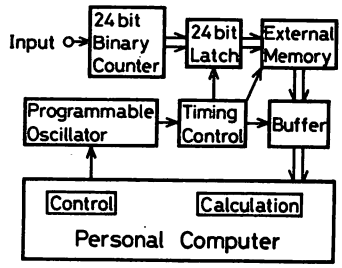

Fig. 3. Block diagram of an improved Allan variance real-time processing system (ARPS).

1/6 times that of the previous system, and the Allan variance could be measured for $1\ \mu s \leqq \tau \leqq 1000$ s.

For spectral linewidth reduction, a linear part of a slope of resonance curve of the light transmitted from the same Fabry–Perot interferometer was used as a frequency discriminator. A phase lag–lead compensating circuit in block (b) in Fig. 2 was employed to compensate for the phase delay due to the FM response characteristics of the master laser. Its transfer function $H_P(f)$ is expressed as

$$H_P(f) = n_1 \cdot \frac{1 + jf/f_1}{1 + (jf/f_1) \cdot n_1} \cdot \frac{1 + (jf/f_2) \cdot n_2}{1 + jf/f_2} \tag{1}$$

where j represents the imaginary unit. Parameters n_1, n_2, f_1, and f_2 were chosen so that the bandwidth and gain of the feedback loop of block (b) in Fig. 2 could become maximum [10]. Since the optimum values of these parameters depended on FM response characteristics of the master laser, these characteristics were measured by using a microwave network analyzer. Furthermore, the open loop transfer function of the feedback loop of block (b) in Fig. 2 was also measured. The field spectral profile was observed by the delayed self-homodyne technique [11] using a single mode optical fiber 2 km long. Furthermore, the power spectral densities of the FM noise of the master laser under free-running and feedback conditions were measured by a microwave spectral analyzer and were compared with each other.

As the second step, frequency tracking of the slave laser to the master laser, i.e., an experiment of realizing a heterodyne-type frequency locked loop, was carried out. For this purpose, a technique of frequency offset locking was employed by using a stable microwave synthesizer as a reference oscillator. Its experimental setup is shown in Fig. 1. Two kinds of feedback loops were employed to improve the performance of this system as compared with that of previous systems [7]. Block(a) of Fig. 1 represents a slow feedback loop to reduce a long-term frequency drift of the heterodyne signal and to extend the capture range. By this feedback loop, long-term frequency stability of the heterodyne signal was improved by locking the phase of the heterodyne signal to that of microwave synthesizer #1 or #3 in Fig. 1. Phase comparator #1 was a digital phase comparator with a wide dynamic range of $\pm 2\pi \times 2^{11}$ rad [7]. Block(b) is a fast feedback loop to improve a

short-term frequency tracking stability. Phase comparator #2 was a wide-band and analogue phase comparator (Motorola, MC1496G, maximum operation frequency = 80 MHz). The frequency of microwave synthesizer #2 was fixed to the product of the frequency of microwave synthesizer #1 and the division rate M of the prescaler. Total bandwidth of these two feedback loops was 3 MHz. The Allan variance of $\sigma_{yH}^2(\tau)$ of the residual frequency fluctuations of the heterodyne signal was measured by the ARPS to evaluate the performance of this system quantitatively.

As the last step, the frequency of synthesizer #1 or #3 in Fig. 1 was swept slowly to sweep the frequency of the slave laser in a stable manner under the condition of frequency locking. In block (a) of Fig. 1, a double-balanced mixer and synthesizer #3 were used for frequency down-conversion to extend the range of stable frequency sweep. The division rate M of the prescaler was fixed within the range of $3 \leqq M \leqq 2000$.

III. Experimental Results and Discussions

A. Frequency Control of Master Laser

Fig. 4 shows the result of center frequency stabilization of the field spectrum of the master laser. This result is expressed by the square root of the Allan variance $\sigma_{yM}^2(\tau)$ of the residual frequency fluctuations $\delta\nu$ normalized to the optical frequency ν ($y = \delta\nu/\nu$). Curves A and B represent the values under free-running and feedback conditions, respectively. Since the bandwidth of the feedback loop for center frequency stabilization (block (a), Fig. 2) was 20 kHz, the value of curve B was lower than that of curve A for the range of $\tau \geqq 50$ μs. The minimum of curve B was $\sigma_{yM}(\tau) = 1.4 \times 10^{-10}$ at $\tau = 3$ s, which corresponds to fluctuations of 50 kHz. Higher frequency stability can be expected by using absorption spectral lines in stable atoms or molecules, e.g., Rb, Cs, H_2O, NH_3, and so on [12], [13].

Figs. 5 and 6 show the transfer function $H_L(f)$ of the FM response characteristics of the master laser and the open loop transfer function $H(f)$ of the linewidth reduction loop (block (b), Fig. 2), respectively, measured by a microwave network analyzer. It is clearly seen from Fig. 5 that the arg $[H_L(f)]$ was almost constant up to 100 MHz. This characteristic made it easy to design a wide-band frequency control loop. Curve A in Fig. 6 shows an open loop transfer function when the phase compensating circuit was not used. The bandwidth of the curve A was 3.9 MHz. By using an optimized phase compensating circuit, the loop transfer function was measured, which was represented by curve B in this figure. The optimized values of n_1, n_2, f_1, and f_2 in (1) were 0.8, 0.5, 8.8 MHz, and 16 MHz, respectively. As the result of this optimization, the bandwidth of the feedback loop for linewidth reduction (block(b), Fig. 2) was expanded to 24 MHz.

Fig. 7 shows the result of spectral linewidth reduction of the master laser. Since this figure represents spectral

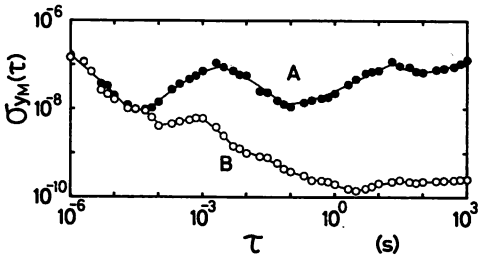

Fig. 4. Square root of the Allan variance $\sigma_{yM}^2(\tau)$ of the residual frequency fluctuations of the master laser. τ is integration time of measurement. Curves A and B represent the values under free-running and feedback conditions, respectively.

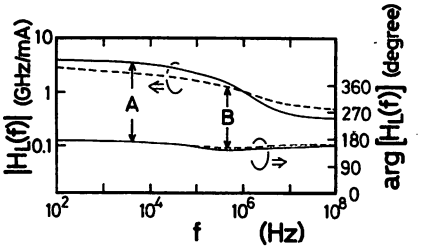

Fig. 5. Transfer function $H_L(f)$ of FM response characteristics of the master laser. DC injection currents I normalized to its threshold value I_{th} are 1.84 and 1.28 for curves A and B, respectively.

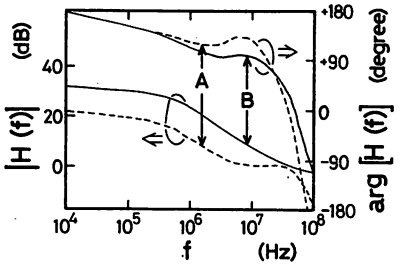

Fig. 6. Open loop transfer function $H(f)$ of the feedback loop for linewidth reduction. Curve A shows the result when a phase compensating circuit was not used. Curve B shows the result by using an optimized phase compensating circuit.

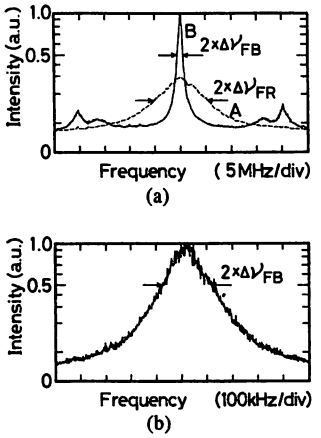

Fig. 7. Spectral profiles of the master laser observed by a delayed self-homodyne technique. (a) Curve A represents a result under free-running condition. The linewidth $\Delta\nu_{FR}$ was 5 MHz. Curve B represents a result under feedback condition. (b) Magnified profile of the curve B in (a). The linewidth $\Delta\nu_{FB}$ was 100 kHz.

profiles obtained by a delayed self-homodyne technique, the linewidth of these profiles correspond to the twice those (FWHM) of the field spectral profiles of laser oscillations. DC injection current I of the master laser normalized to its threshold value I_{th} was 2.0. Curves A and B in Fig. 7(a) show the spectral profiles under free-running condition and under feedback condition, respectively. The value of the linewidth (FWHM) $\Delta\nu_{FR}$ of the free-running laser given by curve A was 5 MHz. The curve in Fig. 7(b) shows the magnified profile of curve B in Fig. 7(a). The value of the linewidth (FWHM) $\Delta\nu_{FB}$ measured from Fig. 7(b) was 100 kHz, which was 1/50 times that of $\Delta\nu_{FR}$. Fig. 8 shows a relation between $(I/I_{th} - 1)^{-1}$ and the linewidth of the field spectrum of the master laser. Curves A and B show the linewidths under free-running $\Delta\nu_{FR}$ and feedback $\Delta\nu_{FB}$ conditions, respectively. Comparison between these two curves shows that the larger linewidth reduction $(\Delta\nu_{FR}/\Delta\nu_{FB})$ was obtained at a higher dc bias level. The reasons were as follows. 1) The gain of the feedback loop was increased by the increase of the detecting power at Si-APD in the block (b) of Fig. 2. 2) With increasing the dc bias level, the linewidth under free-running condition becomes narrower, which made the required bandwidth of the feedback loop narrower and made the design of the higher gain feedback loop easier.

The theoretical limit of bandwidth reduction by negative electrical feedback is discussed in the following. The frequency fluctuation $\delta\nu(t)$ under feedback condition can be expressed by the following quantum mechanical Langevin equation of motion [10].

$$\delta\nu(t) = \kappa\{\Gamma_s(t) + \Gamma_c(t)\} - \int_0^\infty h(\tau) \cdot \{\delta\nu(t-\tau) + \Gamma_n(t-\tau)\}\, d\tau \tag{2}$$

where κ represents a loss of a laser cavity. Γ_s and Γ_c represent the quantum noise sources due to spontaneous emission and carrier density fluctuations, respectively. A relation between the magnitudes of these noise sources is expressed as $\Gamma_c = \alpha^2 \cdot \Gamma_s$, where α is the linewidth enhancement factor [14]. The impulse response of the feedback loop is given by $h(\tau)$. $\delta\nu(t-\tau)$ is the FM noise detected by the frequency discriminator of the feedback loop, and Γ_n is the magnitude of noise originated from electrical circuits in the feedback loop. The Fourier transform of (2) gives

$$F(f) = \frac{1}{1 + H(f)} \cdot \kappa(1+\alpha^2) \cdot \Pi_s(f) - \frac{H(f)}{1 + H(f)} \cdot \Pi_n(f) \tag{3}$$

where F, Π_s, H, and Π_n represent the Fourier transforms of $\delta\nu$, Γ_s, h, and Γ_n, respectively. $H(f)$ corresponds to the open loop transfer function shown in Fig. 6. By increasing the gain of the feedback loop ($|H| \to \infty$), the value of the first term of the right-hand side of (3) approaches zero, while that of the second term approaches $|\Pi_n|$. This means that the contributions from the two quantum FM noise sources can be suppressed by negative feedback, and that the FM noise can be reduced to a value limited by the noise originated from the feedback loop. In other words, if a high-gain and low-noise feedback loop is employed, the magnitude of the FM noise can be reduced to a value which is lower than that determined by spontaneous emission fluctuations of the free-running laser. Based on the facts that curve A of Fig. 8 corresponds to the magnitude of $\kappa(1+\alpha^2)\Pi_s$ of (3) [i.e., $\kappa(\Gamma_s + \Gamma_c)$ in (2)] and that the value of the linewidth enhancement factor α of CSP-type semiconductor lasers has been estimated as $1.3 \leqq \alpha \leqq 5.4$ [14], the contribution of the spontaneous emission $\kappa \cdot \Pi_s$, i.e., the Schawlow–Townes' limit of the linewidth can be estimated as is given by the meshed area of Fig. 8. It was found from this figure that the value of curve B at $(I/I_{th} - 1)^{-1} = 1$, i.e., 100 kHz, was smaller than the value represented by the meshed area. From this fact, it was confirmed that the frequency fluctuations of the master laser were reduced to a value lower than those determined by spontaneous emission fluctuations. This fact agreed with the theoretical discussion given above.

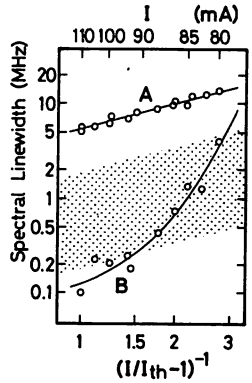

Fig. 8. Relation between $(I/I_{th} - 1)^{-1}$ and the linewidth of the master laser. Curves A and B represent values under free-running and feedback conditions, respectively. The meshed area represents the estimated value of the linewidth determined by the magnitude of the spontaneous emission [14].

The power spectral density of the frequency fluctuation of the master laser was measured to estimate a relation between the Fourier frequency f and the FM noise reduction ratio. Fig. 9 shows a ratio between the power spectral density of the FM noise $S_{\nu FB}(f)$ under feedback condition and $S_{\nu FR}(f)$ of the free-running laser. Curve A in Fig. 9 represents the experimental result. Curve B in Fig. 9, which represents a calculated result obtained by using the measured frequency transfer function of the feedback loop $H(f)$, agrees well with curve A. It can be seen from this figure that a reduction ratio as high as -27 dB was obtained at $f = 100$ kHz.

Curve A has a resonant peak near the cut-off frequency of the feedback loop ($f_c = 24$ MHz). The FM sideband of curve B in Fig. 7(a) is caused by this reasonant peak.

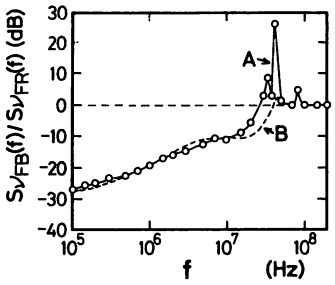

Fig. 9. Power spectral densities $S_{\nu FB}(f)$ of the FM noise of the master laser under feedback conditions, which was normalized to that of the free-running laser $S_{\nu FR}(f)$. Curve A represents experimental result, and curve B represents calculated result by using the measured transfer function $H(f)$.

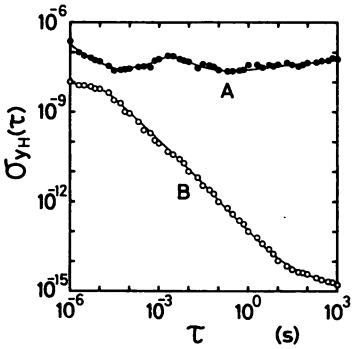

Fig. 10. Square root of the Allan variance $\sigma^2_{yH}(\tau)$ of the residual frequency fluctuations of the heterodyne signal. Curves A and B represent the values under free-running and feedback conditions, respectively.

This resonant peak was due to the slight excess gain of the feedback loop which enhanced the positive feedback around f_c. Therefore, if this laser is used for the optical measurement system whose bandwidth is wider than 24 MHz, this resonant peak could deteriorate the performance of the system. However, since most of the systems given by [1] and [2] have a bandwidth narrower than 24 MHz, this laser can be effectively used for these systems. On the other hand, since the frequency fluctuations were not reduced at $f > 24$ MHz, it could be rather difficult to use this laser directly in medium-to-high bit rate coherent optical communication systems. However, one may find several possibilities for using it for low bit rate systems, i.e., with a bit rate lower than 24 MB/s.

B. Frequency Control of the Heterodyne Signal and the Slave Laser

The linewidth of the heterodyne signal between the master and the slave lasers was about 25 MHz when the linewidth of the master laser was not reduced. However, this linewidth was reduced to about 15 MHz by reducing the linewidth of the master laser to as narrow as 500 kHz. If the bandwidth of the heterodyne-type frequency locked loop was sufficiently wide and its gain was high enough, the linewidth of the heterodyne signal could be reduced to zero. However, since the bandwidth of the present loop was about 3 MHz, the linewidth was still as wide as 15 MHz. However, as the spectral peak height of the heterodyne signal was increased by reducing the linewidth of the master laser, the detection sensitivity of the heterodyne signal was also increased. By this increase, the residual frequency fluctuations of the heterodyne signal were reduced to 1/10 times that obtained by using the free-running master laser.

Fig. 10 shows the square root of the Allan variance $\sigma^2_{yH}(\tau)$ of the heterodyne frequency fluctuations, which was normalized to the optical frequency. Curves A and B represent the values under free-running and feedback conditions, respectively. In this experiment, the heterodyne frequency ν_H and the division rate M of the prescaler were set to 30 MHz and 3, respectively.

The value of σ_{yH} was 1.0×10^{-14} at $\tau = 100$ s, which corresponded to fluctuations of 4.3 Hz. This was 1/6 times that of the previous experiment [7]. The minimum of σ_{yH} was 1.7×10^{-15} at $\tau = 1000$ s, i.e., the residual frequency fluctuation was as low as 0.6 Hz. Such low fluctuations at a longer integration time could be obtained since the long-term frequency drift was reduced by comparing and controlling the phase difference between the heterodyne signal and the reference signal. Furthermore, the value of σ_{yH} under feedback conditions was 1/10 times that of the free-running laser at an integration time τ as short as 1 μs. This improvement of the short-term stability was the result of widening the bandwidth of the feedback loop to as wide as 3 MHz. By comparing curve B of Fig. 10 and curve B of Fig. 4, it can be clearly seen that $\sigma^2_{yH}(\tau) \ll \sigma^2_{yM}(\tau)$, which means that the residual frequency fluctuations of the slave laser were almost equal to those of the master laser, i.e., the slave laser frequency tracked accurately to that of the master laser.

The heterodyne frequency ν_H can be easily swept by sweeping the frequency of the reference microwave synthesizer. Fig. 11 shows the range of a continuous sweep of the heterodyne frequency ν_H. The heterodyne frequency ν_H was varied by a stepwise sweep of the frequency of microwave synthesizer #1 or #3 with 1 MHz interval at every 10 s. This figure shows that the locking range of this loop, i.e., the frequency range in which this frequency tracking condition can be maintained, was 2.01 GHz, i.e., a stable sweep was carried out for 0.02 GHz $\leqq \nu_H \leqq$ 2.03 GHz, while the previous result was 0.08 GHz $\leqq \nu_H \leqq$ 1.3 GHz [7]. The reason for this improvement was that the range of the heterodyne frequency for 0.5 GHz $\leqq \nu_H \leqq$ 2.03 GHz was converted to the lower frequency by using a wide-band DBM. The upper limit of the locking range was limited by the response speed of the Si-APD used for the heterodyne signal detection. This upper limit can be increased by using a faster Si-APD and an amplifier of a wider bandwidth. Fig. 12 shows a relation between the square root of the Allan variance σ^2_{yH} and the heterodyne frequency ν_H. It can be confirmed from this figure that the frequency stability of the heterodyne signal could be maintained high enough irrespective of the heterodyne frequency ν_H. Fig. 13 shows an experimental result of the frequency tracking error, i.e., a difference between the reference frequency and the locked heterodyne frequency ν_H. The standard deviation of these

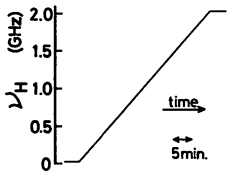

Fig. 11. Range of continuous sweep of the heterodyne frequency ν_H. The heterodyne frequency ν_H was varied by a stepwise sweep of the frequency of microwave synthesizer #1 or #3 with 1 MHz interval at every 10 s.

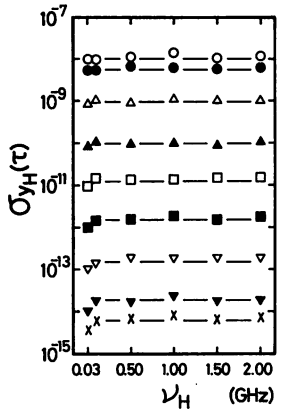

Fig. 12. The relation between the heterodyne frequency ν_H and the square root of the Allan variance $\sigma^2_{y_H}(\tau)$. The integration times τ of the fluctuation measurements were 1 μs (○), 10 μs (●), 100 μs (△), 1 ms (▲), 10 ms (□), 100 ms (■), 1 s (▽), 10 s (▼), and 100 s (×). The division rate M of the prescaler was 3 at ν_H = 0.03 GHz and was 10 at the other values of ν_H.

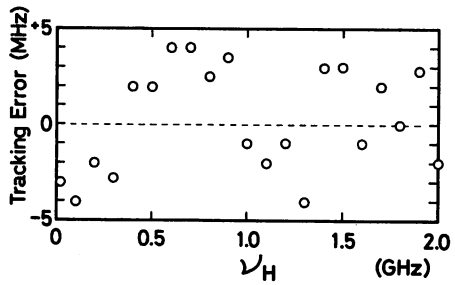

Fig. 13. Experimental results of the tracking error. Tracking error was defined by a difference between the frequency of the microwave synthesizer and the locked heterodyne frequency ν_H.

data was 2.7 MHz. It can be confirmed from the results of Figs. 11, 12, and 13 that the present system realized a high frequency stability, and accurate and wide-band frequency sweep of the heterodyne signal.

Fig. 14 shows a relation between the division rate M of the prescaler and the capture range of the heterodyne-type frequency locked loop. Here, the capture range was defined as the frequency difference between the initial heterodyne frequency and the reference signal (i.e., equivalents to the product of M and the frequency of the microwave synthesizer); within these, two signals can be locked when the loop is closed. The capture range was increased by increasing the division rate M, and the maximum of the capture range was 1.8 GHz at M = 2000. The capture range was saturated at $M > 2000$, which was

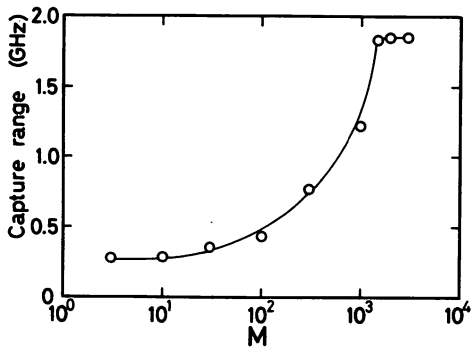

Fig. 14. The relation between the division rate M of the prescaler and the capture range of the frequency tracking loop.

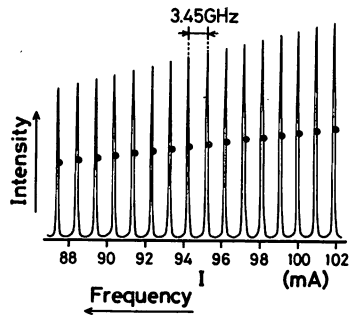

Fig. 15. Transmission spectral lineshapes of the Fabry–Perot interferometer which were used as the frequency reference for the master laser. The black circles are the points to which the master laser frequency was locked.

due to the limited bandwidth of the Si-APD for the heterodyne signal detection. At $M < 3$, the feedback loop did not work because the heterodyne frequency divided by the prescaler exceeded the maximum operation frequency of the digital phase comparator. Thus, the prescaler was used within in the range of $3 \leqq M \leqq 2000$. It was confirmed by the experiments that the residual frequency fluctuations of the heterodyne signal was increased with increasing M, while the capture range was increased by increasing M. When curve B of Fig. 10 was obtained, this increase of the frequency fluctuations of the heterodyne signal was prevented by using a programmable divider which was connected at the next stage of the prescaler. That is, after the heterodyne frequency was captured by using a large value of M, the value of M was decreased by the programmable divider, and finally, the value of M was decreased to 3 to obtain curve B of Fig. 10.

There can be several ways for further increases of the range of the frequency sweep of the slave laser. One of them can be a discrete tuning of the master laser frequency by locking it to successive frequencies of a frequency reference grid which are nearly-equally spaced. By tracking the frequency of the slave laser to each locked frequency of the master laser, a wide-band sweep of the slave laser can be realized. As shown by black circles in Fig. 15, the master laser frequency was locked to 16 successive resonance frequencies of the Fabry–Perot interferometer. By this method, the total range of continuous

frequency sweep of the slave laser was extended to 64.3 GHz. (The value of the previous experimental results was 37 GHz [7].) This range was limited by the mode-hopping phenomenon of the master laser. If the improved single-longitudinal-mode laser [15] will be used, it can be expected that the range would be increased to as wide as 1 THz.

IV. Summary

A synthesized method by negative electrical feedback was proposed to improve the coherence in semiconductor lasers. Based on this method, experiments were carried out for stabilization of center frequency of the field spectrum, linewidth reduction of the field spectrum, frequency tracking to another highly coherent laser, and stable and wide-band frequency sweep. The results are summarized as follows.

1) Stabilization of center frequency of the field spectrum: the minimum of the square root of the Allan variance σ_{yM}^2 of residual frequency fluctuations was $\sigma_{yM}(\tau) = 1.4 \times 10^{-10}$ at $\tau = 3$ s, which corresponded to frequency fluctuations of 50 kHz. By the improvement of the Allan variance real-time processing system (ARPS), frequency stability could be measured for 1 μs $\leqq \tau \leqq$ 1000 s with a shorter time for measurement.

2) Linewidth reduction of the field spectrum: the linewidth of the master laser (FWHM) was reduced to 100 kHz, which was 1/50 times that of the free-running laser. It was confirmed that this linewidth was narrower than that determined by spontaneous emission fluctuations.

3) Frequency tracking: the square root of the Allan variance σ_{yH}^2 of residual frequency fluctuations of the heterodyne signal between the master and the slave lasers was 1.7×10^{-15} at $\tau = 1000$ s. This corresponds to the residual frequency fluctuations of 0.6 Hz. It was also confirmed that the slave laser frequency tracked accurately to that of the master laser.

4) Wide-band frequency sweep: locking range of the heterodyne frequency was 2.01 GHz, i.e., the heterodyne frequency was swept for 0.02 GHz $\leqq \nu_H \leqq$ 2.03 GHz. The range of the continuous frequency sweep of the slave laser was extended to 64.3 GHz by making a discrete tuning of the master laser by successive locking to one of the frequency reference grids. The standard deviation of the tracking error was 2.7 MHz. The maximum of the capture range was 1.8 GHz at $M = 2000$.

Acknowledgment

The authors thank T. Kato of the Tokyo Institute of Technology for his experimental support.

References

[1] M. Ohtsu and S. Araki, "Using a 1.5 μm DFB InGaAsP laser in a passive ring cavity-type fiber gyroscope," *Appl. Opt.*, vol. 26, pp. 464-470, 1987.

[2] M. Hashimoto and M. Ohtsu, "Experiments on a semiconductor laser pumped rubidium atomic clock," *IEEE J. Quantum Electron.*, vol. QE-23, pp. 446-451, 1987.

[3] T. Okoshi, "Recent progress in heterodyne/coherent optical-fiber communications," *J. Lightwave Technol.*, vol. LT-2, pp. 341-346, 1984.

[4] P. Kartaschoff, *Frequency and Time.* London, England: Academic, 1978.

[5] A. Brillet and P. Cerez, "Laser frequency stabilization by saturated absorption," *J. de Physique*, vol. 42, pp. 73-82, 1981.

[6] M. Ohtsu, "Realization of ultrahigh coherence in semiconductor lasers by negative electrical feedback," *J. Lightwave Technol.*, vol. 6, pp. 245-256, 1988.

[7] K. Kuboki and M. Ohtsu, "Frequency offset locking of AlGaAs semiconductor lasers," *IEEE J. Quantum Electron.*, vol. QE-23, pp. 388-394, 1987.

[8] D. W. Allan, "Statistics of atomic frequency standards," *Proc. IEEE*, vol. 54, pp. 221-230, 1966.

[9] I. Siio, M. Ohtsu, and T. Tako, "Development of the Allan variance real-time processor," *Trans. IECE Japan*, vol. J64-C, pp. 204-208, 1981 (in Japanese).

[10] M. Ohtsu and N. Tabuchi, "Electrical feedback and its network analysis for linewidth resolution of a semiconductor laser," *J. Lightwave Technol.*, vol. 6, pp. 357-369, 1988.

[11] T. Okoshi, K. Kikuchi, and A. Nakayama, "Novel method for high resolution measurement of laser output spectrum," *Electron. Lett.*, vol. 16, pp. 630-631, 1980.

[12] M. Hashimoto and M. Ohtsu, "Laser spectroscopy and frequency stabilization of a semiconductor laser for a ^{87}Rb atomic clock," *Trans. IEE Japan*, vol. 108-C, pp. 706-712, 1988 (in Japanese).

[13] M. Ohtsu, H. Kotani, and H. Tagawa, "Spectral measurements of NH_3 and H_2O for pollutant gas monitoring by 1.5 μm InGaAsP/InP lasers," *Japan. J. Appl. Phys.*, vol. 22, pp. 1553-1557, 1983.

[14] M. Osiński and J. Buus, "Linewidth broadening factor in semiconductor lasers—An overview," *IEEE J. Quantum Electron.*, vol. QE-23, pp. 9-29, 1987.

[15] Y. Tohmori, K. Komori, S. Arai, and Y. Suematsu, "Low-threshold-current CW operation of 1.5 μm GaInAsP/InP bundle-integrated-guide distributed-Bragg-reflector (BIG-DBR) lasers," *Electron. Lett.*, vol. 21, pp. 743-745, 1985.

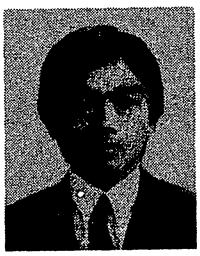

Katsuhiko Kuboki was born in Chiba, Japan, on November 28, 1960. He received the B.S. degree in computer engineering from the Tokyo Institute of Technology, Tokyo, Japan, in 1984.

Currently, he is a doctoral student of the Graduate School of the Tokyo Institute of Technology. He is interested in the frequency control of semiconductor lasers for coherent optical communications.

Mr. Kuboki is a member of the Institute of Electronics, Information and Communication Engineers of Japan and the Japan Society of Applied Physics.

Motoichi Ohtsu (M'88), for a photograph and biography, see p. 38 of the January 1989 issue of this JOURNAL.

JAPANESE JOURNAL OF APPLIED PHYSICS
VOL. 28, NO. 10, OCTOBER, 1989, pp. L 1839–L 1841

Frequency Stabilization of Laser Diodes to the Cs-D_2 Line with the Zeeman Modulation Method

Takeshi IKEGAMI, Shin-ichi OHSHIMA and Motoichi OHTSU†

National Research Laboratory of Metrology,
1-1-4, Umezono, Tsukuba-shi, Ibaraki-ken 305
†Graduate School at Nagatsuta, Tokyo Institute of Technology,
4259 Nagatsuta, Midori-ku, Yokohama-shi, Kanagawa-ken 227

(Received May 29, 1989; accepted for publication September 12, 1989)

The frequencies of AlGaAs laser diodes were stabilized to the $F=4\rightarrow F'=5$ component of the Cs-D_2 line with the Zeeman modulation method, in which the laser frequency remains unmodulated. Allan variance measurements were made on the beat note between two laser diodes thus stabilized and a frequency stability of 2.4×10^{-10} was obtained at an averaging time of 1s. By changing the dc magnetic field applied to the Cs cell, the frequency of the laser diodes could be tuned almost linearly in the range of -180 MHz to 180 MHz.

KEYWORDS: Cs-D_2 line, Zeeman spectra, unmodulated frequency stabilization of a laser diode, Zeeman modulation, frequency sweep of a laser diode

§1. Introduction

Unmodulated frequency stabilization of a laser diode (LD) is necessary in many kinds of optical experiments. In experiments of laser cooling of atoms, for example, the frequency of a laser must be stabilized without frequency modulation and, at the same time, must be tuned over the range of more than a couple of hundred megahertz. Several methods may be used for this purpose including a method using an acousto-optic modulator (AOM),[1] and an offset locking method.[2] However, these methods are somewhat complicated because some additional components are necessary: in the former method, an AOM and an rf driver and in the latter, another laser called a master laser.

Compared with these methods, the Zeeman modulation method is very simple in setup. In addition, this method has the advantage that the frequency of the atomic spectral line to which the laser is locked can be tuned only by changing the magnetic field strength. This simple method has already been applied to laser diodes.[3-6] However, the frequency stability was not yet precisely evaluated in the previous report.

In the present study, we examined the frequency stability and the tunability of laser diodes which were stabilized to the $F=4\rightarrow F'=5$ component of the Cs-D_2 line by the Zeeman modulation method. Allan variance measurements were made on the beat note between two such stabilized lasers. Stabilities comparable with those obtained by the electrical feedback methods ($\sim10^{-10}$)[7] and a tunability as wide as the Doppler width of the thermal Cs (~300 MHz) were obtained.

§2. Energy Levels of Cs

The magnetic field dependence of the energy levels relevant to the Cs-D_2 line is obtained by diagonalizing the hyperfine Hamiltonian[8,9]

$$\mathcal{H}=hAI\cdot J+hB\frac{[6(I\cdot J)^2+3(I\cdot J)-2I^2J^2]}{2I(2I-1)2J(2J-1)}+g_I\mu_B(I\cdot B)+g_J\mu_B(J\cdot B). \quad (1)$$

The symbols are the same as those in ref. 8 except that the magnetic field strength H is replaced by the magnetic flux density B. The energy levels calculated from this Hamiltonian are shown in Fig. 1. In the figure, F and F' denote the quantum numbers of the total angular momenta in the ground state and the excited state, respectively. The transition α (or β when the magnetic field is reversed) in Fig. 1 is suitable for the present experiment, because its frequency changes linearly with the magnetic field.

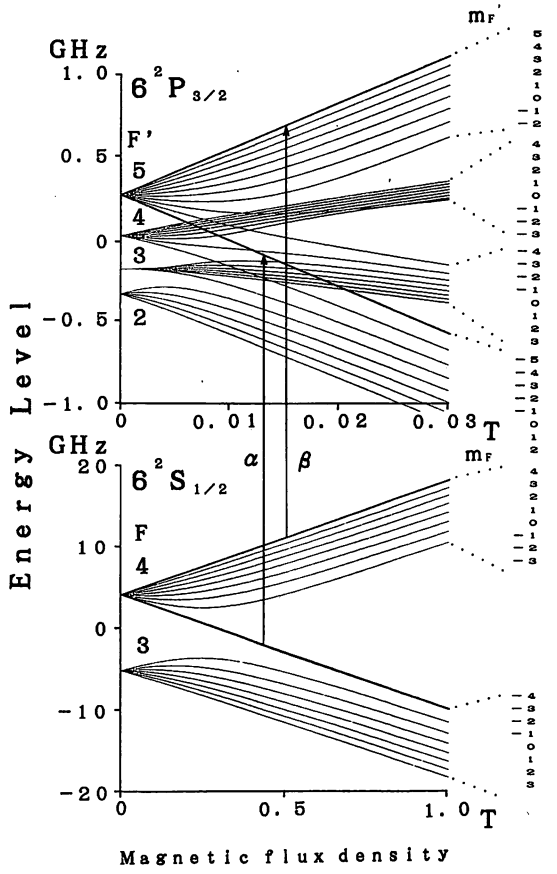

Fig. 1. Energy level diagram of ^{133}Cs in the $^2S_{1/2}$ ground state and the $^2P_{3/2}$ excited state as a function of the applied magnetic field.

If we irradiate the atom with right circularly polarized light, either σ^- or σ^+ transition occurs according to whether the applied magnetic field is parallel or antiparallel to the wave vector of the light beam. Furthermore, when the Zeeman splitting is smaller than the spectral linewidth of the LD, the saturated absorption line intensity of the $F=4\rightarrow F'=5$ transition is expected to be insensitive to the magnetic field strength because most of the atoms in the $F=4$ state are optically pumped to the $m_F=-4$ or $m_F=+4$ Zeeman sublevel, and the contribution to the saturated absorption line comes mainly from the $F=4$, $m_F=-4\rightarrow F'=5$, $m_{F'}=-5$ or the $F=4$, $m_F=+4\rightarrow F'=5$, $m_{F'}=+5$ component. On the other hand, intensities of the $F=4\rightarrow F'=3$ and the $F=4\rightarrow F'=4$ components are expected to be weakened because of Zeeman splitting.

§3. Experimental Apparatus

The experimental setup is shown in Fig. 2. The light beam from a LD is linearly polarized. Passing through a $\lambda/4$ plate, this light is changed to circular polarization to cause only the σ^- or σ^+ transition and introduced into a Cs cell installed at the center of a solenoid coil. The laser power at the entrance of the solenoid coil is typically 1.8 mW. A small fraction (below 1 percent) of this light is reflected by a mirror (M). A polarization beam splitter (PBS) is used to avoid the optical feedback to the LD and the reflected beam is monitored by a PIN photodiode to observe saturated absorption. Fine frequency tuning of the LD is performed by controlling the injection current.

The solenoid coil, 9 cm in length and 4 cm in diameter, consists of 72×7 turns of 1 mm copper wire, and the magnetic field of 53.5×10^{-4} T/A can be generated. In Zeeman modulation, the ac current is superimposed on the dc current of the solenoid coil and a lock-in amplifier is used to obtain the first derivative signal. The output signal from the lock-in amplifier is fedback to the current source of the laser diode through the PI controller to stabilize the laser frequency.

§4. Results

Figure 3(a) shows the saturated absorption spectra observed at various values of the dc current of the solenoid coil. The current was changed from -2.08 A to 2.08 A corresponding to the magnetic field from -110×10^{-4} T to 110×10^{-4} T. The positive sign in the current means that the magnetic field direction in the solenoid coil is parallel to the wave vector of the saturating light beam. We can see that the center frequency of the $F=4\rightarrow F'=5$ saturated absorption peak, denoted by c in Fig. 3, shifts almost linearly with the strength of the applied magnetic field as we expected. To show the magnetic field dependence in detail, we plotted this shift in Fig. 4. The solid line shows the theoretical shift of the frequency of the $F=4$, $m_F=-4\rightarrow F'=5$, $m_F'=-5$ transition under the positive field and the $F=4$, $m_F=+4\rightarrow F'=5$, $m_{F'}=+5$ transition in the negative field calculated by eq. (1). The frequency shift under the negative magnetic field agrees very well with the calculated value of the transition frequency because the line is close to the center of the Doppler broadened spectrum (see Fig. 3). Under the positive magnetic field, on the other hand, the frequency shift deviates slightly from the calculated value because

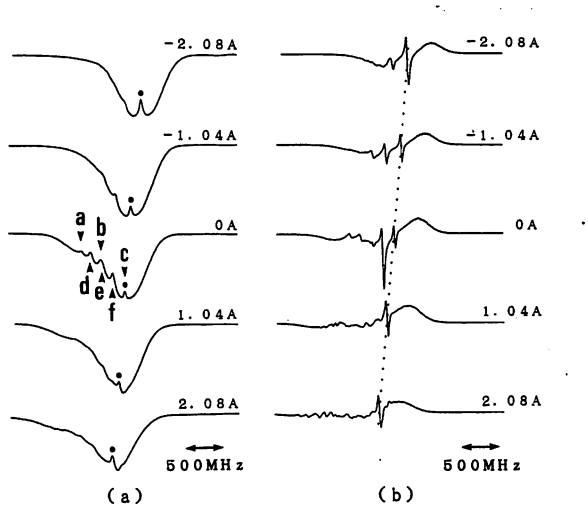

Fig. 3. (a) Magnetic field dependence of the saturated absorption spectrum of the Cs-D_2 line. Symbols a, b and c denote the principal resonances, $F=4\rightarrow F'=3$, $F=4\rightarrow F'=4$ and $F=4\rightarrow F'=5$, respectively. Symbols d, e and f denote the crossover resonances. (b) Magnetic field dependence of the Zeeman modulated spectra. The center of the c-component is connected by a dotted line.

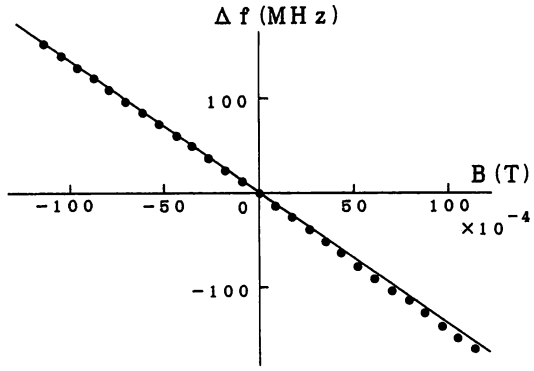

Fig. 4. Observed frequency shift of the $F=4\rightarrow F'=5$ saturated absorption peak as a function of the applied magnetic field. Solid line shows the theoretical shift of the center frequency of the $F=4$, $m_F=-4\rightarrow F'=-4\rightarrow F'=5$, $m_{F'}=-5$ or $F=4$, $m_F=+4\rightarrow F'=4$, $m_{F'}=+5$ transition according to whether magnetic field B is positive or negative.

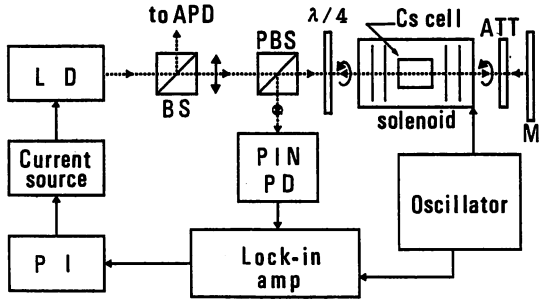

Fig. 2. Experimental setup. LD: laser diode, APD: avalanche photodiode, BS: beam splitter, PBS: polarization beam splitter, $\lambda/4$: $\lambda/4$ wave plate, ATT: attenuator, M: mirror, PIN PD: pin photodiode, PI: proportional amplifier and integrator.

the line is on the side slope of the Doppler profile and also because it is not isolated from the adjacent Zeeman components.

To obtain the first derivative signal, the modulation current at a frequency of 2 kHz with a peak-to-peak amplitude of 50 mA is superimposed on the dc current of the solenoid coil, which corresponds to the magnetic field amplitude of 2.5×10^{-4} T. The output of the lock-in amplifier is shown in Fig. 3(b). The time constant of the low-pass filter of the lock-in amplifier was 3 ms.

Finally, we made two sets of apparatus as shown in Fig. 2 to stabilize two laser diodes to the $F=4\rightarrow F'=5$ line independently and measured the frequency stability of the beat note between the two lasers. The dc currents to each solenoid coil were 0.64 A and -0.64 A, respectively. The beat frequency was divided by 64 by a prescaler, and the square root of the Allan variance, $\sigma_y(\tau)$, was measured as a function of the averaging time, τ, by a computing counter. As shown in Fig. 5, $\sigma_y(\tau)$ is proportional to $\tau^{-1/2}$ for $\tau\leqq1$s, and therefore the frequency fluctuation is almost attributable to the white noise in this range. The minimum of $\sigma_y(\tau)$ is 2.4×10^{-10} at $\tau=1$s and the $\sigma_y(\tau)$ is less than 1×10^{-8} almost throughout the entire range of τ.

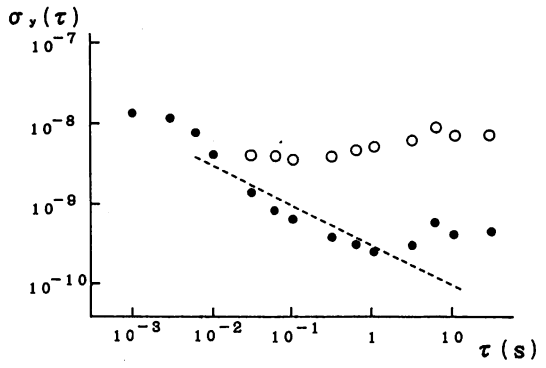

Fig. 5. Frequency stability of a Zeeman stabilized laser diode measured by the heterodyne method. ○: free running. ●: stabilized. The broken line represents the slope of the $\tau^{-1/2}$ dependence.

§5. Summary

The experimental results can be summarized as follows.

(1) The frequency of the $F=4\rightarrow F'=5$ saturated absorption peak changes almost linearly with the magnetic field even when the Doppler broadened profile exists and this agrees well with the calculation.

(2) The frequency of the stabilized laser diode can be swept in the range of -180 MHz to 180 MHz by changing the magnetic field.

(3) A frequency stability of 2.4×10^{-10} is obtained at $\tau=1$s.

Acknowledgement

We thank Dr. Y. Koga and Mr. Y. Nakadan for valuable advice and discussion and for careful reading of the manuscript.

References

1) K. Akiyama, S. Yoshitake, A. Ohte, Y. Koga, Y. Nakadan and S. Ohshima: T. IEE Jpn. **109C** (1989) 22 [in Japanese].
2) K. Kuboki and M. Ohtsu: IEEE J. Quantum Electron. **QE-23** (1987) 388.
3) T. Yabuzaki, T. Kawamura and T. Ogawa: *Proc. 10th Int. Conf. Atomic Physics* (Tokyo, 1986) p. 184.
4) R. A. Valenzuera, L. J. Cimini, R. W. Wilson, K. C. Reichmann and A. Grot: Electron. Lett. **24** (1988) 725.
5) J. Deng, Y. Tan, Y. Xiang and X. Zhu: *Proc. Second European Frequency and Time Forum* (Newchatel, 1988) p. 555.
6) A. Weis and S. Derler: Appl. Optics **27** (1988) 2662.
7) G. P. Barwood, P. G. Gill and W. R. C. Rowley: J. Phys. E. **21** (1988) 966.
8) E. Arimondo, M. Inguscio and P. Violino: Rev. Mod. Phys. **49** (1977) 31.
9) I. Hirano: Metrologia **21** (1985) 27.

総合報告

8.8, 8.9

半導体レーザーの周波数制御とその応用

大津元一・中川賢一

東京工業大学総合理工学研究科 〒227 横浜市緑区長津田 4259

(1989年6月30日 受理)

レーザーの周波数制御は光量子エレクトロニクス分野において最も基本的な研究課題であるが，半導体レーザーに対するそれは他種レーザーと非常に異なった様相を呈する．これは半導体レーザー共振器損失が大きいこと，キャリア密度変動が大きく，高速であること，などに起因する．本稿では半導体レーザーにおける周波数制御の原理，手法，結果，限界，およびその広範な分野への応用と将来について展望する．

Keywords: semiconductor laser, frequency, feedback control, cavity quantum electrodynamics, optical sensing, spectroscopy, quantum optics, laser cooling, parity violation

1. まえがき

連続発振半導体レーザーのいくつかの性能は他種レーザーのそれを凌ぐまでになっている．これを踏まえ広範な光応用システムの開発が進んでいるが，そのためには半導体レーザーの光周波数を制御する必要がある場合が多い．歴史的に見ても周波数制御可能な光源に対する要求がレーザーの発明の大きな引き金であった[1]．

周波数制御はレーザー発明後も世界の主要研究機関が継続して取り組んでいる基本的な研究課題であり[2]，レーザー物理，量子光学，光学，電子工学，などの総合的知識を必要とする科学技術である．本稿では半導体レーザーの周波数制御の方法の現状と将来，およびその応用に関して概説する．

2. あらかじめ注意すべき特性

半導体レーザーの利得スペクトルの幅は共振器縦モード周波数間隔に比べ約100倍大きいので，半導体レーザーは本質的に単一縦モード発振しない．すなわち，次の現象を示す：

（1）モードホッピング；結晶のへき開面を利用したファブリー・ペロー (FP) 共振器構造を持つ半導体レーザーは注入電流，周囲温度を適当に設定しないと通常は多縦モード発振する．このとき，各縦モードパワーのスイッチングが生ずる．

（2）モード分配；特定の縦モードパワーが他にくらべ大きい場合，すなわち擬単一縦モード発振状態，でも主縦モードパワーが過渡的に減少し(パワードロップアウト)，他の縦モードパワーが過渡的に増加する．

両現象とも各モードに混入する自然放出光揺らぎに駆動され，伝導帯内キャリア緩和に基づくモード間相互利得飽和によって生ずる量子現象である．各モードパワー揺らぎの統計的性質はポアッソン過程に従い，熱力学における相転移現象との類推が成立ち，統一的理論モデルも提示されている[3]．この類推から，これらのパワー揺らぎの発生頻度はバイアスレベルの増加とともに指数関数的に減少することが指摘されている．相互利得飽和の度合を強めても減少する．そのために，可飽和吸収体のドーピングが試みられている[4,5]．

光通信用の波長 1.3 μm, 1.5 μmInGaAsP レーザーでは縦モード制御するために回折格子を素子内に作り付け，共振器構造をDFB形またはDBR形にしている．最近では 0.8 μmAlGaAs レーザ

Frequency Control of Semiconductor Lasers and Its Applications. Motoichi OHTSU and Ken'ichi NAKAGAWA. Graduate School at Nagatsuta, Tokyo Institute of Technology. 4259, Nagatsuta, Midori-ku, Yokohama 227.

ーに対しても試みられている[6]．しかし，この場合でも，主縦モードパワーを他モードパワーの40 dB 以上にしないとモード分配現象が無視できず，高精度光応用システムへの使用の障害となる[7]．最近では電極を分割して，空間的ホールバーニングを抑圧し，主縦モードパワーを増加させる努力がなされている[8]．

以上の点を考慮して単一縦モード（正確には擬単一縦モード）発振が実現しても，半導体レーザーの出射光が外部反射面で反射され，レーザーに再注入すると決定論的不安定が生ずる[9,10]．これを避けるには分離比 60 dB 以上の光アイソレーターが必要である．次節以降の議論は以上の問題がすべて解決したことを前提として行う．

3. 単一縦モード半導体レーザーの光周波数の特性

光周波数揺らぎの統計的特性を表す基本的尺度はパワースペクトル密度またはアラン (Allan) 分散である．前者はフーリエ周波数領域，後者は時間領域での尺度である[11,12]．揺らぎが白色雑音であればレーザー発振スペクトル形状はローレンツ形となり，その半値幅を便宜的な尺度とすることもできる．

揺らぎ源のうちレーザー内部で発生するものを図1に示す．そのうち基本的なものは自然放出光揺らぎである．これはフリーランニング・レーザーの揺らぎの量子雑音限界（発振スペクトル半値幅の Schawlow-Townes 限界[13] に対応）を与える．自然放出は真空の0点揺らぎに駆動される誘導放出に対応し，広いフーリエ周波数領域にわたり白色とみなせる．この自然放出の発生確率は共振器モード数に比例し，自然放出に起因する光周波数揺らぎの大きさは共振器損失にも比例する．**4.** の手法により上記の自然放出光揺らぎのレベルが実現したとき，レーザーはコヒーレント状態にあるといわれる．

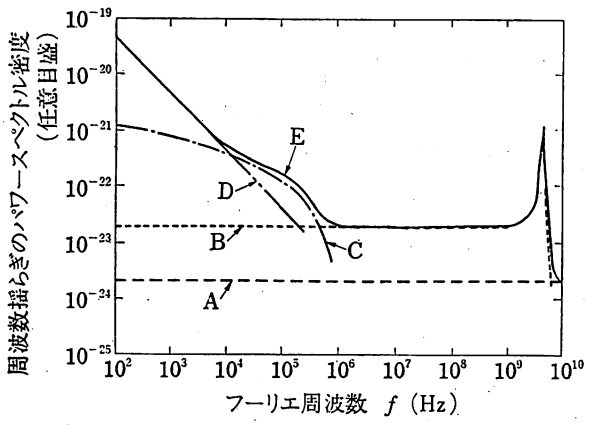

図 1　半導体レーザーの周波数揺らぎのパワースペクトル密度．A：自然放出光揺らぎ．B：キャリア密度揺らぎ．C：温度揺らぎ．D：$1/f$ 揺らぎ．E：全揺らぎ．

さらに，この自然放出に駆動されてキャリア密度が揺らぎ，これにより共振器屈折率が揺らいで第2の源となる．他種レーザーと異なり半導体レーザーのキャリア密度変動は高速なので，その効果は断熱近似による消去不可能であり，キャリア密度揺らぎは無視できない．この源による光周波数揺らぎはキャリアの帯間緩和時間および光子寿命による2次遅れ特性を持ち，キャリアの緩和振動周波数において遮断する低域通過特性を有する．半導体レーザーの複素利得スペクトルの実部，虚部の中心周波数は互いに離調しているためにキャリア密度揺らぎによりレーザーパワー揺らぎと同時に光周波数揺らぎが誘起される．上記の自然放出光揺らぎ，キャリア密度揺らぎが光周波数揺らぎに与える寄与の大きさの比を α^2 で表す．パラメーター α は線幅増大係数，α パラメーター，などと呼ばれおよそ2～9の値をとる[14]．

第3の源は上記のキャリア密度揺らぎに誘起された電流揺らぎ，すなわちそれに起因するレーザーの自己発熱量の揺らぎ（温度揺らぎ）である．これはレーザー素子の熱応答時定数によって決まる低域通過特性を有する．以上の3つの源がレーザー内部で発生する量子雑音を与える．

この他に，低フーリエ周波数領域では $1/f$ 揺らぎが現れる．これはレーザーパワーに依存しない発振スペクトル幅を与える[15]．この揺らぎの発生原因はまだ十分明かにされていないが，キャリア易動度の揺らぎ[16]，をはじめいくつかの解釈がある[17]．さらに，外来雑音源として，定電流源の電流揺らぎ，周囲温度の揺らぎ，などがあり，これら全てがフリーランニング時のレーザー周波数揺らぎを与える[18]．

これらの揺らぎを抑圧するためにはレーザーの直接周波数変調特性を利用する．この特性は **4.** の電気的負帰還制御法のみならず光帰還法の性能

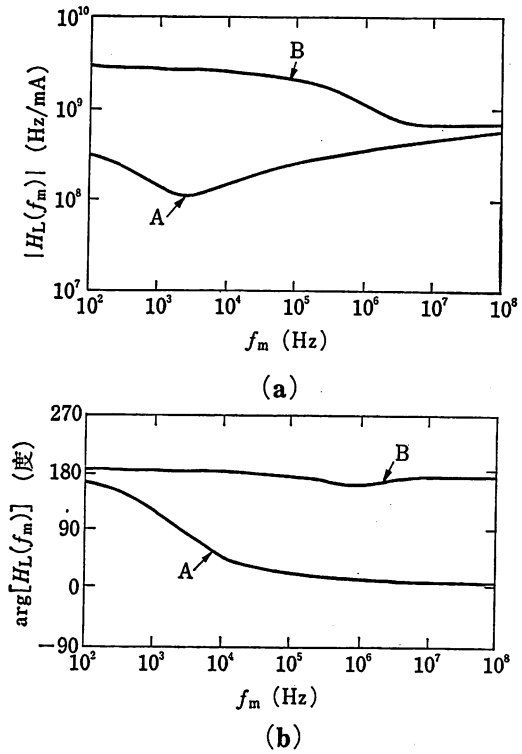

図 2　周波数直接変調特性を表す複素伝達関数の絶対値 (**a**) および (**b**) 位相部分[19]. $H_L(f_m)=d\nu(f_m)/di(f_m)$. ν はレーザー光周波数. i は変調のための注入電流. f_m は変調周波数. A：波長 1.5 μmInGaAsP レーザー. B：波長 0.8 μmAlGaAs レーザー (CSP 形).

にも影響を与える場合がある. **図 2** には波長 1.5 μmInGaAsP レーザー, 0.8 μmAlGaAs レーザー (CSP 形) の特性を示す[19]. 変調の素過程は温度変調効果（低フーリエ周波数領域）およびキャリア密度変調効果（高フーリエ周波数領域）であり，それぞれレーザー素子の熱応答時定数，キャリアの緩和振動によって決まるフーリエ周波数で遮断する. 図 2 の特性はこの 2 つの効果の合成によって決まるので，一般には広いフーリエ周波数領域にわたって均一な特性にはならない. この特性はキャリア密度，α パラメーターの共振器横方向空間特性に依存する[20]. 特に位相遅れ特性は周波数制御帯幅を制限する. 最近は電極を分割し，各注入電流値を調節して，キャリア密度分布を制御し，均一な周波数変調特性を得る試みがなされている[21].

上記の緩和振動周波数は数 GHz の値をとるので，変調帯幅は他種レーザーに比べてきわめて広い. すなわち，レーザーの周波数制御は半導体レーザーに対して，初めて可能になる手法といえる. このように光の状態を制御することが光量子エレクトロニクスの基本的な研究課題であるといえよう.

4. 周波数制御の原理と実際

3. の量子雑音源によって生ずるレーザー周波数揺らぎの大きさ $\delta\nu(t)$ は次のランジュバン方程式により定式化される[22,23].

$$\delta\nu(t)=\kappa\cdot(1+\alpha^2)\cdot\Gamma_s(t)-\int_0^\infty h(\tau)\cdot\{\delta\nu(t-\tau)+\Gamma_n(t-\tau)\}\cdot d\tau \quad (1)$$

ここで，κ は共振器損失，α は **3.** に記した α パラメーター，$\Gamma_s(t)$ は自然放出揺らぎの大きさ，である. 以上がフリーランニング時の量子雑音源を表す. **3.** で指摘した温度揺らぎ，$1/f$ 揺らぎ，をさらに加えてもよい. ここで **4.1** のように電気的負帰還制御を施す場合，その制御の効果が右辺の積分で表されている. すなわち，$h(\tau)$ は制御系のインパルス応答関数，$\delta\nu(t-\tau)$ は制御系で検出された周波数揺らぎ，$\Gamma_n(t-\tau)$ は制御系で発生する雑音である. この式をもとにすると周波数揺らぎを抑圧するために少なくとも次の 4 手法が考えられる：(1) 電気的負帰還制御法[23]，(2) 光帰還法[24]，(3) レーザー素子改良法，(4) Cavity QED (Cavity Quantum Electrodynamics) の利用. 以下にこれらの手法について比較概説する.

4.1 電気的負帰還制御法

(1) 式右辺の積分で表されるように，量子雑音に伴う揺らぎを検出し，それを補正するようにレーザーの動作パラメーターを変化させる（例えば図 2 の特性を利用し，注入電流を制御する）. この方法の特徴は次の通りである：(1) レーザー共振器構造の変更不要. (2) 制御系は高利得，狭〜中帯幅. (3) 特定のフーリエ周波数帯域内のみでの選択的制御可能. この場合，極めて高い制御利得が得られる（共振形重力波検出アンテナ用の超長基線レーザー干渉計などに有望）. (4) 高利得・低雑音の制御系使用によりフリーランニング時の自然放出揺らぎのレベル（コヒーレント状態）以下の揺らぎ（ハイパー・コヒーレント状態と称する[2]）が実現できる. すなわち，(1) 式をフーリエ変換し，まとめると

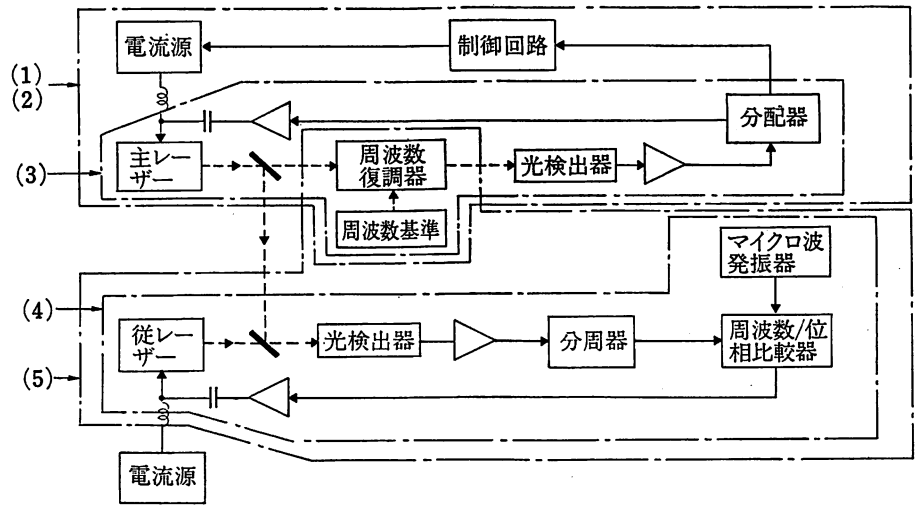

図 3　5つの課題を同時に実現するための電気的負帰還制御法による統合的システムのブロック図[23]．（1）発振スペクトル中心周波数の安定化．（2）発振スペクトル中心周波数の確度向上．（3）発振スペクトル線幅狭窄化．（4）周波数追随．（5）周波数掃引．

$$F(f)=\frac{\kappa\cdot(1+\alpha^2)}{1+H(f)}\cdot\Pi_s(f)-\frac{H(f)}{1+H(f)}\cdot\Pi_n(f) \qquad (2)$$

となる．ここで f はフーリエ周波数，F, Π_s, Π_n H はそれぞれ（1）式中の $\delta\nu$, Γ_s, Γ_n, h のフーリエ変換である．この式によると無限大の制御利得の極限状態（$|H|\to\infty$）では右辺第1項，すなわち量子雑音の寄与は0となる．第2項の大きさは $|\Pi_n|$，すなわち制御系の雑音の大きさに収束する．すなわち，揺らぎ抑圧限界は制御系内の光検出器で発生するショット雑音により決まる．換言するとこれが電気的負帰還制御時の量子雑音限界に相当する．（5）負帰還制御なので安定性が高い．（6）アナログ電子回路における負帰還制御技術の手法が使えるので，計算機を用いた回路シミュレーションが可能で，これにより制御系の最適設計ができる．そしてこの最適設計により再現性の高い実験結果が得られる．

光応用システム用光源の1つの理想的な形態として，周波数揺らぎの少ない光スイープジェネレーターが考えられる．そのためには少なくとも以下の **4.1.1～4.1.5** に示す5つの課題を同時に実現する必要がある．これを同時に実現するためには電気的負帰還制御法による統合的システムが有望である．

5つの課題を同時に実現するシステムのブロック図を**図3**に示す[23]．この装置は複雑に見えるが他種レーザーを使った場合の同様の装置に比べ非常に小型であり，使われている一連の電気的，光学的素子の一部分は半導体レーザーとともに集積化可能である．

4.1.1　発振スペクトル中心周波数の安定化

DC 制御を施し，約 1 Hz 以下の低フーリエ周波数領域の揺らぎ（**3.** で指摘した温度揺らぎおよび $1/f$ 揺らぎによる）を抑圧して発振スペクトル中心周波数のドリフトを抑える．特にドリフトの少ない，安定な周波数基準および周波数復調器が不可欠である．そのような周波数基準として，原子・分子気体の共鳴スペクトル線が使用可能である．

アンモニア[25]，水蒸気[26]，アセチレン[27]，シアン[28]，などの有機分子の振動回転遷移の高調波または結合調の吸収スペクトル線は多数分布しているので，これを使うことができる．欠点はスペクトル線幅が広いこと，吸収強度が弱いこと，スペクトル線の同定が難しいことである．この欠点を補うものとして，波長 0.8 μm 付近に電子遷移による強い吸収を有し，スペクトル線の同定が行われているルビジウム（Rb），セシウム（Cs）蒸気が使われている[29,30]．これらの蒸気は，幅の狭いドプラーフリーの飽和吸収スペクトルが得られること，装置が超小型になること，などの利点を有する．この他，単原子分子である希ガスの光ガルバノスペクトルの信号強度も大きい[31]．この場合，ガスのプラズマ不安定に伴う周波数のシフトなどのために高い安定度を得ることは難しいが，小型

の放電ランプを用いて波長 1.5 μmInGaAsP レーザー用の簡易な基準周波数が考案されている[32].

このレーザーは光通信用の重要な光源であるが，最近はこのレーザーの内部で発生する第二高調波と Rb の強い吸収スペクトルとを使う方法が試みられている[33]. この第二高調波パワー自身は小さいが，AlGaAs レーザーとのヘテロダインにより，吸収スペクトル測定感度が向上し，また，AlGaAs レーザー光を Rb の励起光源として使えばドプラーフリーの飽和吸収スペクトルが測定可能である[34]. したがって，第二高調波パワーが小さいことは本質的に問題ではない. さらに効率向上のために有機非線形光学材料を用いた第二高調波発生用導波路の使用が試みられている[34].

波長 0.67 μm の可視 AlGaInP レーザー用の安定な基準周波数としてリチウムなど多数の原子蒸気が考えられる. 以上のように最近の傾向として，分子の振動回転遷移の高調波または結合調スペクトルよりも原子の電子遷移スペクトルの方が，より高性能の基準周波数であると見なされている.

ファブリー・ペロー (FP) 干渉計は簡便な基準周波数として従来より使われてきたが，周波数の絶対値が不確実であることが欠点である. しかし，最近ではフィネス 10,000 以上の FP 干渉計が実現しており，フーリエ周波数 10^{-4} Hz 以上（積分時間 10^4 秒以下）の短期安定度に関しては原子・分子スペクトルを用いるよりもよい結果が得られることが確認されている[35].

これらの基準周波数を用い，注入電流を制御して 2×10^{-12}（積分時間 100 秒におけるアラン分散の平方根値）の周波数安定度が得られている[36]. 安定度測定は二台の独立に安定化されたレーザー間のビート周波数の揺らぎ測定から推定するのが最も正確である. 制御系の誤差信号による評価は誤差が大きい. 正確な評価をするためのアラン分散の実時間測定装置も開発されている[37,38]. 上記の安定度はフリーランニング時の自然放出揺らぎによる量子雑音レベル，すなわちコヒーレント状態，に達している. 制御系の改良によりショット雑音レベルが実現すれば 1×10^{-15} の安定度が期待できる[23].

4.1.2 発振スペクトル中心周波数の確度向上

(1)の方法で安定化された周波数を利用するとき，その絶対値を高精度評価すること，すなわち確度向上，が必要である. 確度を制限する要因として，レーザー素子の熱抵抗の経時変化による光波長のブルーシフト（約 26 MHz/h）がある[39]. また，基準周波数自身のわずかなドリフトが確度を制限する. Rb 原子蒸気の飽和吸収スペクトルは入射レーザー光パワー，Rb 蒸気圧により周波数シフトを示すが[40]，これらの値は水蒸気スペクトルの場合[41]の約 1/10 である. したがって，分子より原子の方が，より良好な基準といえる. 確度評価には光周波数絶対測定が必要であり，従来は MIM 点接触ダイオード，またはジョセフソン素子を用いたハーモニックミキサーが使われている. ただし，前者は低感度，後者は低速であるため[42]，1.5 μm よりも短波長の半導体レーザーに対しては利用の可能性が少ない. そこで，便宜的に光の波長測定により確度評価を行っている. 走査マイケルソン干渉計形の波長計により誤差 1×10^{-7}〜1×10^{-8} で確度評価が行われている[25,26].

最近は高温超伝導薄膜と金属薄膜との間のトンネル接合を利用して高感度高速光検出器を実現する試みが報告されている[43]. これがハーモニックミキサーとして使用できれば光周波数絶対測定が可能となり，確度 1×10^{-10} が期待される. これはチャネル数 1,000 以上の周波数超多重コヒーレント光通信システムに応用可能である.

4.1.3 発振スペクトル線幅狭窄化

周波数揺らぎが白色雑音であるとき，その大きさを表す便宜的な尺度として発振スペクトルの半値幅を使う場合がある. すなわち，これは広いフーリエ周波数域にわたる揺らぎの大きさを表す大まかな尺度として使われている. したがって，広帯幅の制御によりこの半値幅を狭窄化できる. そのために必要な制御帯幅 B はフリーランニング時のスペクトル半値幅の値 $\Delta\nu_{FR}$ 以上である ($B>\Delta\nu_{FR}$). 高利得・広帯幅の制御系を実現するためには光周波数揺らぎを検出するための周波数復調器の高感度化・広帯幅化が必須である. そのために **4.1.1** でも述べた高フィネス FP 干渉計，特にその反射モードの利用が提案されている[44,45]. 反射モードには光周波数を時間微分する機能が含ま

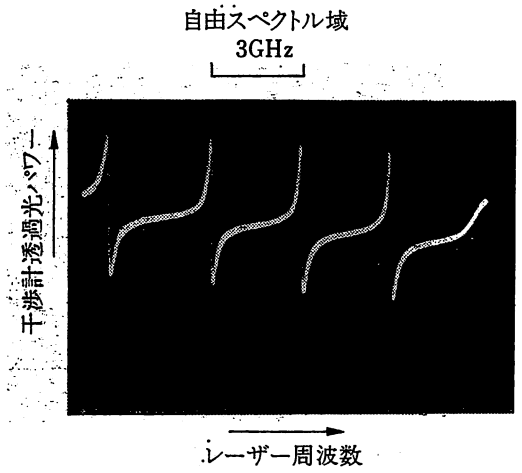

図 4　FP 干渉計とマッハ・ツェンダー干渉計とを組み合わせて得られる周波数復調曲線[47]．分散形曲線の中心の鋭い傾斜部分を周波数復調に利用する．

れるので，広い帯幅が得られる[44~46]．

この他には FP 干渉計とマッハ・ツェンダー干渉計を組み合わせてレーザー周波数無変調で**図 4** のような分散形の周波数復調曲線を得る方法[47]，FP 干渉計の中にブリュースター板を設置する方法[48] なども提案されている．

図 2 の周波数直接変調特性，周波数復調器の伝達関数，などの値をもとに計算機シミュレーションにより制御利得と帯幅とを最大にするように最適設計し，これをもとに AlGaAs レーザー (CSP 形）に対して実験を行った結果を**図 5** に示す．これはレーザーの周波数揺らぎのパワースペクトル密度の値を表し，曲線 A はフリーランニング時の

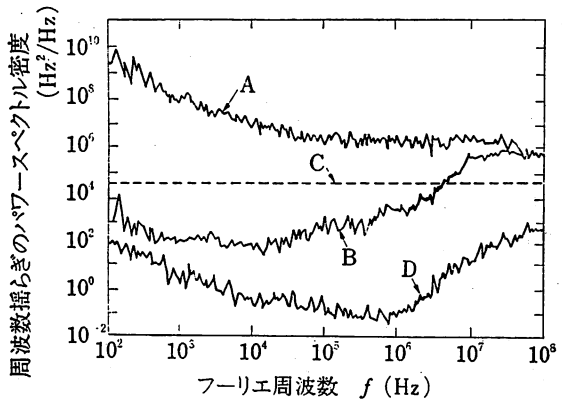

図 5　波長 0.8 μmAlGaAs レーザー (CSP 形）の周波数揺らぎのパワースペクトル密度[44,45]．
A：フリーランニング時．B：電気的負帰還制御時．C：フリーランニング時の自然放出雑音レベル．D：レーザーパワー揺らぎにより制限される周波数復調器の感度限界．

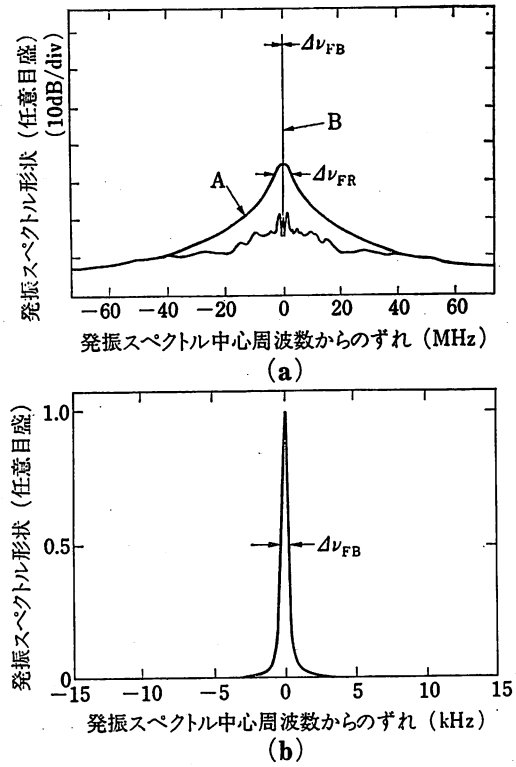

図 6　図 5 に対応する発振スペクトル形状[44,45]．(**a**) A：フリーランニング時．B：電気的負帰還制御時．(**b**) (a) の曲線 B の拡大図．曲線 A, B の半値幅 $\Delta\nu_{FR}$，$\Delta\nu_{FB}$ はそれぞれ 4.5MHz, 560 Hz.

値，曲線 B は制御結果である．両曲線を比較すると制御帯幅 40 MHz，とくにフーリエ周波数範囲 100 Hz～1 kHz の範囲では周波数揺らぎは 60～70 dB 抑圧されている．曲線 C はこのレーザーの α のパラメーターの値を 9 と仮定して[14] 推定されたフリーランニング時の自然放出雑音レベル，すなわちコヒーレント状態の値を表す．フーリエ周波数 4.4 MHz 以下では曲線 B の値は曲線 C の値以下である．すなわち，ハイパー・コヒーレント状態が実現している．

現在の制御系の周波数復調器の感度限界（周波数揺らぎ抑圧限界）はレーザー光のパワー揺らぎにより制限されており，曲線 D で表されている．バランストミキサー[49~51] を使いこのパワー揺らぎの影響を除去すれば制御系内の光検出器のショット雑音が復調器感度限界を与える．図 5 の曲線 A，B の値をもとにフーリエ変換の手法によってレーザー発振スペクトル形状を得た結果を**図 6** (**a**) の曲線 A，B に示す．曲線 A のスペクトル半値幅は 4.5 MHz である．曲線 B は制御の結果であり，スペクトル中心周波数のまわり ±40 MHz

以内で周波数揺らぎが抑圧されていることがわかる．図6 (b) は中心部の拡大図で，これより半値幅560 Hzであることがわかる．これは現在報告されている値のうちで最小のものである．図5の曲線Dに対応する発振スペクトル半値幅は約 1 Hz，ショット雑音レベルに対応する値は約 50 mHz である[23]．

図6では周波数揺らぎのパワースペクトル密度を図5のように正確に測定し，フーリエ変換の手法を用いて発振スペクトル形状を正確に求めた．発振スペクトル形状を求める方法として，この他に2台のレーザー間のヘテロダイン信号スペクトルを測定する方法があるが，この場合は両レーザーの周波数ドリフトを十分抑圧しておく必要がある．また，光ファイバーを用いる遅延自己ホモダインまたはヘテロダイン法があるが[52]，これは低域遮断特性を有し，分解能が低い．半値幅100 kHz以上の発振スペクトル形状測定には高フィネス走査形 FP 干渉計を光スペクトラムアナライザーとして用いることもできる．

4.1.4　周波数追随

4.1.1～4.1.3 の課題を実現し，周波数揺らぎを抑えたレーザーを主レーザーとして用い，第二のレーザー（従レーザー）の周波数をこれに追随させることは，ヘテロダイン，ホモダイン方式光応用システムのための必須技術である．このための手法として注入同期法が考えられる[53]．これはロッキングレンジが広いので，パルスレーザーのチャーピング抑制にも有効である[54]．しかし，非線形光学現象を使っているため，性能がレーザー動作条件に依存し，系の不安定性を誘起する．

より安定な方法として，図3のようなヘテロダイン形周波数同期ループが考えられる．この場合，局部発振器であるマイクロ波発振器の出力周波数と2台のレーザー間のヘテロダイン信号周波数とが一致するように従レーザーの注入電流を制御する．これによりヘテロダイン周波数揺らぎは積分時間100秒において0.2 Hz (光周波数で規格化し，アラン分散の平方根値で表すと 5×10^{-16}) が得られる[55,56]．この揺らぎは **4.1.1** で示した主レーザー周波数揺らぎより小さい．このことは従レーザー周波数は主レーザーのそれに高精度で追随していること，すなわち，従レーザーは主レーザーのレプリカとなっていることを意味する．このループのキャプチャレンジ，ロックレンジはヘテロダイン受信機である光検出器の帯幅により決まるので，2 GHz 程度の大きな値となる[55]．

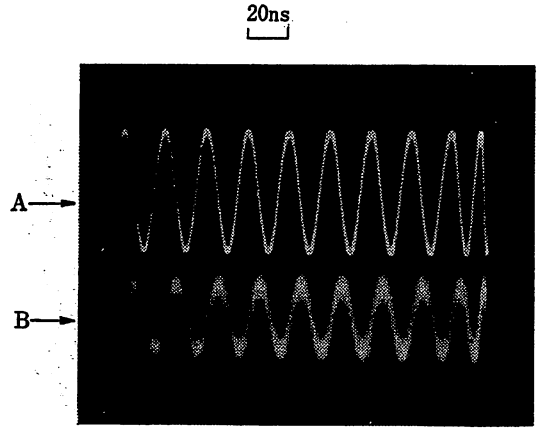

図7　ヘテロダイン形光位相同期ループにおけるヘテロダイン信号波形[56]．周波数は 50 MHz．曲線 A，B はそれぞれ，局部発振器からのマイクロ波信号，2台のレーザー間のヘテロダイン信号波形．

ヘテロダイン信号用の周波数／位相比較器をはじめとする制御系の性能向上により上記の揺らぎを約 1×10^{-18} まで抑圧することが可能であると試算されている[55,56]．この性能向上によりヘテロダイン信号位相揺らぎを1ラジアン以下にすること，すなわちヘテロダイン形光位相同期ループが可能である[57]．**図7** にその結果の一例を示す．図中の2曲線は局部発振器からのマイクロ波信号，および2台のレーザー間のヘテロダイン信号の波形を示す[56]．後者は残留位相揺らぎのために波形がぼやけているが，このぼやけの量から残留位相揺らぎの実効値を推定し[58]，約0.6ラジアンが得られている[56,59]．この他に，ホモダイン形位相同期ループも可能である．これらの位相同期ループの性能の定量的評価には，従来の装置[37,38]より約100倍の高い精度をもつ揺らぎ測定装置[59]が必要である．

干渉測長などでは2モードレーザーを光源とし，それらのモード間のヘテロダイン信号周波数を測定する場合が多い．この場合の測定精度はヘテロダイン信号周波数揺らぎにより制限される．この精度を向上するために各モードに混入する自然放出揺らぎ間に相関をもたせる方法が提案されている[60]．自然放出は真空の0点揺らぎに駆動さ

れる誘導放出過程と考えられるから，通常は各モードに混入する自然放出光揺らぎは互いに無相関である．しかし，レーザー遷移に関与する上準位が複数である場合，外部からの共鳴変調などによりこれら上準位間に量子的相関を与えると自然放出光揺らぎに相関が生ずる．このことは気体レーザー[61]および半導体レーザー[62]に関してすでに実験的に確認されているが，この相関特性の一部は強制モード同期と類似しているので混同を避ける必要がある．最近，短期位相揺らぎのアラン分散値を精密に測定する方法が提案され，相関の高精度評価が可能になってきた[63]．この相関自然放出を利用して，面の傾きおよびピストンセンサー[64]，さらには重力波検出用アンテナ[63]への応用が提案されている．

4.1.5 周波数掃引

注入同期法において主レーザー周波数を掃引すれば従レーザーのそれを掃引できる．しかし，その掃引精度，再現性は高くない．これに対し**4.1.4**の周波数同期ループを利用すると高精度掃引ができる．すなわち**4.1.4**における局部発振器であるマイクロ波発振器周波数を掃引すれば従レーザー周波数は**4.1.4**の性能を保ったまま高精度で掃引される．FP 共振器構造を持つ半導体レーザーでは連続掃引範囲 64 GHz が得られており[55]，これは高分解能分光分析，測長などの応用に対してすでに十分大きな値である．この値はモードホッピング現象により制限されているので，DFB，DBR レーザーなど，縦モード制御されたレーザーを使えば約 1 THz の連続掃引が可能である[65]．さらに有機非線形光学材料によるパラメトリック波長変換を併用すれば 10 THz 以上の値が可能であると試算されている[66]．

以上の5課題についての実験結果の現状と将来予測値を**表1**にまとめる．現時点ですでに高精度の光スィープジェネレーターとしての機能が実現しており，今後その性能の向上が期待される．

4.2 光帰還法

この場合(1)式右辺の積分項はない．その代わりに共振器構造を変更して共振器損失 κ を減少させる．この方法の特徴は(1)制御系は中～高利得，狭～中帯幅（共振器内の光子寿命の逆数で決まる）．(2)構成が簡便（15 年以上の歴史を持つ[24]）．(3) Coherent collapse[67]など，決定論的不安定[9,10]発生の可能性（これを避けるためにはレーザー端面の AR コートにより強い光帰還が必要．さらに外部共振器長の自動制御が必要で，実際には Opto-mechanical feedback というべき古典的方法である．ハイパー・コヒーレント状態は実現しない）．(4)外部共振器モード間のホッピングが発生．このホッピングを検出抑圧する方法が考案されている[68,69]．(5)周波数直接変調効率の消滅．

表1 電気的負帰還制御法の性能の現状，将来予測の概略値．

課　題	現 状	将来予測の概略値
発振スペクトル中心周波数の安定度（積分時間 100 秒において）	2×10^{-12}	1×10^{-15}
発振スペクトル中心周波数の確度	1×10^{-8}	1×10^{-10}
発振スペクトル半値幅	560 Hz	50 mHz
周波数追随精度（積分時間 100 秒において）	5×10^{-16}	1×10^{-18}
周波数掃引範囲	64 GHz	10 THz

光帰還法のうち，レーザー外部に置かれた1つの反射体からの反射光をレーザーに再注入する方法では約 2 kHz の発振スペクトルの半値幅が得られている[70]．反射体として回折格子を使えばレーザー周波数掃引も可能であるが，外部共振器モード間のホッピングが生ずるために連続掃引は困難である．

なお，量子井戸構造を導入してレーザー素子をつくり，この外部に回折格子を設置し，この回折格子面を回転させて周波数掃引する際，量子井戸中のキャリアの第一量子状態によるレーザー遷移から第二量子状態によるレーザ遷移に切り替えるように共振器損失と発振利得とのバランスをとりながら，100 nm 以上の範囲にわたる波長掃引が試みられている[71]．

反射光の位相を調節し系の安定性を保つためにレーザー端面と反射体の間の光路長をピエゾ・セラミックスなどにより自動調節する必要がある．この調整を不要にするために外部反射体として自己ポンプ形位相共役媒質を利用する方法が試みられている[72]．ただし，位相共役媒質の応答性がきわめて遅いことが性能を制限している．

単一反射体による方法よりも優れた方法として

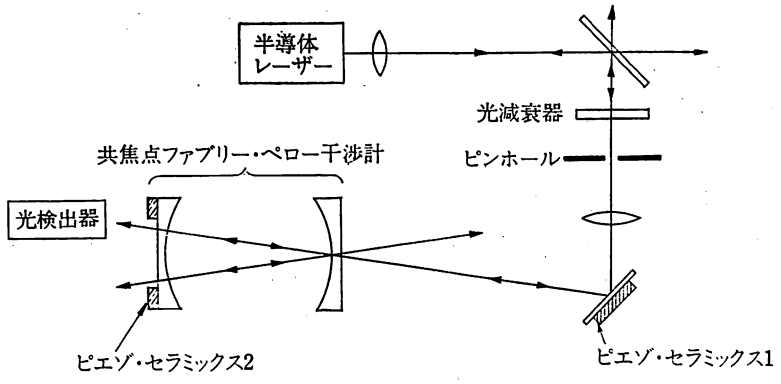

図 8　共焦点系ファブリー・ペロー (FP) 干渉計を用いる光帰還法の原理図[73].

図8に示すように共焦点 FP 干渉計を用いる方法が提案され，約 10 kHz の発振スペクトル半値幅が得られている[73]．この方法では FP 干渉計にレーザーを入射させ，共振後しみだしてきた光をレーザーに再注入させる．すなわち，FP 干渉計は周波数選択性のある反射体として機能し，レーザー周波数は FP 干渉計の共振周波数に自動的に引き込まれ，周波数揺らぎが抑圧される．制御帯幅は FP 干渉計内の光子寿命の逆数で与えられる．上記の単一反射体を使う場合と同様，FP 干渉計とレーザーとの間の光路長を自動調節する必要があるが，その精度は低くてもよい[74]．この他，次の2つの利点がある：(1) FP 干渉計からの強い光帰還は不要なのでレーザー本来の共振器構造はほぼ不変に保たれ，外部共振器モード間のホッピングは存在しない．(2) レーザーの注入電流を FP 干渉計の自由スペクトル域の有理数倍の周波数で変調するとレーザー周波数は変調可能[74,75]．

この FP 干渉計をマイクロ・オプティクス，ファイバー・オプティクスの技法により作成し，周波数変調可能なレーザーモジュールが開発されている[56,76,77]．最近は波長 0.67 μm の可視 AlGaInP レーザーにもこの方法が適用されている[78]．

4.3　レーザー素子改良法

上記 **4.1**, **4.2** の手法ではレーザー素子に外付け素子を付加する．しかし，システム設計者は外付け素子の使用を嫌う場合がある．そこで，レーザー素子自身の性能を向上させる試みがなされている．これはレーザー素子製作技術者にとっても興味のある方法である．この方法の特徴として，低～中制御利得，中～広帯幅（レーザー共振器の光子寿命は **4.2** の場合にくらべ短い），が挙げられる．この場合利得が小さいので **4.1** の手法と組み合わせるのが必須である．

手法は次の2つに分けられる：(1) レーザー素子の長共振器化により共振器損失を減少させ，さらに電極を分割して各電極に流す電流を調節し，空間的ホールバーニングを抑圧してモード間競合を抑える．さらに，量子井戸構造を導入し，**4.2** で述べた複素利得スペクトルの実部，虚部の中心周波数を同調させ，α パラメーターの値を小さくする[79]．

(2) **4.1**, **4.2** の手法の集積化．光帰還法に対応し，外部反射端を付ける試みが報告されている[80]．さらに，この単一反射体の場合の決定論的不安定の回避のために，レーザー発光部，外部反射体としての DBR，レーザーと反射体との光路長を調節するための位相変調器，を集積化することが試みられ，発振スペクトル半値幅が数 100 kHz まで狭窄化されている[81,82]．また，FP 干渉計を利用した図8の光帰還法に対応して，2つの DBR と光導波路を用い，これにより波長 1.5 μm InGaAsP レーザーの発振スペクトル半値幅が 150 kHz まで狭窄化されているが[83]，今後これらの外部素子をレーザーと共に集積化することが課題である．電気的負帰還制御法では制御帯幅を制限する要因の1つは制御ループ長である．光周波数復調器，光検出器，増幅器，などのうちのいくつかをレーザーと集積化することができれば，その性能は向上する．すなわち，電気的負帰還制御法は光集積回路技術と整合性がよい．

4.4　Cavity QED (Cavity Quantum Electrodynamics) の利用

(1) 式右辺の Γ_s の値，すなわち自然放出光揺

らぎの大きさを減少させる．そのために微小共振器に光を閉じ込め，共振器モード数を減らして自然放出確率を減少させる（これは Cavity QED :Cavity Quantum Electrodynamics) と呼ばれる研究分野である[84]）．特徴としては(1)低雑音レーザー発振が可能．(2)レーザー発振開始のためのトリガー法の考案が必要(3)低出力光パワー，が挙げられる．

従来はマイクロ波領域での実験が行われていた．しかし，最近は光領域でも微小共振器を作ることが可能になり，光領域での自然放出を制御する試みがなされている[85]．別の手法として，光を閉じ込める媒質の屈折率を周期的に変化させる構造にし，光子を局在化して光子エネルギー構造にバンドギャップを生成させ，自然放出光揺らぎを除去する試みも提案されている[86,87]．さらに，励起準位間の量子的干渉効果を利用し，反転分布の不要なレーザー発振の可能性も検討されている[88]．このように新しく発見された量子光学現象を積極的に利用することにより，将来は量子雑音の少ない高性能レーザーの実現が期待される．

5. 応　　用

半導体レーザーの応用範囲は広い．しかし，その一部は他種レーザーでも可能であるが半導体レーザーを使うと実用的（小型，低価格，低消費電力）であるという理由のみで使われている場合がある．しかしここでは，周波数揺らぎの少ない半導体レーザーではなくてはできない応用を列挙する．

5.1 光　計　測

(1)受動リング共振型ファイバージャイロ：ファイバー損失を最小に抑えるために半導体レーザーが不可欠で，感度向上のためにはその発振スペクトル半値幅は 100 kHz 以下でなくてはならない[89]．最近，レーザー周波数揺らぎを抑圧することにより地球の自転角速度以下の回転速度が測定可能になってきた[89,90]．さらに，このシステムに使うための高性能レーザーモジュールも開発されている[56,76,77]．

(2) 2 周波高速ドプラー速度計：ヘテロダイン干渉計により運動物体の速度を測るとき，2 周波数差の値によって測定可能速度限界が制限されていた．気体レーザーを使った市販品の典型的な性能は差周波数 20 MHz, 測定可能最大速度 1.8 m/s である[91]．これに対し，**4.1.4** の手法による主，従レーザーの組合せを使えば差周波数は約 2 GHz まで増加させることが可能であり，したがって測定可能速度は従来の 100 倍になる．これは将来半導体素子加工用にX線露光法が採用されるようになったとき，高速ステッパーの速度制御に威力を発揮する．

(3)ヘテロダイン形変位測定：従来は CO_2 レーザーに外部位相変調器を取り付け，周波数の up-chirp, down-chirp 法により物体の変位，さらには速度，を測定していた．しかし，CO_2 レーザー用の位相変調器の性能が必ずしも十分でないので，システム性能が限られていた．半導体レーザーの周波数直接変調特性は図 2 に示すように高効率，広帯幅であるので自由度の大きい chirp が可能となり，性能が向上する．

(4)宇宙空間での測長：半導体レーザーで CW-FM コヒーレント・ライダーを作ると 1～100 m 程度の高精度測長が可能である．これは特に宇宙空間でのアンテナ，建造物などの建築をするときに使われ，そのために **4.1**, **4.2** の方法により周波数揺らぎの少ない半導体レーザーの開発が進められている[92]．

5.2 分光分析

(1)レーザー・レーダー：半導体レーザーは他種のレーダー用レーザーに比べ低パワーであるのが難点であるが，擬似ランダム変調 CW レーザー・レーダー方式の採用により測定距離 1 km（エアロゾルに対し），3～5 km（雲，排煙に対し），距離分解能 9 m という高精度が得られている[93]．これを実現するためには図 2 の周波数直接変調特性，さらに **4.1.1** が不可欠である．

(2)同位体分離：医用診断用トレーサーのための原子の同位体分離には従来色素レーザーなどが用いられている．Rb, Cs などの同位体分離のためにレーザー誘起ドリフト法（レーザー励起により原子の衝突断面積を変化させ，バッファ気体中をドリフトさせる方法）[94] が提案されているが，光励起の際の脱励起のために分離効率は十分高くなかった．しかし，図 2 に示す半導体レーザーの周波数直接変調特性を利用し，FM 側波帯を用い

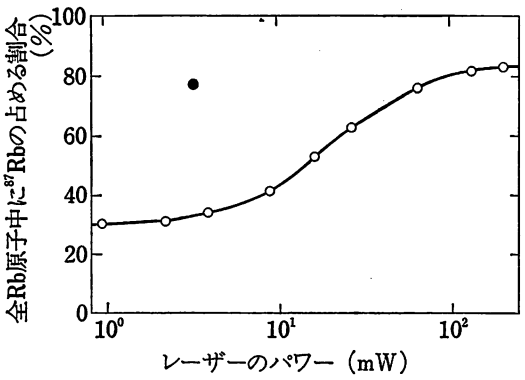

図 9　レーザー誘起ドリフト法による^{87}Rbの同位体分離の実験結果[94]．黒丸は半導体レーザー，白丸および実線は色素レーザーを使った結果．

て循環形の光励起を行い，さらに**4.1.1**を併用することにより分離効率が向上する[95]．すなわち，**図9**に示すように，従来用いていた色素レーザーパワー（150 mW）に対し，約 1/50 の半導体レーザーパワーを用いても同程度の高効率の同位体分離ができる[94]．この他にもバリウム，ガリウムなどの同位体分離に周波数制御された半導体レーザーが使われている[96]．核融合用に重要なウランの同位体分離には可視半導体レーザーが有望である[95]．

（3）SiH_x の分析：CVD によるアモルファスシリコン膜の形成において SiH_x の種の分析，同定は定量的な膜形成制御のために重要である．たとえば SiH_2 ラジカルは紫外光照射によるフォトリシスにおいて振動準位間の遷移に伴う蛍光を発する[97]．その波長は可視の AlGaInP レーザー付近に存在するので，このレーザーにより分析，同定が可能である[95]．

5.3　マイクロ波原子発振器の光励起

マイクロ波通信，航法，地震予知，天文学，などには周波数高安定なマイクロ波原子発振器が基本素子であり，ここでは実用的な次の2つについて述べる．

（1）Rb 原子発振器（6.8 GHz）：波長 0.78 μm の光により光励起し，光・マイクロ波二重共鳴信号を得て，その信号スペクトル中心周波数にマイクロ波周波数を安定化する．周波数制御された半導体レーザーにより光励起すると3準位 Rb 原子の非線形応答によりマイクロ波から光への変調移乗効果が発生し[98,99]，従来の 1/20 程度の狭い幅をもつ二重共鳴スペクトルが得られる．これにより，マイクロ波周波数の短期安定度が従来にくらべ約 40 倍向上する．

さらに，マイクロ波の FM 周波数に対応するフーリエ周波数領域のみで**4.1**の電気的負帰還制御法により選択的にレーザー周波数揺らぎを抑圧すると，二重共鳴信号の S/N 値が向上し，短期安定度がさらに向上することが確認される[100]．レーザー周波数揺らぎの抑圧限界であるショット雑音レベルが実現すると短期安定度は現状のさらに 1,000 倍向上することが試算されている[101]．

一方，レーザー照射によって Rb 原子に生ずる AC シュタルク効果，それに伴う二重共鳴スペクトル中心周波数のシフト，を定量的に評価し，このシフトが無くなるように電気的負帰還制御によりレーザ周波数を制御することができる．この自己同調システムによって，**図10**に示すようにマイクロ波周波数ドリフトが従来の 1/40 以下まで抑圧されている[101,102]．これらの値は市販・可搬形の高精度発振器である Cs 原子発振器より優れていることが確認されている[101]．

（2）Cs 原子発振器（9.2 GHz）：Rb 原子発振器より大型であるが，上位性能を有する発振器である．Cs 原子ビームのエネルギー準位選別を波長 0.85 μm 半導体レーザーによる光励起で行い，選別効率を上げる．さらに，マイクロ波遷移をした

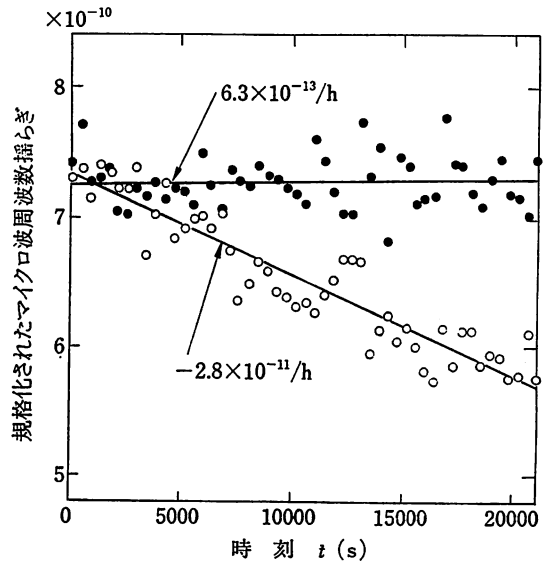

図 10　半導体レーザー周波数制御による自己同調形 Rb 原子発振器のマイクロ波周波数ドリフトの測定結果[101,102]．白丸：フリーランニング・レーザー使用時．黒丸：周波数制御されたレーザー使用時．

原子検出も半導体レーザーによる蛍光検出で行い感度を上げる．この方法は 10 年以上前に提案されていたが[103]，最近 **4.1.1**，**4.1.2** の性能が向上し，実用化研究が盛んになってきた[104]．さらに，レーザー冷却法を併用する試みも報告されている[105]．

5.4 光 通 信

（1）周波数超多重コヒーレント光通信：光ファイバー伝送損失が最小となる波長 1.55 μm を中心に低伝送損失の帯幅が約 20 THz である．この中にチャネル間隔数 GHz で 1,000 チャネル以上を用意し，周波数超多重化が提案されている[106]．そのとき **4.1.1**，**4.1.2**，**4.1.5** の課題が不可欠である．この超多重化が行われれば伝送レートはそれほど高くなくても大容量伝送可能である．**4.1.3** により 50 THz に達する大きな GB 積が得られているので，このレーザーを低〜中ビットレートのコヒーレント光通信システムに使う時には十分低い位相誤差分散を与えることが確認されている[44]．

（2）宇宙光通信：コヒーレント・レーザー・レーダーと同様，**4.1** の手法で制御された AlGaAs レーザーが使用できる[107]．問題は高パワー化，レーザービーム追尾である．

5.5 量子光学・基礎物理学

（1） 原子・分子の高分解能分光

レーザーを利用した高分解能分光は原子・分子の構造，励起状態の動的特性などに関する多くの精密な知見を与えており，特に可視域においては波長可変色素レーザーが頻繁に用いられてきた．しかし，近年 **4.** に示したように半導体レーザーの性能が著しく向上したのに伴い，これを用いた近赤外域（波長 0.7 μm〜1.6 μm）での高分解能分光が行われつつある．この半導体レーザーを用いた分光の特長は，図 2 に示す特性を利用して電流，温度により広範囲にわたる周波数掃引が可能なこと，さらに周波数変調分光により高感度検出が容易に行えることである[108]．

すでにアンモニア[25]，水蒸気[26]の振動回転遷移の高調波，結合調の分光が行われ，さらに最近では DFB レーザーを用いて周波数 1.5 THz 以上の範囲にわたりアセチレン[27]の分光，さらには，シアン[28]，アンモニア[109]の倍音振動スペクトルの高分解能分光が行われている．また，半導体レーザー媒質中で発生する内部第二高調波を用いて，波長 0.4 μm 付近の紫外域でのカリウム，アルミニウムの分光も試みられている[110]．

（2） パリティ非保存の検証およびその関連研究

原子を構成している粒子，すなわち電子，陽子，中性子間の弱い相互作用の存在が Weinberg-Salam の統一理論（電弱理論）によって予言されている．この弱い相互作用の存在を検証するためには従来，加速器を用いた大がかりな高エネル

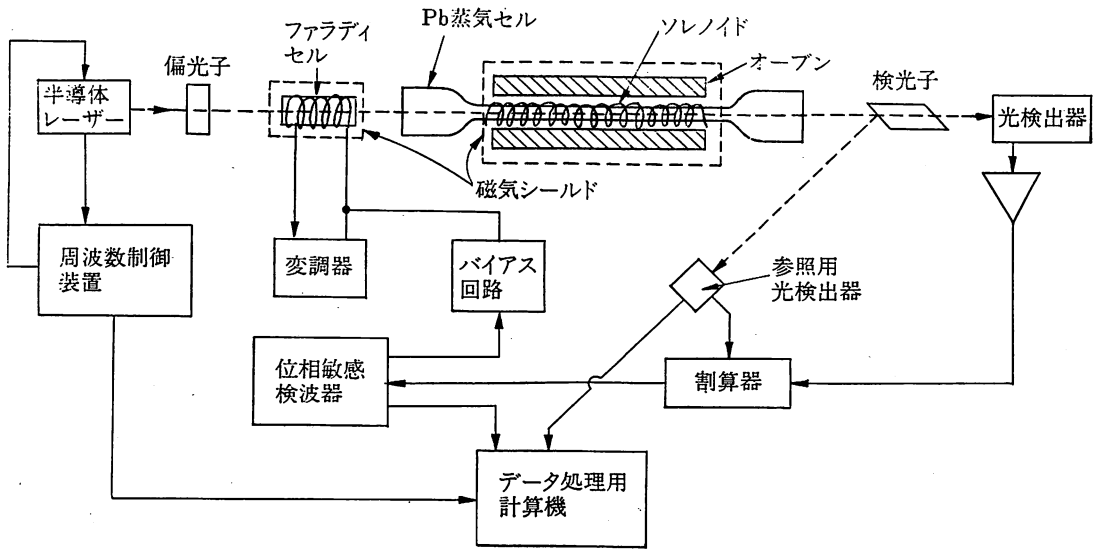

図 11 鉛 (Pb) 原子のパリティ非保存の実験装置[113]．オーブン中の Pb 蒸気に波長 1.3 μm 半導体レーザー光を照射している．その波長は鉛 (Pb) 原子の磁気双極子遷移に共鳴している．ここでは，オーブンを透過するレーザー光の偏光状態変化を検出している．

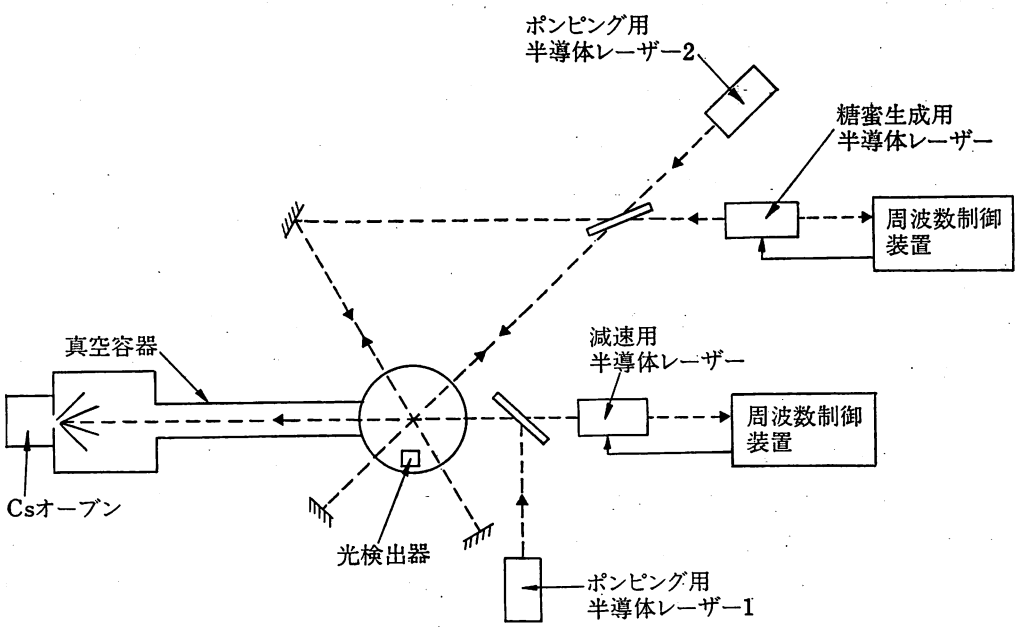

図 12　セシウム (Cs) 原子のレーザー冷却の実験装置[120]. 複数の半導体レーザーを用いて Cs 原子ビームの減速，冷却，さらに光による糖蜜生成を行っている.

ギー実験によっていたが，精密レーザー分光を用いても実験的検証が可能であることがわかってきた[111,112].

すなわち，弱い相互作用により原子の波動関数のパリティ保存が成立しなくなるので，これにより誘起される微弱な光学的遷移をレーザー分光によって測定しうる. 例えば，波長 1.3 μm InGaAsP レーザー光を用いて鉛 (Pb) 原子の磁気双極子遷移を測定し，その際パリティ非保存によって誘起される透過光の偏光状態変化を**図 11** に示す装置によって精密測定した例が報告されている[113]. これらの測定精度は約 1×10^{-14} に達しており，これは理論精度よりも高いとされている[112].

一方，周波数制御された AlGaAs レーザーを用いて Cs 原子のシュタルク係数を精密測定し，パリティ非保存検証に必要な構造定数が推定されている[114].

（3）　レーザー冷却，イオントラップ

Hänsch および Schawlow[115] によって提案されたレーザー光による中性原子の減速（これはレーザー冷却と呼ばれている）および閉じ込めの研究が，最近のレーザー周波数制御技術などの進歩により急速に進歩している. 現在までのところレーザー冷却限界はドップラー効果による値以下 (<40 μK)[116,117]，さらにごく最近の類似の実験では原子と光子との衝突に伴う反跳効果による値以下 (<2 μK)[118] にまで達している.

また，レーザー冷却の手法を用い，真空中で約 10^7 個の原子を約 10^{11} 個/cm^3 の高密度で数分以上の長時間にわたって閉じ込めることが可能になっている[119]. すなわち，この場合，原子集団は動きの少ない粘性流体状になっている. したがって，これを「光による糖蜜 (Optical Molasses)」と呼んでいる.

これらの実験に関し，周波数変調と制御が容易な半導体レーザーを用いることが有利である. これを**図 12** に示す装置中で用い，Cs 原子の冷却，光による糖蜜の生成[120]，さらに，Rb 原子の冷却が行われている[121]. また，最近は希ガス原子の冷却に半導体レーザーを使う試みも提案されている[122].

一方，イオンなどの荷電粒子を高周波磁場などによる電磁的トラップ中に閉じ込め，さらにレーザー冷却の手法を併用するイオントラップの研究の進歩も著しい. 特に，30 年以上前から議論されている量子ジャンプ[123] の現象が，一個のイオンを冷却し，閉じ込めることにより観測されている[124]. さらに，最近では閉じ込めの性能が向上し，イオンの位置と運動量の不確定性の間のスクイージング現象が観測されるようになった[125].

さらに，多数のイオンの冷却，閉じ込めによりイオン結晶，固体プラズマと同様の振る舞いの観

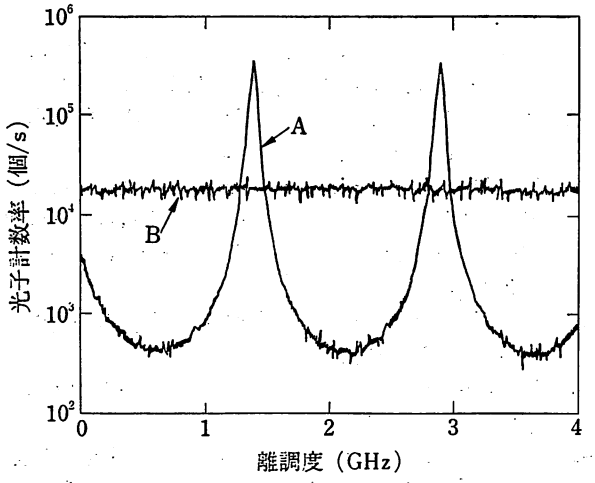

図 13　FP 共振器中のイッテルビウム (Yb) 原子の自然放出の制御の実験結果[128]．Yb 原子に照射するレーザー光周波数は Yb 原子共鳴周波数に同調している．共焦点形 FP 共振器中の Yb 原子ビームからの自然放出光強度と縦軸に取っている．また，横軸は Yb 原子共鳴周波数からの FP 共振器共振周波数の離調度である．曲線 A は FP 共振器を用いた場合の結果である．共振器の共振周波数が原子の共鳴周波数に同調した場合，自然放出光強度が増大しており，離調した場合，抑制されている．曲線 B は FP 共振器を用いない場合，すなわち自由空間での自然放出光強度を示す．

測が報告されている[126]．このイオントラップのために必要なレーザー光源の波長は可視～紫外領域に属するので，この短波長の光を発生させるために従来は色素レーザーなどの複数台のレーザーを注意深く周波数制御し，その SHG または和周波混合を使っていた．したがってその発生効率は非常に低い．そこで周波数制御の容易な半導体レーザーを導入することが検討されている[125]．

（4）　Cavity QED (Cavity Quantum Electrodynamics)

4.4 でも触れたように，近年，電磁波の波長程度の寸法をもつ微小共振器，さらに，低損失共振器内での原子の自然放出を抑制または増強する試みが行われている．現在までのところリドベルグ状態の原子からのマイクロ波の自然放出を抑制することが実験的に確認されている[127]．この実験においては複数個の AlGaAs レーザーが Cs 原子をリドベルグ状態に多段階励起するための光源として使われている．さらに，**図 13** に示すように光領域でも低損失 FP 共振器内の自然放出を抑制または増強できることが確認されている[128]．

また，**4.4** で示したような低雑音半導体レーザーを実現するために，微小共振器を用いた半導体発光素子が理論的および実験的に研究されている[129,13]．

6. むすび

半導体レーザーは共振器損失が大きいために大きな周波数揺らぎを持つが，その制御効率も高い．本稿では，後者をたくみに利用して光の状態を制御し，従来にない良質の光を得る手法について述べた．このような光を用いて広範な応用が可能となる．しかし，そのためには従来半導体レーザー製造技術者が electron control and manipulation に従事し，良質なレーザー素子を実現してきたのに加え，今後は photon control and manipulation が要求されよう．半導体レーザー周波数制御にはレーザー素子から光システムにわたる総合的知識を必要とするので，本稿ではそれに関する文献を必ずしも公平には網羅できていないことをご容赦いただきたい．技術的詳細に関しては文献 23), 36), 131) などの総説を参考にされたい．

謝　辞

本稿のうち著者の研究に関しては国内外の多数の研究者諸氏からのご指導，ご討論をいただいた．また，東京理科大学の田幸敏治教授，東京工業大学の末松安晴教授，伊賀健一教授，池田光男教授，からのご指導，ご鞭撻，さらに著者の研究室所属の学生諸氏の積極的なご協力に深く感謝いたします．

文　献

1) J. L. Bromberg: Phys. Today **41** (1988) 26.
2) 大津元一：サイエンス 1989 年 3 月号 p. 64.
3) M. Ohtsu and Y. Teramachi: IEEE J. Quantum Electron. **25** (1989) 31.
4) N. Chinone, T. Kuroda, T. Otoshi, T. Takahashi and T. Kajimura: IEEE J. Quantum Electron. **QE-21** (1985) 1264.
5) M. Ohtsu, Y. Teramachi and T. Miyazaki: Opt. Commun. **61** (1987) 203.
6) 小島啓介，野田　進，光永一正，藤原賢三，久間和生：電子通信学会技術研究報告 OQE 85-37 (1985).
7) K. -Y. Liou, M. Ohtsu, C. A. Burrus, Jr., U. Koren and T. L. Koch: IEEE J. Quantum Electron. **7** (1989) 632.
8) 宇佐見正士，秋葉重幸，松島裕一：第 49 回応用物理学会学術講演会予稿集 (1988) p. 882.

9) R. Lang and K. Kobayashi: IEEE J. Quantum Electron. **QE-16** (1980) 347.
10) 大津元一：フィジックス **6** (1985) 297.
11) P. Kartaschoff: *Frequency and Time* (Academic Press, London, 1978) Chap. 2.
12) 大津元一：レーザーと原子時計（オーム社，東京，1986）第3章.
13) A. Blaquiere: Compt. Rend. **26** (1962) 2929.
14) M. Oshinski and J. Buus: IEEE J. Quantum Electron. **QE-23** (1987) 9.
15) D. Welford and A. Mooradian: Appl. Phys. Lett. **40** (1982) 560.
16) M. Ohtsu and S. Kotajima: Jpn. J. Appl. Phys. **23** (1984) 760.
17) 大津元一：半導体レーザーの基礎，応用物理学会編，（オーム社，東京，1987）第2章.
18) M. Ohtsu, H. Fukada, T. Tako and H. Tsuchida: Jpn. J. Appl. Phys. **22** (1983) 1157.
19) M. Ohtsu and M. Tabuchi: J. Lightwave Technol. **6** (1988) 357.
20) O. Nilsson and Y. Yamamoto: Appl. Phys. Lett. **46** (1985) 22.
21) Y. Yoshikuni and G. Motosugi: J. Lightwave Technol. **LT-5** (1987) 516.
22) Y. Yamamoto, O. Nilsson and S. Saito: IEEE J. Quantum Electron. **QE-21** (1985) 1919.
23) M. Ohtsu: J. Lightwave Technol. **6** (1988) 245.
24) A. Mooradian: "*High Resolution Tunable Infrared Lasers*", *Laser Spectroscopy*, ed. R. G. Brewer and A. Mooradian (Plenum Press, New York, 1973) 223.
25) M. Ohtsu, H. Kotani and H. Tagawa: Jpn. J. Appl. Phys. **22** (1983) 1553.
26) K. Fukuoka, M. Ohtsu and T. Tako: Jpn. J. Appl. Phys. **23** (1984) L 117.
27) 衣川　茂，佐々田博之，上原喜代治：第49回応用物理学会学術講演会予稿集 (1988) p. 815.
28) H. Sasada: J. Chem. Phys. **88** (1988) 767.
29) 橋本　実，大津元一：電気学会論文誌 C **108** (1988) 706.
30) T. Yabuzaki, A. Ibaragi, H. Hori, M. Kitano and T. Ogawa: Jpn. J. Appl. Phys. **20** (1981) L 451.
31) S. Yamaguchi and M. Suzuki: Appl. Phys. Lett. **41** (1982) 597.
32) Y. C. Chung: *Proc. Int. Conf. Integrated Optics and Optical Fiber Communication* (*IOOC '89*) *Kobe 1989*, (IEICE, Tokyo, 1989) 21 D 4-3.
33) M. Ohtsu and E. Ikegami: Electron. Lett. **25** (1989) 22.
34) 池上英次，楠沢英夫，中川賢一，大津元一：第50回応用物理学会学術講演会予稿集 (1989) 発表予定.
35) Ch. Salomon, D. Hills and J. L. Hall: J. Opt. Soc. Am. B. **5** (1988) 1576.
36) M. Ohtsu: Opt. Quantum Electron. **20** (1988) 283.
37) 加藤　徹，久保木勝彦，大津元一：第48回応用物理学会学術講演会予稿集 (1987) p. 701.
38) K. Kuboki and M. Ohtsu: IEEE Trans. Instrum. and Meas. 投稿中.
39) M. Ohtsu, M. Hashimoto and H. Ozawa: *Proc. the 39th Annual Frequency Control Symposium, Philadelphia, 1985* (IEEE Piscataway, 1985) p. 43.
40) H. Furuta and M. Ohtsu: Appl. Opt. **20** (1989)，9月号掲載予定.
41) V. Pevtschin and S. Ezekiel: Opt. Lett. **12** (1987) 172.
42) 三木幸信：昭和62年度計量研究所研究講演会資料，「量子的計測を中心にして」，日本産業技術振興協会編，p. 19.
43) 榎本陽一，村上敏明：第36回応用物理学関係連合講演会予稿集 (1989) p. 1112.
44) M. Ohtsu, M. Murata and M. Kourogi: *Proc. Conf. Lasers and Electro-Optics* (*CLEO '89*), *Baltimore, 1989* (LEOS/IEEE and OSA, Washington, D. C., 1989) THK 30.
45) M. Ohtsu, M. Murata and M. Kourogi: IEEE J. Quantum Electron. 投稿中.
46) 村田守啓，大津元一：第35回応用物理学関係連合講演会予稿集 (1988) p. 867.
47) 興梠元伸，清原章公，大津元一：第50回応用物理学会学術講演会予稿集 (1989) 発表予定.
48) T. W. Hänsch and B. Couillaud: Opt. Commun. **35** (1980) 441.
49) H. P. Yuen and V. W. S. Chan: Opt. Lett. **8** (1983) 177.
50) G. L. Abbas, V. W. S. Chan and T. K. Yee: J. Lightwave Technol. **LT-3** (1985) 1110.
51) S. B. Alexander: J. Lightwave Technol. **LT-5** (1987) 523.
52) T. Okoshi, K. Kikuchi and A. Nakayama: Electron. Lett. **16** (1980) 630.
53) S. Kobayashi and T. Kimura: IEEE J. Quantum Electron., **QE-17** (1981) 681.
54) C. Lin and F. Mengel: Electron. Lett. **20** (1984) 1073.
55) K. Kuboki and M. Ohtsu: IEEE J. Quantum Electron., 1989年10月掲載予定.
56) C. -H. Shin, M. Teshima, M. Ohtsu, T. Imai, J. Yoshida and K. Nishide: *Proc. the 7th Int. Conf. Integrated Optics and Optical Fiber Communication* (*IOOC '89*), *Kobe 1989* (IEICE, Tokyo, 1989) 21 D 4-5.
57) 申　哲浩，久保木勝彦，大津元一：電気学会論文誌 C 108 (1988) 678.
58) J. L. Hall, M. Long-Sheng and G. Kramer: IEEE J. Quantum Electron. **QE-23** (1987) 427.
59) 申　哲浩，手島光啓，大津元一：第50回応用物理学会学術講演会予稿集 (1989) 発表予定.
60) M. O. Scully: Phys. Rev. Lett. **55** (1985) 2802.
61) P. E. Toschek and J. L. Hall: *Proc. 15th Int.*

Quantum Electronics Conf. (*IQEC '87*), *Baltimore 1987* (OSA, Washington, D. C., 1987) 102.
62) M. Ohtsu and K. -Y. Liou: Appl. Phys. Lett. **52** (1988) 10.
63) M. Winters: JILA, Univ. Colorado (1989) 私信.
64) J. D. Newman, R. C. Short, D. L. Clark: *Proc. Conf. Lasers and Electro-Optics* (*CLEO '89*), *Baltimore, 1989* (LEOS/IEEE and OSA, Washington, D. C., 1989) THK 37.
65) Y. Tohmori, K. Komori, S. Arai and Y. Suematsu: Electron. Lett. **21** (1985) 743.
66) 楠沢英夫，池上英次，中川賢一，大津元一：第50回応用物理学会学術講演会（1989）発表予定.
67) D. Lenstra, B. H. Verbeek and A. J. den Boef: IEEE J. Quantum Electron. **QE-21** (1985) 674.
68) M. Ohtsu, K. -Y. Liou, E. C. Burrows, C. A. Burrus and G. Eisenstein: Electron. Lett. **23** (1987) 1111.
69) M. Ohtsu, K. -Y. Liou, E. C. Burrows, C. A. Burrus and G. Eisenstein: J. Lightwave Technol. **7** (1989) 68.
70) N. A. Olsson and J. P. Van der Ziel: J. Lightwave Technol. **LT-5** (1987) 510.
71) D. Mehuys, M. Mittelstein and A. Yariv: *Proc. Conf. Lasers and Electro-Optics* (*CLEO '89*), *Baltimore 1989* (LEOS/IEEE and OSA, Washington, D. C., *1989*) FL 4.
72) K. Vahala, K. Kyuma, A. Yariv, S. K. Kwong, M. Cronin-Golomb and K. Y. Kau: Appl. Phys. Lett. **49** (1986) 1563.
73) B. Dahmani, L. Hollberg and R. Drullinger: Opt. Lett. **12** (1987) 876.
74) 大津元一：電子情報通信学会技術研究報告 OQE 87-135 (1987).
75) L. Hollberg and M. Ohtsu: Appl. Phys. Lett. **53** (1988) 944.
76) 吉田純一，今井　享，西出健一，申　哲浩，手島光啓，大津元一：レーザー学会研究会報告 RTM-88-37 (1989).
77) 今井　享，吉田純一，西出健一，申　哲浩，手島光啓，大津元一：第 36 回応用物理学関係連合講演会予稿集（1989）p. 955.
78) 鈴木宏昌，輿石伊佐央，中川賢一，大津元一：第50回応用物理学会学術講演会予稿集（1989）発表予定.
79) Y. Arakawa and A. Yariv: IEEE J. Quantum Electron. **QE-22** (1986) 1887.
80) T. Fujita, J. Ohya, K. Matsuda, M. Ishino, H. Sato and H. Serizawa: Electron. Lett. **21** (1985) 374.
81) I. Mito and K. Kitamura: *Proc. Conf. Lasers and Electro-Optics* (*CLEO '89*), *Baltimore 1989* (LEOS/IEEE, OSA, Washington, D. C., 1989) TUD 5.
82) H. Imai: *Proc. Conf. Lasers and Electro-Optics* (*CLEO '89*), *Baltimore 1989* (LEOS/IEEE, OSA, Washington, D. C., 1989) FB 4
83) N. A. Olsson, C. H. Henry, R. F. Kazarinov, H. J. Lee, B. H. Johnson and K. J. Orlowsky: Appl. Phys. Lett. **51** (1987) 1141.
84) S. Haroche and D. Kleppner: Phys. Today (January, 1989) p. 24.
85) A. Anderson, S. Haroche, E. A. Hinds, W. Jhe, D. Meschede and L. Moi: *Proc. 15th Int. Quantum Electronics Conf.* (*IQEC '87*), *Baltimore, 1987* (OSA, Washington, D. C., 1987) p. 128.
86) E. Yablonowitch: *Proc. 15th Int. Quantum Electronics Conf.* (*IQEC '87*), *Baltimore 1987* (OSA, Washington, D. C. 1987) p. 130.
87) E. Yablonovitch: *Proc. Conf. Quantum Electronics and Laser Science* (*QELS '89*) *Baltimore, 1989* (OSA, Washington, D. C., 1989) TUKK 6.
88) S. E. Harris: *Proc. Conf. Quantum Electronics and Laser Science* (*QELS '89*) *Baltimore, 1989* (OSA, Washington, D. C., 1989) TULL 3.
89) M. Ohtsu and S. Araki: Appl. Opt. **26** (1987) 464.
90) 田井修市，高橋正信，久間和生：レーザー学会研究会報告，RTM-88-40 (1989).
91) 西村哲治：第 26 回全日本光学測定機展技術講演会資料（日本光学測定機工業会編，1989）p. 1.
92) R. G. Beausoleil, J. A. McGarvey, R. L. Hagman and C. S. Hong: *Proc. Conf. Lasers and Electro-Optics* (*CLEO '89*), *Baltimore 1989* (LEOS/IEEE, OSA, Washington, D. C., 1989) WN 3.
93) 竹内延夫：国立公害研究所研究報告第 122 号 (1989).
94) A. D. Streatere, J. Mooibroek and J. P. Woerdman: Appl. Phys. Lett. **52** (1988) 602.
95) 大津元一：光波センシング技術研究会講演論文集 LST 1-4 (1988).
96) J. Lawrenz, A. Obrebski and K. Niemax: Anal. Chem. **59** (1987) 1232.
97) I. Dubois: Canadian J. Phys. **46** (1968) 2485.
98) M. Hashimoto and M. Ohtsu: IEEE J. Quantum Electron. **QE-23** (1987) 446.
99) M. Hashimoto and M. Ohtsu: J. Opt. Soc. Am. B, 1989 年 10 月掲載予定.
100) 鈴木宏昌，橋本　実，大津元一：第 50 回応用物理学会学術講演会予稿集（1989）発表予定.
101) 大津元一，橋本　実，鈴木宏昌：電気学会第 2 回精密位相同期回路技術調査専門委員会資料 2-1 (1989).
102) M. Hashimoto and M. Ohtsu: IEEE Trans. Instrum. and Meas. 投稿中.
103) J. L. Picque: Metrologia **13** (1977) 115.
104) 中段和宏，大嶋新一，池上　健，古賀保喜：第 49 回応用物理学会学術講演会予稿集（1988）p. 27.
105) D. W. Sesko and C. E. Wieman: Opt. Lett.

14 (1989) 269.
106) B. Glance: AT & T Bell Labs., 1989, 私信.
107) R. G. Marshalek and G. A. Koepf: Opt. Eng. **27** (1988) 663.
108) W. Lenth: Opt. Lett. **8** (1983) 575.
109) 中川賢一：東京大学博士論文, 1989 年.
110) K. Sakurai and N. Yamada: Opt. Lett. **14** (1989) 233.
111) S. L. Gilbert and C. E. Wieman: Phys. Rev. A **34** (1986) 792.
112) M. C. Noecker, B. P. Masterson and C. E. Wieman: Phys. Rev. Lett. **61** (1988) 310.
113) T. P. Emmons, J. M. Reeves and E. N. Forston: Phys. Rev. Lett. **51** (1983) 2089.
114) C. E. Tanner and C. E. Wieman: Phys. Rev. A **38** (1988) 162.
115) T. W. Hänsch and A. L. Schawlow: Opt. Commun. **13** (1975) 68.
116) P. D. Lett. R. N. Watts, C. I. Westbrook, W. D. Phyllips, P. L. Gould and H. J. Metcalf: Phys. Rev. Lett. **61** (1988) 169.
117) R. N. Watts, P. D. Lett., C. I. Westbrook, S. L. Rolston, C. E. Tanner and W. D. Phillips: *Proc. Conf. Quantum Electronics and Laser Science* (*QELS '89*) *Baltimore, 1989* (OSA, Washington, D. C., 1989) THLL 1.
118) A. Aspect, E. Arimond, R. Kaiser, N. Vansteenkiste and C. Cohen-Tannoudji: Phys. Rev. Lett. **61** (1988) 826.
119) E. L. Raab, M. G. Prentiss, A. E. Cable, S. Chu and D. E. Pritchard: Phys. Rev. Lett. **59** (1987) 2631.
120) D. Sesko, C. G. Fan and C. E. Wieman: J. Opt. Soc. Am. B **5** (1988) 1225.
121) R. N. Watts, D. H. Yang, B. Sheehy and H. Metcalf: *Proc. 15th Int. Quantum Electronics Conf.* (*IQEC '87*) *Baltimore 1987* (OSA, Washington, D. C., 1987) p. 66.
122) 清水富士夫：東京大学, 1989 年, 私信.
123) E. Schrödinger: British J. Phil. Sci. **3** (1952) 109.
124) J. C. Bergquist, R. G. Hulet, W. M. Itano and D. J. Wineland: Phys. Rev. Lett. **57** (1986) 1699.
125) J. Bergquist: NIST, 1989 年, 私信.
126) S. L. Gilbert, J. J. Bollinger and D. Wineland: Phys. Rev. Lett. **60** (1988) 2022.
127) D. Meschede, H. Walther and G. Muller: Phys. Rev. Lett. **54** (1985) 551.
128) D. J. Heinzen, J. J. Childs, J. F. Thomas and M. S. Feld: Phys. Rev. Lett. **58** (1987) 1320.
129) 井桁和浩, 山本喜久, 町田 進, 上田正仁：第 49 回日本物理学会年会 (1989 年 3 月) 28-a-SB-6.
130) Y. Yamamoto, S. Machida, K. Igeta and Y. Horikoshi: *The 6th Rochester Conf. Coherence and Quantum Optics*, June 1989, MCd 2.
131) M. Ohtsu and T. Tako: "Coherence in Semiconductor Lasers". *Progress in Optics XXV*, ed. E. Wolf, 1988 (Elsevier, Amsterdam) p. 191.

FM Noise Reduction and Subkilohertz Linewidth of an AlGaAs Laser by Negative Electrical Feedback

MOTOICHI OHTSU, MEMBER, IEEE, MORIHIRO MURATA, AND MOTONOBU KOUROGI

Abstract—**Negative electrical feedback was applied to a CSP-type AlGaAs laser, by which its FM noise was reduced at the Fourier frequency range of $f \leqq 40$ MHz. The magnitude of the FM noise was far lower than the quantum noise level of the free-running laser at 100 Hz $\leqq f \leqq 4.4$ MHz. Especially, it was as low as $1 \times 10^{-7} \sim 1 \times 10^{-6}$ that of the free-running laser at 100 Hz $\leqq f \leqq 1$ kHz. The full width at half maximum of the field spectrum was reduced to 560 Hz. The major factors necessary for realizing the very low FM noise level were 1) the presently used laser had almost constant FM response characteristics for a wide Fourier frequency range, 2) a high-finesse Fabry-Perot interferometer was employed for highly-sensitive FM noise detection and to get higher feedback gain, 3) the reflection mode of the Fabry-Perot interferometer was employed to increase the bandwidth and efficiency of the FM noise detection, and 4) a computer simulation was utilized for optimum design of the feedback loop.**

I. Introduction

IMPROVEMENT of temporal coherence in lasers is a fundamental and important topic of study in the field of quantum electronics, and has been carried out successively from the advent of lasers [1]. Development of highly-coherent semiconductor lasers has been intensively carried out [2], [3] because they have been required for several important applications. These applications are coherent optical measurements such as resonator-type fiber gyroscopes [4], high-resolution laser spectroscopy, such as optical pumpings of rubidium [5] and cesium [6], cooling of atoms [7], and coherent optical communication systems. A simple method of optical feedback has been proposed to reduce the linewidth of the field spectrum of the semiconductor laser, and the linewidth as narrow as 2 kHz has been realized [8]. As an alternative method, the authors have proposed a method of negative electrical feedback [9], [10] and a linewidth of 360 kHz has been realized for an InGaAsP laser of 1.5 μm wavelength [10]. Advantages of this method are as follows. 1) The system has high stability and reproducibility because the feedback is negative. 2) The feedback loop can be designed accurately through computer simulation, as is the case when designing conventional analog feedback electronic circuits. 3) The magnitude of the FM noise can be reduced to a value lower than the quantum noise limit of the free-running laser, and, as was pointed out in [10], a linewidth as narrow as 58 mHz $\sim$ 2.9 Hz is possible. 4) Since a very low magnitude of the FM noise can be realized at the low Fourier frequency range, e.g., $f < 100$ MHz, this method is useful for highly-sensitive and narrow-bandwidth coherent optical measurements, and high-resolution laser spectroscopy.

In the present paper, a very low magnitude of the FM noise and a subkilohertz linewidth of the field spectrum were obtained by improving the performance of the negative electrical feedback loop. A CSP-type AlGaAs laser of 0.83 μm wavelength was used because it is considered a more appropriate laser device for negative electrical feedback. The reflection mode of a high-finesse Fabry-Perot interferometer was used for highly-sensitive and wide-band FM noise detection. Furthermore, optimum design of the feedback loop was carried out by using a computer simulation.

II. Experimental Setup and Characteristics of the Laser

An AlGaAs laser of 0.83 μm wavelength (CSP-type, Hitachi HL8314E) was used at room temperature (20.0°C). Its threshold current I_{th} was 56.5 mA at this temperature. The output optical intensity was 28 mW at the dc bias current I of 104 mA, i.e., at $I/I_{th} = 1.84$. The temperature of the heat sink was controlled by a Peltier electric cooler and a thermistor bridge, by which the temperature fluctuations were suppressed within 0.2 mK. Fig. 1 shows the experimental setup. All of the components in this setup were mounted on an optical bench to reduce the effect of mechanical vibration. Furthermore, they were installed in a carefully designed shield box, made of lead plates and glass wools, to reduce the effect of acoustic vibration. Ambient temperature of the components was stabilized within ± 0.5 K as a result of using this box. The slopes of resonance curves of two kinds of Fabry-Perot interferometers were used for the FM noise detection of the laser. By using the carefully designed shield box and the optical bench, the effects of ambient temperature fluctuations and acoustical and mechanical vibrations were sufficiently reduced so as to foster the use of the Fabry-Perot interferometers as stable frequency references throughout the present paper. One Fabry-Perot interferometer (FP1) was made of a cylindrical rod of fused silica, which was 3 cm long corresponding to the free spectral range of 3.45 GHz. Dielectric multilayers were coated on both ends of the rod, which gave a finesse of 25, i.e., the full width at half maximum (FWHM) of the resonance curve was 138 MHz. The second was a confocal Fabry-

Manuscript received April 4, 1989; revised August 18, 1989.

The authors are with the Graduate School at Nagatsuta, Tokyo Institute of Technology, Midori-ku, Yokohama 227, Japan.

IEEE Log Number 8932613.

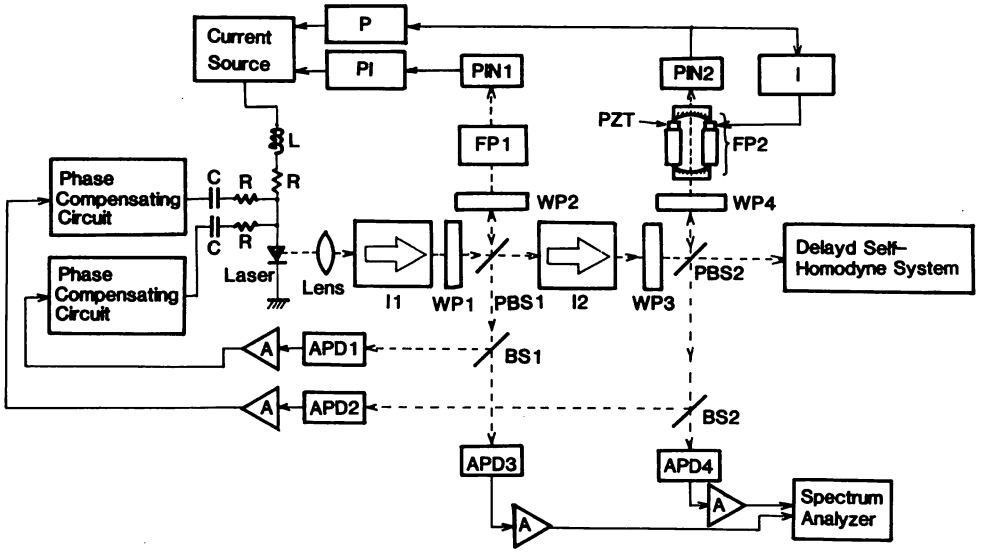

Fig. 1. Experimental setup. FP1 and FP2: Fabry-Perot interferometers with the finesse of 25 and 3500, respectively. I1 and I2: Optical isolator modules in which two Faraday isolators of 30 dB optical isolation were installed. WP1-WP4: Quarter-wave plates. PBS1 and PBS2: Polarizing beam splitters. BS1 and BS2: Beam splitters. APD1-APD4: Avalanche photodiodes. PIN1 and PIN2: p-i-n photodiodes. PI: PI-controller composed of a proportional amplifier and an integrator used to control the injection current of the laser. P: P-controller composed of a proportional amplifier used to control the injection current of the laser. I: I-controller composed of an integrator used to control the piezoelectric transducer (PZT) of FP2. All of the components were mounted on an optical bench, and were installed in a carefully designed shield box made of lead plates and glass wools. The feedback loop using the FP1 and APD1 was called the feedback loop 1), and that using the FP2 and APD2 was called the feedback loop 2) in the present paper.

Perot interferometer (FP2), for which a 5 cm long super-Invar cylinder was used as a spacer for the two concave mirrors. A cylindrical 2.5 mm long piezoelectric transducer (PZT) was fixed on one end of the spacer for fine adjustment of the interferometer length. Two concave mirrors were fixed on the spacer and the PZT by epoxy resin.

Fig. 2 shows the measured profile of the resonance curve of FP2. This figure represents a relation between the optical frequency and the light intensity reflected from FP2. For this measurement, a negative electrical feedback loop by using FP1 was applied to the free-running laser, by which its linewidth was reduced to 30 kHz in order to use it as a narrow-linewidth light source. It can be seen from this figure that the FWHM of the resonance curve was 850 kHz, which corresponded to a finesse of 3500. Highly-sensitive FM noise detection can be expected by using the very steep slope of the resonance curve of the high-finesse Fabry-Perot interferometer. Efficiency of the transmitted light from FP2, i.e., the intensity ratio between input and output lights of FP2, was 4 percent. On the other hand, that of the reflected light from FP2, i.e., the depth of the dip of the curve in Fig. 2 normalized to the input light intensity, was as high as 30 percent. The reason for the higher efficiency of the reflected light is that the reflected light contained a high-intensity light directly reflected from the input mirror of FP2. High efficiency of

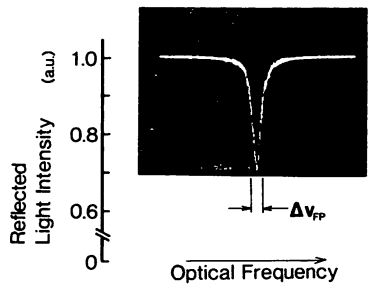

Fig. 2. The measured profile of the resonance curve of FP2. This curve represents a relation between the optical frequency and the light intensity reflected from FP2. For this measurement, the laser linewidth was preliminarily reduced to 30 kHz. The FWHM of this curve $\Delta\nu_{FP}$ was 850 kHz.

the reflected light was advantageous for sensitive FM noise detection. Two optical isolator modules (I1 and I2) were used to suppress the laser oscillation instability, which could be induced by injection of the reflected light from FP1 and FP2. Each module contained two Faraday isolators of 30 dB optical isolation.

Slow feedback loops were applied to the laser to reduce the drift of the laser frequency. That is, the injection current of the laser was controlled by a PI controller (a proportional amplifier and an integrator) and a P controller (a proportional amplifier). For this control, the transmitted lights from FP1 and FP2 were detected by p-i-n-photodiodes PIN1 and PIN2, respectively. The value of the

high-frequency cutoff of the PI controller and P controller were fixed to 200 Hz. Furthermore, in order to reduce the drift of the resonance frequency of the high-finesse FP2 induced by the ambient temperature fluctuations, the applied voltage for the PZT of FP2 was simultaneously controlled by an I controller (an integrator).

Faster feedback loops were simultaneously used for wide-band FM noise reduction. For this purpose, intensity fluctuations of the reflected light from FP1 and FP2, induced by the FM noise of the laser, were detected by avalanche photodiodes APD1 and APD2, respectively. The polarization of the light was controlled by four quarter-wave plates (WP1 ~ WP4) and two polarizing beam splitters (PBS1 and PBS2) to increase the light intensities incident to APD1 and APD2. Wide-band preamplifiers, passive phase compensating circuits, and bias-T circuits (the circuits composed of C, R, and L, as shown in Fig. 1) were connected in series to APD1 and APD2, and the injection current of the laser was controlled by the output signals from the bias-T circuits.

About 10 percent of the light intensities reflected from FP1 and FP2 were extracted from the feedback loops by beamsplitters BS1 and BS2 to measure the magnitude of the FM noise by using two avalanche photodiodes (APD3 and APD4) and a microwave spectrum analyzer (Anritsu, MS560J). This spectrum analyzer allowed the measurement of the power spectral density of the FM noise within the Fourier frequency range of 100 Hz $\leqq f \leqq$ 100 MHz. The values of the power spectral density measured by APD3 and APD4 were mutually compared and calibrated for precisely evaluating the FM noise. The transmitted light from PBS2 was used to measure the field spectral profile of the laser by a delayed self-homodyne technique by using a 2 km long single-mode fiber. Resolution of this measurement was 100 kHz [11].

Curve A of Fig. 3(a) shows the measured power spectral density $S_\nu(f)$ of the FM noise of the free-running laser. Curve B in this figure represents the sensitivity limit of this FM noise detection imposed by the laser IM noise, whose details will be discussed in Section III-B. A part of curve A at 100 kHz $\leqq f \leqq$ 100 MHz is composed of a white noise, which is due to the quantum noise induced by spontaneous emission and carrier density fluctuations. The flicker noise ($1/f$ noise) can be seen at $f <$ 100 kHz [12]. The profile of the field spectrum $I(\nu)$ of the free-running laser was simultaneously measured by the delayed self-homodyne technique. The result is shown by the solid curve in Fig. 3(b), from which it can be found that its FWHM ($\Delta\nu_{FR}$) was 4.5 MHz. On the other hand, this spectral profile can also be derived from the power spectral density of curve A in Fig. 3(a) by using the following formula [13]:

$$I(\nu) = 4 \cdot \mathrm{Re}\left[\int_0^\infty \exp\left\{i \cdot 2\pi(\nu_0 - \nu) \cdot \tau - 2 \cdot (\pi\tau)^2 \cdot \sigma_\nu^2(\tau)\right\} \cdot d\tau\right] \quad (1)$$

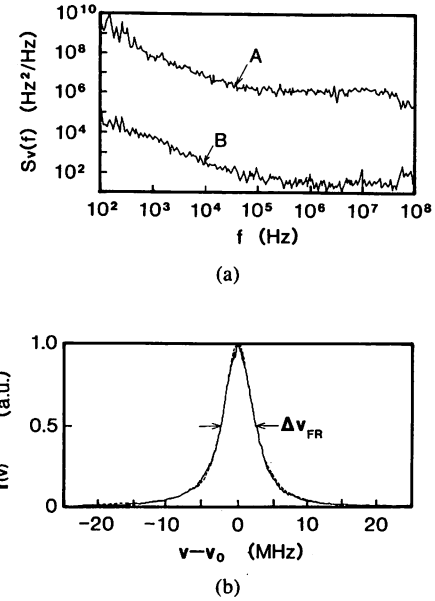

Fig. 3. (a) Curve A: power spectral density of the FM noise of the free-running laser measured by using FP1 and APD3. Curve B: the sensitivity limit of the FM noise detection by using FP1. This limit was estimated by the measured magnitude of the IM noise of the laser. (b) Solid curve: the profile of the field spectrum of the free-running laser measured by the delayed self-homodyne technique. Broken curve: the profile of the field spectrum of the free-running laser calculated by using curve A in Fig. 3(a), (1), and (2). The FWHM's of these two curves were $\Delta\nu_{FR}$ = 4.5 MHz.

where Re represents taking the real part of the complex number in the bracket, ν_0 is the nominal frequency of the laser, and $\sigma_\nu^2(\tau)$ is the variance given by

$$\sigma_\nu^2(\tau) = 2\int_0^\infty S_\nu(f) \cdot \frac{\sin^2(\pi f\tau)}{(\pi f\tau)^2} \cdot df. \quad (2)$$

Since the Fourier frequency range measurable by the microwave spectrum analyzer was 100 Hz $\leqq f \leqq$ 100 MHz, the upper and lower limits for the numerical integrals of (1) and (2) were not exactly ∞ and 0, respectively. They were 10 ms and 10 ns for (1), and 100 MHz and 100 Hz for (2), respectively. The broken curve in Fig. 3(b) represents the calculated result by using curve A in Fig. 3(a), (1), and (2). This curve agreed well with the solid curve. From this agreement, it can be confirmed that numerical integral based on (1) and (2) can be used for accurately estimating the narrow spectral profile which will be obtained by the experiments in Section IV.

The solid curves in Fig. 4 show the characteristics of direct frequency modulation of the laser, which was measured by a microwave network analyzer based on the method given in [10]. These characteristics can be interpreted as the complex transfer function $H_L(f)$ of the laser. This figure shows the measured values of $|H_L(f)|$ and arg $[H_L(f)]$. It is seen that these two quantities take almost constant values for a wide range of f. On the other hand, these characteristics of an InGaAsP laser of 1.5 μm wavelength were considerably different from those of Fig. 4 because, as shown in [10], $|H_L(f)|$ of the InGaAsP laser strongly depended on f in a very complicated manner

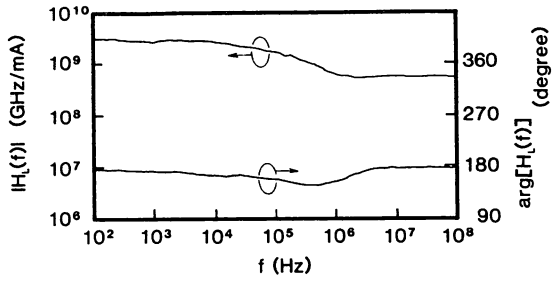

Fig. 4. Measured characteristics of direct frequency modulation of the laser at $I/I_{th} = 1.84$, which correspond to the complex transfer function $H_L(f)$ of the laser. Two curves represent the values of $|H_L(f)|$ and arg $[H_L(f)]$.

and the value of arg $[H_L(f)]$ changed as much as 180°. The fact that $|H_L(f)|$ and arg $[H_L(f)]$ of the present laser took almost constant values was advantageous for designing a wide-band negative electrical feedback loop for FM noise reduction. One of the reasons for reducing the FM noise to a far lower level than that of the previous work [10] was due to this advantageous property of the present laser.

III. Computer Simulation of the FM Noise Reduction

A. Transfer Function of a Fabry-Perot Interferometer

A Fabry-Perot interferometer served as one of the servo-control elements in the feedback loops in Fig. 1. Its transfer function $H_{FP}(f)$ corresponds to a relation between the modulated optical frequency incident into the interferometer and the modulated optical intensity emitted from the interferometer. This relation can be calculated by the method given in [10, Appendix A]. In the present paper, the transfer functions were calculated for the cases of using the reflected and transmitted light from the Fabry-Perot interferometer. Curves *A* and *B* in Fig. 5(a) and (b) represent the calculated transfer functions of the reflection mode and the transmission mode of the Fabry-Perot interferometer, respectively. In Fig. 5(a), the value of $|H_{FP}(f)|$ is given by normalizing to the value at $f = 0$. This figure shows that the FWHM ($\Delta\nu_{FP}$) of the resonance curve of the Fabry-Perot interferometer gives a high-frequency cutoff of the transfer function. Furthermore, it is seen that the value of the slope of curves *A* and *B* are different with respect to each other at $f \geqq \Delta\nu_{FP}$. They are −20 and −40 dB/decade, respectively. Due to this difference in the slopes between these modes, the transfer function of the reflection mode has a wider bandwidth than that of the transmission mode. The difference between the two modes has been briefly and qualitatively discussed in [14]. On the basis of our analysis, this difference can be summarized as follows. Comparing with the transmission mode, the reflection mode has an additional effect of temporally differentiating the optical frequency of the incident light, and this effect clearly appears at $f \geqq \Delta\nu_{FP}$. That is, the reflected light contains the high-intensity directly reflected light from the input mirror of the Fabry-Perot interferometer and also the transmitted light after the resonance inside the Fabry-Perot interferometer. Since the incident optical frequency varies nonadiabatically in the range of $f \geqq \Delta\nu_{FP}$, the former bears the present optical frequency, while the latter bears the past averaged optical frequency due to the resonance inside the interferometer. Therefore, the measurement of the reflection mode corresponds to measuring the difference between these present and past optical frequencies, and this difference can be approximated as the temporal differentiation of the optical frequency. On the other hand, the transmission mode does not have the differentiating effect because it does not contain the directly reflected light from the input mirror which serves as a reference for differentiation. Therefore, by this differentiating effect, the slope of the reflection mode is +20 dB/decade larger than that of the transmission mode at $f \geqq \Delta\nu_{FP}$. Furthermore, Fig. 5(b) shows that the change in the value of arg $[H_{FP}(f)]$ of the transmission mode is as large as −180°, while that of the reflection mode is only −90°. This difference is also due to the differentiating effect.

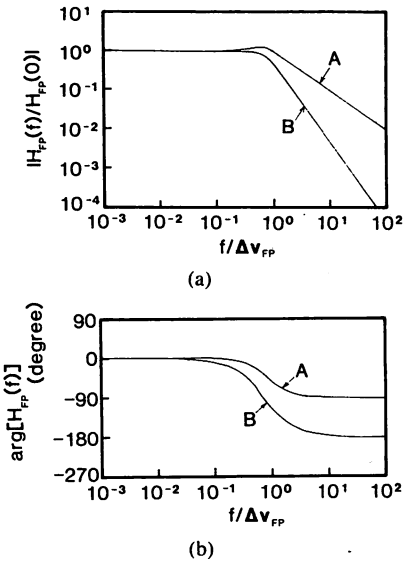

Fig. 5. Calculated transfer function of a Fabry-Perot interferometer $H_{FP}(f)$ represented as a function of $f/\Delta\nu_{FP}$, where $\Delta\nu_{FP}$ is the FWHM of the resonance curve of the Fabry-Perot interferometer. (a) and (b) represent the values of $|H_{FP}(f)|$ and arg $[H_{FP}(f)]$, respectively. Curves *A* and *B* represent the results for the reflection and transmission modes, respectively.

To experimentally confirm this difference, the free-running laser was used as a white FM noise generator. That is, the power spectral density of the FM noise of the free-running laser was measured within the range of 1 MHz $\leqq f \leqq$ 1 GHz by using FP1 in Fig. 1 and a high-frequency microwave spectrum analyzer. The high-frequency cutoff (= $\Delta\nu_{FP}$ = 140 MHz) of the transfer function of FP1 fell within this Fourier frequency range. Measured results are shown by curves *A* and *B* of Fig. 6 for the reflection and the transmission modes, respectively. Although the FM noise of the laser is a white noise within this Fourier frequency range, curves *A* and *B* have slopes of −20 and −40 dB/decade, respectively, at $f \geqq \Delta\nu_{FP}$. The difference between these slopes can be attrib-

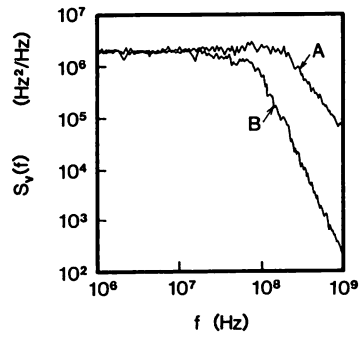

Fig. 6. Power spectral density of the free-running laser, which was measured by using the reflection (curve *A*) and transmission (curve *B*) modes of FP1 within the range of 1 MHz $\leqq f \leqq$ 1 GHz.

uted to the characteristics given by Fig. 5(a), from which the characteristics of the Fabry–Perot interferometer of Fig. 5(a) was confirmed experimentally. Since the transfer function of the reflection mode has a wider bandwidth and a smaller phase change than that of the transmission mode, it can be concluded that using the reflection mode could be advantageous for wide-band FM noise detection and for designing a wide-band negative electrical feedback loop.

B. Sensitivity of FM Noise Detection

The discussion on the limit of FM noise reduction by negative electrical feedback has been given in [10], which can be summarized as follows. The effect of negative electrical feedback can be expressed by the following quantum-mechanical Langevin equation of motion:

$$\delta\nu(t) = \Gamma_s(t) + \Gamma_c(t) - \int_0^\infty h(\tau) \cdot \{\delta\nu(t-\tau) + \Gamma_n(t-\tau)\} \cdot d\tau, \quad (3)$$

where $\delta\nu(t)$ is the frequency fluctuation at time t. Langevin forces Γ_s and Γ_c represent the two quantum FM noise sources for the free-running laser due to spontaneous emission and carrier density fluctuations, respectively. The ratio of the magnitudes between these two quantum noise sources Γ_c/Γ_s is given by α^2, where α is a linewidth broadening factor [15]. The convolution integral on the right-hand side of this equation represents the effect of negative electrical feedback, where $\delta\nu(t-\tau)$ is the detected FM noise, $\Gamma_n(t-\tau)$ is the noise magnitude generated from the feedback loop, and $h(\tau)$ is the impulse response of the feedback loop. The Fourier transform of (3) gives

$$F(f) = \frac{(1+\alpha^2)}{1+H(f)} \cdot \Pi_s(f) - \frac{H(f)}{1+H(f)} \cdot \Pi_n(f) \quad (4)$$

where F, Π_s, $\alpha^2\Pi_s$, Π_n, and H represent the Fourier transform of $\delta\nu$, Γ_s, Γ_c, Γ_n, and h, respectively. In this equation, the value of the first term of the RHS approaches zero for infinite gain of the feedback loop ($|H(f)| \rightarrow \infty$), while that of the second term approaches $|\Pi_n|$. This means that the contributions from the two quantum noise sources can be suppressed by a high feedback gain and that the magnitude of the FM noise can be ultimately reduced to a value limited by the noise generated from the feedback loop. In other words, if a high-gain, low-noise feedback loop is employed, the magnitude of the FM noise can be reduced to a value which is lower than the quantum FM noise level of the free-running laser.

It was found by preliminary measurements that the principal noise source generated from the feedback loop in Fig. 1 was the intensity fluctuation (IM noise) of the laser itself. For example, in the case of using FP1, the FM noise of the laser was converted to the intensity fluctuation of the light reflected from FP1, and was detected by APD1. This result of FM noise detection was given by curve *A* of Fig. 3(a). However, the intensity of the light incident into APD1 also fluctuated due to the intrinsic IM noise of the laser. The magnitude of this fluctuation was far larger than those of other noises generated from electronic circuits in the feedback loop and that of the resonance frequency fluctuation of FP1. Therefore, it was confirmed that this fluctuation corresponded to $|\Pi_n(f)|$ of (4), which limited the sensitivity of FM noise detection as well as FM noise reduction. The magnitude of IM noise introduced into this FM noise detection system was measured by using APD3 and by placing a flat mirror in front of FP1. The measured result of FM noise detection limit imposed by this IM noise is given by curve *B* of Fig. 3(a). The ratio between the values of curves *A* and *B* in this figure is about 1×10^4, from which it can be expected that the FM noise is reduced to 1×10^{-4} times that of the free-running laser by the feedback loop using the reflection mode of FP1 [feedback loop 1)]. On the other hand, as will be explained in Section IV, after the FM noise of the free-running laser was preliminarily reduced by feedback loop 1), the magnitude of residual FM noise was measured by APD3. The result is given by curve *B* in Fig. 10. The limit of this residual FM noise reduction is given by curve *D* in this figure. As was the case for curve *B* in Fig. 3(a), this limit was also estimated from the magnitude of IM noise of the laser, which was measured by APD4 under the condition of the frequency control by the feedback loop 1). For this IM noise measurement, a flat mirror was also placed in front of FP2. The measured value of the power spectral density of the IM noise was stored in a personal computer. This value was then divided by the transfer function of FP2 [i.e., curve *A* of Fig. 5(a)] by using this computer. Curve *D* represents the result of this division. The ratio between the values of curves *B* and *D* is also about 1×10^4, which means that FM noise reduction of about 1×10^{-8} that of the free-running laser can be expected if the residual FM noise of curve *B* is reduced by also employing the feedback loop using the reflection mode of FP2 [feedback loop 2)]. In the discussion given above, it was assumed that the magnitude of the IM noise did not change even if the negative electrical feedback was applied to the laser for FM noise

reduction. Validity of this assumption will be given at the end of Section IV.

C. Network Analysis of the Feedback Loop and Computer Simulation of FM Noise Reduction

The normalized residual FM noise can be defined as a ratio between the power spectral densities of the free-running laser [$S_{\nu FR}(f)$] and of the laser under negative electrical feedback [$S_{\nu FB}(f)$]. This is given by [10]

$$\frac{S_{\nu FB}(f)}{S_{\nu FR}(f)} = \left|\frac{1}{1 + H(f)}\right|^2 \tag{5}$$

where $H(f)$ represents the open loop transfer function of the feedback loop appeared in (4). To minimize the normalized residual FM noise, optimum design of the feedback loop is necessary so as to maximize the value of $|H(f)|$. Network analysis was employed as a powerful tool for this optimum design, whose details are described in the following.

The loop transfer function $H(f)$ of feedback loop 1) or 2) is given by

$$H = H_T \cdot H_L \cdot H_{FP} \cdot H_A \cdot H_P \cdot H_D \tag{6}$$

where H_T, H_L, H_{FP}, H_A, H_P, and H_D are transfer functions of the bias-T circuit, FM response of the laser, the Fabry–Perot interferometer, the APD with a preamplifier, the phase compensating circuit, and the delay of signal propagation in the feedback loop, respectively. The transfer function of the circuit composed of the C and R in the bias-T circuit of Fig. 1 is expressed as

$$H_T(f) = \frac{1}{1 + f_T/if}. \tag{7}$$

For feedback loops 1) and 2), the values of f_T in this equation were fixed to 200 Hz. This value of f_T gave a -3 dB low-frequency cutoff of the feedback loop. The measured values of Fig. 4 were used as the transfer function of the FM response of the laser $H_L(f)$. The calculated values of Fig. 5(a) and (b) were used as the transfer functions of the Fabry–Perot interferometers $H_{FP}(f)$. Since the bandwidths of APD1, APD2, and the preamplifier were sufficiently wider than those of the other transfer functions in (6), the value of $H_A(f)$ was assumed to be constant at 100 Hz $\leqq f \leqq$ 100 MHz. The transfer function of the phase compensating circuit connected to the preamplifier is expressed as

$$H_P(f) = \frac{1 + if/f_1}{1 + if/n_1 f_1} \cdot \frac{n_2 + if/f_2}{1 + if/f_2}. \tag{8}$$

The first and the second parts of the RHS of this equation represent the effect of phase-lag compensation and phase-lead compensation, respectively. The values of the parameters f_1, n_1, f_2, n_2 in this equation were adjusted for the optimum design to maximize the $|H(f)|$. The transfer function representing the delay of signal propagation in the feedback loop is expressed as

$$H_D(f) = \exp(-i2\pi f t_D) \tag{9}$$

where t_D represents the total delay time, which included all contributions from the lengths of the electrical cables and optical paths and those of the APD and preamplifier. Measured values of t_D for feedback loops 1) and 2) were 8.4 and 10 ns, respectively.

The loop transfer function of the feedback loop could be calculated by substituting the value of the transfer function of each servo element into (6). This loop transfer function could also be directly measured by inserting a microwave network analyzer between the phase compensating circuit and the bias-T circuit in Fig. 1. Since these two results agreed well with each other, it was concluded that the network analysis was accurate enough. [The validity of this conclusion was proven by comparing curves A (calculated result) and B (measured result) in Fig. 9 of Section IV. Good agreement can be actually seen between these two curves for the optimized feedback loop 1)].

Fig. 7 shows the results of computer simulation for estimating the magnitude of the normalized residual FM noise by using the network analysis based on (5) ~ (9). Since the purpose of this computer simulation was to investigate dependence of normalized residual FM noise on the characteristics of the reflection mode and the transmission mode of the Fabry–Perot interferometer, it was assumed for simplicity that only one feedback loop was applied to the laser by using one Fabry–Perot interferometer. Therefore, the magnitude of the normalized residual FM noise given by this figure is different from that of the experimental result (Fig. 10) obtained by using two feedback loops. However, the results of the following discussion could offer useful information for designing actual feedback loops. Fig. 7(a) and (b) show calculated results obtained by using the reflection and transmission modes of a Fabry–Perot interferometer, respectively. Curves A, B, C, and D in this figure are the results obtained by assuming the FMHM of the resonance curve of the Fabry–Perot interferometer as $\Delta\nu_{FP}$ = 100, 10, 1, and 0.1 MHz, respectively. To obtain the four curves in Fig. 7(a), the values of the parameters in (8) were optimally adjusted for maximizing the value of $|H(f)|$. Their optimized values fell within the ranges of 50 MHz $\leqq f_1 \leqq$ 90 MHz, $0.1 \leqq n_1 \leqq 0.5$, $f_2 = \infty$, and $n_2 = 1$. For the four curves in Fig. 7(b), the optimized values were within the ranges of 100 kHz $\leqq f_1 \leqq$ 40 MHz, $0.2 \leqq n_2 \leqq 0.5$, 300 kHz $\leqq f_2 \leqq$ 50 MHz, and $0.3 \leqq n_2 \leqq 0.6$. It is seen by comparing four curves in Fig. 7(a) that the magnitude of the normalized residual FM noise decreased by decreasing the value of $\Delta\nu_{FP}$. This is because a smaller value of $\Delta\nu_{FP}$ gave a steeper slope of the resonance curve of the Fabry–Perot interferometer, which resulted in higher sensitivity of FM noise detection and higher gain of the feedback loop. On the contrary to the case of Fig. 7(a), comparison between the four curves in Fig. 7(b) shows that the normalized residual FM noise increased with decreasing $\Delta\nu_{FP}$. This was attributed to the narrower bandwidth of the transfer function of the transmission mode of the Fabry–Perot interferometer. That is, because the bandwidth of the $H_{FP}(f)$ of the transmission mode

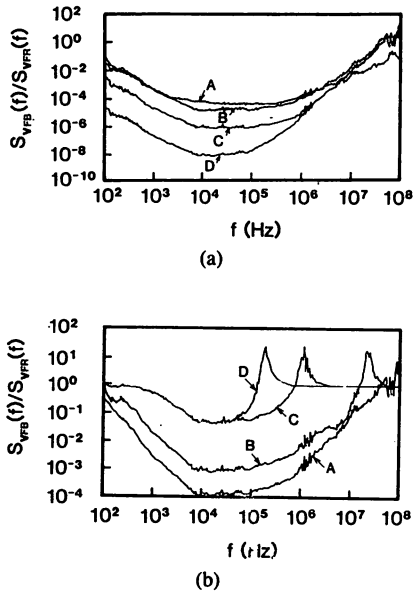

Fig. 7. Results of computer simulation for estimating the magnitude of the normalized residual FM noise. (a) and (b) represent the results for the reflection and the transmission modes, respectively. Curves *A*, *B*, *C*, and *D* are the results obtained by assuming the FWHM of the resonance curve of the Fabry–Perot interferometer as $\Delta\nu_{FP}$ = 100, 10, 1, and 0.1 MHz, respectively.

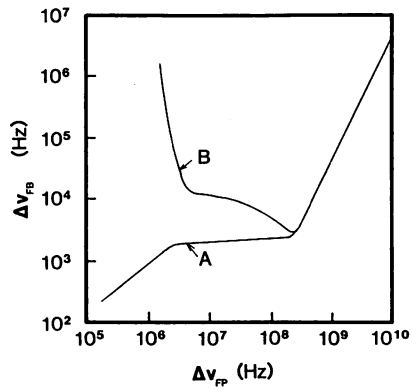

Fig. 8. Results of computer simulations for a relation between the FWHM ($\Delta\nu_{FP}$) of the Fabry–Perot interferometer and the FWHM ($\Delta\nu_{FB}$) of the field spectrum of the laser under feedback. Curves *A* and *B* represent the results for the reflection and transmission modes, respectively.

was narrower and the change of arg $[H_{FP}(f)]$ was larger, the feedback loop became, then, unstable at the Fourier frequency of taking arg $[H(f)] = -180°$ if the feedback loop gain was increased excessively. Resonant peaks can actually be seen on the four curves in Fig. 7(b), which represent this instability. To maintain the heights of these peaks low enough to stabilize the feedback loop, the allowable maximum of the feedback loop gain was limited, which limited the magnitude of the FM noise reduction. Since the bandwidth of the reflection mode was wider and the change in arg $[H_{FP}(f)]$ was smaller, the effect of the limited bandwidth was not clearly visible in Fig. 7(a). Therefore, it can be concluded that the use of reflection mode realizes a wider bandwidth for FM noise reduction. This wider bandwidth increased the allowable maximum of the feedback loop gain, by which the lower magnitude of the normalized residual FM noise was realized by using the reflection mode.

The profile of the field spectrum $I(\nu)$ of the laser under negative electrical feedback can be calculated by using the curves in Fig. 7, curve *A* in Fig. 3(a), and (1) and (2). Fig. 8 shows a relation between the FWHM ($\Delta\nu_{FP}$) of the resonance curve of the Fabry–Perot interferometer and the FWHM ($\Delta\nu_{FB}$) of the field spectrum of the laser under feedback obtained by this calculation. Curves *A* and *B* in this figure represent the results for the reflection and the transmission modes of the Fabry–Perot interferometer, respectively. The values of $\Delta\nu_{FB}$ on both curves decreased with decreasing $\Delta\nu_{FP}$ if $\Delta\nu_{FP} \geqq 230$ MHz. These decreases were attributed to the increases in the sensitivity of FM noise detection and in the feedback loop gain, which resulted because the slope of the resonance curve of the Fabry–Perot interferometer became steeper by decreasing the $\Delta\nu_{FP}$. However, at $\Delta\nu_{FP} < 230$ MHz, curve *B* shows that the $\Delta\nu_{FB}$ increased by decreasing the $\Delta\nu_{FP}$. This was because the allowable maximum of the feedback loop gain was limited by the narrower bandwidth of the transfer function of the transmission mode of the Fabry–Perot interferometer, as was explained for Fig. 7(b). By this limited gain, the profile of curve *B* has a V-shape. This V-shaped profile has been presented in [10, Fig. 17] as a result of simpler calculations. On the other hand, curve *A* shows that $\Delta\nu_{FB}$ decreased monotonously by decreasing $\Delta\nu_{FB}$ because the reflection mode of the Fabry–Perot interferometer has a larger gain and a wider bandwidth. From the result given by curve *A*, a subkilohertz linewidth of the laser can be expected by using the reflection mode of a high-finesse Fabry–Perot interferometer such as FP2 (i.e., $\Delta\nu_{FP} < 1$ MHz).

IV. Experiments on FM Noise Reduction

By following the discussions of the Section III, experiments on FM noise reduction were carried out by using negative electrical feedback. The reflection mode of the Fabry–Perot interferometer was employed to realize a higher loop gain than that of the previous experiment [10]. As will be pointed out later, using the reflection mode of FP2 gave an essential contribution to the FM noise reduction in the present work. Prior to using feedback loop 2), auxiliary feedback loop 1) was applied to the free-running laser to reduce preliminarily the FM noise. This feedback loop had a wider bandwidth than that of feedback loop 2) because of a larger value of the $\Delta\nu_{FP}$ of FP1. To maximize the gain of the feedback loop 1), the values of the parameters in (8) were optimally adjusted. They were $f_1 = 2.5$ MHz, $n_1 = 0.14$, $f_2 = \infty$, and $n_2 = 1$. The -3 dB high-frequency cutoff of the feedback loop 1) depended on the value of f_1. Curves *A* and *B* in Fig. 9(a) and (b) show the calculated and measured values of the loop transfer function using the optimized phase compensating circuit, respectively. These two curves agree with each other, from which high accuracy of the network analysis based on (6)–(9) can be confirmed. Curves *C* in Fig. 9(a) and (b) represent the measured values without

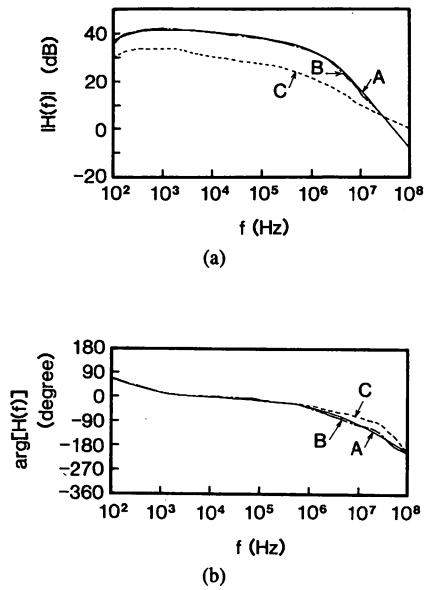

Fig. 9. (a) and (b) represent the values of $|H(f)|$ and arg $[H(f)]$ of the feedback loop 1), respectively. Curves *A* and *B*: calculated and measured results, respectively, for which the optimally designed phase compensating circuit was used. Curve *C*: measured result without any phase compensating circuits.

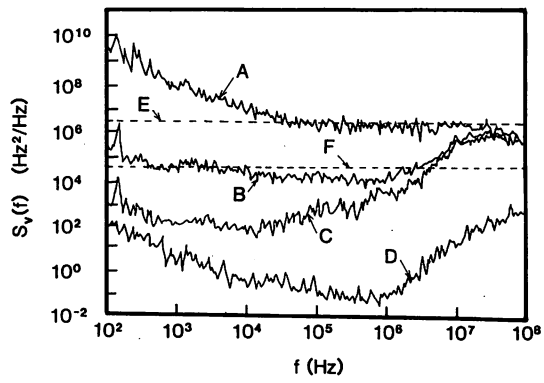

Fig. 10. Measured power spectral density of the FM noise of the laser. Curve *A*: FM noise of the free-running laser, which is identical to curve *A* in Fig. 3(a). Curve *B*: residual FM noise of the laser under auxiliary feedback by using the feedback loop 1). Curve *C*: residual FM noise of the laser under feedback by using both the feedback loops 1) and 2). Curve *D*: the limit of the residual FM noise detection by FP2 under the auxiliary feedback by the feedback loop 1). This limit was estimated by the measured magnitude of the IM noise of the laser. Curve *E*: magnitude of the white noise component in the curve *A*, which is due to the spontaneous emission and carrier density fluctuations. Curve *F*: minimum of the magnitude of the quantum FM noise due to spontaneous emission, which was estimated by using curve *E* and $\alpha = 9.0$.

using the phase compensating circuit. It is seen by comparing curves *B* and *C* that the loop gain could be increased 10 dB and approached as high as 40 dB by using this phase compensating circuit while the loop bandwidth was slightly decreased. It can be seen from (5) that this value of the gain was almost as high as that required to reduce the FM noise of the free-running laser [curve *A* of Fig. 3(a)] to the value limited by the IM noise [the curve *B* of Fig. 3(a)], from which the usefulness of the phase compensating circuit can be confirmed. Curve *B* in Fig. 9 shows that the high-frequency cutoff at which the loop gain decreased to 0 dB was 40 MHz. It means that the FM noise can be reduced within the Fourier frequency range as wide as 40 MHz in spite of the fact that the −3 dB high-frequency cutoff of the feedback loop was about 200 kHz. This frequency range, 40 MHz, depended on the value of the delay time t_D of the signal propagation in feedback loop 1).

Another phase compensating circuit was also used for feedback loop 2). Since the precise measurement of its loop transfer function was rather difficult because of a very narrow FWHM of the resonance curve of FP2, fully quantitative measurements of the loop transfer function were not carried out. Design of the phase compensating circuit for this loop was made empirically, by which the optimized values of the parameter in (8) were $f_1 = 20$ kHz, $n_1 = 0.14$, $f_2 = \infty$, and $n_2 = 1$. The 3 dB high-frequency cutoff of feedback loop 2) depended on the value of f_1. However, as was the case of feedback loop 1), the loop gain decreased to 0 dB at the Fourier frequency larger than this value of f_1.

Fig. 10 shows the experimental results of FM noise reduction. Curve *A* represents the power spectral density of the FM noise of the free-running laser, which is identical to curve *A* of Fig. 3(a). Curve *B* represents the residual FM noise of the laser under the condition of an auxiliary frequency control by using feedback loop 1). This FM noise was measured by using FP1 and APD3. Curve *C* is the result obtained by applying feedback loop 2) to the preliminarily controlled laser. This FM noise was measured by using FP2 and APD4. Curve *D* represents the limit of the residual FM noise detection by FP2 under the condition of auxiliary feedback loop 1). As was described in Section III-B, this limit was estimated from the measured magnitude of the IM noise of the laser because the main contribution to this limit was found to be the intrinsic IM noise of the laser. The power spectral density of this IM noise was carefully measured by APD4 in Fig. 1. After this value of the power spectral density was stored into a personal computer, it was divided by the transfer function of FP2, i.e., the curve *A* of Fig. 5(a), by using this computer. Curve *D* represents the result of this division. The reason for the increase in the value of curve *D* at $f \geqq 1$ MHz was the result of this division. That is, this increase was due to the limited bandwidth of the transfer function of FP2 used for the residual FM noise detection. Curve *D* gave the limit of FM noise reduction for the case of using both feedback loops 1) and 2).

It can be seen by comparing curves *A* and *B* that the auxiliary feedback loop 1) reduced the FM noise within the range of $f \leqq 40$ MHz. This range agreed with the range of curve *B* in Fig. 9, where the gain of feedback loop 1) was larger than 0 dB. It can be also seen by comparing curves *B* and *C* that further reductions of the FM noise were realized by feedback loop 2) within the range of $f \leqq 5$ MHz, which means that the gain of feedback loop 2) was larger than 0 dB within this range. The broken line *E* represents the magnitude of the white noise component in curve *A*, which corresponded to the value of $|(1$

$+ \alpha^2) \cdot \Pi_s|$ of (4) due to the spontaneous emission and carrier density fluctuations. Since the maximum of the linewidth broadening factor α of the laser used for the present experiments has been estimated as 9.0 (the open circle in Fig. 4A of [15]), the minimum of the $|\Pi_s|$ in (4) can be estimated from this value of α and the broken line *E*. The result is given by the broken line *F*. The value of curve *C* was lower than that of line *F* in the range of 100 Hz $\leqq f \leqq$ 4.4 MHz, which means that the magnitude of the FM noise in this range was reduced to a value lower than the quantum FM noise level of the free-running laser. This experimental result supports the validity of the result of theoretical discussion of Section III-B. Especially at 100 Hz $\leqq f \leqq$ 1 kHz, it is seen by comparing curves *A* and *C* that the magnitude of the FM noise was reduced to as low as $1 \times 10^{-7} \sim 1 \times 10^{-6}$ that of the free-running laser.

At $f <$ 100 Hz, slow-frequency fluctuations were also reduced by the PI and P controls by using the transmission modes of FP1 and FP2. The square root of the Allan variance $\sigma_A^2(\tau)$ of these fluctuations was measured because it has been known that the Allan variance is a more accurate measure for evaluating a slow-frequency fluctuation [16] than the power spectral density. The Allan variance real-time processing system was used for this measurement [17]. The measured value was $1 \times 10^{-12} \leqq \sigma_A(\tau) \leqq 1 \times 10^{-11}$ at the integration time of 10 ms $\leqq \tau \leqq$ 100 s. The value of the power spectral density was derived from the $\sigma_A(\tau)$ by using a conversion formula [18], and the result was $1 \times 10^5 f^{-1} \leqq S_\nu(f) \leqq 1 \times 10^7 f^{-1}$ at 10 mHz $\leqq f \leqq$ 100 Hz, which was about 1×10^{-6} that of the free-running laser. Since these slow fluctuations were sufficiently reduced, feedback loops 1) and 2) were kept very stable and the very-low FM noise level given by curve *C* was also maintained for more than 3 h. Furthermore, it was also confirmed that these slow fluctuations were low enough so that the estimated result of the very narrow field spectrum given below (Fig. 11) was independent of them.

A very narrow linewidth of the field spectrum of the laser can be expected with such a low magnitude of the FM noise. When the field spectral profile under feedback was measured by the delayed self-homodyne system in Fig. 1, periodical side lobes were clearly seen on this profile [19]. It was because the linewidth of the field spectrum was far narrower than the resolution of this system (= 100 kHz), which means that the FWHM of the field spectrum under feedback cannot be accurately evaluated by the presently used delayed self-homodyne system. Therefore, instead of using this system, the FWHM was estimated by calculating the field spectral profile $I(\nu)$ by using curves *B* and *C* of Fig. 10, and (1) and (2). The value of FWHM estimated from the curve *B* was 30 kHz. Curve *A* in Fig. 11(a) represents the field spectral profile estimated from curve *C* in Fig. 10. The unit of the vertical axis in this figure is in dB. Curve *B* represents the profile of the free-running laser, which is identical to the broken curve in Fig. 3(b). It can be seen by comparing curves *A* and *B* in this figure that the effect of feedback loop appears in the range of $|\nu - \nu_0| \leqq$ 40 MHz, which corresponds to the Fourier frequency range in which the gain of the feedback loop 1) was larger than 0 dB. Several low-level side lobes on curve *A* were caused by the roughness of curve *C* in Fig. 10. Since the linewidth of curve *A* is too narrow to measure, its central part was magnified and was shown by Fig. 11(b). A linear scale was employed for the vertical axis of this figure. The FWHM value of this spectral profile was estimated from this figure as $\Delta\nu_{FB}$ = 560 Hz. This value of FWHM could give, to the authors' knowledges, one of the narrowest linewidths which have been documented so far.

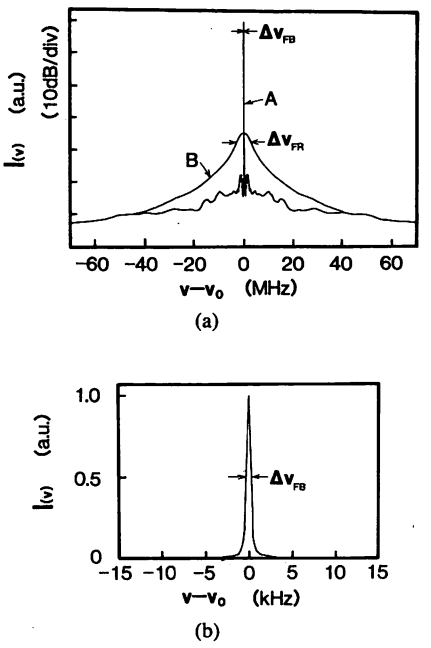

Fig. 11. (a) Profile of the field spectrum of the laser. ν_0 is the nominal optical frequency of the laser. Curve *A*: the result under feedback using feedback loops 1) and 2), which was estimated by using curve *C* in Fig. 10. Curve *B*: the result of the free-running laser, which is identical to the broken curve in Fig. 3(b). (b) Magnified profile of the central part of curve *A* in (a). The FWHM ($\Delta\nu_{FB}$) is measured to be 560 Hz from this profile.

Curve *C* in Fig. 11 has a resonant peak at f = 150 Hz, which was caused by a low-level residual acoustic vibration and a higher harmonic of the ac electric power source for electronic circuits. It was found that the FWHM of the field spectrum of Fig. 11(b) was slightly increased by this peak. Narrower linewidth can be expected by more careful acoustic shield and rejection of the higher harmonic of the ac electric power source, and finally, the magnitude of the FM noise can be reduced to the value given by curve *D* of Fig. 11 by further improvements of the performances of the feedback loops.

The −3 dB high-frequency cutoff of the feedback loop 2) was 20 kHz, which was determined by the value of f_1 of (8). This feedback loop became unstable when this value was increased to far larger than 20 kHz. It was found that this instability was induced because the gain of feedback loop 1) was decreased to 0 dB at a Fourier frequency as low as 40 MHz, as was shown by curve *B* in Fig. 9.

From this limited bandwidth of feedback loop 1), the −3 dB high-frequency cutoff of feedback loop 2) was also limited to 20 kHz to maintain this loop stably enough. Since this value of −3 dB high-frequency cutoff was smaller than the value of FWHM $\Delta\nu_{FP}$ (= 850 kHz) of FP2, one may think that feedback loop 2) did not fully utilize such advantageous characteristics of the reflection mode as presented by Figs. 5 and 7. However, as was shown by curve C in Fig. 11, this feedback loop had a gain larger than 0 dB for a Fourier frequency up to 5 MHz, which was larger than the value of the high-frequency cutoff (= $\Delta\nu_{FP}$) of the transfer function of FP2. Therefore, when the transmission mode of FP2 was used in a preliminary experiment instead of using the reflection mode, the excessively increased gain of feedback loop 2) induced an instability and a resonant peak appeared, as was shown by Fig. 7(b). From the comparison between this preliminary experimental result and curve C of Fig. 11, it was confirmed that the advantageous characteristics of the reflection mode of FP2 gave an essential contribution to reduce the magnitude of the FM noise to as low as $1 \times 10^{-7} \sim 1 \times 10^{-6}$ that of the free-running laser.

For FM noise detection under the condition of feedback, the error signals of the feedback loops, i.e., intensity fluctuations of the reflected lights from FP1 and FP2 induced by the FM noise were extracted from the feedback loops by using BS1 and BS2 of Fig. 1, and they were detected by APD 3 and APD 4. Therefore, if the magnitude of the IM noise of the laser was drastically increased by the feedback for the FM noise reduction, the inaccuracy of the FM noise detection could be increased, and the estimated limit of the FM noise reduction may become invalid. To check this possibility, a simultaneous measurement of the magnitude of the IM noise was carried out under a condition of frequency control by using the other APD placed between PBS2 and the delayed self-homodyne system in Fig. 1. As a result of this measurement, it was found that the increase in the IM noise under feedback using both the feedback loops 1) and 2) was within 60 percent that of the free-running laser. Thus, it was confirmed that the increase in the magnitude of the IM noise did not give any significant effects on the FM noise detection. Such a negligible increase in the magnitude of the IM noise has been discussed theoretically in Appendix B of [10]. The validity of this discussion was confirmed by the present paper.

V. Summary

FM noise in an AlGaAs laser was reduced by negative electrical feedback at the Fourier frequency range of $f \leqq 40$ MHz. It was confirmed that the magnitude of the FM noise was reduced to the value lower than the quantum noise level of the free-running laser at the Fourier frequency range of 100 Hz $\leqq f \leqq$ 4.4 MHz. Especially, the magnitude of the FM noise was as low as $1 \times 10^{-7} \sim 1 \times 10^{-6}$ that of the free-running laser at 100 Hz $\leqq f \leqq$ 1 kHz. The FWHM of the field spectrum was reduced to 560 Hz.

Major factors necessary for realizing such a low-level FM noise and a subkilohertz linewidth can be summarized as follows. 1) The laser had almost constant FM response characteristics for a wide Fourier frequency range. 2) High sensitivity of the FM noise detection and high gain of the feedback loop were obtained by using a high-finesse Fabry–Perot interferometer. 3) Use of the reflection mode of the high-finesse Fabry–Perot interferometer (FP2) improved the bandwidth and the sensitivity of the FM noise detection. 4) Results of optimum design of the feedback loops by a careful computer simulation were utilized for actual assembly of the electronic circuits of the feedback loops.

Further FM noise reduction and narrower linewidth of the field spectrum can be expected by decreasing the delay time of the feedback loop and by rejecting residual acoustic vibrations and electronic noises.

Acknowledgment

The authors would like to express their thanks to Dr. L. Hollberg of the National Institute of Standards and Technology for his valuable comments on the use of a high-finesse Fabry–Perot interferometer. They also thank C.-H. Shin of the Graduate School at Nagatsuta, Tokyo Institute of Technology, for his careful reading of the manuscript.

References

[1] Ch. Salomon, D. Hills, and J. L. Hall, "Laser stabilization at the millihertz level," *J. Opt. Soc. Amer. B*, vol. 5, pp. 1576–1587, 1988.

[2] For example, see M. Ohtsu and T. Tako, "Coherence in semiconductor lasers," in *Progress in Optics XXV*, E. Wolf, Ed. Amsterdam, The Netherlands: Elsevier, 1988, pp. 191–278, and references therein.

[3] For example, see M. Ohtsu, "Realization of ultrahigh coherence in semiconductor lasers by negative electrical feedback," *J. Lightwave Technol.*, vol. 6, pp. 245–256, 1988, and references therein.

[4] M. Ohtsu and S. Araki, "Using a 1.5 μm DFB InGaAsP laser in a passive ring cavity-type fiber gyroscope," *Appl. Opt.*, vol. 26, pp. 464–470.

[5] M. Hashimoto and M. Ohtsu, "Experiments on a semiconductor laser pumped rubidium atomic clock," *IEEE J. Quantum Electron.*, vol. QE-23, pp. 446–451, 1987.

[6] J. L. Picque, "Hyperfine optical pumping of a cesium atomic beam, and applications," *Metrologia*, vol. 13, pp. 115–119, 1977.

[7] D. Sesko, C. G. Fan, and C. E. Wieman, "Production of a cold atomic vapor using diode-laser cooling," *J. Opt. Soc. Amer. B*, vol. 5, pp. 1225–1227, 1988.

[8] N. A. Olsson and J. P. van der Ziel, "Performance characteristics of 1.5 μm external cavity semiconductor lasers for coherent optical communication," *J. Lightwave Technol.*, vol. LT-5, pp. 510–515, 1987.

[9] M. Ohtsu and S. Kotajima, "Linewidth reduction of a semiconductor laser by electrical feedback," *IEEE J. Quantum Electron.*, vol. QE-21, pp. 1905–1912, 1985.

[10] M. Ohtsu and N. Tabuchi, "Electrical feedback and its network analysis for linewidth reduction of a semiconductor laser," *J. Lightwave Technol.*, vol. 6, pp. 357–369, 1988.

[11] T. Okoshi, K. Kikuchi, and A. Nakayama, "Novel method for high resolution measurement of laser output spectrum," *Electron. Lett.*, vol. 16, pp. 630–631, 1980.

[12] M. Ohtsu and S. Kotajima, "Derivation of the spectral width of a 0.8 μm AlGaAs laser considering $1/f$ noise," *Japan. J. Appl. Phys.*, vol. 23, pp. 760–764, 1984.

[13] A. Yariv, *Quantum Electronics*, 2nd ed. New York: Wiley, 1975, sect. 13.3.

[14] R. W. P. Drever, J. L. Hall, F. V. Kowalski, J. Hough, G. M. Ford, A. J. Munley, and E. Ward, "Laser phase and frequency stabilization using an optical resonator," *Appl. Phys. B*, vol. 31, pp. 97–105, 1983.

[15] M. Osiński and J. Buus, "Linewidth broadening factor in semiconductor lasers—An overview," *IEEE J. Quantum Electron.*, vol. QE-23, pp. 9-29, 1987.
[16] D. W. Allan, "Statistics of atomic frequency standards," *Proc. IEEE*, vol. 54, pp. 221-230, 1966.
[17] K. Kuboki and M. Ohtsu, "The Allan variance real-time processing system for frequency stability measurement of semiconductor lasers," *IEEE Trans. Instrum. Meas.*, submitted for publication.
[18] P. Kartaschoff, *Frequency and Time*. London, England: Academic, 1978, ch. 2.
[19] L. E. Richter, H. I. Mandelberg, M. S. Kruger, and P. A. McGrath, "Linewidth determination from self-heterodyne measurements with subcoherence delay times," *IEEE J. Quantum Electron.*, vol. QE-22, pp. 2070-2074, 1986.

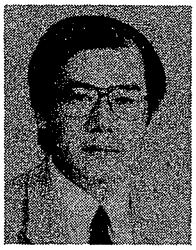

Motoichi Ohtsu (M'88) was born in Kanagawa, Japan, on October 5, 1950. He received the B.S., M.S., and Ph.D. degrees in electronics engineering from the Tokyo Institute of Technology, Tokyo, Japan, in 1973, 1975, and 1978, respectively.

In 1978 he was appointed a Research Associate and in 1982 became an Associate Professor at the Tokyo Institute of Technology. From September 1986 to July 1987, while on leave from the Tokyo Institute of Technology, he joined the Crawford Hill Laboratory, AT&T Bell Laboratories, Holmdel, NJ. His main fields of interest are the frequency control of lasers, analysis of the dynamic behavior of lasers and its applications to coherent optical measurements, optical communications, and microwave atomic clocks.

Dr. Ohtsu has written over 80 papers and received two patents. He is the author or coauthor of eight books. He is a member of the Institute of Electronics, Information and Communication Engineers of Japan, the Institute of Electrical Engineers of Japan, the Japan Society of Applied Physics, and the Optical Society of America. In 1982 he was awarded a prize from the Japan Society of Applied Physics. He was also awarded the Issac Koga Gold Medal from the International Union of Radio Science (URSI) in 1984. In 1988, he received the Japan IBM Science Award.

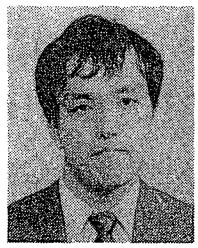

Morihiro Murata was born in Shizuoka, Japan, in 1963. He received the B.S. degree in electronics engineering and the M.S. degree in information processing from the Tokyo Institute of Technology, Tokyo, Japan, in 1987 and 1989, respectively.

Presently, he is with the Yamaha Corporation. His research interests include the frequency control of semiconductor lasers for coherent optical sensing and communications.

Mr. Murata is a member of the Japan Society of Applied Physics.

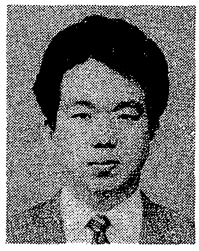

Motonobu Kourogi was born in Shiga, Japan. He graduated from Shizuoka University of Engineering in 1988.

Currently, he is a graduate student at the Tokyo Institute of Technology, Tokyo, Japan. He is engaged in research on frequency control of semiconductor lasers for coherent optical sensing and communications.

Mr. Kourogi is a member of the Japan Society of Applied Physics.

FM Characteristics and Compact Modules for Coherent Semiconductor Lasers Coupled to an External Cavity

CHUL-HO SHIN, MITSUHIRO TESHIMA, MOTOICHI OHTSU, MEMBER, IEEE, TOHRU IMAI, JUNICHI YOSHIDA, AND KENICHI NISHIDE

Abstract—**FM responses of a semiconductor laser optically coupled off-axis to a confocal Fabry-Perot cavity were measured. It was found that this cavity acted as a frequency discriminator and as a phase comparator for slow and fast frequency fluctuations, respectively. The crossover between them was determined by a half linewidth of the cavity. Based on these investigations, we made two kinds of coherent semiconductor laser modules. External FP cavities were made by using an optical fiber and a hemispherical micro-lens, respectively. Linewidths of these lasers were less than 25 kHz.**

INTRODUCTION

OPTICALLY stabilized semiconductor lasers (SL) using an external confocal Fabry-Perot cavity (CFP) have high spectral purity with relatively long-term frequency stability [1] and frequency modulation (FM) capability [2]. They are thus considered as good candidates for optical local oscillators and/or light sources in coherent communication systems and optical measurements. Frequency noise characteristics of semiconductor lasers coupled to a resonant external cavity have been theoretically analyzed [3]–[5] and experimentally evaluated [3], [6], [7]. However, precise evaluations of FM response have not yet been carried out. We report here measured and calculated results of the frequency response of the direct FM characteristics of a semiconductor laser coupled to a CFP cavity (CFP-SL). This is very important for investigating FM noise suppression characteristics by this optical feedback, and for the design of coherent optical systems, e.g., an optical phase-locked loop by using this laser as the local oscillator. Based on these investigations, we developed two kinds of coherent semiconductor laser modules as the compact-sized version of the CFP-SL for practical applications. Their external cavities were made by using an optical fiber and a hemispherical micro-lens, respectively.

OPERATING PRINCIPLE AND FM RESPONSES

Fig. 1(a) shows a semiconductor laser system coupled off-axis with a CFP cavity, which was used to evaluate the FM response characteristics. All the lasers described in this letter are commercial AlGaAs semiconductor lasers (Hitachi HL8312E). The emitted light from the laser is spectrally purified by the resonance of the external cavity. And then, a part of the cleaned light field built within the cavity returns to the laser through the cavity input mirror at resonance. The oscillating frequency of the laser is thus locked to the resonance of this CFP cavity, i.e., optical self-locking takes place. Thereby, the spectral linewidth becomes very narrow, and the center frequency of the laser field spectrum is also stabilized substantially. The free spectral range (FSR) and the finesse of the CFP cavity were 1.5 GHz and 75, respectively. This means that the linewidth of the CFP cavity $\Delta\nu_c$ was 20 MHz. The frequency-locking range of the CFP-SL was in the range of 500–800 MHz with a moderate feedback level. The system could, therefore, endure fluctuations of the injection current and the temperature variation of the laser mount, which was suppressed within 1 mK with the temperature control circuit consisting of Peltier coolers and thermistor sensors. Stable locking was maintained up to about 1 h without any other additional stabilizing circuits. This period could be lengthened by using a simple electrical feedback loop to control the feedback phase by the PZT-Φ in Fig. 1(a) [7]. The field spectral linewidth of the CFP-SL was about 10 kHz at the bias level of 1.4 times the threshold current value. The linewidth was measured by heterodyning between two CFP-SL's. The linewidth at free-running condition was about 25

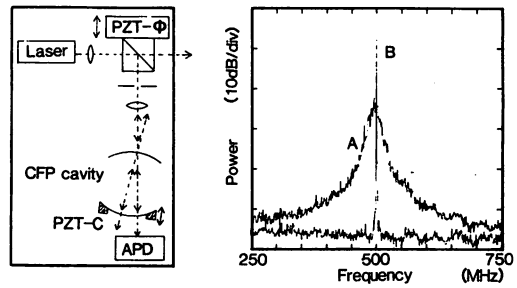

Fig. 1. (a) Semiconductor laser coupled to a confocal Fabry-Perot cavity (CFP-SL). PZT-Φ and PZT-C are used for optimizing the phase of the feedback light and the fine control of the laser oscillating frequency under optical feedback, respectively. Both PZT's can also be used to maintain long-term locking stability together with simple electrical circuits for an external control loop. (b) An example of the beat spectra, where curve *A* was obtained with a CFP-SL and a free-running laser and curve *B* with two CFP-SL's.

Manuscript received October 4, 1989; revised December 29, 1989.

C.-H. Shin, M. Teshima, and M. Ohtsu are with the Graduate School at Nagatsuta, Tokyo Institute of Technology, 4259 Nagatsuta, Midori-ku, Yokohama 227, Japan.

T. Imai, J. Yoshida, and K. Nishide are with Tokyo Aircraft Instrument Company, Ltd., 35-1, Izumi-Honcho, 1-Chome, Komae-shi, Tokyo 201, Japan.

IEEE Log Number 8934143.

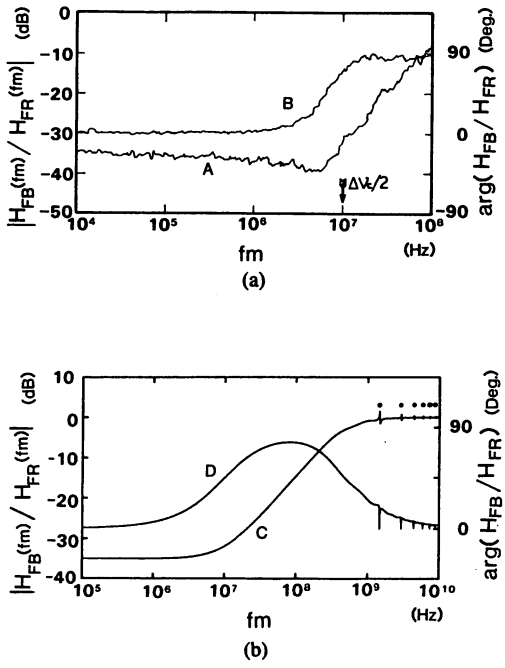

Fig. 2. The FM transfer function $H_{FB}(f_m)$ of the CFP-SL, which represents the frequency response. These values have been normalized to that under free-running condition $H_{FR}(f_m)$. (a) Measured results. (b) Calculated results, where the calculating parameters used were the same values as that of (a). Curves A and C are the frequency responses of the FM efficiency, and curves B and D are those of the phase.

MHz. An example of the heterodyned beat spectra is shown in Fig. 1(b).

Fig. 2(a) shows the transfer function $H_{FB}(f_m)$ of a CFP-SL as a function of the modulation frequency f_m of the injection current, which represents the frequency response of FM efficiency. It was measured by an RF network analyzer and the values shown in this figure have been normalized to the transfer function of the free-running condition $H_{FR}(f_m)$. Another FP cavity was used as a frequency discriminator for these measurements. Fig. 2(b) is the calculated results of a frequency response corresponding to Fig. 2(a). Details of the calculation will be published elsewhere. The curves in this figure show that the FM response has high-pass characteristics. The 3 dB cutoff frequency is determined by $\Delta\nu_c/2$. For $f_m < \Delta\nu_c/2$, FM efficiency and its phase were flat. The phase changed 90° at $f_m \simeq \Delta\nu_c/2$. On the other hand, for $f_m > \Delta\nu_c/2$, FM efficiency is increased with the rate of 20 dB/dec. And then, arg $[H_{FB}/H_{FR}]$ is returned to zero at the limit of $f_m \to \infty$.

It was also confirmed that the CFP-SL can be modulated with high efficiency up to or even more than that under free-running condition when the f_m is an integer multiple of the FSR of the CFP cavity as has been demonstrated previously [2], [7]. This results from the positive optical feedback effects at the modulation frequencies of the integer multiple of the FSR as marked by dots in Fig. 2(b).

From these figures, suppression of frequency noise of the CFP-SL can be explained as the following by using an idea similar to that of Drever *et al.* [8] and Salomon *et al.* [9]: For Fourier frequency $f < \Delta\nu_c/2$, feedback light from the input mirror of the cavity can be considered as the time delayed version of the instantaneous laser phase itself because the

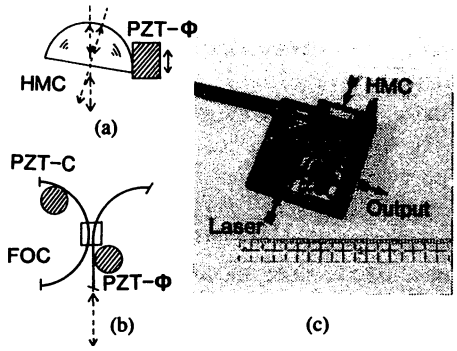

Fig. 3. Fiber optic cavity (FOC) (a) and a hemispherical micro-lens cavity (HMC) (b), which were used as the external cavity of compact modules. (c) Picture of the miniature-packaged HMC-SL module.

cavity responds to such slow variations. Feedback light from the cavity can thus be considered as the frequency reference, which is mixed destructively with the instantaneous laser field fluctuation in the laser medium. However, for $f > \Delta\nu_c/2$, the output of the cavity can be considered as the time-averaged version of past phase of the laser because the cavity does not respond instantaneously to faster variations than the cavity storage time, so the cavity provides a phase reference. The phase change of 90° stems from the crossover between the frequency of the phase comparison.

The heterodyne signal between the two CFP-SL's with S/N ratio of 52.5 dB as seen by Fig. 1(b) was also observed with 2.2 GHz span. However, any side mode could not be observed. From this measurement, it was confirmed that the side mode suppression ratio of this external cavity semiconductor laser was at least 52.5 dB, which proves a reliable single-mode oscillation. The longitudinal side mode suppression ratio of the laser itself was, at least, not affected by this optical feedback. The suppression ratio was too high to measure by a conventional monochromator.

Compact Modules

Two new type semiconductor laser modules coupled to different types of optical cavities were developed as shown in Fig. 3(a) and (b) and their good performances were also confirmed. Fig. 3(a) shows a fiber optics cavity (FOC) made of single-mode optical fiber. The FOC was aluminum coated at both ends, and its FSR and finesse were 100 MHz and 20, respectively. The laser light was coupled with the FOC by a 96:4 fiber coupler, of which the coupling-end to the laser and the opposite end were cut with the tilted angles of 4° and 8°, respectively, for preventing the direct reflection from fiber ends. The laser field spectral linewidth was 20 kHz at the maximum feedback level under stable locking condition.

Fig. 3(b) shows a hemispherical micro-lens cavity (HMC). The HMC was made of BK7 glass and its diameter and the reflectivity were 10 mm and 90%, respectively. Because the FSR of the cavity (10 GHZ) was higher than the relaxation oscillation frequency of the solitary laser, reduction of AM and FM excess noises at that frequency can be expected as pointed out in [4]. The miniature-packaged MHC-SL module is shown in Fig. 3(c). The size of the module is 50 × 50 × 30 mm. The linewidth of the laser under free-running condition

used in this module was 21 MHz with a bias level of 1.9 times the threshold current. The minimum linewidth and the locking range at that time were 25 kHz and 1 GHz, respectively. However, under operating conditions with a moderate feedback level, the linewidth was maintained at/around 70 kHz. Under the operating condition, FM efficiency of this laser module was 180 MHz/mA at 1 Hz $\leq f_m \leq$ 100 kHz, of which the free-running condition was 3.2 GHz/mA. The available output power of this module under this condition was about 6 mW because of the loss by a beam splitter used in this module. The FM efficiency was high and the linewidth was narrow enough for practical applications such as a passive ring-resonator-type optical fiber gyroscope [10]. Performances of the gyroscope by using this HMC-SL module will be published elsewhere.

Summary

FM characteristics of a CFP-SL were measured and calculated. For the frequency noise reduction by optical feedback, the resonant type external cavity provided a frequency reference of $f_m < \Delta\nu_c/2$, and a phase reference for $f_m > \Delta\nu_c/2$. The linewidth of the CFP laser was less than 10 kHz. Based on these results, we developed two kinds of the miniature-packaged version of the CFP-SL by using an HMC cavity and an FOC cavity, respectively. Minimum attainable linewidths of these lasers were less than 25 kHz. It is expected that these highly coherent semiconductor laser modules will be useful as reliable light sources of the coherent lightwave systems.

Acknowledgement

The authors thank M. Kourogi and Dr. K. Nakagawa of Tokyo Institute of Technology for their fruitful discussion on the calculation of the FM responses.

References

[1] B. Dahmani, L. Hollberg, and R. Drullinger, "Frequency stabilization of semiconductor lasers by resonant optical feedback," *Opt. Lett.*, vol. 12, pp. 876–878, 1987.

[2] L. Hollberg and M. Ohtsu, "Modulatable narrow-linewidth semiconductor lasers," *Appl. Phys. Lett.*, vol. 53, pp. 944–946, 1988.

[3] P. Laurent, A. Clairon, and C. Brent, "Frequency noise analysis of optically self-locked diode lasers," *IEEE J. Quantum Electron.*, vol. 25, pp. 1131–1142, 1989.

[4] D. R. Hjelme, "Temporal and spectral properties of semiconductor lasers," Ph.D. dissertation, Univ. of Colorado, 1988.

[5] H. Li and N. B. Abraham, "Analysis of a laser diode with optical feedback from a high finesse resonator," *IEEE J. Quantum Electron.*, vol. 25, pp. 1782–1793, 1989.

[6] H. Li and H. R. Telle, "Efficient frequency noise reduction of GaAlAs semiconductor lasers by optical feedback from an external high-finesse resonator," *IEEE J. Quantum Electron.*, vol. 25, pp. 257–264, 1989.

[7] C. H. Shin, M. Teshima, M. Ohtsu, T. Imai, J. Yoshida, and K. Nishide, "Modulatable, high coherent and compact semiconductor laser modules," in *Proc. 7th Int. Conf. Integrated Opt. and Opt. Fiber Commun. (IOOC)*, Kobe, Japan, July 1989, paper 21D4-5.

[8] R. W. P. Drever, J. L. Hall, F. V. Kowalski, J. Hough, G. M. Ford, A. J. Munley, and H. Ward, "Laser phase and frequency stabilization using an optical resonator," *Appl. Phys. B*, vol. 31, pp. 97–105, 1983.

[9] C. Salomon, D. Hills, and J. L. Hall, "Laser stabilization at the millihertz level," *J. Opt. Soc. Amer. B*, vol. 5, pp. 1576–1587, 1988.

[10] M. Ohtsu and S. Araki, "Using a 1.5 μm DFB InGaAsP laser in a passive ring cavity-type fiber gyroscope," *Appl. Opt.*, vol. 26, pp. 464–470, 1987.

Heterodyne Optical Phase-Locked Loop by Confocal Fabry–Perot Cavity Coupled AlGaAs Lasers

CHUL-HO SHIN AND MOTOICHI OHTSU, MEMBER, IEEE

Abstract—**Two external confocal Fabry–Perot cavity coupled 0.83 μm AlGaAs lasers have been phase-locked to one another by a heterodyne optical phase-locked loop. The phase error under phase locking conditions was measured using the square root of the Allan variance. The result confirmed that the heterodyne signal was a full replica of the spectrum of the reference RF signal within the loop bandwidth. The estimated phase error variance σ_ϕ^2 was 0.02 rad², i.e., $\sigma_\phi \simeq 8.1°$.**

I. Introduction

THE heterodyne [1]–[4] and homodyne [5]–[9] optical phase-locked loops (OPLL's) are required for achieving various coherent optical systems in the fields of precise optical measurements and coherent optical communication systems. The heterodyne OPLL is known as the frequency offset locking [3], [4], translation loop [10], indirect loop [11], and so on. The heterodyne OPLL has advantages as follows: 1) a well-developed microwave phase comparator can be used for detecting the phase difference between two lasers at the reference frequency ν_R, which determines the heterodyne frequency. 2) The loop can be ac-coupled. It means that a bandpass filter can be used preceding the phase comparator, thus rejecting dc drift at the photodetector and then improving signal-to-noise ratio. 3) The oscillating frequency of the slave laser can be precisely swept by sweeping the ν_R. So the heterodyne OPLL will be a key technique for the optical frequency sweep generator in the near future. It can also be expected that the coherently combined beam of two lasers heterodyne-phase-locked together with can be used in optical measurements such as using a two-frequency laser [12]. So far, the heterodyne OPLL's have been demonstrated experimentally by several authors by using gas lasers [1], external cavity semiconductor lasers [2], [3], and Nd: YAG lasers [4]. We report here experimental results on the heterodyne OPLL using semiconductor lasers, of which frequencies were stabilized by optical feedback from a confocal Fabry–Perot (CFP) cavity. Previous heterodyne OPLL experiments by external cavity semiconductor lasers did not report the loop parameters and phase errors at all. In this paper, they are indicated and discussed in details. To confirm the phase locking of the heterodyne OPLL, the Allan variance of residual frequency fluctuations of the phase-locked heterodyne signal was measured when the heterodyne signal was locked to the RF reference signal. This type of quantitative measurement was demonstrated for the first time in case of the heterodyne OPLL. The results showed excellent frequency and phase tracking capability between two semiconductor lasers by the heterodyne OPLL.

Manuscript received December 16, 1989; revised February 1, 1990.
The authors are with Graduate School at Nagatsuta, Tokyo Institute of Technology, 4259 Nagatsuta, Midori-ku, Yokohama 227, Japan.
IEEE Log Number 9034857.

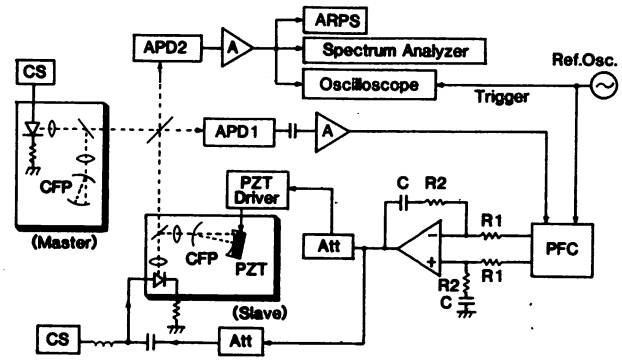

Fig. 1. General experimental arrangement of the heterodyne optical phase-locked loop. Abbreviations used here are as follows: LD—semiconductor laser diode; CS—current source; CFP—confocal Fabry–Perot cavity (Finesse: 75, Free spectral range 1.5 GHz); APD—avalanche photo diode, A—amplifier with 40 dB gain, PFC—phase/frequency comparator, ARPS—Allan variance real-time processing system; and ATT—RF attenuator.

II. Experiments

Fig. 1 is the experimental arrangement of the heterodyne OPLL. Commercial 0.83 μm AlGaAs semiconductor lasers (Hitachi HL8314) were used as the master and the slave lasers in the experiment. We employed a frequency stabilizing scheme using optical feedback for these lasers similar to one used by Dahmani *et al.* [13]. Each of the lasers was coupled off-axis with a CFP cavity (finesse: 75, free spectral range: 1.5 GHz) so that optical feedback of directly reflected light at the cavity input mirror can be avoided. The laser oscillation frequency can be fine tuned by the PZT attached for adjusting the length of the CFP cavity. The PZT and the injection current frequency tuning coefficients were 79 MHz/V and 31 MHz/mA, respectively. The characteristics of frequency noise reduction and direct frequency modulation of the lasers have been measured and reported in [14], [15]. The linewidth of the unlocked heterodyne signal between two lasers was measured as less than 30 kHz at the total sweep time of 50 ms and about 2 MHz including long term frequency drifts at the total sweep time of 100 s by an RF spectrum analyzer. The heterodyne

1041-1135/90/0400-0297$01.00

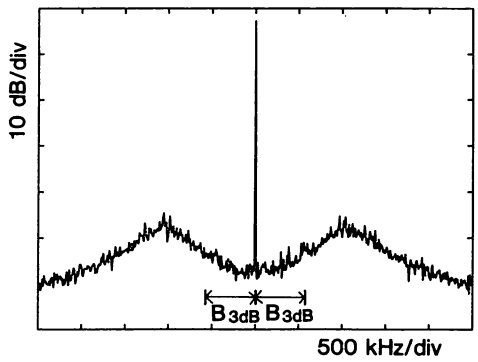

Fig. 2. Field spectral shape of the heterodyne signal under phase locking condition. The total sweep time and the resolution bandwidth were 15 s and 1 kHz, respectively. B_{3dB} is the calculated 3 dB bandwidth of the loop. The center frequency of the heterodyne signal was 25 MHz.

frequency drift was less than 100 kHz/s. Optical feedback stabilization of the lasers was maintained for longer than one hour without any additional long-term stabilizing scheme under consideration, which is a servo-loop to control the optical feedback phase and the injection current so that the laser is operating within the optical feedback locking range of about several 100 MHz at moderate feedback level. This limited the phase locking period of the OPLL.

The heterodyne signal was detected with two commercial Si avalanche photodiodes (APD). These APD's act only as optical frequency down converters, but the shot noise generated by detecting process become one of phase error sources. The first detector was used for OPLL and the second detector for measurements. The power of ~ 3.7 μW of each laser was used for the OPLL. The heterodyne signal was phase-frequency compared with the reference microwave signal from a stable RF local oscillator by a digital phase/frequency comparator (PFC). The digital PFC was consisted of a high-speed voltage comparator (PLESSEY SP9687) for converting the analog heterodyne signal to the emitter coupled-logic (ECL) level, and an ECL PFC IC chip (Motorola MC12040). The active phase comparison range of the digital PFC is $\pm 2\pi$ with the linearity over the entire range, and the PFC provides sweep-frequency acquisition capabilities if the loop is unlocked [10]. The phase/frequency error signal was passed through a first order active loop filter, of which the transfer function $F(s) = (1 + \tau_2 s)/(\tau_1 s)$ with $\tau_1 = R_1 C$, $\tau_2 = R_2 C$ and s is the Laplace variable. The control signal at the output of the loop filter was divided by two, and fedback to the slave laser via a PZT driver for slow components of the control signal and injection current for fast components of the control signal. RF attenuators were used for adjusting the balance between the gains of these two control routes.

Time constants of the loop filter τ_1 and τ_2 were 3.30 and 1.00 μs, respectively. By following the conventional PLL theory [10], [11], the natural angular frequency ω_n and the damping factor ζ of this second-order OPLL were calculated as 1.65×10^6 rad/s and 0.82, respectively. In this calculation, we used the measured parameter values as follows: the gain of the PFC $K_D = 0.16$ V/rad, the gain of the slave laser $K_0 = 4.96 \times 10^8$ rad/s/V and the attenuation coefficient between the PFC and the slave laser was 0.11. The noise bandwidth B_n and the 3 dB loop bandwidth of this OPLL B_{3dB} were thus calculated as 925 and 580 kHz, respectively. B_{3dB} was calculated by the expression of $B_{3dB} = \omega_n \{2\zeta^2 + 1 + [(2\zeta^2 + 1)^2 + 1]^{1/2}\}^{1/2}/(2\pi)$ [Hz] [10], [11].

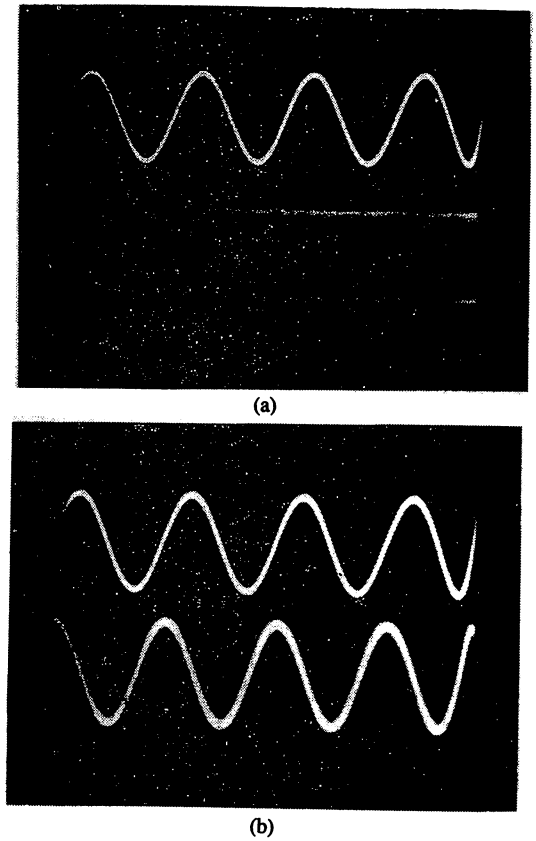

(a)

(b)

Fig. 3. The heterodyne signals (lower traces) observed in the time domain by an RF oscilloscope under unlocking (a) and phase-locking (b) conditions. In (a) and (b), upper traces are the triggering signals from the reference signal to which the heterodyne signal has been locked.

III. Results and Discussion

Fig. 2 shows a spectral shape of the phase-locked heterodyne signal measured by an RF spectrum analyzer. From this figure, the frequency/phase noise within the 3 dB loop bandwidth B_{3dB} was drastically controlled and effectively suppressed up to about 1 MHz from the center frequency of the spectral shape. We have observed this spectral shape with a span of 1 kHz and a 30 Hz resolution bandwidth, and confirmed that its linewidth was maintained within the resolution bandwidth. Furthermore, comparing the spectral shape of the heterodyne signal under phase locking condition with that of the reference RF signal, we found that both spectral shapes have the same linewidth and S/N ratio. This means that the optical phase locking between the heterodyne signal and the reference signal has successfully been carried out by this OPLL. In particular, the same S/N ratio means that the performance of this OPLL was reached to the limit determined by the spectral quality of the reference RF signal. To confirm the phase locking between heterodyne signal and reference signal and to observe residual phase fluctuations of the heterodyne signal under phase locking condition, its waveform was observed with an oscilloscope triggered by the

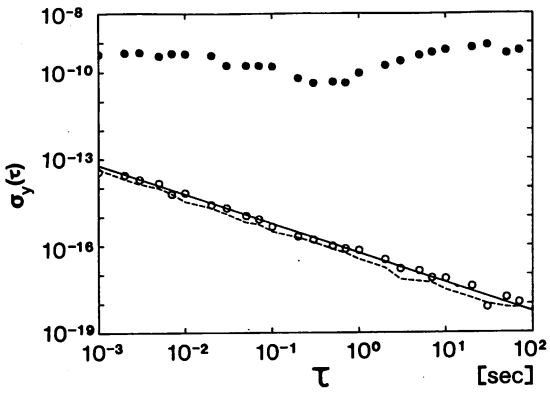

Fig. 4. Measured results of Allan variances of residual frequency fluctuations of the heterodyne signal. $\sigma_y(\tau)$ and τ are the square root of Allan variance and the integration time, respectively. The values of $\sigma_y(\tau)$ was normalized to the norminal optical frequency ν_0 of the lasers used in this experiment. Closed circles, open circles, and a broken curve are the measured results for under free running conditions, under phase locking conditions and for the reference signal, respectively. A solid curve is a least-squares approximation of the results for the phase-locked heterodyne signal, which is expressed as $\sigma_y(\tau) = 6.3 \times 10^{-17} \cdot \tau^{-1}$.

reference signal. This method was first used by Hall *et al.* [1]. Comparing (a) and (b) of Fig. 3, it can be confirmed that the heterodyne signal is successfully phase-locked to the reference signal. The rms residual phase fluctuations was estimated to be less than 0.1 rad by measuring the timing jitter of the waveform of the phase-locked heterodyne signal. The result is 2.1 times smaller than that of [1]. The reason of this smaller value can be that our OPLL had larger bandwidth and thus higher control gain could be secured within the bandwidth.

To quantitatively measure the phase locking quality between two lasers in the time domain, we have measured the square root of Allan variances $\sigma_y(\tau)$ of residual frequency fluctuations of the heterodyne signal by a new Allan variance real-time processing system (ARPS) using the heterodyne and period measurement method, which was developed for this work. The principle of operation of the ARPS is as follows: the heterodyne frequency is down-converted to 1 kHz, which generates a short-period pulse signal per a cycle. The pulse signal acts as the latch enable signal and the micro-computer interrupt signal. A 32 bits nonstop counter is continuously counting the 5 MHz signal from a stable crystal oscillator, and the counted value is latched by the latch enable signal. Thus, there is no deadtime. When the interrupt signal comes, the microcomputer acquires the latched value and stores it in the memory. The integration time and the number of samples are set by the keyboard input, and the calculation of the Allan variances are carried out by the software. If neglecting the instabilities of the 5 MHz signal and the system noise of the ARPS, this new ARPS can measure a very stable signal with 1/5000 times frequency fluctuations of the measurement limit of an old version ARPS (employing a direct frequency counting method), which was determined by ± 1 count uncertainty [16].

The measured results are shown by Fig. 4. The square root of Allan variance of residual frequency fluctuations of the heterodyne signal $\sigma_y(\tau)$ can be approximated by $6.3 \times 10^{-17} \cdot \tau^{-1}$ (the solid line in Fig. 4), which is normalized by the nominal optical frequency of the laser $\nu_0 \cdot \tau$ is the integration time. In particular, the experimental result of $\sigma_y(\tau)$ was 1.1×10^{-18} at $\tau = 70$ s. The stability of the heterodyne signal is almost same level as that of the reference signal as shown in Fig. 4. The results show the phase tracking capability between two lasers by this OPLL. From this measurements, the phase error variance σ_ϕ^2 were estimated as 0.02 rad^2 ($\sigma_\phi = 8.1°$), where the conversion formula $\sigma_\phi^2 = (2\pi\tau\nu_0)^2\sigma_y^2(\tau)$ was used. The phase error by the heterodyne frequency drift of about 100 kHz/s was calculated to $1.4 \times 10^{-5}°$. The noise spectral density of the system noise including the shot noise, the intensity noises of the lasers and the amplifier noise was 270 nV/Hz$^{1/2}$, which induces the phase error of 0.14°. If the beat linewidth of 30 kHz is purely attributed to the Lorentzian component of phase noises of two lasers, it results in the phase error of 10.8°. Comparing it with the measured result, the value of the beat linewidth was overestimated. The result suggests that the actual beat linewidth should be narrower than 17 kHz, and that a spetral linewidth measurement is not accurate to estimate the phase error. So the Allan variance measurement is a suitable method for this purpose. The phase error of the OPLL was mainly determined by the laser phase noise and the stability of the reference RF signal. Further improvement of the OPLL can be made by the increase of the loop bandwidth and using a more stable reference signal. The resulting phase error variance of the OPLL is sufficiently low for applications in coherent optical communication systems, e.g., the heterodyne PSK scheme, with a low bit error ratio (BER), because it requires σ_ϕ less than 11° for the BER of 10^{-9} [17], [18].

IV. Conclusion

We have demonstrated a second order heterodyne OPLL using semiconductor lasers coupled to an external confocal Fabry–Perot cavity. The phase error of the OPLL was estimated by measuring the Allan variance of residual frequency fluctuations of the heterodyne signal. The result confirmed that the heterodyne signal was a full replica of the reference RF signal within the loop bandwidth. The phase error σ_ϕ was estimated as 8.1°. The phase control capability of the heterodyne OPLL using confocal FP cavity coupled AlGaAs lasers is sufficiently high for applications such as coherent optical communication systems, remote sensing, and high-resolution spectroscopy.

Acknowledgment

The authors thank M. Teshima of Tokyo Institute of Technology for his assistance preparing the lasers used in this experiment and one reviewer for fruitful comments.

References

[1] J. L. Hall, L.-S. Ma, and G. Kramer, "Principles of optical phase-locking: Application to internal mirror He-Ne lasers phase-locked via past control of the discharge current," *IEEE J. Quantum Electron.*, vol. QE-23, pp. 427–437, 1987.

[2] R. C. Steele, "Optical phase-locked loop using semiconductor diode lasers," *Electron. Lett.*, vol. 19, pp. 69–70, 1983.

[3] J. Harrison and A. Mooradian, "Linewidth and offset frequency locking of external cavity GaAlAs lasers," *IEEE J. Quantum Electron.*, vol. QE-25, pp. 1152–1155, 1989.

[4] T. J. Kane, A. C. Nilsson, and R. L. Byer, "Frequency stability and offset locking of a laser-diode-pumped Nd:YAG monolithic nonplanar ring oscillator," *Opt. Lett.*, vol. 12, pp. 175–177, 1987.

[5] W. R. Leeb, H. K. Plipp, A. L. Scholtz, and E. Bonek, "Frequency synchronization and phase locking of CO_2 lasers," *Appl. Phys. Lett.*, vol. 41, pp. 592–594, 1982.

[6] G. Wenke and S. Saito, "Phase locking of semiconductor lasers using homodyne detection and negative electrical feedback," *Japan J. Appl. Phys.*, vol. 24, pp. L908–L910, 1985.

[7] D. J. Malyon, D. W. Smith and R. Wyatt, "Semiconductor laser homodyne optical phase-locked-loop," *Electron. Lett.*, vol. 22, pp. 421–422, 1986.

[8] J. M. Kahn, B. L. Kasper, and K. J. Pollack, "Optical phaselock receiver with multi-gigaheltz signal bandwidth," *Electron. Lett.*, vol. 25, pp. 626–628, 1989.

[9] L. G. Kazovsky and D. A. Atlas, "A 1320 nm experimental optical phase-locked loop," *IEEE Photon. Technol. Lett.*, vol. 1, pp. 395–397, 1989.

[10] F. M. Gardner, *Phaselock Techniques,* 2nd ed. New York: Wiley, 1979.

[11] A. Blanchard, *Phase-Locked Loops: Application to Coherent Receiver Design.* New York: Wiley, 1975.

[12] M. Hercher and G. Wyntjes, "Precision Angle measurement with a 2-frequency HeNe leaser," *SPIE,* vol. 741, pp. 174–185, 1987.

[13] B. Dahmani, L. Hollberg, and R. Drullinger, "Frequency stabilization of semiconductor lasers by resonant optical feedback," *Opt. Lett.*, vol. 12, pp. 876–878, 1987.

[14] C. H. Shin, M. Teshima, M. Ohtsu, T. Imai, J. Yoshida and K. Nishide, "Modulatable, high coherent and compact semiconductor laser modules," presented at 7th Int. Conf. Integrated Opt. Opt. Fiber Commun. (IOOC), Kobe, Japan, No. 21D4-5, July 1989.

[15] ——, "FM characteristics and compact modules of coherent semiconductor lasers coupled to an external cavity," *IEEE Photon. Technol. Lett.*, vol. 2, pp. 167–169, Mar. 1990.

[16] K. Kuboki and M. Ohtsu, "The Allan variance real-time processing system for frequency stability measurement of semiconductor lasers," *IEEE Trans. Instrum. Measure.*, 1989.

[17] K. Kikuchi, T. Okoshi, M. Nagamatsu, and N. Henmi, "Degradation of bit-error rate in coherent communications due to spectral spread for the transmitter and the local oscillator," *J. Lightwave Technol.*, vol. LT-2, pp. 1024–1033, 1984.

[18] L. G. Kazovsky, "Balanced phase-locked loops for optical homodyne receivers: performance analysis, design considerations, and laser linewidth requirements," *J. Lightwave Technol.*, vol. LT-4, pp. 182–195, 1986.

——招待論文

半導体レーザの周波数・位相制御

正員 大津 元一[†]　正員 申 哲浩[†]　正員 楠澤 英夫[†]
非会員 興梠 元伸[†]　非会員 鈴木 宏昌[†]

Frequency and Phase Controls of Semiconductor Lasers

Motoichi OHTSU[†], Chul-Ho SHIN[†], Hideo KUSUZAWA[†], *Members*,
Motonobu KOUROGI[†] *and* Hiromasa SUZUKI[†], *Nonmembers*

あらまし 半導体レーザの周波数，位相を制御するための筆者らの最近の実験結果について報告した．発振スペクトル半値幅を狭さく化するために電気的負帰還制御法を用い，560 Hz の値が得られた．共焦点ファブリーペロー干渉計を用いた光帰還法を採用し，発振スペクトル半値幅 25 kHz を有する小形レーザ装置を製作した．波長 0.67 μm の AlGaInP レーザにこの方法を適用し，50 kHz 以下のスペクトル半値幅を得た．ホモダイン形光位相同期ループを構成し，制御帯域 10 MHz，残留位相ゆらぎ 2×10^{-9} (radian^2/Hz) を得た．ヘテロダイン形光位相同期ループを構成し，残留位相ゆらぎのアラン分散の平方根として 0.14 (radian) を得た．更に，半導体レーザと非線形光学素子とを組み合せた，広帯域周波数掃引可能な光スイープジェネレータのシステムを提案した．

1. まえがき

半導体レーザはその共振器損が大きいこと，キャリヤ密度変動量が大きくかつ高速であること，などの理由により大きな周波数，位相ゆらぎを示す．しかし直接周波数変調効率が大きいこと，安価かつ低消費電力であること，などのために各種の実用的な光応用システムに広く用いられている．各々の光応用システムの仕様を満たすために新しい構造をもつ半導体レーザデバイスの開発，光帰還法の開発，などが行われており，これらについては本特集の他の論文で紹介されるはずであるので，ここでは電気的負帰還制御法，および光帰還法の一形態に関する筆者らの最近の研究を報告する．

光センシング，基礎科学分野での光応用システムには周波数掃引可能範囲が約1ペタヘルツ ($\equiv1\times10^{15}$ ヘルツ) の周波数可変・高コヒーレント光源，すなわちペタヘルツ級のハイパーコヒーレント光スイープジェネレータの開発[(1)]が有用であり，筆者らはその実現を目指している．そのためには現存の高精度マイクロ波スイープジェネレータと同様，少なくとも次の五つの課題を実行することが必要である：

(1)発振スペクトル中心周波数の安定化，(2)発振スペクトル中心周波数の再現性と確度の向上，(3)発振スペクトル半値幅の狭さく化，(4)主レーザへの周波数，位相の追随，(5)安定かつ高精度の周波数掃引．

これらの課題を電気的負帰還制御法によって同時に実現するための統合的なシステムの構成を図1に示す[(2)]．(1)，(2)の結果については紙数の節約のために筆者らによる最近の解説論文[(2)]にゆずり，(3)～(5)についての実験結果のみについて報告する．

2. 発振スペクトル半値幅の狭さく化

周波数制御帯域 B の値がフリーランニング時の発振スペクトル半値幅 $\Delta\nu_{FR}$ の値よりも大きければ (すなわち $B>\Delta\nu_{FR}$) 半値幅は制御により減少する．そのための方法として電気的負帰還制御法と光帰還法とについての実験結果を示す．

2.1 電気的負帰還制御法

光センシング，基礎科学 (一般相対論の検証，原子物理学，量子光学，など) 実験用のレーザには帯域は狭～中 (約 10 MHz 以下) でよいが，高利得の制御が必要であり，それには図1に示すような電気的負帰還制御

† 東京工業大学大学院総合理工学研究科，横浜市
The Graduate School at Nagatsuta, Tokyo Institute of Technology, Yokohama-shi, 227 Japan

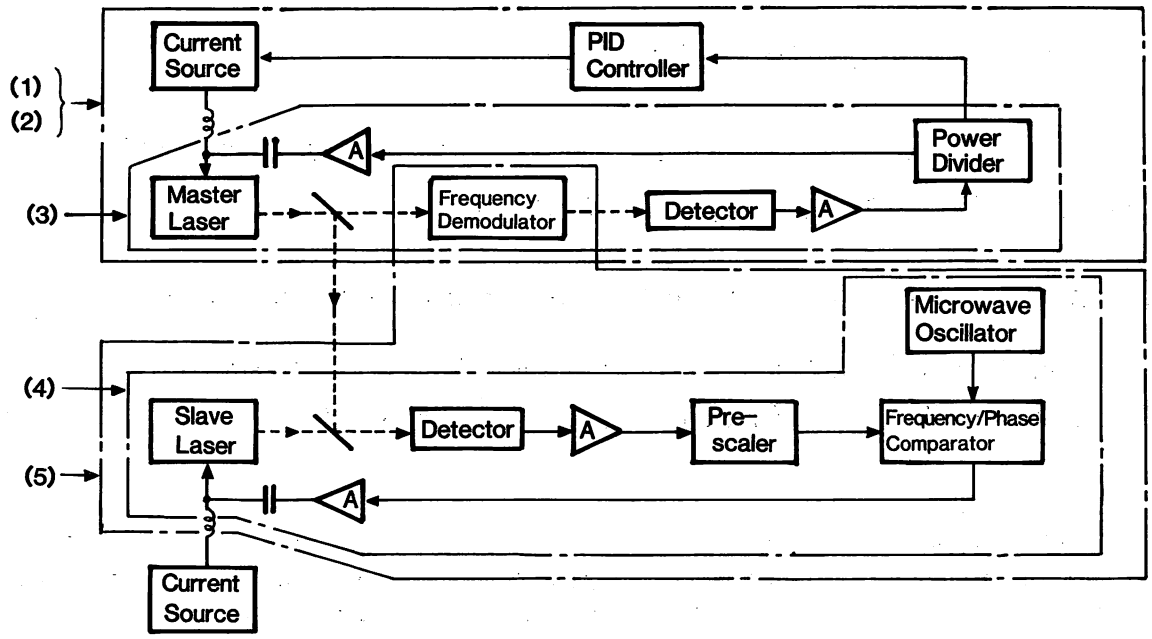

図1 電気的負帰還制御法による統合的システムの構成[2]. 図中の五つのブロック中の装置によって五つの課題を実行する. すなわち, (1)発振スペクトル中心周波数の安定化, (2)発振スペクトル中心周波数の再現性と確度の向上, (3)発振スペクトル半値幅の狭さく化, (4)主レーザへの周波数, 位相の追随, (5)安定かつ高精度の周波数掃引

Fig. 1 Bock diagram of the synthesized system by negative electrical feedback[2]. Five blocks in this figure are for (1) stabilization of the center frequency of the field spectrum, (2) improvements of the reproducibility and accuracy of the center frequency of the field spectrum, (3) linewidth reduction of the field spectrum, (4) frequency and phase trackings to the master laser, and (5) stable and accurate frequency sweep.

法が適している. そのためには, 周波数ゆらぎを抑圧するために半導体レーザの注入電流を制御する. 高利得を得るために高フィネスのファブリーペロー(FP)干渉計を周波数復調器に用いる. 更に, FP干渉計の反射モード(反射光のパワーゆらぎを光検出器で受信する方法)を使うほうが透過モードよりも広帯域制御が可能となる. これは $f > \Delta\nu_{FP}/2$ (f はフーリエ周波数, $\Delta\nu_{FP}$ はFP干渉計の共振曲線の半値全幅)では反射モードには光周波数を時間微分する機能が含まれるからである[3]. このほかに半導体レーザの周波数変調特性を表す伝達関数をはじめ, 電気的負帰還制御ループ中の各要素の伝達関数の値を測定または計算によって求め, これらの結果をもとにループ伝達関数の利得, 帯域が最大になるようにループ中の位相補償回路を最適設計する. この最適設計された制御ループを用い, 波長0.8 μm AlGaAsレーザに対して実験を行った結果得られた周波数ゆらぎのパワースペクトル密度を図2に表す[3]. 曲線A(フリーランニング時), B(制御時)の比較により $f \leqq 40$ MHz で制御の効果が現れていることがわかる. 曲線Cはフリーランニング時の自然放出光ゆらぎによる周波数ゆらぎの推定値(コヒーレント状態におけるゆらぎの大きさに対応)を表す. 曲線Bの値は $f \leqq 4.4$

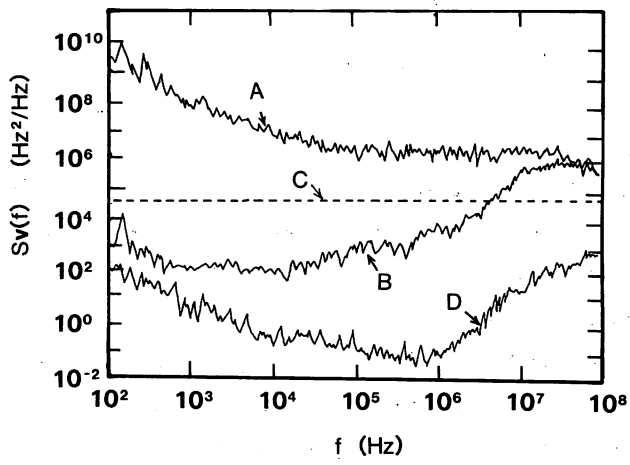

図2 波長0.83 μm AlGaAsレーザ(CSP形)の周波数ゆらぎのパワースペクトル密度 $S_\nu(f)$[3]. A: フリーランニング時, B: 電気的負帰還制御時, C: フリーランニング時の自然放出光ゆらぎにより決まる値, D: レーザ強度ゆらぎにより制限される周波数ゆらぎ検出限界

Fig. 2 Power spectral density $S_\nu(f)$ of the frequency fluctuations of a 0.83 μm-wavelength AlGaAs laser (CSP-type)[3]. A: free-running laser, B: under negative electrical feedback, C: the value determined by the spontaneous emission fluctuations of the free-running laser, D: limit of frequency fluctuations detection imposed by the laser intensity fluctuations.

MHzでは曲線Cの値より小さい. すなわち, この範囲では電気的負帰還制御によりハイパーコヒーレント状

態[3]~[5]が実現している．特に$f \leqq 1$ kHzでは周波数ゆらぎ抑圧度はフリーランニング時の60～70 dBに達しており非常に高利得の制御が実現している．

図3は発振スペクトル形状を表す．フリーランニング時のスペクトル半値幅は4.5 MHzであるが，制御時は560 Hzになっていることが確認されている[3]．図2の曲線Dはレーザの強度ゆらぎによって決まる周波数ゆらぎ検出限界である．制御系の性能向上により周波数ゆらぎがこの曲線Dの値まで減少すれば，発振スペクトル半値幅は更に狭くなると期待される[3]．

FP干渉計をマッハ・ツェンダ干渉計の中に設置し，その出力を光バランス検出器により測定する周波数復調器を用いればレーザ強度ゆらぎの影響が除去でき，更にFP干渉計の反射モードを使った場合よりも10 dB大きな周波数復調利得が得られることが指摘され，その性能が実験的に評価されている[6]．これにより周波数ゆらぎ検出限界が光検出器のショット雑音レベルに達すれば，スペクトル半値幅は58 mHzに達すると推定されている[7]．筆者らの製作した光バランス検出器を用いて実験を行った結果，$f \leqq 40$ MHzにおいてレーザ強度ゆらぎの寄与を20～30 dB抑圧できた[8]．

2.2 光帰還法

外部反射体からの反射光を半導体レーザに再注入させて周波数ゆらぎを抑圧する光帰還法は，その構成が簡単なために15年以上前から使われている[9]．レーザと反射体との距離が変動するとレーザ発振の不安定を誘起するので[10]注意が必要である．この方法のうち，比較的安定な方法として，図4(a)に示すように，共焦点FP干渉計からの反射光をレーザに再注入する方法が提案されている[11]．フィネス75，自由スペクトル域(FSR)1.5 GHzの共焦点FP干渉計を用い，波長0.83 μm AlGaAsレーザの周波数ゆらぎを抑圧した場合の周波数ゆらぎのパワースペクトル密度の抑圧度の測定結果を図5に示す[12]．この図からもわかるように，周波数ゆらぎ抑圧のための制御帯域の3 dB遮断周波数f_{3dB}は共焦点FP干渉計の共振曲線の半値半幅$\Delta\nu_{FP}/2$(＝10 MHz)に等しい．この実験の結果，スペクトル半値幅として10 kHzが得られている[12]．0 dB遮断周波数は原理的に無限大であるが，FSRの整数倍のフーリエ周波数における正帰還のため周波数ゆらぎの値はフリーランニング状態の場合よりも大きくなる．これは理論的にも確認されている[13]．この正帰還のため，直

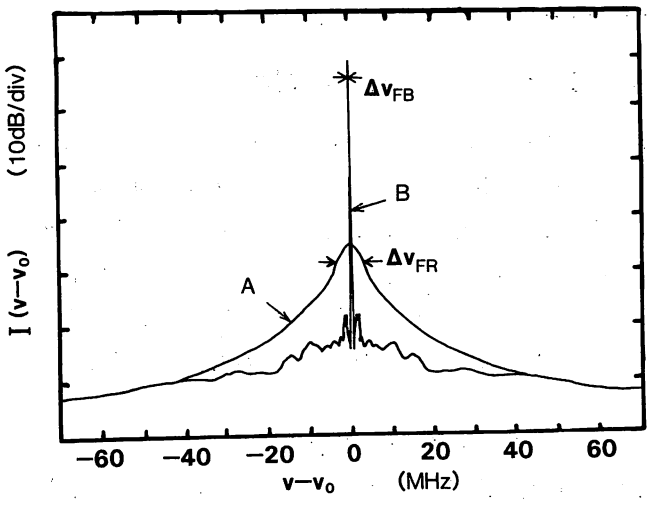

図3　図2の曲線AとBに対応する発振スペクトル形状I($\nu-\nu_0$)[3]．ν_0はスペクトル中心周波数．A：フリーランニング時，B：電気的負帰還制御時．曲線A，Bの半値幅$\Delta\nu_{FR}$，$\Delta\nu_{FB}$はそれぞれ4.5 MHz，560 Hz

Fig. 3　Field spectral profile I($\nu-\nu_0$) corresponding to the curves A and B of Fig. 2. ν_0 represents the center frequency of the spectrum. A : free-running laser, B : under negative electrical feedback. The half linewidth of the curves A and B are $\Delta\nu_{FR}$=4.5 MHz and $\Delta\nu_{FB}$=560 Hz, respectively.

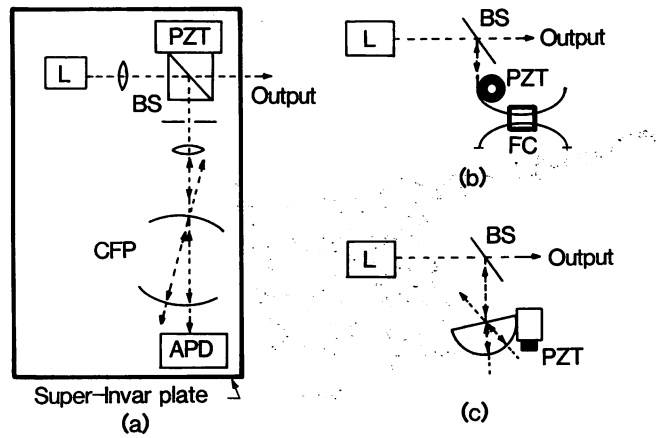

図4(a)　共焦点ファブリーペロー(FP)干渉計からの光帰還による周波数ゆらぎ抑圧法の原理図[11],[12],[15]．L：半導体レーザ，BS：ビームスプリッタ，PZT：光路長調整用ピエゾ圧電素子，CFP：共焦点FP干渉計
(b)　共焦点FP干渉計を光ファイバを用いたFP干渉計で置き換えたもの．FC：ファイバカプラ
(c)　共焦点FP干渉計を半球形レンズ面に反射膜を蒸着したもので置き換えたもの

Fig. 4(a)　Setup for reducing the frequency fluctuations of the laser by using an optical feedback from a confocal Fabry-Perot (FP) interferometer[11],[12],[15]. L : semiconductor laser, BS : beam splitter, PZT : piezo ceramics for controlling the optical pass length, CFP : confocal FP interferometer.
(b)　Setup obtained by replacing a confocal FP interferometer by an optical fiber-FP interferometer. FC : fiber coupler.
(c)　Setup obtained by replacing a confocal FP interferometer by a hemispherical lens on which a high reflection films are coated.

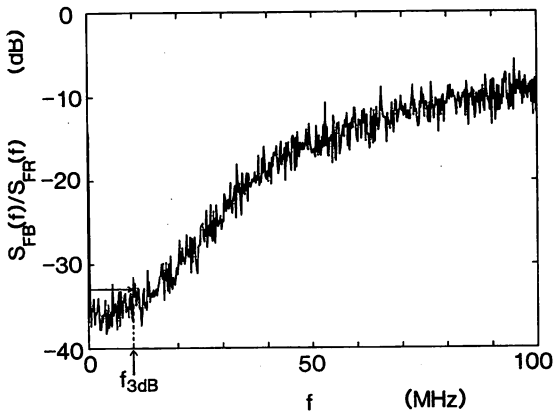

図5 共焦点ファブリーペロー干渉計を用いた光帰還法により波長0.83 μm AlGaAsレーザの周波数ゆらぎを抑圧した場合の抑圧度[12]. $S_{FR}(f)$, $S_{FB}(f)$はそれぞれフリーランニング時, 光帰還時の周波数ゆらぎのパワースペクトル密度. f_{3dB}は光帰還による周波数制御帯域の3 dB遮断周波数

Fig. 5 Reduction factor of the frequency fluctuations of a 0.83 μm wavelength AlGaAs laser by the optical feedback from a confocal Fabry-Perot interferometer[12]. $S_{FR}(f)$ and $S_{FB}(f)$ represent the power spectral densities under free-running and feedback conditions, respectively. The 3 dB cutoff frequency of the optical feedback bandwidth is represented by f_{3dB}.

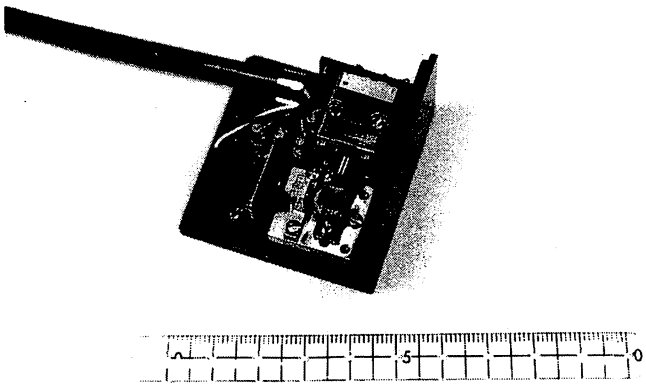

図6 ファブリーペロー干渉計からの光帰還法を用いた発振スペクトル線幅25 kHzを有する小形レーザモジュール[16]

Fig. 6 A 25 kHz linewidth compact laser module by optical feedback from a Fabry-Perot interferometer[16].

接周波数変調効率もこのフーリエ周波数において増大することが実験により指摘されている[14]. また, この共焦点FP干渉計は図4(b), (c)に示すように両端研磨した光ファイバ, または半球形レンズ面に反射膜を蒸着したもの, により作成することもできる[15]. 特に, 図4(c)のように直径10 mmの半球形レンズを用いることにより図6に示すように寸法5 cm×5 cm×3 cmの容器に納まり, ファイバジャイロなどに用いられるような小形装置が作られている[16]. この場合, 25 kHzのスペクトル幅が得られている. また, 最近は波長0.67 μm AlGaInPレーザのスペクトル半値幅もこの方法で狭さく化されている[17]. 遅延自己ホモダイン法[18]によって測定したスペクトル形状を図7に示す. これよりスペクトル半値幅は50 kHzであることがわかるが, これは測定に用いたファイバの長さ(2 km)によって決まる測定分解能と同じ値である. この実験では外部回折格子からの反射光も同時にレーザに戻している. このとき, 回折格子面を回転させることにより波長を5 nmの範囲で掃引することができた.

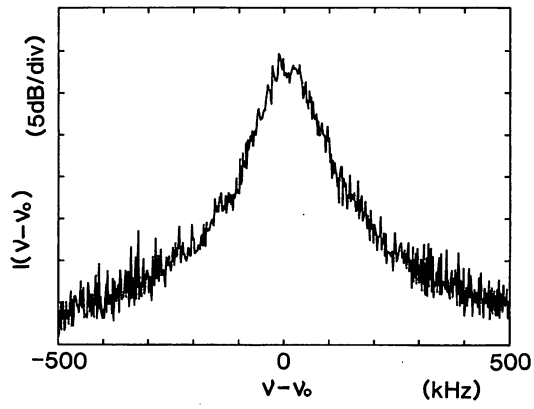

図7 共焦点ファブリーペロー干渉計を用いた光帰還法を波長0.67 μm AlGaInPレーザに適用して得られた発振スペクトル形状 $I(\nu-\nu_0)$[17]

Fig. 7 Field spectral profile $I(\nu-\nu_0)$ of a 0.67 μm wavelength AlGaInP laser under the optical feedback from a confocal Fabry-Perot interferometer[17].

3. 主レーザへの周波数追随

前章までで得られた周波数ゆらぎの少ないレーザを主レーザとして用い, これにもう一つのレーザ(従レーザ)の周波数, 位相を追随させることはヘテロダイン形, またはホモダイン形の光センシングシステム, 更には光通信システム, などでは有用な技術である. 本章ではこれらの実験についての筆者らの最近の結果を報告する.

3.1 ホモダイン形光位相同期ループ

2.1の電気的負帰還制御法により得られたAlGaAsレーザを主レーザとして用い, ホモダイン形光位相同期ループを構成する実験を行って得られた位相ゆらぎのパワースペクトル密度の値を図8の曲線Aに示す. 従レーザには補助的な電気的負帰還法を施し, 両レーザ間のビート信号スペクトルの半値幅を300 kHzに狭めた状態で位相同期実験を行った. 従来の報告では光帰還法によるレーザを用いた実験が報告されているが[19],

電気的負帰還法による主，従レーザを用いた例はない．曲線Bは位相同期がかかっていない場合の位相ゆらぎの推定値である．制御帯域は10 MHzであり，制御帯域内では位相ゆらぎは約2×10^{-9} (radian^2/Hz)まで抑圧されていることがわかる．この値は従来のフリーランニング状態の2台のレーザ(ビート信号スペクトルの半値幅15 MHz)を用いた実験結果に比べ，1/5以下の値になっている[20]．

上記の光位相同期ループの制御帯域を制限する主要因は光路長，ケーブル長，などに依存する制御信号伝搬の時間遅れと考えられた．そこで，制御帯域を拡大するために光路長およびケーブル長を短縮することを試みた．短縮化の妨げとなっていたものは従レーザのスペクトル半値幅を狭さく化するための補助的な電気的負帰還制御素子だったので，これを実験台から取り除いた．すなわち，従レーザをフリーランニング状態で使用した．この状態で，光位相同期ループ中での光路長，ケーブル長を実測し，これらによる遅延時間を推定したところ約0.5 nsまで短縮されたことがわかった．そして実際の光位相同期ループを構成したところ制御帯域は約75 MHz(0 dB遮断周波数)となった．このとき，フーリエ周波数範囲$1\,\mathrm{MHz}\leqq f\leqq75\,\mathrm{MHz}$において位相ゆらぎのパワースペクトル密度は約$2\times10^{-9}$ (radian^2/Hz)以下となり，図8とほぼ同等の位相ゆらぎが得られた．一方，ネットワークアナライザを用いて光位相同期ループの全遅延時間を測定した結果，約2 nsの値が得られた．従って，以上の改良により，全遅延時間を決定する主要因は光路長，ケーブル長ではなく，半導体レーザおよび光検出器の群遅延であること，すなわち，制御帯域はこれらの群遅延で決まる値まで拡大したこと，が確認された．この制御帯域は従来の類似の実験結果(約10 MHz)[20]に比べ大きな値である．以上の結果より，良好な光位相同期ループが実現していることがわかった．

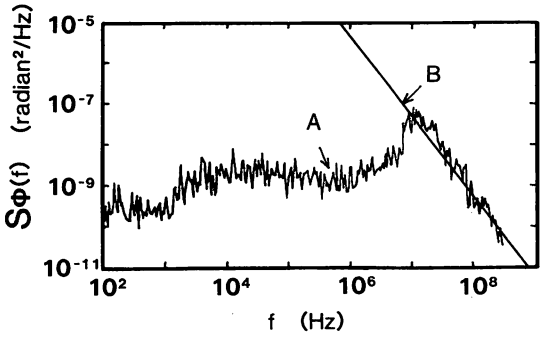

図8　電気的負帰還制御された2台のAlGaAsレーザを用いたホモダイン形光位相同期ループにより得られた残留位相ゆらぎのパワースペクトル密度$S_\phi(f)$[20]．曲線A，Bはそれぞれ位相同期成立時，フリーランニング時の値

Fig. 8　Power spectral density $S_\phi(f)$ of the residual phase fluctuations of the homodyne optical phase locked loop by using two AlGaAs lasers under negative electrical feedback[20]. The curves A and B represents the value under phase locked and unlocked conditions, respectively.

3.2　ヘテロダイン形光位相同期ループ

ヘテロダイン形光位相同期ループは次章で述べる安定かつ高精度の周波数掃引のために必要な技術である．筆者らは既にヘテロダイン形光周波数同期ループを構成し[21],[22]，ヘテロダイン周波数ゆらぎが積分時間$\tau=1{,}000$ (s)において0.6 (Hz)であることを報告した[22]．その性能を更に向上させるために，ここではその一例として，**2.2**で示した光帰還法によりあらかじめ周波数ゆらぎを抑圧した2台のレーザを用いた実験結果[23]について示す．

1台目のレーザを主レーザとして用い，2台目のレーザ(従レーザ)とのヘテロダイン信号周波数が，別に用意した局部発振器(高安定マイクロ波周波数シンセサイザ)からの信号周波数と一致するように従レーザ周波数を制御した．この制御のために，従レーザの注入電流を制御し，同時に電気ひずみ素子(PZT)に印加する電圧を制御して光帰還用の共焦点FP干渉計の長さを調節した．ヘテロダイン信号のスペクトル形状を図9(a)，(b)に示す†．図9(a)は縦軸を対数表示してある．この図はスペクトル中心周波数のまわりに±1.0 MHz以内で周波数ゆらぎが抑圧されていること，すなわち，ヘテロダイン周波数制御の帯域は1.0 MHzであることを示している．図9(b)は縦軸を線形表示したものである．スペクトル幅は非常に小さいが，これは測定に用いたRFスペクトラムアナライザの分解能を制限するフィルタ帯域幅(30 Hz)以内の値である．更に，局部発振器として用いたマイクロ波周波数シンセサイザの出力信号スペクトル形状と比較した結果，両者の形状にはとんど差は見られなかった．このことは，従レーザ周波数は局部発振器の周波数安定度で制限される精度で主レーザ周波数に追随していることを意味する．このことを，より定量的に示したものが図10である†．図10の白丸はヘテロダイン信号周波数のゆらぎを表すアラン分散の平方根σ_yの測定結果である．σ_yはヘテロダイン信号周波数ゆらぎをレーザの光周波数ν_0(361

† C.-H. Shin and M. Ohtsu: "Heterodyne optical phase-locked loop by confocal Fabry-Perot cavity coupled AlGaAs lasers", to be published in April issue of IEEE Photonics Technol. Lett..

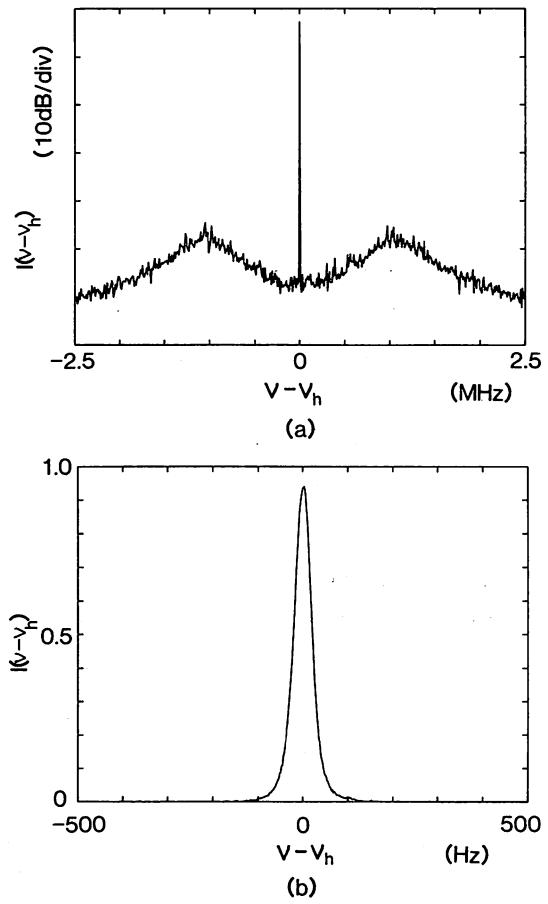

図9 共焦点ファブリーペロー干渉計を用いた光帰還法を採用した2台のAlGaAsレーザを用いたヘテロダイン形光位相同期ループにより得られたヘテロダイン信号のスペクトル形状 $I(\nu-\nu_h)$†. ν_h はスペクトル中心周波数. (a), (b)は縦軸をそれぞれ対数表示, 線形表示したものである

Fig. 9 Field spectral profile $I(\nu-\nu_h)$ of the heterodyne signal between two lasers under optical feedback obtained by using heterodyne optical phase locked loop†. ν_h represents the center frequency of the spectrum. Logarithm and linear scales were employed for the ordinates of (a) and (b), respectively.

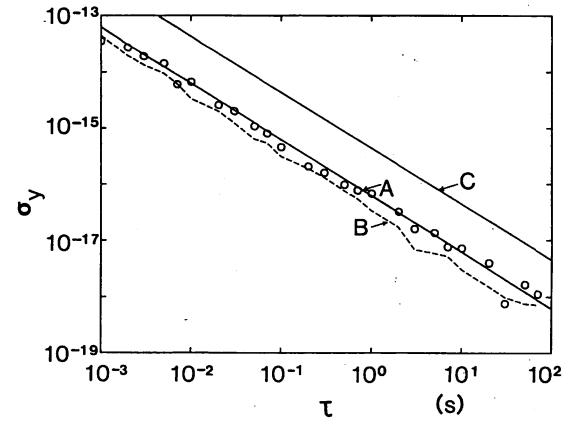

図10 共焦点ファブリーペロー干渉計を用いた光帰還法を採用した2台のAlGaAsレーザを用いたヘテロダイン形光位相同期ループにより得られたヘテロダイン信号周波数ゆらぎの大きさを表すアラン分散の平方根の値 σ_y†. 周波数ゆらぎはレーザの光周波数 ν_0 (=361 THz)で規格化して表してある. τ は測定の際の積分時間, 白丸は測定結果. 直線Aは白丸の測定結果を最小2乗近似したもの. Bは局部発振器として使ったマイクロ波周波数シンセサイザの周波数ゆらぎを表す. Cは位相ゆらぎのアラン分散の平方根が1(radian)になるのに必要な σ_y の値を表す

Fig. 10 The square root of the Allan variance σ_y of the heterodyne frequency fluctuations of the heterodyne optical phase locked loop by using two AlGaAs lasers under optical feedback†. Magnitude of the frequency fluctuations has been normalized to the laser optical frequency ν_0 (=361 Thz). τ represents the integration time of measurements. Open circles represent the experimental results. The solid line A represents the result least-square fitted to the open circles. The broken curve B represents the measured value of the frequency fluctuations of the microwave frequency synthesizer used as a local oscillator. The solid line C represents the value of σ_y at which the square root of the Allan variance of the phase fluctuations is 1 radian.

THz)で規格化して表してある. これらは $\sigma_y=6.3\times10^{-17}\cdot\tau^{-1}$ なる式(これを図10中の直線Aに示す)で近似できる. 特に, 積分時間 $\tau=70$ (s)において, 1.1×10^{-18} なる測定値が得られている. この値は0.40 mHzのヘテロダイン周波数ゆらぎに相当する. 曲線Bは局部発振器として用いたマイクロ波周波数シンセサイザのゆらぎの大きさをレーザの光周波数で規格化して表したものである. この値と白丸の値とがほぼ等しいことから, ヘテロダイン信号周波数ゆらぎは局部発振器の周波数ゆらぎの値まで抑圧されていることがわかる. なお, このような小さな周波数ゆらぎを測定するためには, 従来筆者らが開発して用いていたアラン分散実時間測定装置[23]よりも精度が約5000倍優れたものを新たに開発して用いた[24]. 直線Cはヘテロダイン信号の位相ゆらぎのアラン分散の平方根 σ_ϕ が1ラジアンの値に対応する σ_y の値を示したものである. 但し, σ_y と σ_ϕ との間に成り立つ関係式, $\sigma_\phi=2\pi\tau\nu_0\sigma_y$, を用いている. 直線Aの値をこの式に代入することにより, 位相ゆらぎ $\sigma_\phi=0.14$ (radian)が得られたこと, すなわち, ヘテロダイン形光位相同期ループが実現したことが確認できる.

4. 安定かつ高精度の周波数掃引

3.2のヘテロダイン形光位相同期ループにおいて, 局部発振器の周波数を掃引すれば従レーザの周波数を掃引することができる. このとき, 掃引の時定数が同期ループの帯域内であれば従レーザの周波数安定度は主レーザのそれと同等に保たれ, 安定かつ高精度の掃引

が可能である．この方法で筆者らは既に0.8 μm AlGaAsレーザ(CSP形)の周波数を安定に64 GHzの範囲で連続掃引できたこと，更に，この連続掃引範囲はこのレーザ固有のモードホッピング現象によって制限されていること，DFB，DBRレーザのような動的単一モードレーザを使えば連続掃引範囲は約1 THzまで可能であること，を示した[22]．

筆者らはこのような安定性かつ高精度性を保ったまま，更に掃引範囲を広げる方法を最近提案した[1]．このシステム構成の概念図を図11に示す[1]．これには現在の半導体レーザ素子製作技術により製作し得る波長1.56，1.34，0.78，0.67 μmレーザを光源として用いる．波長0.78 μmレーザ周波数ゆらぎを**2.**および**3.**の手法により抑圧し，これを第1の主レーザとして用いる．このレーザに波長1.56 μmレーザの第2高調波周波数を**3.2**の手法を用いて追随させる．これとは別の分光的手法として波長0.78 μmレーザ光と波長1.56 μmレーザの第2高調波とをRb原子に同時入射させてRbのドップラーフリー光-光2重共鳴スペクトルを検出し，このスペクトル中心周波数に二つの光周波数を固定することも提案されている[26]．以上の方法により波長0.78 μmレーザと1.56 μmレーザとの間の周波数同期が可能となる．予備実験として波長1.56 μmレーザの活性層内部で発生する第2高調波を利用した実験が行われている[26]．この場合，第2高調波パワーは小さい(約2 pW)が，実験上の不都合はない．但し，実用的にはより高い第2高調波パワーが得られることが望ましいので，第2高調波発生用の有機非線形光学導波路(材料

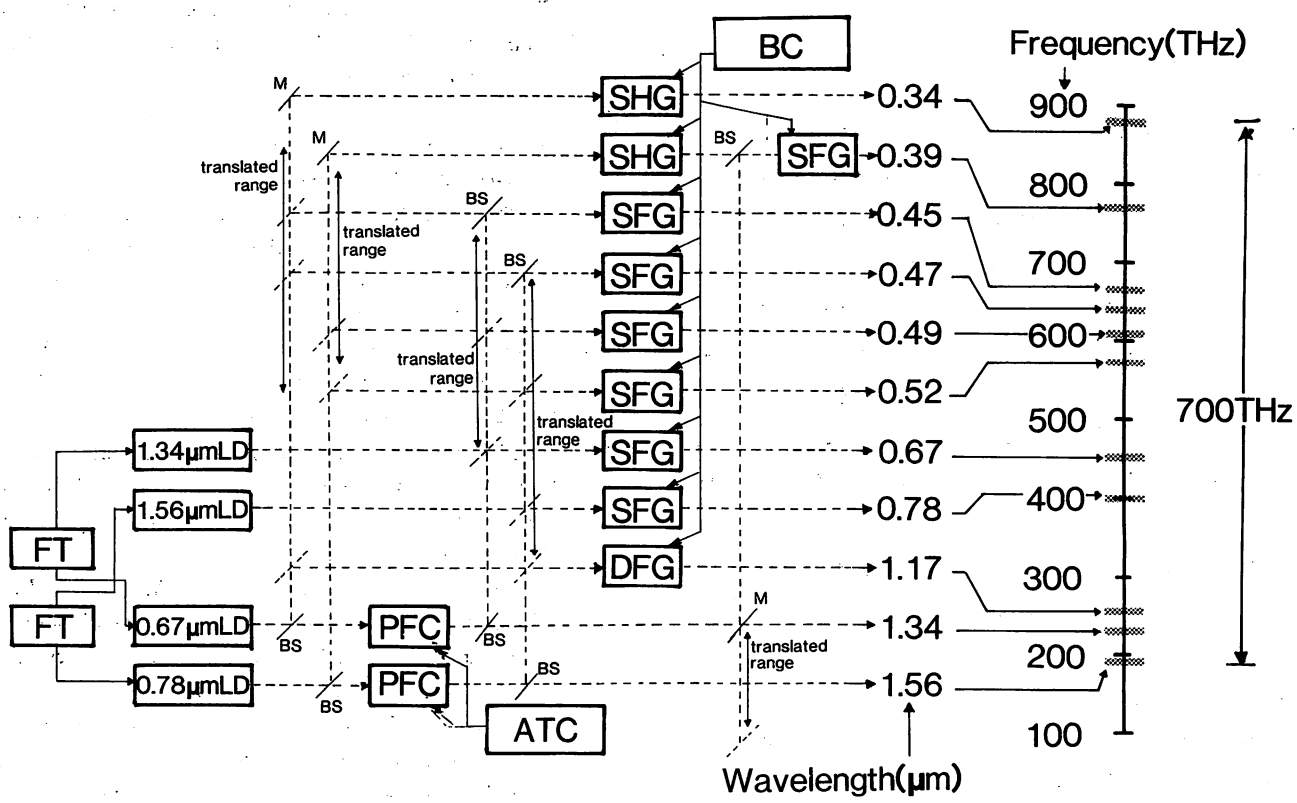

図11　提案された周波数安定かつ広帯域可変レーザシステム[1]．右端の周波数軸上のメッシュを施した範囲が周波数連続掃引可能範囲を表す．
ATC：非線形光学結晶への光の入射角調整による周波数掃引機構，BC：非線形光学結晶の複屈折率制御機構，BS：可動のビームスプリッタ，DFG：非線形光学結晶による差周波数発生器，FT：電気的負帰還によるレーザ間の周波数追随用制御機構，M：可動の鏡，PFC：非線形光学結晶によるパラメトリック周波数変換器，SFG：非線形光学結晶による和周波数発生器，SHG：非線形光学結晶による第2次高調波発生器

Fig. 11　Block diagram of a stable and wideband tunable laser system proposed by the authors[1]. Meshed area on the frequency axis of the right hand side of this figure represent continuously tunable ranges.
ATC : frequency tuning mechanism by controlling the incident angle of the light into the nonlinear optical crystals, BC : control mechanism of the birefringence in the nonlinear optical crystals, BS : translatable beam splitter, DFG : difference frequency generator by nonlinear optical crystals, FT : frequency tracking system between the two lasers by negative electrical feedback, M : translatable mirror, PFC : parametric frequency converter by nonlinear optical crystals, SFG : sum frequency generator by nonlinear optical crystals, SHG : second harmonic generator by nonlinear optical crystals.

はDAN)の使用が試みられている[25]．波長0.67 μmレーザを第2の主レーザとし，同様な方法で波長1.34 μmレーザとの周波数同期が可能である．光-光2重共鳴法を採用するとすればLi原子が適していることが指摘されている[1]．以上の4種類の光源をもとに有機，および無機非線形光学結晶を用いたパラメトリック周波数変換，和および差周波数発生，により波長1.56 μm～波長0.34 μmまで，すなわち周波数範囲700 THzにわたる周波数掃引の可能性が示されている．但し，現在作成し得る有機，無機非線形光学結晶および非線形導波路の性能を考慮すると700 THzにわたる連続掃引は必ずしも直ちに実現し得るわけではなく，周波数掃引不可能範囲が不連続に存在する．これを差し引くと周波数連続掃引範囲は図11の右端の周波数軸上のメッシュを施した部分になり，その合計は約140 THzであると試算されている[27]．

5. むすび

本論文では半導体レーザについて，その発振スペクトル半値幅の狭さく化，主レーザへの周波数と位相の追随，安定かつ高精度の周波数掃引，に関する筆者らの最近の実験結果をまとめて報告した．一方，文献(2)中の表1にはその執筆時点でのこれらの実験結果の現状および将来予測を示した．これと比較すると，本論文の結果の中で特にヘテロダイン形光位相同期ループによる周波数，位相追随の精度に関しては**3.2**に示したように当時の将来予測値に達していることが確認される．また，**4.**の後半に示した広帯域周波数掃引システムが実現すればペタヘルツ(=1×10^{15} Hz)級のハイパーコヒーレント光スイープジェネレータが将来実現すると期待される．

なお，本論文ではフリーランニング状態の半導体レーザの周波数ゆらぎの大きさを決めている自然放出光そのものの特性は制御せず，自然放出光ゆらぎがレーザ周波数ゆらぎに寄与する大きさを電気的負帰還制御法，または光帰還法により補正する方法について述べた．一方，最近はCavity Quantum Electrodynamics (Cavity QED)の手法を用いて自然放出発生確率そのものを制御することが試みられている[28]．この試みはいまだ初期段階にあるが，この手法を用いれば量子雑音の少ない，新しい光源の可能性が期待される．

謝辞 日ごろ御指導頂く，東京工業大学伊賀健一教授に感謝致します．また，筆者らの研究は東京工業大学の中川賢一博士，同大学院学生の吉田浩之，池上英次，輿石伊佐央，手島光啓，の各氏，更に研究生の今井享氏，の積極的な御協力なしには実現し得なかったものであり，ここに感謝致します．

文　献

(1) M. Ohtsu: "Progress toward highly coherent semiconductor lasers", Proc. the seventh International Conf. on Integrated Opt. and Opt. Fiber Commun., (IOOC '89), Kobe, Japan, paper number 19A3-1 (July 1989).

(2) 大津元一，中川賢一："半導体レーザーの周波数制御とその応用"，応用物理，**58**, 10, pp. 1428-1444 (平1-10).

(3) M. Ohtsu, M. Murata and M. Kourogi: "FM noise reduction and sub-kHz linewidth of an AlGaAs laser by negative electrical feedback", IEEE J. Quantum Electron., **26**, 2, pp. 231-241 (1990).

(4) 大津元一："ハイパー・コヒーレント光の実現"，サイエンス，平成元年3月号，pp. 64-73.

(5) M. Ohtsu: "Spectroscopy by Semiconductor Lasers, Chapter 4 of "Semiconductor Lasers for Coherent and Quantum Optics" ", Ed. by Y. Yamamoto, (John-Wiley, New York, 1990) to be published.

(6) 興梠元伸，清原章公，大津元一："半導体レーザのFM雑音抑圧のための電気的負帰還システムの高性能化"，信学技報，**OQE89**-62 (1989-09).

(7) M. Ohtsu and N. Tabuchi: "Electrical feedback and its network analysis for linewidth reduction of a semiconductor laser", J. Lightwave Technol., **6**, 3, pp. 357-369 (March 1989).

(8) 手島光啓，申　哲浩，大津元一："ホモダイン光位相同期のための光帰還半導体レーザの周波数変調特性"，第50回応物秋季予稿集，29p-ZL-3 (平1-09).

(9) A. Mooradian: "High Resolution Tunable Infrared Lasers", in "Laser Spectroscopy", Ed. by R. G. Brewer and A. Mooradian, pp. 223-236, Plenum Publishing Corp., New York (1977).

(10) D. Lenstra, B. H. Verbeek and A. J. den Boef: "Coherence collapse in single-mode semiconductor lasers due to optical feedback", IEEE J. Quantum Electron., **QE-21**, 6, pp. 674-679 (June 1985).

(11) B. Dahmani, L. Hollberg and R. Drullinger: "Frequency stabilization of semiconductor lasers by resonant optical feedback", Opt. Lett., **12**, 11, pp. 876-878 (Nov. 1987).

(12) 申　哲浩，手島光啓，大津元一："光位相同期のための高コヒーレント半導体レーザ"，第36回応物春季予稿集，4P-ZC-1 (平1-04).

(13) C. -H. Shin, M. Teshima and M. Ohtsu: "FM characteristics and compact modules of coherent semiconductor lasers coupled to an external cavity", to be published in March issue, 1990, IEEE Photonics Technol. Lett..

(14) L. Hollberg and M. Ohtsu: "Modulatable narrow-linewidth semiconductor lasers", Appl. Phys. Lett., **53**, 11, pp. 944-946 (Sept. 1988).

(15) C.-H. Shin, M. Teshima, M. Ohtsu, T. Imai, J. Yoshida and K. Nishide: "Modulatable, high coherent and compact semiconductor laser modules", Proc. the seventh International Conf. on Opt. and Opt. Fiber Commun. (IOOC '89), Kobe, Japan, paper number 21D4-5 (July 1989).
(16) 今井　享，吉田純一，西出健一，申　哲浩，手島光啓，大津元一："光ファイバジャイロ用高コヒーレント半導体レーザ"，第36回応物春季予稿集，4P-ZC-2 (平1-05).
(17) 鈴木宏昌，興石伊佐央，大津元一，寺町康昌："可視半導体レーザの周波数制御"，第50回応物秋季予稿集，29p-ZL-7 (平1-09).
(18) T. Okoshi, K. Kikuchi and A. Nakayama: "Novel method for high resolution measurement of laser output spectrum", Electron. Lett., **16**, 16, pp. 630-631 (July 1980).
(19) J. M. Kahn: "1 Gbit/s PSK homodyne transmission system using phase locked semiconductor lasers", IEEE Photonics Technol. Lett., **1**, 10, pp. 340-342 (Oct. 1989).
(20) G. Wenke and S. Saito: "Phase locking of semiconductor lasers using homodyne detection and negative electrical feedback", Jpn. J. Appl. Phys., **24**, 12, pp. L908-L910 (Dec. 1985).
(21) K. Kuboki and M. Ohtsu: "Frequency offset locking of AlGaAs semiconductor lasers", IEEE J. Quantum Electron., **QE-23**, 4, pp. 388-394 (April 1987).
(22) K. Kuboki and M. Ohtsu: "A synthesized method to improve coherence in semiconductor lasers by electrical feedback", IEEE J. Quantum Electron., **QE-25**, 10, pp. 2084-2090 (Oct. 1989).
(23) 加藤　徹，久保木勝彦，大津元一："周波数オフセットロックシステムの性能評価"，第48回応物秋季予稿集，20p-ZQ-4 (昭62-10).
(24) 申　哲浩，手島光啓，大津元一："半導体レーザによるヘテロダイン型光位相同期ループ"，第50回応物秋季予稿集，29p-ZL-4 (平1-09).
(25) 池上英次，楠澤英夫，中川賢一，大津元一："半導体レーザ光スイープジェネレータ用の有機非線形導波路 I (周波数同期)"，第50回応物秋季予稿集，28p-ZP-16 (平1-09).
(26) M. Ohtsu and E. Ikegami: "Frequency stabillization of 1.5 μm DFB laser using internal second harmonic generation and atomic ^{87}Rb line", Electron. Lett., **25**, 1, pp. 22-23 (Jan. 1989).
(27) 楠澤英夫，池上英次，中川賢一，大津元一："半導体レーザによるペタヘルツ級超高コヒーレント光スイープジェネレータの基礎研究"，第4回光波センシング研究会予稿集，LST4-8 (平1-12).
(28) S. Haroche and D. Kleppner: "Cavity quantum electrodynamics", Phys. Today, pp. 24-30 (Jan. 1989).

(平成元年12月25日受付)

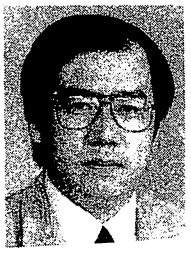

大津　元一

昭48東工大・工・電子卒．昭53同大学院博士課程了．東工大・精研・助手を経て現在，同大学院総合理工・助教授．この間，昭61から62，AT&Tベル研究所研究員．光量子エレクトロニクス，レーザ制御と応用，などの研究に従事．電気学会，応用物理学会，OSA，IEEE各会員．昭57応用物理学会賞(B)，昭59電波科学国際連合(URSI)よりI. KOGAゴールドメダル，昭63日本IBM科学賞(エレクトロニクス部門)受賞．著書「レーザーと原子時計」，「超高コヒーレント光の発生」など．

申　哲浩

1976年韓国海洋大学卒．1985年同大学院電子航海計器専攻修士課程了．東工大・物理情報工学専攻博士課程在学中．1976年3月大韓船舶株式会社船舶部航海士，1980年(株)三益商船運航部課長代理．1982年3月から韓国国立木浦海洋専門大学専任講師，1984年4月同助教授．現在，半導体レーザの周波数制御，コヒーレント光通信基礎，特に半導体レーザによるヘテロダイン・ホモダイン光位相同期の研究に従事．応用物理学会，大韓電子工学会，韓国航海学会各会員．

楠澤　英夫

昭59信州大・工・情報卒．昭61同大学院修士課程了．昭61スタンレー電気株式会社技術研究所入社．昭63同社退社．現在，東工大・大学院総合理工学研究科博士後期課程在学中．非線形光学効果による半導体レーザの光周波数変換(光スイープジェネレータ)の研究に従事．応用物理学会，同結晶工学分科会会員．

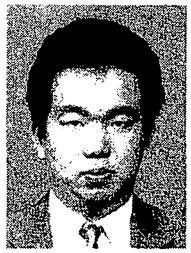

興梠　元伸

昭63静大・工・光電機械卒．同年東工大・大学院総合理工学研究科入学．現在，修士課程在学中．半導体レーザの周波数，位相制御の研究に従事．応用物理学会会員．

鈴木　宏昌

平成元年東工大・理・応物卒．同年東工大・総理工・物情入学．現在，修士課程在学中．可視半導体レーザの周波数制御およびその応用の研究に従事．応用物理学会会員．

4 TH EUROPEAN FREQUENCY AND TIME FORUM NEUCHÂTEL - 13 - 14 - 15 MARCH 1990

Session Number

Laser frequency stabilization with applications to atomic frequency standards

K.Nakagawa and M.Ohtsu

Graduate School at Nagatsuta, Tokyo Institute of Technology
4259 Nagatsuta, Midori-ku, Yokohama 227, Japan

Abstract
Recent works on frequency stabilizations of semiconductor lasers are introduced and several applications are demonstrated. The stability of the Rb atomic clock is expected to be improved by using these stabilized lasers. Several works on optically pumped Rb atomic clock are shown and further improvements are discussed.

1. Introduction

Frequency stabilizations of lasers are very important factors in many applications using lasers. High stability and wide wavelength range of stabilized lasers should be required in many applications of these lasers. Recently, semiconductor lasers are developed and widely used especially for optical communications and optical information systems. Very recently, oscillation wavelength range is extended to 670nm, which is close to that of a red HeNe laser. Available output power is higher than 1W, which is comparable to that of the Ar^+ laser. The frequency fluctuations of semiconductor lasers have been

reduced to be reached to stable gas lasers. These progresses make it possible to use semiconductor lasers in many applications such as high resolution spectroscopy, precise measurement for fundamental physics[1].

In the field of frequency and time standards, optical frequency standard is important and required to be more accurate. The coherent optical communication system requires absolute frequency reference in near-infared region[2]. The frequency stabilized semiconductor lasers will play an essential role in this field. Another important application of semiconductor lasers is optically pumped atomic frequency standard. The usage of stabilized semiconductor lasers can improve further stability and contribute to improve the realiability[3)-6].

In consideration of frequency standards, we show the recent investigations of frequency stabilization of semiconductor lasers and an optically pumped Rb atomic clock of our group.

2. Frequency stabilizations of semiconductor lasers

Magnitude of frequency fluctuation of free running semiconductor lasers is generally larger than that of other stable gas lasers. However, the characteristics of frequency tunability and fast response by the injection current make it possible to stabilize its frequency by feedback techniques. There are mainly two methods of negative feedback for frequency stabilization. One method uses electrical feedback by controlling the injection current and the other uses the optical feedback from an external reflector or cavity.

In the case of electrical feedback method, an external cavity is used as the frequency discriminator and the reflected light from the cavity is detected and fed back to the injection current of the laser[7](Fig.1). In this method, the high feedback gain and desirable feedback bandwidth is available. Figure 2 shows the improvement of the frequency fluctuation by using this electrical feedback. The obtained linewidth is

560Hz which is further less than the Shallow-Townes' limit of linewidth of 55kHz in free running condition. The advantages of this method are that direct frequency modulation is available and the instability induced by the optical feedback is avoidable. This electrical feedback method was also employed to realize a homodyne-type optical phase locked loop. The residual phase variance as low as 0.15 rad^2 was obtained by expanding the feedback of bandwidth of 100 MHz[8].

Another method is to use a optical feedback from an external cavity[9]. This method can reduce frequency fluctuation in wide frequency bandwidth which is determined by the linewidth of the external cavity. The linewidth of less than 10kHz can be easily achieved[10]. We develped compact semiconductor laser modules with using this method for practical applications[10](Fig.3). This method was also applied to the heterodyne type optical phase locked loop[11](Fig.4). The residual phase error variance was reduced to 0.02 rad^2(Fig. 5).

Recently, semiconductor laser oscillations have reached to visible region(<670nm). In the near future, the HeNe laser(633nm) will be replaced by these visible semiconductor lasers in many fields. However, the spectral characteristic of these lasers is still worse than that of the near-infrared semiconductor lasers. The typical linewidth of this laser is order of several hundred MHz. We have improved the linewidth of this visible semiconductor laser of less than 50kHz with using the optical feedback method[12]. This result suggests the potential capability of optical frequency standard of using visible semiconductor lasers. Now we are trying to stabilize these laser frequencies to atomic transitions of Li at 670nm.

In the case of the optical feedback method, a distance between a laser facet and an external reflector should be controlled to adjust the phase of reflected light. This technical inconvenience can be avoided by replacing the external mirror by a phase conjugate mirror(PCM). We have demonstrated the linewidth narrowing by the PCM which use the four-wave mixing process in the semiconductor laser medium[13]. The noncolinear light from the master laser is incident into the slave laser and the phase conjugate light is fed into the master laser. The linewidth of the master was reduced to be less than fifth of that of the

free running and was not affected by varying the distance between two lasers.

Frequency stabilization of the semiconductor lasers has been carried out by using atomic and molecular transitions as frequency references, and the stability as high as 2×10^{-12} was obtained at the integration time of 100s[14]. A novel method of using an internal second harmonics of an InGaAsP laser of 1560 nm was proposed to stabilize its frequency to the Rb absorption spectral line at 780 nm[15](Fig. 6). This method will provide frequency chain between the 1560nm laser and 780nm laser by locking simultaneously to the Rb absorption line. To increase an efficiency of second harmonics of semiconductor lasers, we are trying to use an external SHG from nonlinear material.

3. Application to optically pumped Rb atomic clock

It has been mentioned that the usage of stabilized lasers for optically pumped atomic clock can improve the stability of the atomic clock[3]. We have improved the stability of a Rb atomic clock by employing a frequency stabilized semiconductor laser[4](Fig. 7).

One of the advantage of using a laser instead of a Rb lamp is that an extremely narrow linewidth of 200Hz can be obtained in a optical-microwave double resonance signal and this result contributes to improve a short-term frequency stability of the Rb atomic clock[4),16](Fig. 8). The S/N ratio of the double resonance signal is mainly determined by the FM noise of the semiconductor laser. By employing the electrical feedback method, the FM noise of the laser was reduced at the microwave modulation frequency of 1 kHz and the S/N ratio of the double resonance signal was improved to be more than 10 dB(fig. 9).

The long-term stability of the clock is improved by employing the stabilized lasers[17]. Although the light shift causes the drift and error of the microwave clock frequency, this error is canceled by the self-tuned frequency stabilizing of the semiconductor laser. The slight frequency detuning of the laser from

the Rb transition causes light shift and asymmetry of the line shape of the signal. By employing a computer controlling system, this asymmetry was estimated and the effect of light shift was compensated by the feedback of the injection current of the laser. Figure 10 shows the result of the improvement and the drift was about forty five lower than that of the free running.

The transition frequency of the present clock is affected and shifted by the pressure shift of buffer gases. Now we are constructing a Rb-beam type optically pumped atomic clock.

4. Summary

We have investigated the frequency stabilization of the semiconductor laser. The experimental results are summarized as follows.

center frequency stabilization	2×10^{-12}
linewidth reduction	560 Hz
frequency tracking	1.1×10^{-18}

These stabilization and controlling technics of semiconductor lasers can be directly applied to optical frequency standard in visible and near-infrared region.

The optically pumped Rb atomic clock was stabilized by using the stabilized semiconductor lasers. The short-term stability was improved to be $7.9 \times 10^{-13} \tau^{-1/2}$. Further improvement can be expected by employing the FM noise reduction of more than 60 dB, which can be achived by employing the electrical feedback method(Fig.2). The frequency drift induced by light-shift was reduced by self-tuned controlling system and the long-term stability was obtined to be as low as 6.3×10^{-13}/h.

References

1) C.E.Tanner and C.E.Wieman, Phy.Rev.A **38**, 162-165(1988).
2) S.Sudo, Y.Sakai, H.Yasaka, and T.Ikegami, IEEE Photon. Technol. Lett., Vol.1 281-284(1989).
3) J.L.Picque, Metrologia **13**, 115-119(1977).
4) M.Hashimoto and M.Ohtsu, IEEE J.Quantum Electron. **QE-23**, 446-451(1987).
5) S.Ohshima, Y.Nakadan and Y.Koga, IEEE Trans. Instrum. Meas. **37**, 409-413(1988).
6) D.W.Sesco and C.E. Wieman, Opt. Lett. **14**, 269-271(1989).
7) M.Ohtsu, M.Murata and M.Kourogi, IEEE J.Quantum Electron., **QE-26**, Feb. issue (1990).
8) M.Kourogi and M.Ohtsu, prepared for submission.
9) B.Dahmani, L.Hollberg, and R.Drullinger, Opt. Lett. **12**, 876-878(1987).
10) C.H.Shin, M.Teshima, M.Ohtsu, T.Imai, J.Yoshida, and K.Nishide, IEEE Photonics Technol. Lett., **2**, March issue, (1990) to be published.
11) C.H.Shin and M.Ohtsu, IEEE Photonics Technol. Lett. **2**, April issue, (1990) to be published.
12) H.Suzuki, K.Nakagawa and M.Ohtsu, prepared for submission.
13) I.Koshiishi, H.Suzuki, and M.Ohtsu, prepared for submission.
14) M.Ohtsu, Optical and Quantum Electron. **20**, 283-300(1988).
15) M.Ohtsu and E.Ikegami, Electron. Lett. **25**, 22-23(1989).
16) M.Hashimoto, and M.Ohtsu, J.Opt.Soc.Am.B **6**, 1777-1789(1989).
17) M.Hashimoto, and M.Ohtsu, IEEE Trans. Instrum. Meas. May issue, (1990) to be published.

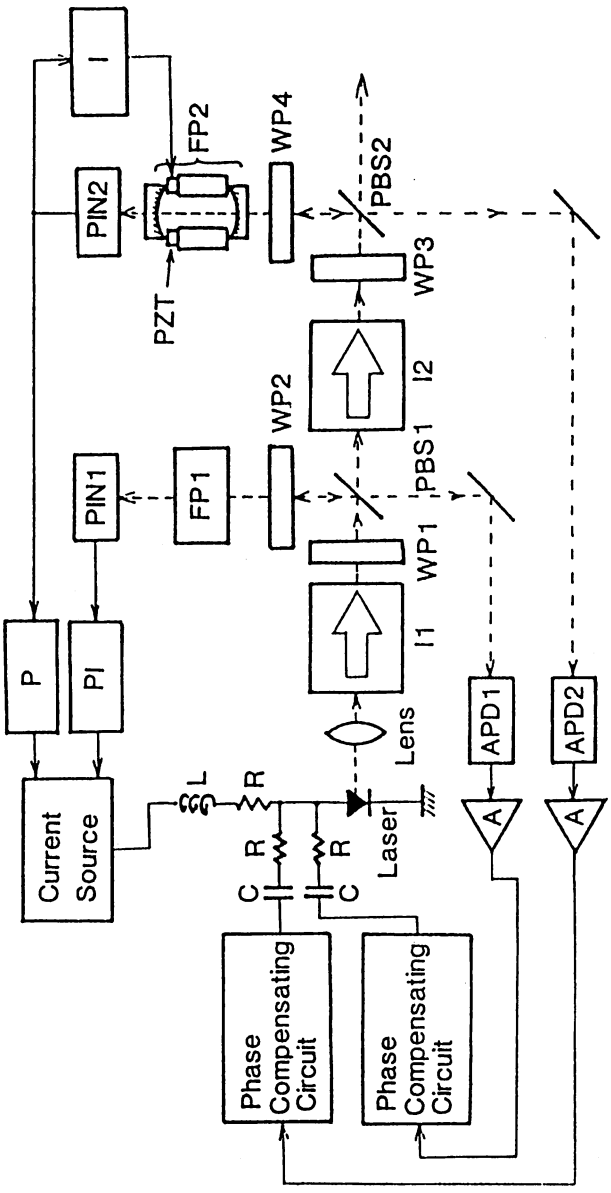

Figure 1. Block diagram of an electrical feedback semiconductor laser(Ref.7).

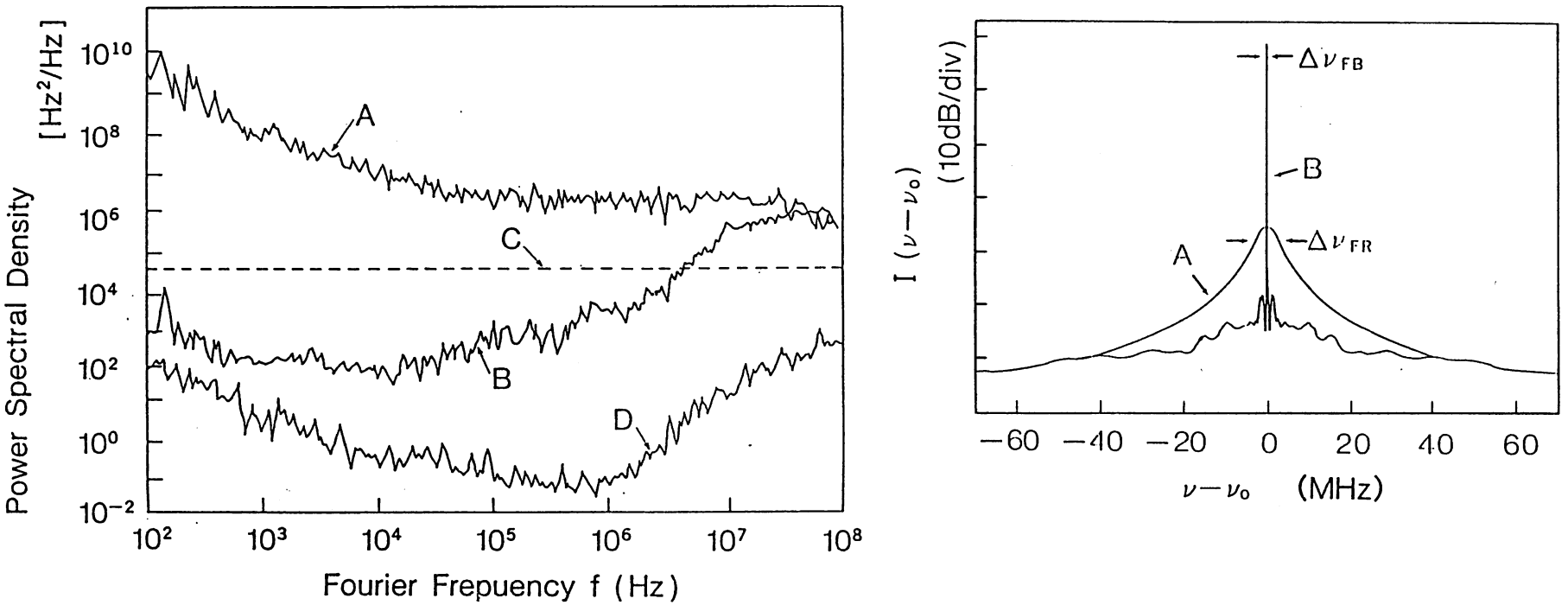

Figure 2. Progress of the experiments on linewidth reduction by electrical feedback(Ref.7). Power spectral densities of frequency fluctuations are shown in (a). Profiles of the field spectrum are shown in (b). A: Free running. B: With electrical feedback. C: Shallow-Townes' limit of the free running laser. D: Detection noise limit of the electrical feedback laser.

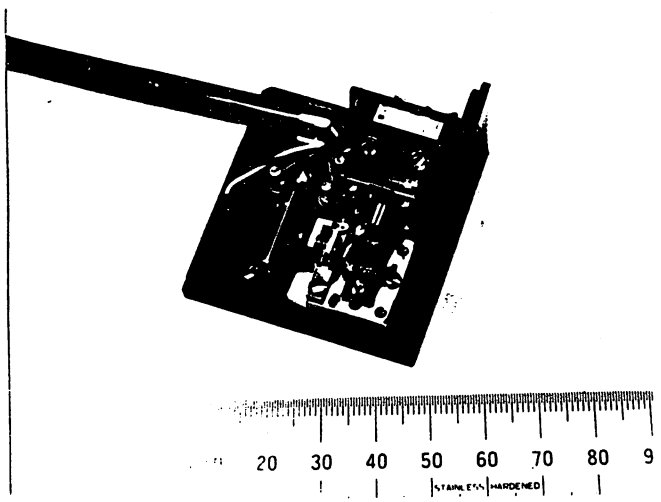

Figure 3. Compact module of an optical feedback semiconductor laser (Ref.10).

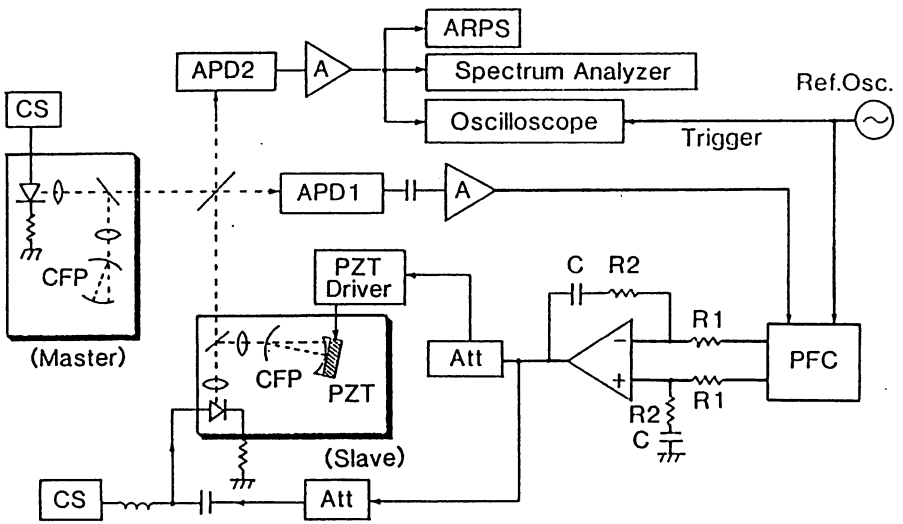

Figure 4. Block diagram of the heterodyne optical phase-locked loop(Ref.11).

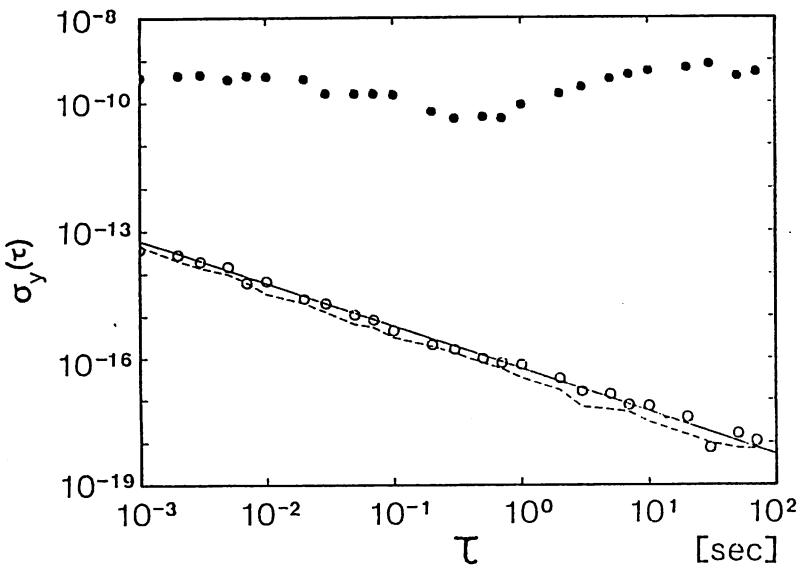

Figure 5. Measured results of Allan variances of residual frequency fluctuations of the heterodyne signal(Ref.11). ● and O represent in free running and phased-locked condition, respectively.

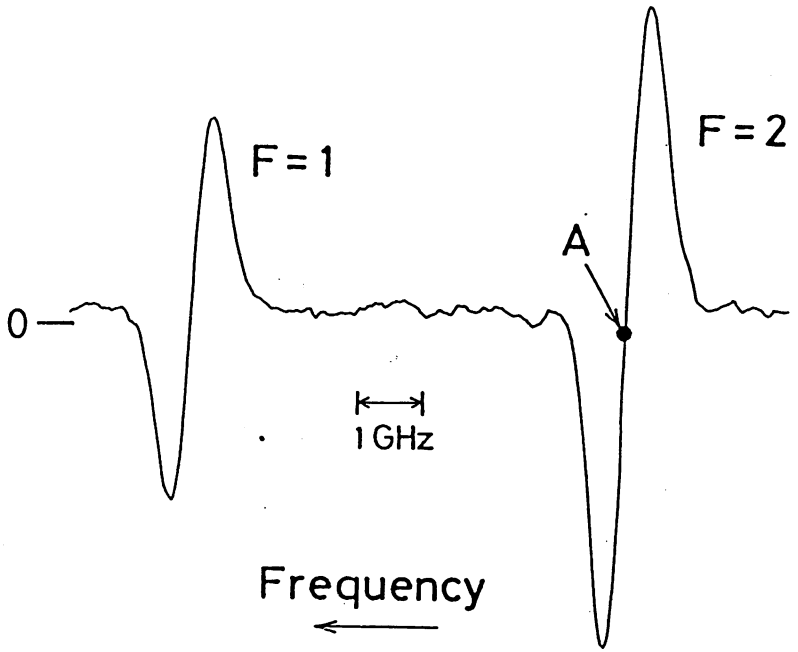

Figure 6. First derivative signal of ^{87}Rb-D_2 spectral lines. The internal second harmonics frequency was locked to point A(Ref.15).

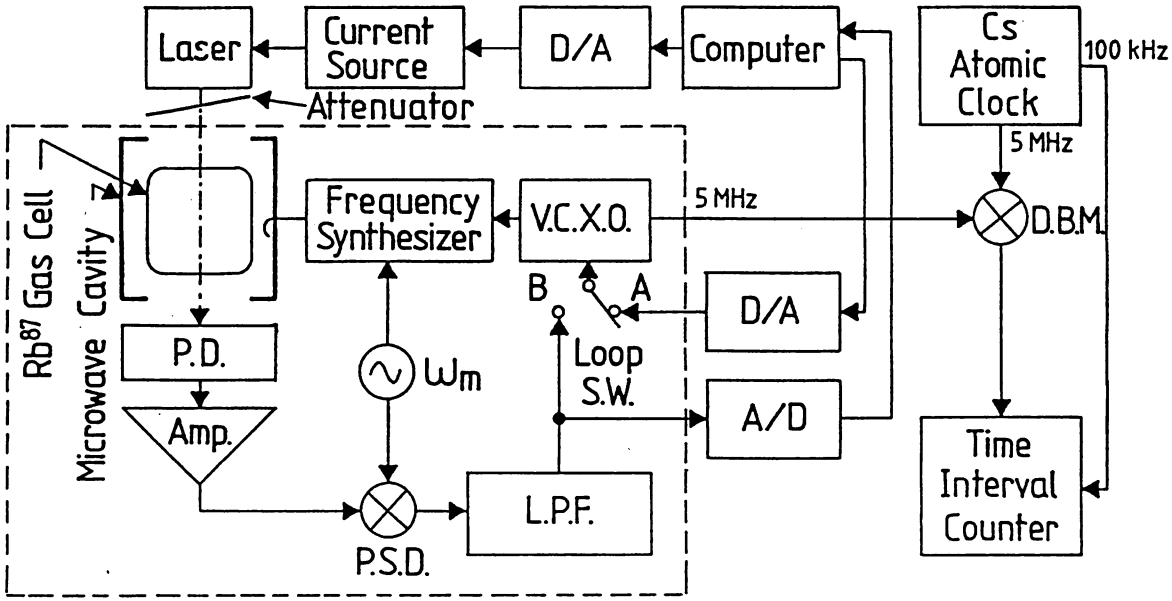

Figure 7. Block diagram of a semiconductor laser pumped Rb^{87} atomic clock(Ref.17).

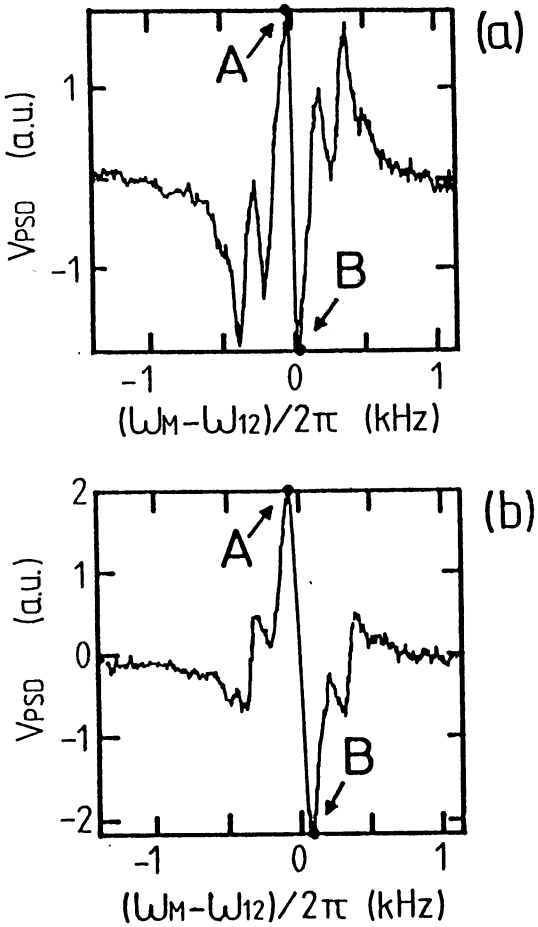

Figure 8. Typical spectral lineshapes of double resonance signal (Ref.16).

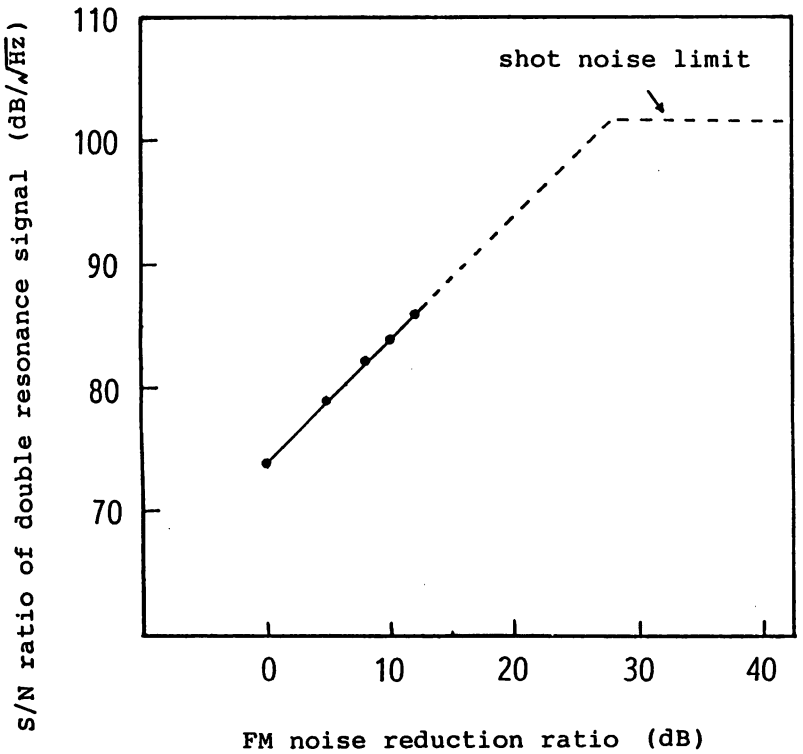

Figure 9. Improvement of the S/N ratio of the double resonance signal.

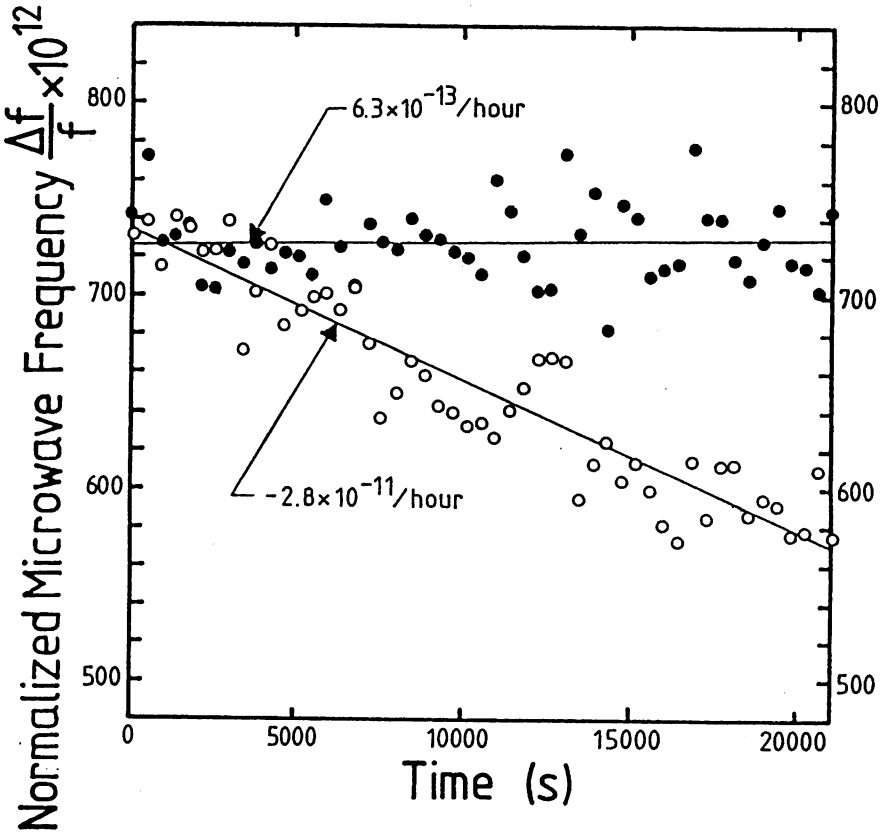

Figure 10. Drift of the microwave frequency. ● and ○ represent the results obtained with and without the self-tuning method, respectively (Ref.17).

9:30 AM Invited paper
CME5 Progress toward a 1-PHz hypercoherent optical sweep generator by semiconductor lasers

M. OHTSU, K. NAKAGAWA, C.-H. SHIN, H. KUSUZAWA, M. KOUROGI, H. SUZUKI, Tokyo Institute of Technology, Graduate School at Nagatsuta, 4259 Nagatsuta, Midori-ku, Yokohama 227, Japan.

We demonstrate that the combination of frequency controlled semiconductor lasers with inorganic and organic nonlinear optical waveguides can make a hypercoherent (FM noise below the Schawlow-Townes limit) optical sweep generator with a frequency tunable range of ~1 PHz (1×10^{15} Hz), i.e., between the 1.56- and 0.34-μm wavelength region. Frequencies of two InGaAsP lasers, an AlGaAs laser, and an AlGaInP laser are controlled; for example, the half linewidth of the 0.8-μm AlGaAs laser was reduced to 560 Hz by negative electrical feedback.[1] This value is less than the Schawlow-Townes limit from which it can be said that hypercoherent state light was generated.[2]

Frequency tracking and sweeping between these lasers are achieved by three steps. The first is second harmonic generation from the 1.56-μm laser using organic (DAN) nonlinear optical waveguides.[3] As the second step, coarse frequency tracking of this second harmonic frequency to the hypercoherent 0.78-μm AlGaAs laser is achieved by optical-optical double resonance in Rb atomic vapor. The coarse frequency tracking of the second harmonics of the 1.34-μm InGaAsP laser to the 0.67-μm AlGaInP laser is also possible using Li atomic vapor. To obtain Doppler-free optical-optical double resonance spectral profiles, the half linewidth of the 0.67-μm AlGaInP laser was reduced to 50 kHz, which is 2.5×10^{-4} times that of the free-running condition. Fine tracking is carried out by heterodyne or homodyne optical phase locking.

Figure 1 shows the experimental results when the residual beat frequency noise was reduced to 1.1×10^{-18} at 70-s integration time, which corresponds to 0.18-rad phase fluctuation. Figure 2 shows that the power spectra of phase fluctuations were lower than 2×10^{-9} rad^2/Hz within the feedback bandwidth of 10 MHz.

As the third step, these lasers are used as the master lasers for parametric frequency conversion by organic (MNA or MBANP) nonlinear optical DFB type waveguides. Figure 3 shows an example of calculated results to estimate the tunable range by a waveguide. In addition to the parametric frequency conversion, sum and difference frequency generation is carried out using inorganic and organic nonlinear optical waveguides. From these considerations, we estimated that the tunable range from 1.56 and 0.34 μm corresponding to 700 THz with a net tuning range of ~100-THz frequency can be achieved.

By assembling the techniques described above, a petahertz class hypercoherent optical sweep generator system can be constructed in the future. For further improvements to this system, a novel method of cavity quantum electrodynamics is proposed to make an inherently low noise light source by controlling the spontaneous emission rate from Rb atoms. Manipulation of Rb atoms is also proposed by this cavity quantum electrodynamics scheme.

1. M. Ohtsu, M. Murata, and M. Kourogi, IEEE J. Quantum Electron. (Feb. 1990).
2. M. Ohtsu, Science (Japanese version of Sci. Am.) 64–73 (in Japanese) (Mar. 1989).
3. M. Ohtsu and E. Ikegami, Electron. Lett. 25, 27–28 (1989).

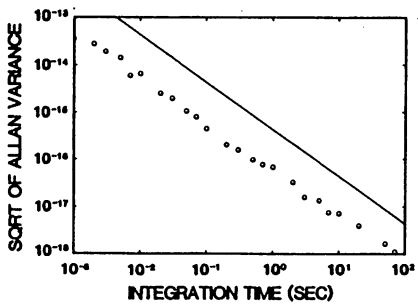

CME5 Fig. 1. Square root of the Allan variance of the residual frequency fluctuations of the beat signal in the heterodyne optical phase-locked loop. The solid line represents the 1-rad phase variance level.

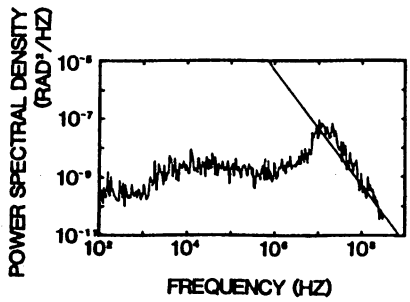

CME5 Fig. 2. Power spectral density of the phase noise of the homodyne optical phase-locked loop. The solid line represents that of the unlocked condition.

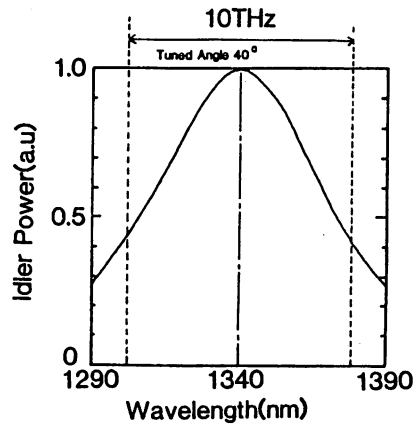

CME5 Fig. 3. Calculated result of the wavelength tunable range by parametric frequency conversion with a nonlinear organic (MNA) optical DFB waveguide.

Proposal of a Semicondoutor Laser Diode Based Peta Hertz Class Coherent Optical Sweep Generator

H.Kusuzawa, E.Ikegami, H.Huruta, K.Nakagawa, and M.Ohtsu
Graduate School at Nagatsuta, Tokyo Institute of Technology
4259 Nagatsuta, Midori-ku, Yokohama 227, Japan

<Abstract>

We proposed an optical sweep generator with the total sweep range of 700THz (≅ one Peta-Hz), and demonstrated the crystal growth of organic nonlinear elements and the possibility of frequency link between two LDs.

1.Introduction

Coherent Optical Sweep Generator (OSG) covering from ultraviolet to infrared is one of ideal light sources requiring for various applications. However, any frequency stabilized and wide range tunable OSG has not yet been realized. Based on this background, we first propose an OSG with optical frequency conversion systems by four semicondoutor laser diodes (LDs). This system employs nonlinear optical elements, the techniques of frequency stabilization, and tracking. In this paper we describe two important techniques for realizing of the proposed OSG. First, two pairs of frequency tracking links,(i.e.,the one between 0.78 μm and 1.56 μm LDs and the other between 0.67 μm and 1.34 μm LDs) by using internal second harmonic waves (SH waves). One LD of each pair was frequency stabilized to an absorption line of atomic vapors. Second, coarse frequcncy tuning can be obtained by parametric frequency conversion using organic nonlinear waveguides (ONLWs) with gratings. It can be expected by using these waveguides that sweep optical frequency span is expanded to 700THz (≅ one Peta-Hz), where the net continuous sweeping range is 140THz.

The output power of this system will be shown, as low as subμW, however, our purposes is to realize a highly accurate frequency sweeping system. General concepts of this system are reviewed by one of the authors in CLEO'90[1]. Technical details are presented here.

2.System configuration

Figure 1 shows a general arrangement of the proposed OSG system. LD modules in this system are optically stabilized narrow linewidth LDs with external cavities[2]. Their wavelengths are 0.67, 0.78, 1.34, and 1.56 μm. Optical frequencies of 0.67μm and 0.78 μm LDs are stabilized to absorption lines of Li atoms and Rb atoms, respectively These frequency are linked with internal SH waves of 1.56 μm and 1.34 μm LDs. On the other hand, the frequency stabilized light of 0.78 μm and 0.67 μm are converted by the parametric frequency conversions (PFC) of using ONLW. And the actual sweep ranges are extended by sum or difference frequency conversions. Some $LiNbO_3$ balk crystals with Fabry-Perot cavity are employed for sum or difference frequency generation (SFG or DFG modules). The center frequency of sweep range by PFC is lifted up by SFG or DFG module. Finally the continuous sweep range is expanded to 140THz by using nine SFG and one DFG modules.

Additionally, a wavelength measurement system will be used to feedback to this system for the precise tuning of the optical frequency. Second harmonic generation (SHG) in Fig. 1 is achieved by using nonlinear optical fiber, in which DAN (4-(N, n-dimethylamino)-3-acet-amidonitrobenzen) is filled.

3.Coarse frequency sweeping by ONLWs

Figure 2 shows an ONLW structure for coarse frequency sweep proposed the first time, where MNA(2-methil-4-nitroaniline)[3] is used as the nonlinear organic material. The coarse frequency sweep is made by the angle turning of the ONLWs. The ONLW is consist of three elements which are optical flat glass, organic nonlinear single crystalline thin film, and SiO_2 evaporated gap spacers. Sinusoidal grating is made by holographic exposure on the upper optical flat glass. The chirped grating[4] will be employed by which requirement of the control of MNA thin film can be relieved. The grating consist of a resonator for pump, idler, and signal waves. Internal optical power increase by this configuration and thereby conversion efficiency are also improved by a factor of 100 times over an ONLW without grating. By employing this structure, the mode dispersion is occurred, and pump, signal, and idler waves satisfy two dimensional phase matching conditions. Figure 3 shows phase matching conditions, i.e., a relation between the output angle of the idler wave and the thickness of the thin film crystal. As shown by Fig. 4 frequency sweep range and output power in this case are 14THz and 3 μW, respectively.The output power of OSG is expected to the 960nW. A most important advantage of ONLW is the fact that the temperature control is not required.

We have confirmed that the ONLW can be grown by vapor pressured crystal growth method. Figure 5 shows an example of ONLW without grating. By this surface photograph, we could confirmed that a single crystalline thin film was fabricated. We have also confrimed a single crystalline organic nonlinear optical fiber, in which MNA or DAN is filled.

4.Frequency stabilization, tracking and fine tuning system

We have stabilized the center frequency of 1.56 μm InGaAsP LD to an absorption line of Rb atomic vapor. The measured stability was 3.0×10^{-9} at the integration time of 100s in square root of Allan variance[5].

Furthermore, 0.78 μm GaAlAs LD and internal SH wave of 1.56 μm InGaAsP LD can be stabilized and tracked with each other by using a Doppler-free optical-optical double resonance Rb spectral line as a reference without modulating the frequency of 1.56 μm LD (see Fig. 6). We have observed an optical-optical double resonance spectrum.(see Fig. 7). This confirms possibility of the frequency link between 1.56μm LD and 0.78μm LD.

5.Summary

We proposed a coherent wideband optical sweep generator. Achievable total sweep range and continuous sweep range are i.e., 700THz (≅one Peta Hertz) and 140THz, respectively, with new type ONLWs. We demonstrated possibility of the frequency link between 1.56μm LD and 0.78μm LD, which is a key element for realizing the proposed OSG.

6.references

[1] M.Ohtsu, K.Nakagawa, C.H.Shin, H.Kusuzawa, M.Kourogi:" Progress toward a Peta-Hz Hyper Coherent Optical Sweep Generator by secmicodcuctor Lasers " to be presented as an invited paper at CLEO'90

[2] C.H.Shin, M.Teshima, M.Ohtsu, T.Imai, J.Yoshida, and K.Nishide: IEEE PTL, 2, to be published in April issue, 1990

[3] R.Morita, N.Ogasawara, S.Umegaki, R.Ito: J. J. Appl. Phys.,Vol.27(6) pp.1131-1133 June (1988)

[4] A.Katzir, C.Livanos, J.B.Shellan, and A.Yariv: "Chirped gratings in Integrated Optics " IEEE J. Quantum Electro., Vol.QE-13, No.4, April 1977

[5] M.Ohtsu, E.Ikegami: " Frequency stabilization of 1.5μm DFB laser using internalsecond harmonic generation and atomic Rb line. " Elect.Let.25, p22, 1989

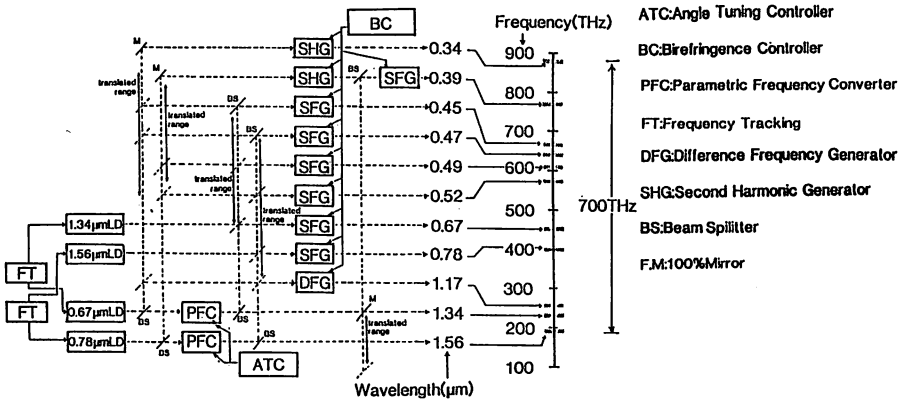

Fig.1 Peta Hertz class optical sweep Generator system

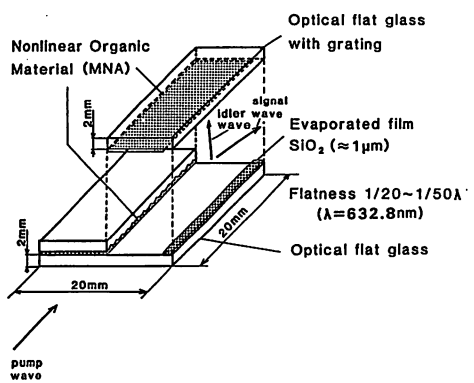

Fig.2 New type of organic nonlinear waveguide structure

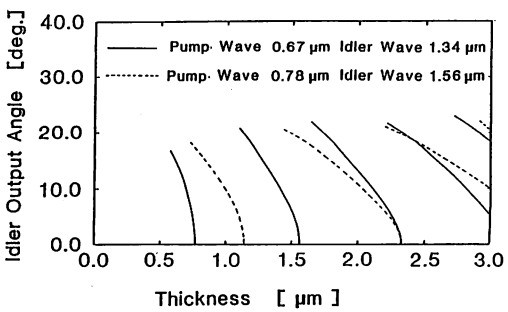

Fig.3 Relation between the idler output angle and the thickness of MNA thin film to meet the Phase matching condition

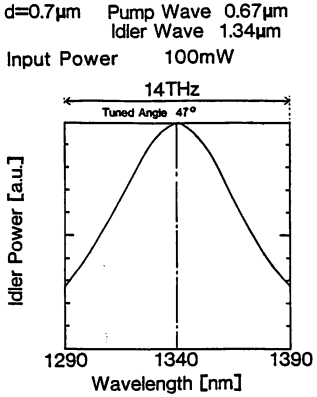

Fig.4 Output power and sweep range of organic nonlinear waveguide by MNA

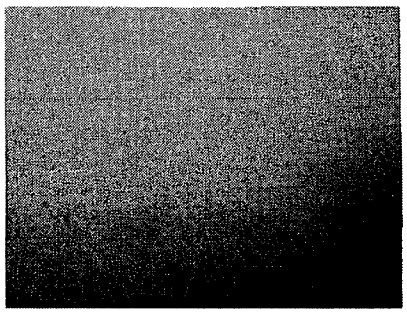

Fig.5 Surface photograph of organic nonlinear waveguide without grating by MNA (x 200)

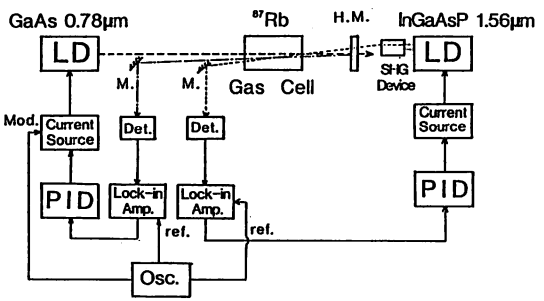

Fig.6 0.78μm and 1.56μm frequency stabilization system with an opticl-optical double resonance Rb spectral line

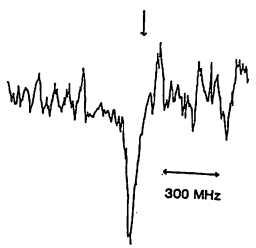

Fig.7 Optical-optical double resonance spectrum of internal SH wave of 1.56μm LD

Optical Phase-Locking Experiments by Confocal Fabry-Perot Cavity Coupled Semiconductor Lasers

Chul-Ho Shin and Motoichi Ohtsu

Graduate School at Nagatsuta, Tokyo Institute of Technology
4259 Nagatsuta, Midori-ku, Yokohama, Japan
Tel 045-922-1111(ext.2526) Fax 045-921-1156

<ABSTRACT>
We have carried out the experiments of the heterodyne and the homodyne optical phase-locked loops using the confocal Fabry-Perot cavity coupled semiconductor lasers with RMS phase errors of 8.1 and 2.6 degrees, respectively.

1. Introduction

Optical phase-locking is a key technology for achieving coherent optical communication systems, precise optical measurements and optical frequency sweep generator, especially by semiconductor lasers because of their merits, i.e., small size, low price, low power consumption, high efficiency and so on. Several experimental results have been reported for homodyne optical phase-locked loops (OPLL)[1]-[6], heterodyne OPLLs [7]-[10] and homodyne OPLL based coherent optical receivers[11]-[14]. A few recent OPLL experiments by external cavity semiconductor lasers have been successfully carried out by utilizing their low quantum phase noises.

The confocal Fabry-Perot cavity (CFP) coupled semiconductor laser diode (CFP-LD) [14]-[16] showed good phase noise suppression, and thereby small linewidth less than 10 kHz, and also improvement of the oscillation center frequency stability of one to two orders comparing with a free running semiconductor laser. Its oscillation frequency can be modulated by modulating the cavity length of the coupled CFP and the injection current directly, and can be, thus, controlled with a wide bandwidth. Using these characteristics of CFP-LD, we carried out the experiments of homodyne and heterodyne OPLLs, and confirmed its excellent frequency and phase tracking capability between two CFP-LDs by the heterodyne OPLL and the homodyne OPLL, respectively. For both of the heterodyne and the homodyne OPLL by CFP-LDs, this presentation is the first report. In case of the heterodyne OPLL, previous experiments by external cavity semiconductor lasers did not report the loop parameters and phase errors at all [7][9]. We measured quantitatively phase errors of the heterodyne OPLL by the Allan variance of residual frequency fluctuations of the phased-locked heterodyne signal, when the heterodyne signal was locked to a RF reference signal. This type measurement of the phase error of the OPLL is reported for the first time.

2. Experiments

The experimental arrangement of the heterodyne OPLL is shown by Fig.1. In this experiment, two commercial 0.83 μm AlGaAs lasers (Hitachi HL8314E) were used as the master and the slave lasers. Temperature fluctuations of the laser mounts were controlled within 1 mK with Peltier coolers. Each of these two lasers was frequency-stabilized by using optical feedback scheme employing a CFP with the finesse of 75 and the FSR (free spectral range) of 1.5 GHz as shown by Fig.1. Optical feedback stabilization of the lasers was maintained upto about one hour, which limited the phase-locking period in case of the heterodyne OPLL. However, the phase-locking period of the homodyne OPLL was mainly limited by DC drifts of the balanced detector used as the phase detector. The linewidth of the unlocked heterodyne signal was estimated to be less than 20 kHz. However, The beat spectral linewidth was 1 to 2 MHz at the 100 sec total sweep time of the RF spectrum analyzer, which resulted from the long term frequency drifts of about 100kHz/sec and noises of lower Fourier frequency bandwidths induced by thermal drifts, acoustics and vibrations. The frequency tuning coefficients of the external cavity length by a PZT and the injection current were 79MHz/V and 31MHz/mA, respectively. The characteristics of frequency noise reduction and direct frequency modulation by the injection current have been reported in [15][16].

First, we explain the experiment of the heterodyne OPLL. The heterodyne signal was detected by two commercial Si-APDs, one for the OPLL and the other for the phase error measurement. The power of about 3.7 μW of each laser was used for the OPLL. The heterodyne signal was phase compared with a stable RF reference signal by a digital phase/frequency comparator (PFC), which is consisted of a high speed voltage comparator and an ECL logic PFC IC. The gain of the PFC is 0.16 Volts/rad. The error signal was passed through a first order active loop filter as shown by Fig.1, and fedback to the slave laser. Two control routes were employed for securing a wide control bandwidth. One is the external cavity length control and the other is the injection current control. The calculated natural angular frequency, the damping factor, the noise bandwidth and the 3dB loop bandwidth by using the measured parameter values were 1.65 x 10^6 rad/sec, 0.82, 925 kHz and 580 kHz, respectively.

Second, in case of the homodyne OPLL, the loop elements from APDs to the PFC in the Fig.1 were replaced by a balanced detector consisted of two commercial Si-pin-PDs with the responsivity of 0.58 A/W. Others were same as those of the heterodyne OPLL. The optical powers for the OPLL were 1 to 60 μW from the master laser and 130 μW from the slave laser. The intensity noise suppression ratio of the balanced phase detector was 35 to 40 dB upto the Fourier frequency of 10 MHz. The natural frequency of the loop was selected from several 100 kHz to 2 MHz.

3. Results and Discussions

<A> Heterodyne OPLL

Three kinds of measurement were carried out to confirm the phase-locking performance and to measure the phase error as indicated in Fig.1. They are as follows: 1) By observing the spectral shape of the heterodyne signal under phase-locked condition by an RF spectrum analyzer, it was confirmed that phase/frequency noises within the 3dB loop bandwidth were fully controlled as shown by Fig.2, and the 3dB linewidth of the heterodyne signal was narrowed to less than the resolution bandwidth of the spectrum analyzer of 30 Hz. 2) By observing the waveform of the heterodyne signal by an oscilloscope triggered with the RF reference signal, we confirmed that the heterodyne signal was successfully phase-locked to the RF reference signal, the rms residual phase fluctuation of the phase locked heterodyne signal was estimated to be less than 0.1 rad by measuring the timing jitter of the heterodyne signal. 3) To quantitatively measure the phase error between two lasers in the time domain, we have measured the square root of the Allan variance $\sigma_y(\tau)$ of the residual frequency fluctuations of the heterodyne signal by an Allan variance real time processing system (ARPS). τ is the integration time. $\sigma_y(\tau)$ was normalized by the optical frequency ν_o. The measured results are shown by Fig.3. The closed circles, open circles and the broken line are the results for heterodyne signal under free running condition, the phase-locked heterodyne signal and the RF reference signal, respectively. The solid line is the approximation of the result for the phase locked heterodyne signal given by the expression of $\sigma_y(\tau) = 6.3 \times 10^{-17}\tau^{-1}$. This kind of quantitative evaluations has not yet been reported. In particular, $\sigma_y(\tau)$ was as low as 1.1×10^{-18} at τ=70s. It corresponds to 0.4 mHz frequency fluctuations, i.e., to authors' knowledge, the minimum values among the

reported results so far. The results confirms that the stability of the phase locked heterodyne signal was almost same level as that of the reference signal. The phase error σ_ϕ was 8.1 degrees, where the relation of $\sigma_\phi = 2\pi\tau\nu_0\sigma_y(\tau)$ was used.

The phase error induced by the heterodyne frequency drift of 100 kHz was calculated to 1.4 x 10^{-5} degrees. The noise spectral density of the system including shot noise, intensity noises of the lasers and amplifier noise was 270 $nV/Hz^{1/2}$, which induces the phase error of 0.14 degrees. The beat linewidth of 20 kHz results in the phase error of 8.7 degrees. These values of the phase errors was calculated by using the loop parameters given in the section 2. The phase error of the OPLL was mainly determined by the laser phase noise, and measured phase error of 8.1 degrees is well agreed with the calculated phase error of 8.8 degrees. Further improvement of the heterodyne OPLL can be realized by increasing the loop bandwidth and using a more stable reference signal.

<B> Homodyne OPLL

Figure 4 shows an example of the phase error power spectral density (PSD) of the homodyne OPLL. The break point of the PSD is about 1.25 MHz, which is order of the natural frequency[5]. We measured the phase error comparing the rms voltage value under phase-locked state with the peak-to-peak amplitude of the beat signal under unlocked state. Under the locking condition of the Fig.4, σ_ϕ was 2.6 degrees. However, the phase error was calculated to 4.1 degrees by using the estimated beat linewidth of 20 kHz and the measured loop parameters. In both type OPLLs, the fact that the measured values of phase errors were smaller than the calculated values, suggests that the estimated linewidth contained not only Lorentzian phase noise components but also noise components by acoustics and vibrations. The locking period was about 10 minutes, limited mainly by DC drifts of the balanced phase detector.

4. Summary

We have carried out the experiments on the heterodyne and the homodyne OPLLs with two CFP semiconductor lasers with the linewidths of less than 10 kHz. The phase errors of the heterodyne and the homodyne OPLL were 8.1 and 2.6 degrees, respectively. It can be considered that the phase controllabilities of the heterodyne and the homodyne OPLL using CFP-LDs is sufficiently high for applications such as coherent optical communication receivers, remote sensings, and high-resolution spectroscopy.

<References>

[1]L.H.Enloe and J.L.Rodda,IEEE proc.,165-166,1965
[2]W.R.Leeb,H.K.Philipp,A.L.Scholtz andE.Bonek,Appl.Phys.Lett.,41,592-594,1982
[3]D.J.Maylon,D.W.Smith and Wyatt,Electron.Lett.,22,421-422,1986
[4]T.J.Kane and E.A.P.Cheng,Opt.Lett.,13,970-972,1988
[5]J.M.Kahn,B.L.Kasper and K.J.Pollock,Electron.Lett.,25,626-628,1989
[6]L.Kazovsky and D.A.Atlas,IEEE PTL,1,395-397,1989
[7]R.C.Steele,Electron.Lett.,19,69-70,1983
[8]J.L.Hall,L.S.Ma and G.Kramer,IEEE J.QE,QE-23,427-437,1987
[9]J.Harrison and A.Mooradian,IEEE J.QE,25,1152-1155,1989
[10]K.J.Williams,L.Goldberg,M.Daganais and J.F.Weller,Electron.Lett.,25,1242-1243,1989
[11]H.K.Philipp,A.L.Scholtz,E.Bonek and W.R.Leeb,IEEE Tran.Com,31,1000-1002,1983
[12]G.Fisher,J.Opt.Comm.,9,27-28,1988
[13]J.M.Kahn,IEEE PTL,1,340-342,1989
[14]B.Dahmani,L.Hollberg and R.Drullinger,Opt.Lett.,V.12,876-878,1987
[15]C.H.Shin,M.Teshima,M.Ohtsu,T.Imai,J.Yoshida and K.Nishide, 7th IOOC in Kobe, Japan,21D4-5,1989
[16]C.H.Shin,M.Teshima,M.Ohtsu,T.Imai,J.Yoshida and K.Nishide,IEEE PTL,2,to be published in March issue,1990

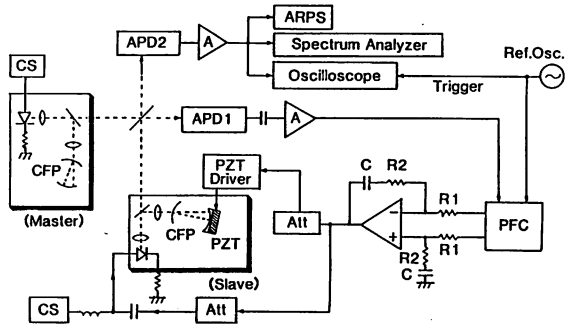

Fig.1 General experimental arrangement of the heterodyne OPLL. LD: semiconductor laser diode, CS: current source, A: Amplifier, Att: RF attenuator. In case of homodyne OPLL, the loop elements of APD1 to PFC were replaced by a balanced phase detector consisted of two Si-pin-PDs.

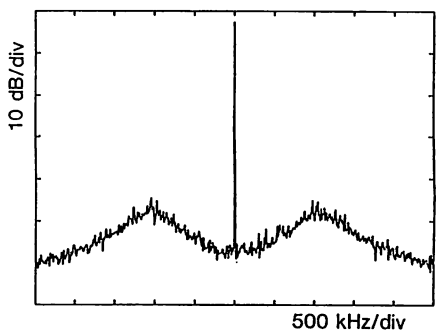

Fig.2 Spectral shape of the heterodyne signal under phase-locking condition.

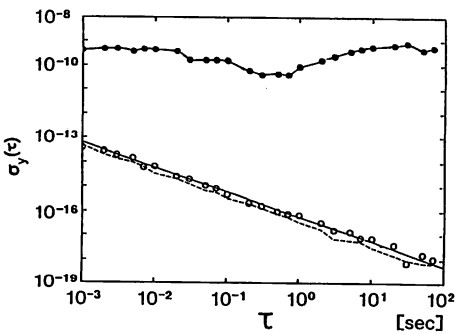

Fig.3 Measured results of square root Allan variances of residual frequency fluctuations of the heterodyne signal under unlocked (closed circles) and phase-locked (open circles) conditions and of the RF reference signal (a broken curve).

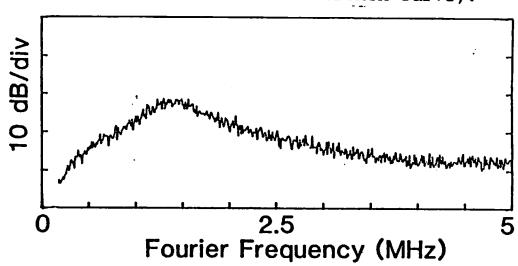

Fig.4 Power spectral density of phase error in homodyne phase-locked loop.

Modulation transfer and optical Stark effect in a rubidium atomic clock pumped by a semiconductor laser

Minoru Hashimoto and Motoichi Ohtsu

Graduate School at Nagatsuta, Tokyo Institute of Technology, 4259 Nagatsuta, Midori-ku, Yokohama 227, Japan

Received November 11, 1988; accepted May 24, 1989

Novel spectral line shapes of optical-microwave double resonance with an extremely narrow linewidth were observed in a rubidium atomic clock pumped by a semiconductor laser. It was confirmed that these novel spectral line shapes of double resonance were due to the modulation-transfer effect. These spectral line shapes were calculated by solving the equation of motion of the density matrix that describes the modulation-transfer process. The calculated results agree with the experimental results. By using the calculated results of the influence of the optical Stark effect on these spectral line shapes, characteristics of the inhomogeneous light shift were evaluated quantitatively for the frequency-modulated microwave. Furthermore, optimum values of modulation parameters were found by computer simulation in order to obtain the highest microwave frequency stability of the atomic clocks. An experiment was carried out employing these optimum parameters, and a short-term frequency stability as high as $\sigma_y(\tau) = 7.9 \times 10^{-13}\,\tau^{-1/2}$ was obtained, where τ is an integration time of measurement.

1. INTRODUCTION

The portable frequency standards most widely used today are the passive ^{87}Rb gas-cell standard and the ^{133}Cs atomic-beam standard. They are required for many applications, such as satellite communications, satellite tracking, and global positioning systems. The development of a stable, monochromatic, and tunable laser operating in the near infrared has made it possible to improve the performance of atomic clocks. Hyperfine pumping and optical detection using a GaAs semiconductor have been proposed for optically pumped ^{133}Cs atomic-beam clocks.[1]

In the case of optical pumping for ^{87}Rb atomic clocks, although replacement of a rf-excited ^{87}Rb lamp by a semiconductor laser has been proposed and preliminary experiments on laser-pumped ^{87}Rb atomic clocks have been reported,[2,3] no novel physical phenomena have been found. The authors have demonstrated the novel spectral line shapes of optical-microwave double resonance with an extremely narrow linewidth by utilizing the advantageous effect of the high temporal coherence of the laser.[4] These spectral line shapes are useful for the improvement of the frequency stability of a ^{87}Rb atomic clock.

However, the physical process of this phenomenon has not yet been fully investigated. On the other hand, the microwave resonance frequency, which is used as the frequency reference for an atomic clock, would be shifted by the optical Stark effect induced by the electric field of the pumping light.[5] This is called the light shift, the process that limits the frequency accuracy of atomic clocks. Precise evaluation of the light shift is thus required if one is to estimate the frequency accuracy of ^{87}Rb atomic clocks. Although the inhomogeneous light shift, which is the result of inhomogeneity in the spatial distribution of laser intensity in the ^{87}Rb gas cell, has been evaluated for nonmodulated microwaves,[6,7] precise evaluations of inhomogeneous light shifts for actual atomic clocks have not been made. This is because a precise evaluation would be rather difficult when the microwave frequency was modulated in order to obtain the frequency discriminator for the microwave frequency stabilization.

In this paper we report theoretical analyses of the novel spectral line shapes of double resonance for a semiconductor-laser-pumped ^{87}Rb atomic clock and of the inhomogeneous light shift. The results are compared with experimental results of the inhomogeneous light shift. In Section 2 observations of some novel double-resonance line shapes are described. The equation of motion of the density matrix is solved in Section 3. Thereby it is pointed out that the novel spectral line shapes of double resonance are caused by the modulation-transfer process, i.e., the modulation signal is transferred from microwave to laser light, which originates from the complex polarizability of three-level ^{87}Rb atoms. In Section 4 the optical Stark effect and its relationship to the inhomogeneous light shift are discussed, using the results of Section 3. Finally, in Section 5, optimum conditions for attaining the highest stability of microwave frequency of the ^{87}Rb atomic clock are found, based on the discussion of the modulation-transfer process. Symbols used in this paper, detailed calculations used to obtain the complex polarization, and an experimental procedure to find the dependence of population inversion on laser frequency detuning are summarized in Appendixes A, B, and C, respectively.

2. OBSERVATION OF THE NOVEL SPECTRAL LINE SHAPE OF OPTICAL-MICROWAVE DOUBLE RESONANCE

Figure 1 is a block diagram of a ^{87}Rb atomic clock pumped by a semiconductor laser, in which a commercially available atomic clock (Fujitsu, 5407A) was used. Most of the parameters, such as microwave signal power, rubidium-vapor pressure, and buffer-gas pressure, have already been optimized. In this experiment, a semiconductor laser rather than an ^{87}Rb lamp was used as an optical pumping source for an

0740-3224/89/101777-13$02.00

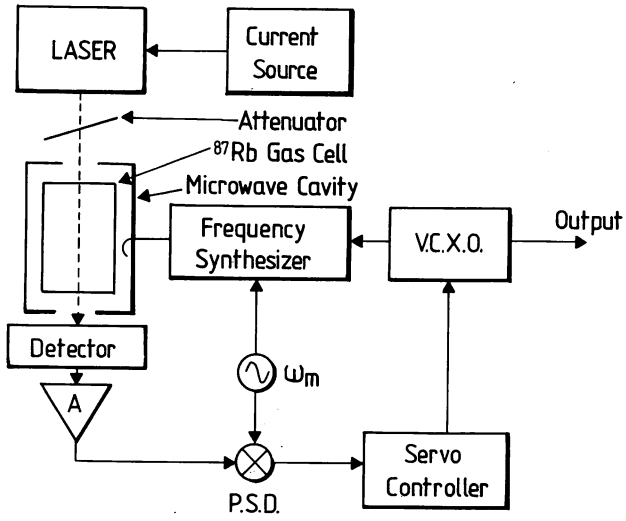

Fig. 1. Block diagram of a semiconductor-laser-pumped ^{87}Rb atomic clock: P.S.D., phase-sensitive detector; V.C.X.O., voltage-controlled crystal oscillator; A, postdetector amplifier; ω_m, angular frequency for microwave frequency modulation.

optimized commercial atomic clock. ^{87}Rb vapor and buffer gases (total pressure 43 Torr, $Ar/N_2 = 1.65$) were contained in a cylindrical glass cell. The ^{85}Rb/^{87}Rb isotope ratio of the rubidium vapor used in our experiments was less than 1%. The temperature of the ^{87}Rb cell was fixed at 48°C. The ^{87}Rb atoms were pumped by a 0.78-μm AlGaAs semiconductor laser (Hitachi, HL7802E). The laser light was linearly polarized. Figure 2 shows examples of the derivatives of novel spectral line shapes of optical-microwave double resonance. The microwave frequency was modulated to obtain these derivatives. The vertical axes of these figures are the output voltage V_{PSD} of the phase-sensitive detector shown in Fig. 1. The line shapes of Figs. 2(a) and 2(b) are quite different. This difference, however, stems only from the difference of the modulation index M, the modulation frequency $\omega_m/2\pi$, and the phase difference θ between the output signal from the postdetector amplifier and the reference signal for the phase-sensitive detector. These signals were obtained by using a reference signal $\cos(\omega_m t - \theta)$ for the phase-sensitive detector.

It is worth mentioning that the peak-to-peak linewidth ($\Delta\nu$) at the center of these spectral shapes, i.e., the separation between points A and B in Figs. 2(a) and 2(b), was narrower than those of conventional ^{87}Rb atomic clocks. In the case of Figs. 2(a) and 2(b) the values of $\Delta\nu$ were 75 and 110 Hz, respectively, while that of a conventional ^{87}Rb atomic clock is 360 Hz. Furthermore, the slopes D [$=2\pi dV_{PSD}/d\omega_M|_{\omega_M=\omega_{12}}$; see Eq. (50) below] of these line shapes at the microwave resonance frequency ($\omega_{12}/2\pi$) were steep, and their values depended on modulation parameters such as M, $\omega_m/2\pi$, and θ. The short-term microwave frequency stability depends on this slope at $\omega_{12}/2\pi$, i.e., the frequency-discrimination sensitivity for the microwave frequency stabilization of a ^{87}Rb atomic clock. If ω_m is smaller than the transverse relaxation constant of the microwave resonance [γ_{21}'; see Eq. (42) below], the square root of the Allan variance $\sigma_y^2(\tau)$ of the short-term microwave frequency stability of the ^{87}Rb atomic clock can be expressed as[8]

$$\sigma_y(\tau) = \frac{0.11}{Q(S/N)}\tau^{-1/2}, \tag{1}$$

where τ is the integration time of measurement, Q is the quality factor of the frequency discriminator, and S/N is the signal-to-noise ratio of the signal from a postdetector amplifier. Since the quality factor Q is defined approximately by

$$Q = \frac{\omega_{12}/2\pi}{\Delta\nu}, \tag{2}$$

Eq. (1) can be transformed into

$$\sigma_y(\tau) = \frac{0.11N}{(\omega_{12}/2\pi)D}\tau^{-1/2}, \tag{3}$$

where $S/\Delta\nu$ was approximated as the frequency-discrimina-

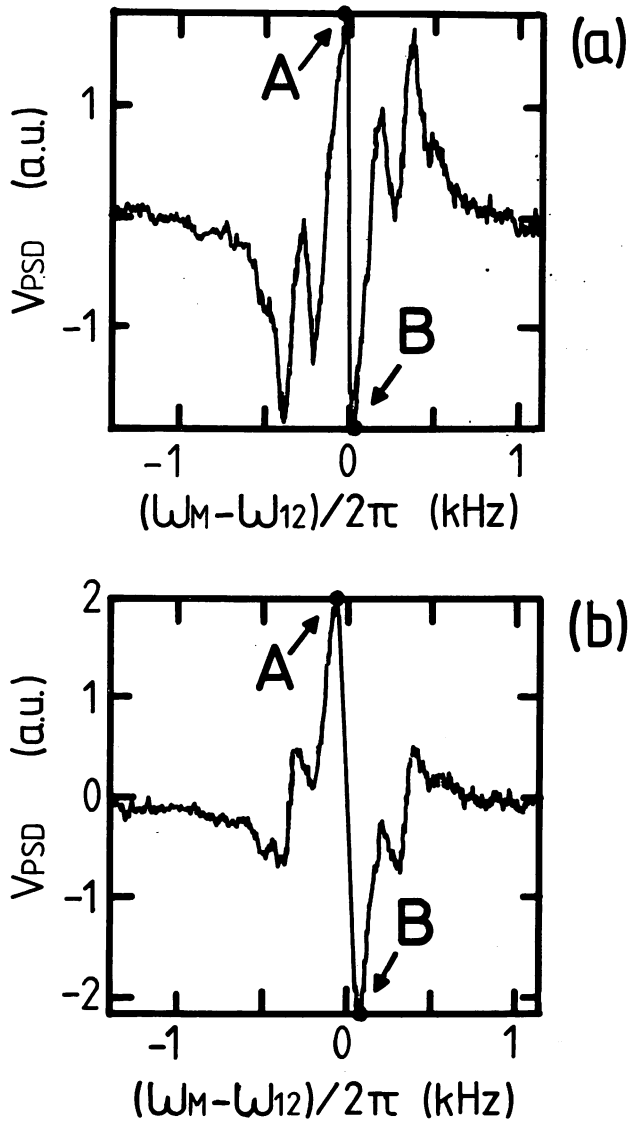

Fig. 2. Examples of novel line shapes of optical-microwave double resonance. (a) Modulation frequency, modulation index, and phase $\omega_m/2\pi$ = 160 Hz, M = 1.8, and θ = 235°, respectively. (b) Modulation frequency, modulation index, and phase $\omega_m/2\pi$ = 200 Hz, M = 1.6, and θ = 270°, respectively. V_{PSD}, Output voltage from the phase-sensitive detector. The laser-light intensity was I_0 = 14.4 μW/cm^2. For definitions of ω_M and ω_{12}, see Appendix A.

tion sensitivity D of the center of the double-resonance spectral shapes. Since the microwave frequency stability $\sigma_y(\tau)$ is inversely proportional to D, the microwave stability can be improved by increasing the value of D.

3. MODULATION-TRANSFER PROCESS

An energy-level diagram of a ^{87}Rb atom is shown in Fig. 3. Two hyperfine levels of the ground state ($5S_{1/2}$), ($F = 1, m_F = 0$) and ($F = 2, m_F = 0$), and of an excited state ($5P_{3/2}$) are relevant to the operation of a ^{87}Rb atomic clock, which are labeled $|1\rangle$, $|2\rangle$, and $|3\rangle$, respectively. The modulated magnetic field of a microwave in the microwave cavity, which would induce the transition between the levels $|1\rangle$ and $|2\rangle$, is expressed as

$$H_M(r, z, t) = \sum_{q=-\infty}^{\infty} J_q(M) H_M \cos[(\omega_M + q\omega_m)t], \tag{4}$$

where

$$H_M = H_{M0} J_0(3.832r/R)\sin[(k_M + qk_m)z]. \tag{5}$$

H_{M0} is the amplitude of the magnetic field, R is the cavity radius, z and r are the cylindrical coordinates along the microwave cavity axis and the radius, respectively, J_q is the qth-order Bessel function, k_M and k_m are the wave vectors of the microwave and modulation signals, respectively, and ω_M is the microwave angular frequency. The contributions of qk_m can be neglected in Eq. (5) because $k_m \ll k_M$. Equation (5) represents the TE_{011}-mode magnetic field in the microwave cavity. Since the laser light used for pumping from level $|1\rangle$ to level $|3\rangle$ was incident upon an edge of the gas cell installed in the microwave cavity, the laser-light field can be expressed as a traveling wave:

$$E_L(z, t) = E_L \cos(\omega_L t - k_L z), \tag{6}$$

where E_L, k_L, and ω_L are the amplitude of the electric field, the wave vector, and the angular frequency, respectively, of the laser light.

The laser light transmitted through the ^{87}Rb vapor was detected by a photodetector. By using the complex polarizability α of ^{87}Rb atoms for the laser field, the laser intensity detected by the photodetector can be expressed as

$$\begin{aligned} I_{\mathrm{DET}}(t) &= c\epsilon_0 |E_L(z, t)\exp[-\alpha L_c]|^2 \\ &\simeq c\epsilon_0 E_L{}^2(1 - \alpha L_c - \alpha^* L_c), \end{aligned} \tag{7}$$

where c is the speed of light, ϵ_0 is the dielectric constant of a vacuum, L_c is the length of the gas cell, and $*$ represents a complex conjugate. The optical length of the vapor can be expressed by $L_d = 1/n_{87}\sigma$, where n_{87} is the rubidium density and σ is the photon-absorption cross section. The value of L_d was as great as 25 cm because $n_{87} = 1.3 \times 10^{10}/\mathrm{cm}^3$ and $\sigma = 1.9 \times 10^{-11}\ \mathrm{cm}^2$ in our experiments. The thin-vapor approximation is valid in relation (7) since the cell length $L_c = 3.5$ cm was sufficiently shorter than the optical length $L_d = 25$ cm.

A rate equation[2] or a local density matrix[6] has been utilized to derive the complex polarizability α in conventional ^{87}Rb atomic clocks. However, the equations of motion of the density matrix of three-level atoms should be solved for a more quantitative evaluation when the atoms are pumped by a coherent light source such as a semiconductor laser.

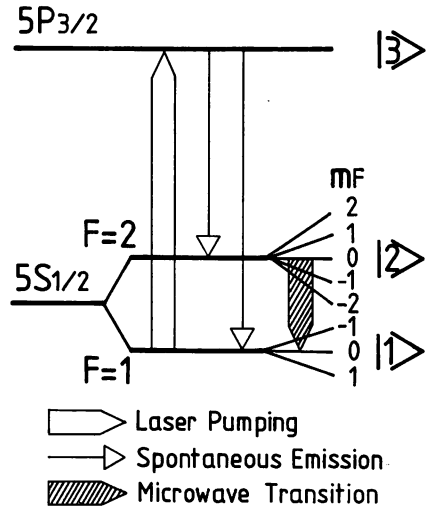

Fig. 3. Energy-level diagram of a ^{87}Rb atom.

The Doppler effect associated with the microwave transition can be neglected because the Doppler broadening of the microwave transition is sufficiently reduced by the buffer gases. Furthermore, the Doppler effect associated with the optical transition is not significant because the pressure broadening of the optical transition is 400–500 MHz, which is as large as the Doppler-broadened width. Therefore the equations of motion of the density matrix elements of three-level atoms can be expressed as

$$\frac{d\rho_{11}}{dt} = -i\left(\frac{\mu_{21}H_M}{\hbar}\rho_{21}^* + \frac{\mu_{31}E_L}{\hbar}\rho_{13} - \frac{\mu_{21}^*H_M^*}{\hbar}\rho_{21} - \frac{\mu_{31}^*E_L^*}{\hbar}\rho_{13}^*\right) - (\rho_{11} - n_1)\gamma_1, \tag{8}$$

$$\frac{d\rho_{22}}{dt} = i\left(\frac{\mu_{21}H_M}{\hbar}\rho_{21}^* - \frac{\mu_{21}^*H_M^*}{\hbar}\rho_{21}\right) - (\rho_{22} - n_2)\gamma_2, \tag{9}$$

$$\frac{d\rho_{33}}{dt} = i\left(\frac{\mu_{31}E_L}{\hbar}\rho_{13} - \frac{\mu_{31}^*E_L^*}{\hbar}\rho_{13}^*\right) - (\rho_{33} - n_3)\gamma_3, \tag{10}$$

$$\frac{d\rho_{21}}{dt} = i\left[(\rho_{22} - \rho_{11})\frac{\mu_{21}H_M}{\hbar} + \frac{\mu_{31}E_L}{\hbar}\rho_{32}^*\right] + i(\omega_{12} + i\gamma_{21})\rho_{21}, \tag{11}$$

$$\frac{d\rho_{32}}{dt} = i\left(\frac{\mu_{21}^*H_M^*}{\hbar}\rho_{13}^* - \frac{\mu_{31}E_L}{\hbar}\rho_{21}^*\right) + i(\omega_{23} + i\gamma_{23})\rho_{32}, \tag{12}$$

$$\frac{d\rho_{13}}{dt} = -i\left[(\rho_{33} - \rho_{11})\frac{\mu_{31}^*E_L^*}{\hbar} + \frac{\mu_{21}^*H_M^*}{\hbar}\rho_{32}^*\right] - i(\omega_{13} - i\gamma_{13})\rho_{13}, \tag{13}$$

where $\hbar$ is Planck's constant divided by 2π, μ_{21} is the magnetic dipole moment, μ_{31} is the electric dipole moment, ω_{ij} is Bohr's angular frequency between the levels $|i\rangle$ and $|j\rangle$, n_j is the equilibrium population of the level $|j\rangle$, γ_j is the longitudinal relaxation constant of the level $|j\rangle$, and γ_{ij} is the transverse relaxation constant. It is well known that $\omega_{12}/2\pi$ and

$\omega_{13}/2\pi$ are 6.8 GHz and 384 THz (780-nm wavelength), respectively. From linewidth measurements of optical absorption and of optical-microwave double-resonance spectral shapes, it was found that $\gamma_{21}/2\pi$ and $\gamma_{13}/2\pi$ ($\simeq\gamma_{23}/2\pi$) were 50 Hz and 1 GHz, respectively. By solving Eqs. (8)–(13) based on the nonperturbation method[9] (see Appendix B), the polarization (p_{13}) between levels $|1\rangle$ and $|3\rangle$ can be obtained. Thus the complex polarizability is expressed as

$$\alpha(t) = -i\frac{k_L\mu_{31}}{2\epsilon E_L^*}p_{13} = \frac{k_L\mu_{31}^2}{2\epsilon\hbar}\left\{\frac{i(\rho_{33}-\rho_{11})}{\Delta_{13}} + \frac{x_M^2}{4} \times \sum_q\sum_p \frac{iJ_{p+q}J_p(\rho_{22}-\rho_{11})}{\Delta_{13}[\Delta_{21}(p)\Delta_{32}^*(p) + x_L^2/4]}\exp(-iq\omega_m t)\right\}, \quad (14)$$

where x_M and x_L are the Rabi angular frequencies of microwave and laser light, respectively. These and Δ_{ij} are defined by Eqs. (B7)–(B11) of Appendix B. Equation (14) indicates that the complex polarizability of a ^{87}Rb atom is modulated by a microwave modulation signal of angular frequency ω_m. In other words, the modulation signal is transferred from the microwave to the laser-light field. This has been called modulation transfer.[10] Although it is well known that the modulation-transfer process plays an important role in four-wave mixing,[11] pump–probe spectroscopy,[12] and saturation spectroscopy,[13] this modulation-transfer process has not yet been fully investigated in the case of optical-microwave double resonance. When Eq. (14) is substituted into relation (7), the light intensity detected by the photodetector is given by

$$I_{\mathrm{DET}}(t) = I_0\left[1 - 2\delta_{\mathrm{OPT}} - \sum_q\sum_p J_{p+q}J_p(\delta_p - i\phi_p)\exp(iq\omega_m t) - \sum_q\sum_p J_{p+q}J_p(\delta_p + i\phi_p)\exp(-iq\omega_m t)\right], \quad (15)$$

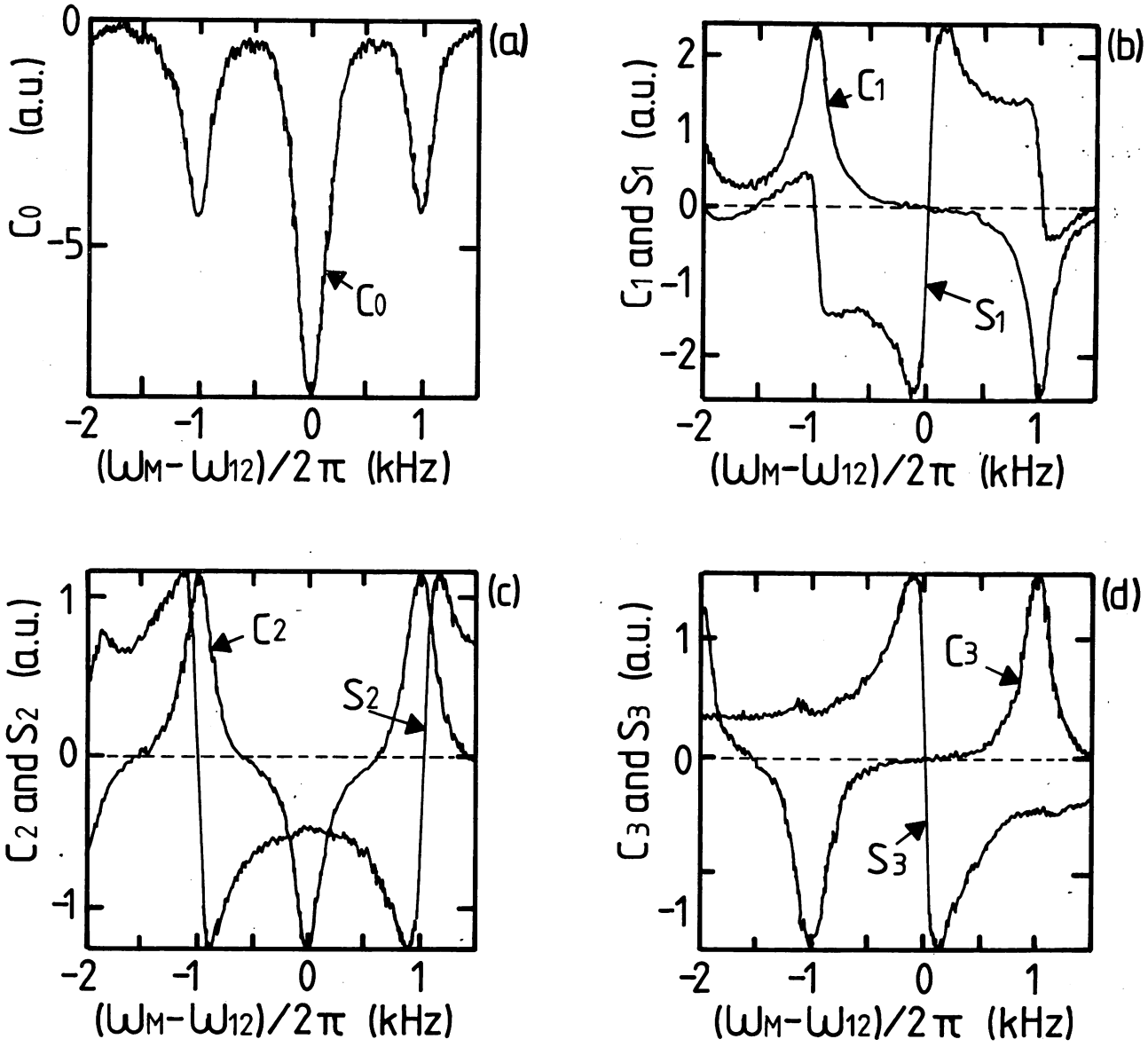

Fig. 4. Measured dependences of C_q and S_q on microwave frequency, where the modulation frequency was $\omega_m/2\pi$ = 1 kHz and the laser-light intensity was I_0 = 74.4 μW/cm^2. Modulation indices M were (a)–(c) 1.4 and (d) 4.3. For definitions of ω_M and ω_{12}, see Appendix A.

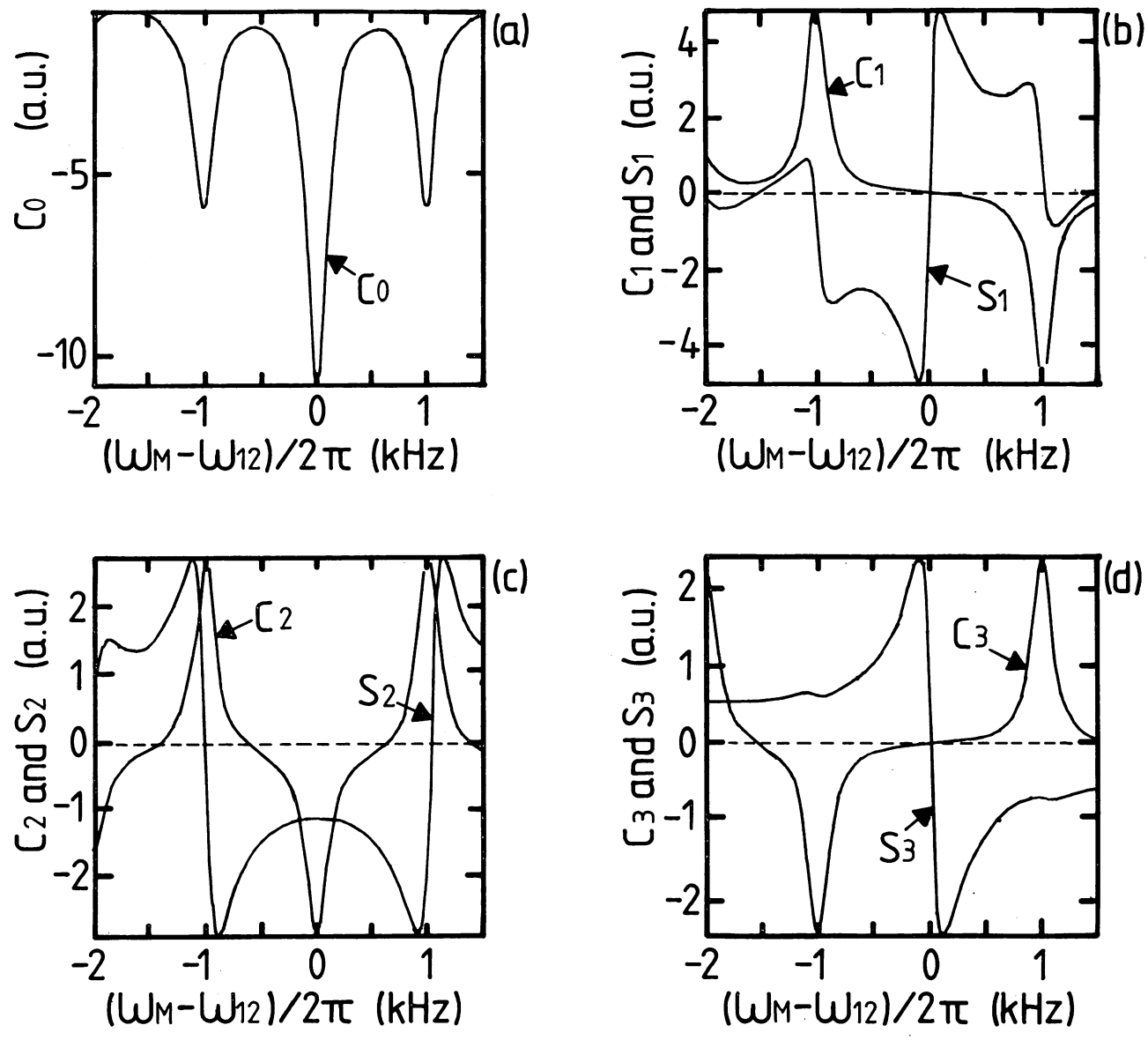

Fig. 5. Calculated dependences of C_q and S_q on microwave frequency. Modulation indices M were (a)–(c) 1.4 and (d) 4.3. The modulation frequency was $\omega_m/2\pi = 1$ kHz, and the laser Rabi frequency was $x_L/2\pi = 400$ kHz. For definitions of ω_M and ω_{12}, see Appendix A.

where

$$I_0 = c\epsilon_0 E_L^2, \tag{16}$$

$$\delta_{\mathrm{OPT}} = \frac{k_L \mu_{31}^2 L_c}{2\epsilon\hbar} \frac{(\rho_{33} - \rho_{11})\gamma_{13}}{(\omega_{13} - \omega_L)^2 + \gamma_{13}^2}, \tag{17}$$

$$\delta_p = \frac{k_L \mu_{31}^2 L_c}{2\epsilon\hbar} \frac{x_M^2}{4} \mathrm{Re}\left\{\frac{i(\rho_{22} - \rho_{11})}{\Delta_{13}[\Delta_{21}(p)\Delta_{32}^*(p) + x_L^2/4]}\right\}, \tag{18}$$

$$\phi_p = \frac{k_L \mu_{31}^2 L_c}{2\epsilon\hbar} \frac{x_M^2}{4} \mathrm{Im}\left\{\frac{i(\rho_{22} - \rho_{11})}{\Delta_{13}[\Delta_{21}(p)\Delta_{32}^*(p) + x_L^2/4]}\right\}, \tag{19}$$

I_0 is the laser-light intensity incident into the ^{87}Rb gas cell, δ_{OPT} is the amplitude attenuation of laser light by the optical transition from level $|1\rangle$ to level $|3\rangle$, and δ_p and ϕ_p are the amplitude attenuation and the phase shift of the laser light by the microwave transition from level $|1\rangle$ to level $|2\rangle$, respectively. In Eq. (15), although all the arguments of the Bessel function are the modulation index M, they have been dropped for the sake of compactness. Detailed discussions on δ_p and ϕ_p are given in Section 4. Equation (15) can be transformed into

$$I_{\mathrm{DET}}(t) = I_0(1 - 2\delta_{\mathrm{OPT}}) + \sum_{q=0}^{\infty} [C_q \cos(q\omega_m t) + S_q \sin(q\omega_m t)], \tag{20}$$

where

$$C_q = -I_0 \sum_{p=-\infty}^{\infty} (J_{p+q} + J_{p-q}) J_p \delta_p \tag{21}$$

and

$$S_q = -I_0 \sum_{p=-\infty}^{\infty} (J_{p+q} - J_{p-q}) J_p \phi_p. \tag{22}$$

C_q and S_q are the in-phase and the quadrature components of the qth-order harmonic, respectively, with respect to the

phase of the microwave frequency-modulation signal. Expressions of C_q and S_q up to the third harmonics are given by

$$C_0 = I_0[-2J_0^2\delta_0 - J_1^2(\delta_1 + \delta_{-1}) - J_2^2(\delta_2 + \delta_{-2}) - J_3^2(\delta_3 + \delta_{-3})], \quad (23)$$

$$C_1 = I_0[-J_0J_1(\delta_1 - \delta_{-1}) - J_1J_2(\delta_2 + \delta_1 - \delta_{-1} - \delta_{-2}) - J_2J_3(\delta_3 + \delta_2 - \delta_{-2} - \delta_{-3}) - J_3J_4(\delta_3 - \delta_{-3})], \quad (24)$$

$$S_1 = I_0[J_0J_1(\phi_1 - 2\phi_0 + \phi_{-1}) + J_1J_2(\phi_2 - \phi_1 - \phi_{-1} + \phi_{-2}) + J_2J_3(\phi_3 - \phi_2 - \phi_{-2} + \phi_{-3}) - J_3J_4(\phi_3 + \phi_{-3})], \quad (25)$$

$$C_2 = I_0[-J_0J_2(\delta_2 + 2\delta_0 + \delta_{-2}) + J_1^2(\delta_1 + \delta_{-1}) - J_1J_3(\delta_3 + \delta_1 + \delta_{-1} + \delta_{-3}) - J_2J_4(\delta_2 + \delta_{-2}) - J_3J_5(\delta_3 + \delta_{-3})], \quad (26)$$

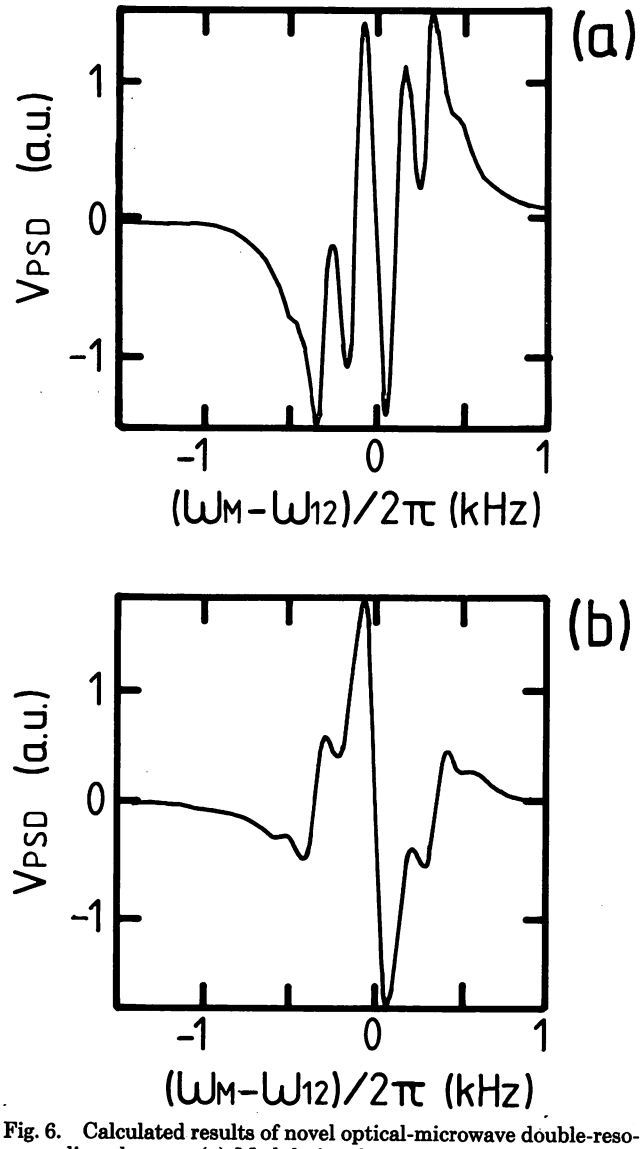

Fig. 6. Calculated results of novel optical-microwave double-resonance line shapes. (a) Modulation frequency, modulation index, and phase $\omega_m/2\pi = 160$ Hz, $M = 1.8$, and $\theta = 235°$, respectively. (b) Modulation frequency, modulation index, and phase $\omega_m/2\pi = 200$ Hz, $M = 1.6$, and $\theta = 270°$, respectively. V_{PSD}, Output voltage from the phase-sensitive detector. The laser Rabi frequency was $x_L/2\pi = 150$ kHz. For definitions of ω_M and ω_{12}, see Appendix A.

Table 1. Constants Used in Our Calculations[a]

Length of gas cell	$L_c = 3.6$ cm
Radius of gas cell	$R_c = 1.6$ cm
Transverse relaxation frequency between the levels $\|2\rangle$ and $\|1\rangle$	$\gamma_{21}/2\pi = 50$ Hz
Transverse relaxation frequency between the levels $\|1\rangle$ and $\|3\rangle$	$\gamma_{13}/2\pi = 1$ GHz
Transverse relaxation frequency between the levels $\|2\rangle$ and $\|3\rangle$	$\gamma_{32}/2\pi = 1$ GHz
Spot size of laser beam	$w = 0.4$ cm
Rabi frequency of microwave	$x_M/2\pi = 100$ Hz

[a] As a result of the linewidth measurements of optical absorption and of optical-microwave double-resonance spectral line shapes, it was found that $\gamma_{21}/2\pi$ and $\gamma_{13}/2\pi$ ($\simeq\gamma_{32}/2\pi$) were 50 Hz and 1 GHz, respectively.

$$S_2 = I_0[J_0J_2(\phi_2 - \phi_{-2}) - J_1^2(\phi_1 - \phi_{-1}) + J_1J_3(\phi_3 - \phi_1 + \phi_{-1} - \phi_{-3}) - J_2J_4(\phi_2 - \phi_{-2}) - J_3J_5(\phi_3 - \phi_{-3})], \quad (27)$$

$$C_3 = I_0[-J_0J_3(\delta_3 - \delta_{-3}) + J_1J_2(\delta_2 - \delta_1 + \delta_{-1} - \delta_{-2}) - J_1J_4(\delta_1 - \delta_{-1}) - J_2J_5(\delta_2 - \delta_{-2}) - J_3J_6(\delta_3 - \delta_{-3})], \quad (28)$$

and

$$S_3 = I_0[J_0J_3(\phi_3 - 2\phi_0 + \phi_{-3}) - J_1J_2(\phi_2 - \phi_1 - \phi_{-1} + \phi_{-2}) - J_1J_4(\phi_1 + \phi_{-1}) - J_2J_5(\phi_2 + \phi_{-2}) - J_3J_6(\phi_3 + \phi_{-3})]. \quad (29)$$

The first terms in these equations give a principal contribution to C_q and S_q. For instance, in the cases of C_1 and S_1 the first terms are the same as those of FM spectroscopy.[14] In particular, if $\omega_m/2\pi \ll \gamma_{21}'/2\pi$, one has

$$C_1 \simeq -I_0J_0J_1(\delta_1 - \delta_{-1}) = -I_0J_0J_1[\delta(\omega_M + \omega_m) - \delta(\omega_M - \omega_m)] \simeq -I_0J_0J_1\frac{d\delta(\omega_M)}{d\omega_M} \quad (30)$$

and

$$S_1 \simeq I_0J_0J_1(\phi_1 - 2\phi_0 + \phi_{-1}) = I_0J_0J_1[\phi(\omega_M + \omega_m) - 2\phi(\omega_M) + \phi(\omega_M - \omega_m)] \simeq I_0J_0J_1\frac{d^2\phi(\omega_M)}{d\omega_M^2}. \quad (31)$$

These equations mean that the spectral line shapes of C_1 and S_1 are proportional to the first derivative of the absorption and the second derivative of the dispersion, respectively.

If a reference signal for the phase-sensitive detector in Fig. 1 is proportional to $\cos(q\omega_m t - \theta)$, the output signal V_{PSD} from it is expressed as

$$V_{PSD} = V_0\left(\frac{C_q}{2}\cos\theta + \frac{S_q}{2}\sin\theta\right), \quad (32)$$

where V_0 is a proportional constant. It is found from Eq. (32) that the contributions from C_q and S_q to V_{PSD} depend on the phase difference θ. The dependences of C_q and S_q on microwave frequency were observed as shown in Fig. 4. The

calculated results corresponding to Fig. 4 are shown in Fig. 5. Figure 6 shows the calculated results fitted to the experimental ones of Fig. 2 by using Eq. (32), for which the values of γ_{21}', M, and θ were used as fitting parameters. The curves in Fig. 6 show the value of V_{PSD}, obtained by using the results given in Fig. 5 and substituting $q = 1$ into Eq. (32). From the agreement between Figs. 2 and 6 it is confirmed that the theoretical analysis given in this section is valid. Numerical values used for these calculations are listed in Table 1.

4. OPTICAL STARK EFFECT

The optical Stark effect, caused by the electric field of the pumping light, induces the light shift, i.e., the shift in microwave resonance frequency. This was investigated theoretically by Mathur.[5] In other experiments, inhomogeneous broadening of spectral line shapes of optical-microwave double resonance has been observed.[5,16] However, certain characteristics of the light shift, and the relationship of these characteristics to this inhomogeneous broadening, have not been fully discussed.

Camparo has pointed out that the observed characteristics of the light shift differ from the theoretical characteristics, owing to inhomogeneity in the spatial distribution of laser-light intensity. Because the center frequency and the linewidth of the double-resonance spectral line shape are strongly influenced by the laser-light intensity, spatial integration of the laser-light intensity distribution is required for correct results. Deformation and asymmetry in spectral line shapes of optical-microwave double resonance can be evaluated quantitatively from these results. This light shift is caused by inhomogeneity of the spatial distribution of laser-light intensity and is therefore called an inhomogeneous light shift. The inhomogeneous light shift for modulated microwaves has been evaluated experimentally.[6,7] However, a fully theoretical evaluation has not been made. However, since the microwave frequency is usually modulated in the practical ^{87}Rb atomic clock, the treatment of an inhomogeneous light shift becomes more complicated because of the FM sidebands of the modulation-signal-induced laser light.

Since the zero-crossing point of V_{PSD} is used as the reference frequency of the ^{87}Rb atomic clock, the light shift can be measured by observing the shift of this point. In preliminary experiments it was found that the highest sensitivity of the light-shift measurement could be obtained by measuring the zero-crossing point of S_3. Figure 7 shows examples of S_3 with respect to various laser frequency detunings. It can be seen from the curves in this figure that the shift of the zero-crossing point was induced by the deformation of these line shapes caused by the intensity and frequency detuning of the laser light. Characteristics of the light shift, i.e., dependences of the zero-crossing point of S_3 on the laser frequency detuning, are shown in Fig. 8. In this figure the light shift could not be measured within the range -4 GHz $\ll (\omega_L - \omega_{13})/2\pi \ll -2.2$ GHz because of the low intensity of the double-resonance signals from the postdetector amplifier. This results from the fact that the magnitude of population inversion between levels $|1\rangle$ and $|2\rangle$ was nearly zero in this range, which was confirmed by experiment. Details of this experiment are given in Appendix C, and the results are shown in Fig. 9.

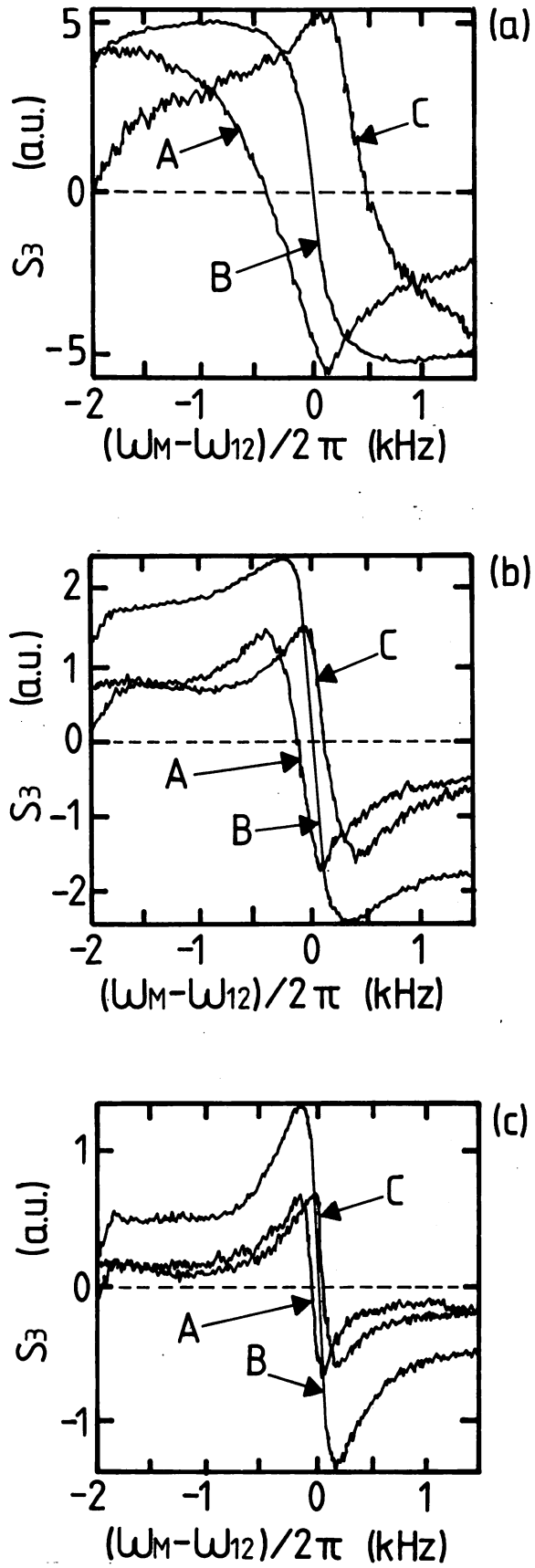

Fig. 7. Measured spectral line shapes of deformed S_3. Laser-light intensities I_0 were (a) 1440 μW/cm^2, (b) 420 μW/cm^2, and (c) 210 μW/cm^2. The laser frequency detuning $(\omega_L - \omega_{13})/2\pi$ was A, 1200 MHz; B, 0 MHz, and C, -1200 MHz. The modulation index was $M = 3.9$. For definitions of ω_L, ω_M, ω_{13}, and ω_{12}, see Appendix A.

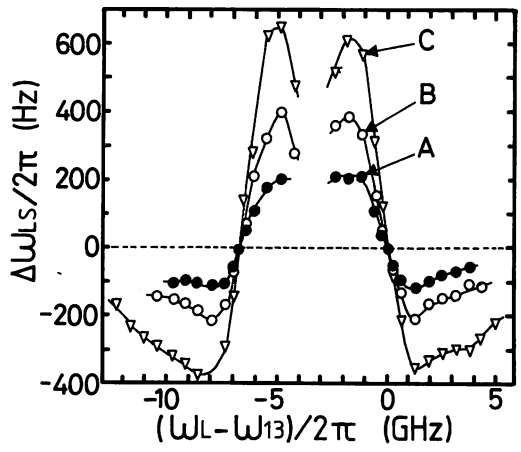

Fig. 8. Measured characteristics of the light shift. The laser-light intensities I_0 were A, 144 μW/cm^2; B, 360 μW/cm^2; and C, 1008 μW/cm^2. The modulation index was M = 3.9. $\Delta\omega_{LS}$, Shift of zero-crossing point of S_3. For definitions of ω_L, ω_{13}, and ω_{12}, see Appendix A.

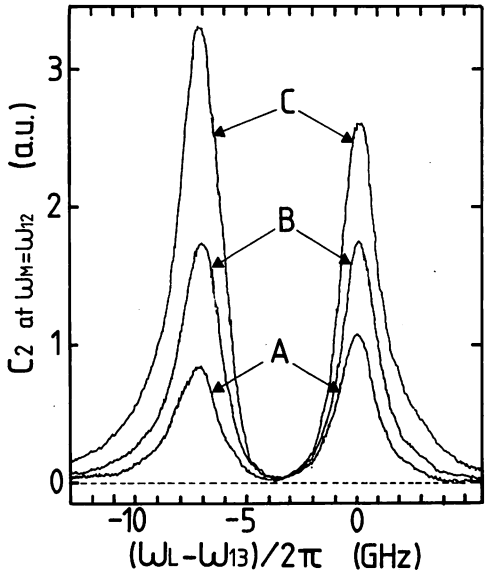

Fig. 9. Measured population inversion between the levels $|1\rangle$ and $|2\rangle$. The laser-light intensities I_0 were A, 144 μW/cm^2; B, 360 μW/cm^2; and C, 1008 μW/cm^2. The modulation index was M = 2.4. C_2, In-phase component of second harmonics. For definitions of ω_L and ω_{13}, see Appendix A.

The physical origins of light shifts and Stark splitting can be found by examining the denominator of the right-hand sides of Eqs. (18) and (19). The denominators of Eqs. (18) and (19) can be reduced to

$$\begin{aligned}\Delta_{13}[\Delta_{21}(p)\Delta_{32}^*(p) + x_L^2/4] &= \Delta_{13}[(\omega_{12} - \omega_M - p\omega_m + i\gamma_{21}) \\ &\times (\omega_{23} - \omega_L + \omega_M + p\omega_m - i\gamma_{32}) + x_L^2/4] \\ &= \Delta_{13}[(\omega_{12} - \omega_M - p\omega_m + i\gamma_{21}) \\ &\times (\omega_{13} - \omega_{12} - \omega_L + \omega_M + p\omega_m - i\gamma_{32} \\ &+ i\gamma_{21} - i\gamma_{21}) + x_L^2/4] \\ &= -\Delta_{13}[\Delta_{21}(p) - \epsilon(+)][\Delta_{21}(p) - \epsilon(-)], \end{aligned} \tag{33}$$

where

$$\epsilon(\pm) = \frac{\omega_{13} - \omega_L - i(\gamma_{32} - \gamma_{21}) \pm \Omega_{13}}{2} \tag{34}$$

and

$$\Omega_{13} = [\{\omega_{13} - \omega_L - i(\gamma_{32} - \gamma_{21})\}^2 + x_L^2]^{1/2}. \tag{35}$$

Ω_{13} is the nutation frequency, which depends on laser-light intensity.[9] Therefore the terms within braces in Eqs. (18) and (19) can be decomposed into partial fractions, i.e.,

$$\{\ \} = \frac{i(\rho_{22} - \rho_{11})}{\Delta_{13}\Omega_{13}}\left[\frac{1}{\Delta_{21}(p) - \epsilon(-)} - \frac{1}{\Delta_{21}(p) - \epsilon(+)}\right]. \tag{36}$$

This equation means that the Stark splitting of optical-microwave double resonance is expressed by two Lorentzian components. Since the complex Taylor series of Eq. (35) converges if $|x_L| \ll |\omega_{13} - \omega_L - i(\gamma_{32} - \gamma_{21})|$, Eq. (35) can be approximated as

$$\begin{aligned}\Omega_{13} &= [\omega_{13} - \omega_L - i(\gamma_{32} - \gamma_{21})] \\ &\times \left[1 + \frac{x_L^2}{\{\omega_{13} - \omega_L - i(\gamma_{32} - \gamma_{21})\}^2}\right]^{1/2} \\ &\simeq \omega_{13} - \omega_L - i(\gamma_{32} - \gamma_{21}) + \frac{x_L^2/2}{\omega_{13} - \omega_L - i(\gamma_{32} - \gamma_{21})}. \end{aligned} \tag{37}$$

Substituting relation (37) into Eq. (34), one has

$$\epsilon(+) = \omega_{13} - \omega_L - i\gamma_{32} + \frac{x_L^2/4}{\omega_{13} - \omega_L - i(\gamma_{32} - \gamma_{21})} \tag{38}$$

and

$$\epsilon(-) = -\frac{x_L^2/4}{\omega_{13} - \omega_L - i(\gamma_{32} - \gamma_{21})}. \tag{39}$$

Therefore Eq. (36) can be transformed into

$$\{\ \} = \frac{i(\rho_{22} - \rho_{11})}{\Delta_{13}\Omega_{13}}\left[\frac{1}{\omega_{12}' - \omega_M - p\omega_m + i\gamma_{21}'} - \frac{1}{\omega_{12}'' - \omega_M - p\omega_m + i\gamma_{21}''}\right], \tag{40}$$

where

$$\omega_{12}' = \omega_{12} + \frac{\omega_{13} - \omega_L}{(\omega_{13} - \omega_L)^2 + (\gamma_{32} - \gamma_{21})^2}\frac{x_L^2}{4}, \tag{41}$$

$$\gamma_{21}' = \gamma_{21} + \frac{\gamma_{32}}{(\omega_{13} - \omega_L)^2 + (\gamma_{32} - \gamma_{21})^2}\frac{x_L^2}{4}, \tag{42}$$

$$\omega_{12}'' = \omega_{12} - \omega_{13} + \omega_L - \frac{\omega_{13} - \omega_L}{(\omega_{13} - \omega_L)^2 + (\gamma_{32} - \gamma_{21})^2}\frac{x_L^2}{4}, \tag{43}$$

and

$$\gamma_{21}'' = \gamma_{32} - \frac{\gamma_{32}}{(\omega_{13} - \omega_L)^2 + (\gamma_{32} - \gamma_{21})^2}\frac{x_L^2}{4}. \tag{44}$$

The last terms on the right-hand sides of Eqs. (41) and (43)

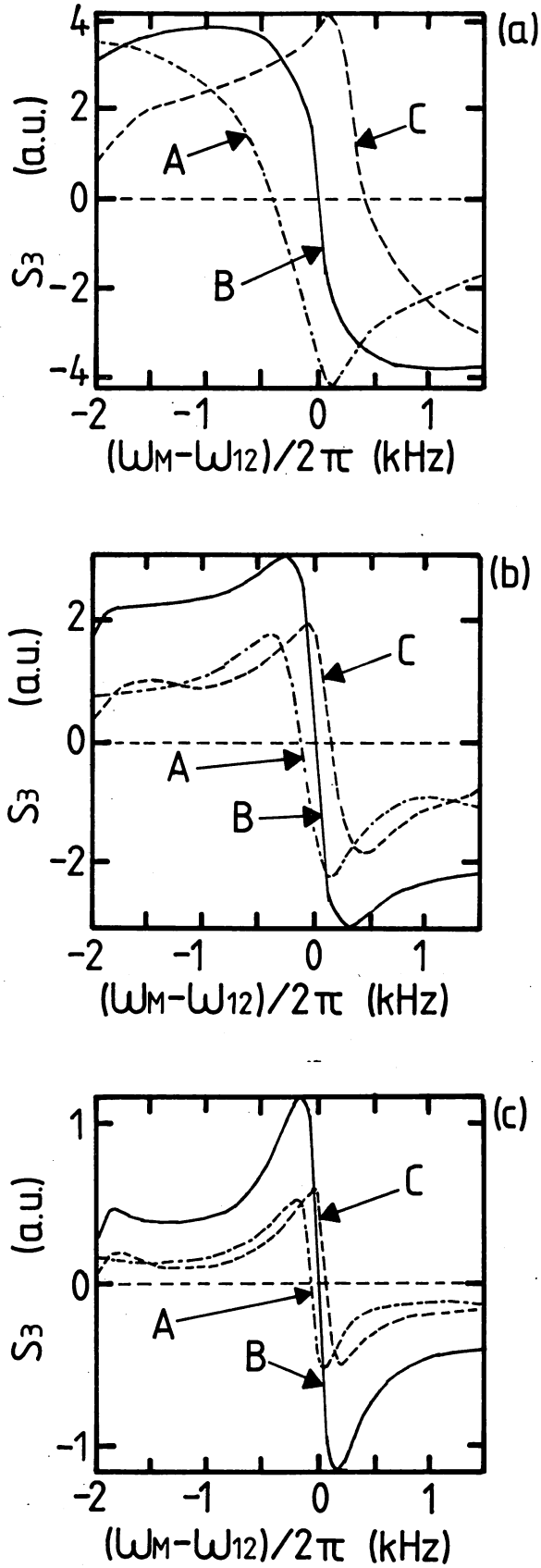

Fig. 10. Calculated line shapes of deformed S_3. Laser Rabi frequencies $x_L/2\pi$: (a) 1800 kHz, (b) 900 kHz, and (c) 500 kHz. The laser frequency detuning $(\omega_L - \omega_{13})/2\pi$ was A, 1200 MHz; B, 0 MHz; and C, −1200 MHz. The modulation index was $M = 3.9$. For definitions of ω_L, ω_M, ω_{13}, and ω_{12}, see Appendix A.

represent the energy-level shift of the microwave resonance frequency, i.e., a light shift, which can be expressed by a dispersive curve similar to that obtained by Mathur.[5] However, the signs of the dispersive curves of Eqs. (41) and (43) are opposite each other. Equations (42) and (44) represent the broadening and narrowing, respectively, of the linewidth induced by the laser power. The second Lorentzian within brackets of Eq. (40) can be neglected because $\gamma_{21}'' \gg \gamma_{21}'$ for $x_L \ll \gamma_{32}$. Since the low-intensity approximation $(x_L \ll \gamma_{32})$ is valid in the present study, Eq. (40) can be reduced to

$$\{\} = \frac{(\rho_{22} - \rho_{11})}{|\Delta_{13}||\Omega_{13}|} \exp(i\zeta) \frac{i(\omega_{12}' - \omega_M - p\omega_m) + \gamma_{21}'}{(\omega_{12}' - \omega_M - p\omega_m)^2 + \gamma_{21}'^2}, \quad (45)$$

where

$$\zeta \simeq \tan^{-1} \frac{\omega_{13} - \omega_L}{\gamma_{13}} - \tan^{-1} \frac{\omega_{13} - \omega_L + \dfrac{\omega_{13} - \omega_L}{(\omega_{13} - \omega_L)^2 + (\gamma_{32} - \gamma_{21})^2} \dfrac{x_L^2}{2}}{\gamma_{32} - \dfrac{\gamma_{32}}{(\omega_{13} - \omega_L)^2 + (\gamma_{32} - \gamma_{21})^2} \dfrac{x_L^2}{2}}. \quad (46)$$

ζ represents the phase shift by the pumping light. Since $x_L \ll \gamma_{32}$ and $\gamma_{32} \simeq \gamma_{13}$, ζ can be approximated as 0. Furthermore, the laser beam has a Gaussian transverse profile, which can be expressed as

$$x_L^2(r) = x_L^2(0) \frac{2}{\sqrt{\pi} w} \exp[-(r/w)^2], \quad (47)$$

where w is spot size of the laser beam. There can be also an effect due to the attenuation of the light intensity along the optical path through the gas cell; however, this apparently has only a small effect on our experiments. Spatial integration of Eqs. (18) and (19) by using Eq. (47) gives the final results of δ_p and ϕ_p, which can be expressed as

$$\delta_p = 2\pi \int_0^{R_c} \frac{k_L \mu_{31}^2 L_c}{2\epsilon\hbar} \frac{x_M^2}{4} \frac{(\rho_{22} - \rho_{11})}{|\Delta_{13}||\Omega_{13}|} \times \frac{\gamma_{21}'}{(\omega_{12}' - \omega_M - p\omega_m)^2 + \gamma_{21}'^2} \frac{2}{\sqrt{\pi} w} \exp[-(r/w)^2] dr \quad (48)$$

and

$$\phi_p = 2\pi \int_0^{R_c} \frac{k_L \mu_{31}^2 L_c}{2\epsilon\hbar} \frac{x_M^2}{4} \frac{(\rho_{22} - \rho_{11})}{|\Delta_{13}||\Omega_{13}|} \times \frac{\omega_{12}' - \omega_M - p\omega_m}{(\omega_{12}' - \omega_M - p\omega_m)^2 + \gamma_{21}'^2} \frac{2}{\sqrt{\pi} w} \exp[-(r/w)^2] dr, \quad (49)$$

where R_c is the radius of the gas cell.

By using ϕ_p calculated by Eq. (49), S_3 could be derived from Eq. (29). The calculated results, which correspond to Fig. 7, are shown in Fig. 10. Asymmetric line shapes can be clearly seen from these figures, which agree with those of Fig. 7. It was confirmed from this agreement that the inhomogeneous light shift for a frequency-modulated microwave can be explained by the modulation-transfer process.

5. IMPROVEMENT OF MICROWAVE FREQUENCY STABILITY

In this section we report the optimum conditions for obtaining the highest discrimination sensitivity of the microwave frequency, which were obtained by computer simulation. The frequency-discrimination sensitivity D can be given by

$$D = 2\pi \left. \frac{dV_{PSD}}{d\omega_M} \right|_{\omega_M=\omega_{12}}, \tag{50}$$

where V_{PSD} is the output voltage from the phase-sensitive detector. It can be seen from Figs. 4 and 5 that both the fundamental components (C_1 and S_1) and the third-harmonic components (C_3 and S_3) are odd functions, while the second-order harmonic components (C_2 and S_2) are even functions. Since the values of D of these odd functions are not zero at $\omega_M = \omega_{12}$, the values can be used as frequency discriminators. It should be noted that V_{PSD} given by Eq. (32) is exactly zero, irrespective of the value of θ at $\omega_M/2\pi = \omega_{12}/2\pi$, since the spectral line shapes of C_1, S_1, C_3, and S_3 cross the abscissa at this frequency when the frequency detuning of the laser is zero. Therefore these spectral line shapes can be used as accurate frequency discriminators.

Since V_{PSD} can be expressed as Eq. (32), the value of θ should be swept to find the maximum value of D. Since the Bessel function $J_q(M)$ determines the magnitudes of C_q and S_q, the modulation index M should also be swept to find the optimum condition. To find the optimum conditions by sweeping these parameters it was assumed that the laser frequency ($\omega_L/2\pi$) was tuned to the optical transition frequency ($\omega_{13}/2\pi$) between levels $|1\rangle$ and $|3\rangle$. By this assumption, the line shapes of δ_p and ϕ_p can be expressed as

$$\delta_p = \frac{\gamma_{21}'}{(\omega_{12} - \omega_M - p\omega_m)^2 + \gamma_{21}'^2} \tag{51}$$

and

$$\phi_p = \frac{\omega_{12} - \omega_M - p\omega_m}{(\omega_{12} - \omega_M - p\omega_m)^2 + \gamma_{21}'^2}. \tag{52}$$

By using Eqs. (51) and (52) the dependence of the value of D on the values of θ, ω_m/γ_{21}', and M was obtained. This dependence for the fundamental components (C_1 and S_1) is shown in Fig. 11. Figure 12 shows the dependence on ω_m/γ_{21}', where M was used as a parameter. The modulation index M in Fig. 11 was fixed at 1.2 because the maximum value of D in Fig. 12 was obtained when M was fixed at this value. The phase difference θ in Fig. 12 was fixed at 120° because the value of D in Fig. 11 took the maximum at this value of phase difference. Figures 13 and 14 show the dependences of the value of D for third-harmonic components (C_3 and S_3) on θ, ω_m/γ_{21}', and M. The modulation index M in Fig. 13 was fixed at 3.6 because the maximum value of D in Fig. 14 was obtained when M was fixed at this value. The phase difference θ in Fig. 14 was fixed at 270° because the value of D in Fig. 13 took the maximum at this value of phase difference. From Figs. 12 and 14 the optimum conditions for obtaining the highest microwave frequency stability were found. They are as follows:

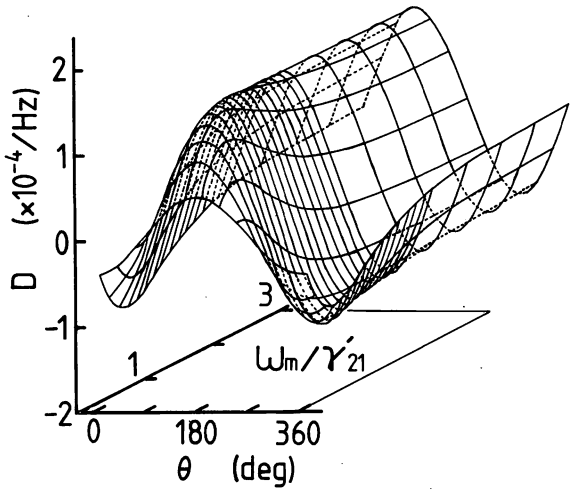

Fig. 11. Calculated dependence of the frequency-discrimination sensitivity D of the fundamental component on the normalized modulation frequency ω_m/γ_{21}' and the phase difference θ, where the modulation index M was fixed as 1.2.

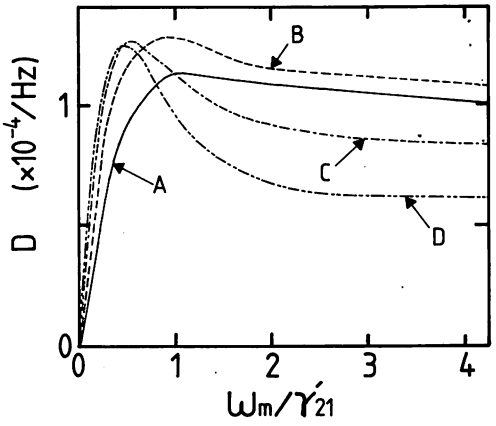

Fig. 12. Calculated dependence of the frequency-discrimination sensitivity D of the fundamental component on the normalized modulation frequency ω_m/γ_{21}', where the phase difference θ was fixed at 120°. The modulation indices M were A, 0.8; B, 1.2; C, 1.6; and D, 1.8.

Fundamental component:

$$D_{MAX} = 1.3 \times 10^{-4}(1/\text{Hz})$$

$$\text{at } M = 1.2,\ \omega_m/\gamma_{21}' = 1.0, \text{ and } \theta = 120°. \tag{53}$$

Third-harmonic component:

$$D_{MAX} = 6.1 \times 10^{-5}(1/\text{Hz})$$

$$\text{at } M = 3.6,\ \omega_m/\gamma_{21}' = 0.5, \text{ and } \theta = 270°. \tag{54}$$

Although the value of D_{MAX} of the third-harmonic component was half of that of the fundamental components, it can be said that the use of the third-harmonic component is more likely to reduce the effects of noise when the system is governed by flicker noise. The optimum values of S/N and $\Delta\nu$ obtained by using fundamental components are summarized in Table 2. The experimental results for a rf-excited ^{87}Rb lamp are also summarized in this table. Although the linewidth $\Delta\nu$ in Table 2 is larger than that in Fig. 2, the

values in Table 2 give the highest frequency stability because the S/N value is also larger than that of Fig. 2. When these values were substituted into Eq. (1), the short-term frequency stabilities of laser-pumped and conventional ^{87}Rb atomic clocks were

$$\sigma_y(\tau) = 7.9 \times 10^{-13}\, \tau^{-1/2} \tag{55}$$

and

$$\sigma_y(\tau) = 5.0 \times 10^{-12}\, \tau^{-1/2}, \tag{56}$$

respectively. The value of $\sigma_y(\tau)$ of a laser-pumped ^{87}Rb atomic clock is approximately one sixth that of conventional ^{87}Rb atomic clocks, which means that the short-term stability was improved by a factor of 6 when a laser-pumping scheme was used. According to the authors' preliminary experiments, it was found that the S/N of a double-resonance signal of a rubidium atomic clock pumped by a semiconductor laser was limited by the magnitude of the FM noise of the semiconductor laser. Therefore a frequency stability as high as that for a fully optimized laser-driven standard[3] can be expected if the technique of FM noise reduction is applied to the semiconductor laser.[17]

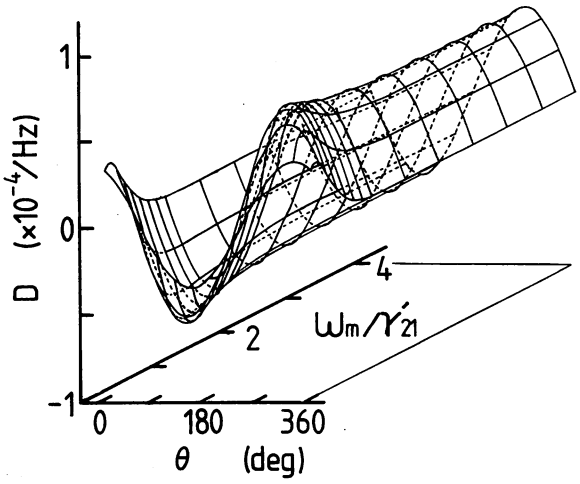

Fig. 13. Calculated dependence of the frequency discrimination sensitivity D of the third-harmonic component on the normalized modulation frequency ω_m/γ_{21}' and the phase difference θ, where the modulation index M was fixed at 3.6.

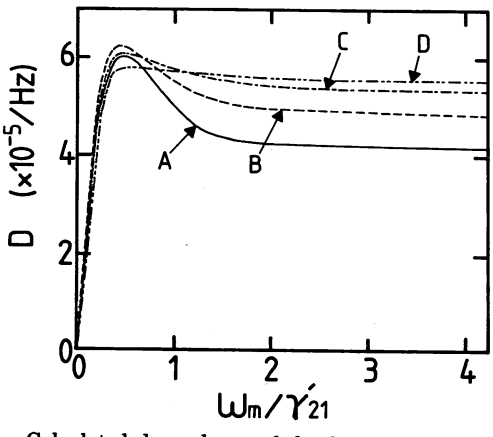

Fig. 14. Calculated dependence of the frequency-discrimination sensitivity D of the third-harmonic component on the normalized modulation frequency ω_m/γ_{21}', where the phase difference θ was fixed at 270°. The modulation indices M were A, 3.4; B, 3.6; C, 3.8; and D, 4.0.

Table 2. Measured Values of S/N and Linewidth ($\Delta\nu$)

Pumping Source	S/N (dB)	Linewidth (Hz)
Semiconductor laser	73	220
Rf-excited ^{87}Rb lamp	61	360

6. SUMMARY

By solving the equations of motion of a density matrix, we have analyzed the modulation-transfer process in optical-microwave double-resonance. We found that the novel spectral line shapes of double resonance were due to the modulation-transfer effect. The calculated results showed good agreement with the experimental ones. We investigated influence of the optical Stark effect on these spectral line shapes. As a result, characteristics of the inhomogeneous light shift were evaluated quantitatively for frequency-modulated microwaves. Furthermore, optimum values of modulation parameters were found by the computer simulation to obtain the highest microwave frequency stability of the atomic clocks. These values are as follows:

Fundamental component:

$D_{MAX} = 1.3 \times 10^{-4}$(1/Hz)

at $M = 1.2$, $\omega_m/\gamma_{21}' = 1.0$, and $\theta = 120°$.

Third-harmonic component:

$D_{MAX} = 6.1 \times 10^{-5}$(1/Hz)

at $M = 3.6$, $\omega_m/\gamma_{21}' = 0.5$, and $\theta = 270°$.

Experiments were carried out by employing these optimum parameters. A short-term frequency stability of an atomic clock as high as $\sigma_y(\tau) = 7.9 \times 10^{-13}$, $\tau^{-1/2}$ (where τ is the integration time) was obtained, which was one sixth that of conventional ^{87}Rb atomic clocks.

APPENDIX A: DEFINITIONS OF SYMBOLS

c, Speed of light
C_q, In-phase component of transmitted laser light
D, Sensitivity of microwave frequency discrimination
$E_L(z, t)$, Electric field of laser light (traveling wave)
E_L, Amplitude of the electric field of laser light
F, Quantum number of hyperfine level
$H_M(r, z, t)$, Magnetic field of a microwave (standing wave)
H_M, Amplitude of magnetic field of a microwave, which is a function of r and z
H_{M0}, Amplitude of magnetic field of a microwave
$\hbar$, Planck's constant divided by 2π
$I_{DET}(t)$, Light intensity detected by a photodetector
I_0, Laser-light intensity
I_q, qth-order Bessel function
$|j\rangle$ ($j = 1, 2, 3$), Wave function

k_L, Wave vector of laser light
k_M, Wave vector of a microwave
L_c, Gas-cell length
L_d, Optical length
M, Modulation index
m_F, Quantum number of the Zeeman sublevel
N, Noise
n_{87}, Rubidium density
n_j ($j = 1, 2, 3$), Population of level $|j\rangle$ at thermal equilibrium
p_{ij} ($i, j = 1, 2, 3,\ i \neq j$), Amplitude of polarization between the levels $|i\rangle$ and $|j\rangle$
Q, Quality factor of the double-resonance spectral line shape
R, Radius of a microwave cavity
R_c, Radius of a gas cell
r, Radial position in cylindrical coordinates
S_q, Quadrature component of transmitted laser light
V_0, Proportional constant
V_{PSD}, Output voltage of a phase-sensitive detector
w, Spot size of a laser beam
x_L, Rabi angular frequency of laser light
x_M, Rabi angular frequency of a microwave
z, Axial position in cylindrical coordinates
$\alpha(t)$, Complex polarizability of ^{87}Rb atoms
γ_j ($j = 1, 2, 3$), Longitudinal relaxation constant of level $|j\rangle$
γ_{ij} ($i, j = 1, 2, 3,\ i \neq j$), Transverse relaxation constant
γ_{ij}' ($i, j = 1, 2, 3,\ i \neq j$), Transverse relaxation constant under perturbation of a laser-light field
γ_{ij}'' ($i, j = 1, 2, 3,\ i \neq j$), Transverse relaxation constant under perturbation of a laser-light field
$\Delta\nu$, Separation (peak to peak) of a double-resonance line shape
$\Delta\omega_{LS}$, Shift of the zero-crossing point of a frequency discriminator
Δ_{ij}, Defined as Eqs. (B9)–(B11) below
δ_{OPT}, Amplitude attenuation of the laser caused by an optical transition
δ_p, Amplitude attenuation of the laser caused by a microwave transition
$\epsilon(\pm)$, Level shifts caused by the optical Stark effect
ϵ_0, Dielectric constant of a vacuum
ζ, Phase shift by the pumping light
θ, Phase difference between the output signal from the postdetector amplifier and the reference signal for the phase-sensitive detector
μ_{21}, Magnetic dipole moment between the levels $|2\rangle$ and $|1\rangle$
μ_{31}, Electric dipole moment between the levels $|3\rangle$ and $|1\rangle$
ρ_{ij} ($i, j = 1, 2, 3$), Elements of the density matrix
σ, Photon absorption cross section
σ_y, Square root of the Allan variance
τ, Integration time of measurement
ϕ_p, Phase shift of the laser caused by a microwave transition
Ω_{13}, Nutation angular frequency, which depends on the laser-light intensity
ω_L, Angular frequency of the laser light
ω_M, Angular frequency of a microwave
ω_m, Angular frequency of the modulation signal
ω_{ij} ($i, j = 1, 2, 3,\ i \neq j$), Bohr's angular frequency between the levels $|i\rangle$ and $|j\rangle$
ω_{ij}' ($i, j = 1, 2, 3,\ i \neq j$), Bohr's angular frequency under perturbation of a laser-light field
ω_{ij}'' ($i, j = 1, 2, 3,\ i \neq j$), Bohr's angular frequency under perturbation of a laser-light field

APPENDIX B: DERIVATION OF COMPLEX POLARIZATION (p_{13})

If the populations are saturated by laser light, the diagonal elements ρ_{jj} ($j = 1, 2, 3$) expressed by Eqs. (8)–(10) can be assumed to be constant.[9,18] Therefore the changes in diagonal elements induced by frequency modulation can be neglected. Only the resonant terms in Eqs. (11)–(13) are kept; the rotating-wave approximation is employed, i.e.,

$$\rho_{21} = \sum_q \frac{p_{21}(q)}{2} \exp[i(\omega_M + q\omega_m)t], \tag{B1}$$

$$\rho_{32} = \sum_q \frac{p_{32}(q)}{2} \exp\{i[(\omega_L - \omega_M - q\omega_m)t - k_L z]\}, \tag{B2}$$

and

$$\rho_{13} = \sum_q \frac{p_{13}(q)}{2} \exp\{-i[(\omega_L + q\omega_m)t - k_L z]\}. \tag{B3}$$

Substituting Eqs. (B1)–(B3) into Eqs. (8)–(13), one has

$$p_{21}(q) = \frac{1}{\Delta_{21}(q)}\left[(\rho_{22} - \rho_{11})x_M + \frac{x_L}{2} p_{32}{}^*(q)\right], \tag{B4}$$

$$p_{32}(q) = \frac{1}{\Delta_{32}(q)}\left[\frac{x_M{}^*}{2} \sum_p J_{p+q} p_{13}{}^*(q) - \frac{x_L}{2} p_{21}{}^*(q)\right], \tag{B5}$$

and

$$p_{13}(q) = \frac{1}{\Delta_{13}(0)}\left[(\rho_{33} - \rho_{11})x_L{}^* - \frac{x_M{}^*}{2} \sum_p J_p p_{32}{}^*(p)\right] \quad (q = 0)$$

$$= \frac{1}{\Delta_{13}(q)}\left[-\frac{x_M{}^*}{2} \sum_p J_{p+q} p_{32}{}^*(p)\right] \quad (q \neq 0), \tag{B6}$$

with the abbreviations

$$x_M = \frac{\mu_{21} H_M}{\hbar}, \tag{B7}$$

$$x_L = \frac{\mu_{31} E_L}{\hbar}, \tag{B8}$$

$$\Delta_{21}(q) = (\omega_{12} - \omega_M - q\omega_m) + i\gamma_{21}, \tag{B9}$$

$$\Delta_{32}(q) = (\omega_{23} - \omega_L + \omega_M + q\omega_m) + i\gamma_{32}, \tag{B10}$$

$$\Delta_{13}(q) = (\omega_{13} - \omega_L - q\omega_m) + i\gamma_{13}, \tag{B11}$$

where x_M and x_L are the Rabi angular frequencies of microwave and laser light, respectively. Equation (B5) can be simplified by neglecting the first term within brackets be-

cause $x_M \ll x_L$. By substituting Eq. (B4) into Eq. (B5), one has

$$p_{32}(q) = -\frac{(\rho_{21}-\rho_{11})J_q}{\Delta_{21}^*(q)\Delta_{32}(q)+x_L^2/4}\frac{x_M^* x_L}{2}. \tag{B12}$$

By substituting Eq. (B12) into Eq. (B6), one has the polarization between $|1\rangle$ and $|3\rangle$:

$$\begin{aligned}\rho_{13} &= \sum_q p_{13}(q)\exp(-iq\omega_m t)\\ &= -\left\{\frac{(\rho_{33}-\rho_{11})}{\Delta_{13}}+\frac{x_M^2}{4}\right.\\ &\quad\times\sum_q\sum_p \frac{J_{p+q}J_p(\rho_{33}-\rho_{11})}{\Delta_{13}[\Delta_{21}(p)\Delta_{32}^*(p)+x_L^2/4]}\\ &\quad\left.\times\exp(-iq\omega_m t)\right\}x_L^*,\end{aligned} \tag{B13}$$

where $\Delta_{13}(q)$ can be approximated as $\Delta_{13}(0)$ because $|q\omega_m| \ll \gamma_{13}$ in this equation.

APPENDIX C: EXPERIMENTAL PROCEDURE FOR FINDING THE DEPENDENCE OF POPULATION INVERSION ON THE LASER FREQUENCY DETUNING

A relation between laser frequency and population inversion between levels $|1\rangle$ and $|2\rangle$ in three-level ^{87}Rb atoms has not been measured so far to our knowledge. Only results calculated by solving rate equations have been presented.[2] However, this relation can be measured by the phase-sensitive detection technique employed in the present study. As shown in Eqs. (18) and (21), the magnitude of C_{2n} ($n = 0, 1, 2, 3\ldots$) at $\omega_M = \omega_{12}$ is proportional to the population inversion between levels $|1\rangle$ and $|2\rangle$ caused by optical pumping. Since the highest sensitivity for measurement was obtained by using the line shape of C_2, a relation between the value of C_2 at $\omega_M = \omega_{12}$ and the laser frequency detuning was measured to find the area where population inversion may not take place depending on the frequency detuning of the pumping source. The result was shown in Fig. 9. It can be seen from this figure that the population inversion was nearly equal to zero within the range $-4\ \text{GHz} \ll (\omega_L - \omega_{13})/2\pi \ll -2.2\ \text{GHz}$. This is why the light shift could not be measured within this frequency range.

ACKNOWLEDGMENTS

The authors express their gratitude to Y. Kasai, X. X. Gounji, and K. Chiba (Fujitsu Company, Ltd.) and to S. Kano (IBM), N. Oura, and N. Kuramochi (Tokyo Institute of Technology) for valuable discussions.

REFERENCES

1. J. L. Picque, "Hyperfine optical pumping of a cesium atomic beam, and applications," Metrologia **13,** 115–119 (1977).
2. L. L. Lewis and M. Feldman, "Optical pumping by lasers in atomic frequency standards," in *Proceedings of the 35th Annual Frequency Control Symposium* (Institute of Electrical and Electronics Engineers, New York, 1981), p. 625.
3. J. C. Camparo and R. P. Frueholz, "Fundamental stability limits for the diode-laser-pumped rubidium atomic frequency standard," J. Appl. Phys. **59,** 3313–3317 (1986).
4. M. Hashimoto and M. Ohtsu, "Experiments on a semiconductor laser pumped Rb atomic clock," IEEE J. Quantum Electron. **QE-23,** 446–451 (1987).
5. W. Happer and B. S. Mathur, "Effective operator formalism in optical pumping," Phys. Rev. **163,** 12–25 (1967).
6. J. C. Camparo, R. P. Frueholz, and C. H. Volk, "Inhomogeneous light shift in a alkali-metal atoms," Phys. Rev. **27,** 1914–1925 (1983).
7. T. McClelland, L. K. Lam, and T. M. Kwon, "Anomalous narrowing of magnetic-resonance linewidths in optically pumped alkali-metal vapor," Phys. Rev. A **33,** 1967–1707 (1986).
8. J. Vanier and L. G. Bernier, "On the signal-to-noise ratio and short-term stability of passive rubidium frequency standards," IEEE Trans. Instrum. Meas. **IM-13,** 221–230 (1981).
9. T. W. Hänsch, "Nonlinear high-resolution spectroscopy of atoms and molecules," in *Nonlinear Spectroscopy*, N. Bloembergen, ed. (North-Holland, Amsterdam, 1977), pp. 17–86.
10. M. Ducloy and D. Bloch, "Theory of degenerate four-wave mixing in resonant Doppler-broadened media. Doppler-free heterodyne spectroscopy via collinear four-wave mixing in two- and three-level systems," J. Phys. (Paris) **43,** 57–65 (1982).
11. R. W. Boyd and M. Sargent III, "Population pulsation and the dynamic Stark effect," J. Opt. Soc. Am. B **5,** 99–111 (1988).
12. M. T. Gruneisen, K. R. MacDonald, and R. W. Boyd, "Induced gain and modified absorption of a weak probe in a strongly driven sodium vapor," J. Opt. Soc. Am. B **5,** 123–128 (1988).
13. J. H. Shirley, "Modulation transfer process in optical heterodyne saturation spectroscopy," Opt. Lett. **7,** 537–539 (1982).
14. G. C. Bjorklund, "Frequency-modulation spectroscopy: a new method for measuring absorptions and dispersions," Opt. Lett. **5,** 15–17 (1980).
15. B. S. Mathur, H. Tang, and W. Happer, "Light shifts in the alkali atoms," Phys. Rev. **171,** 11–19 (1968).
16. G. Busca, M. Tetu, and J. Vanier, "Light shift and light broadening in the ^{87}Rb maser," Can. J. Phys. **51,** 1379 (1973).
17. M. Ohtsu, "Realization of ultrahigh coherence in semiconductor lasers by negative electric feedback," IEEE J. Lightwave Technol. **6,** 245–256 (1988).
18. T. W. Hänsch, "Theory of a three-level gas laser amplifier," Z. Phys. **236,** 213–244 (1970).

A Novel Method to Compensate for the Effect of Light Shift in a Rubidium Atomic Clock Pumped by a Semiconductor Laser

MINORU HASHIMOTO AND MOTOICHI OHTSU, MEMBER, IEEE

Abstract—**Light shift (i.e., microwave resonance frequency shift induced by the electric field of the pumping light) was precisely measured in a rubidium atomic clock pumped by a semiconductor laser. It was confirmed that the spectral lineshape of the microwave resonance, which was used as a frequency discriminator for the atomic clock in the optical microwave double resonance experiment, depends strongly on the spatial distribution of the laser beam intensity, laser frequency detuning, and modulation parameters of the microwave frequency. Based on measurements of the deformation of the resonance lineshape, a self-tuning system was built to compensate for the effect of light shift. As a result of controlling the laser frequency with this system, a long-term drift of the microwave frequency as low as 6.3×10^{-13}/h was obtained.**

I. Introduction

PRECISE microwave frequency oscillators, such as portable low cost rubidium (Rb^{87}) atomic clocks, have been widely used for various applications, e.g., signal sources for the global positioning system (GPS). In order to improve the performance of these clocks, the use of laser techniques has been proposed, and preliminary investigations have been carried out for these improvements [1], [2]. In the case of Rb^{87} atomic clocks, a 780-nm AlGaAs semiconductor laser can be used as an optical pumping source instead of a conventional RF-excited Rb^{87} lamp.

The short-term stability of the microwave frequency can be improved by using a frequency stabilized semiconductor laser [3], [4]. However, it has been difficult to improve the long-term stability of the microwave frequency because of the long-term drift caused in these atomic clocks by light shift, i.e., microwave resonance frequency shift induced by the electric field of pumping light [5], [6]. The origin of drift in these atomic clocks is mostly due to light shift and wall effect. Since wall shift is a very complicated phenomenon, a method to compensate for the effect of wall shift is not proposed here. As is shown explicitly in the title, this paper limits itself to topics relative to the novel method of compensating for the effect of light shift.

It is possible to precisely evaluate the light shift by utilizing an advantageous property of the laser's high temporal coherence [3], [4]. The double resonance deformation, which results from transverse inhomogeneity in spatial distribution of laser beam intensity in the Rb^{87} gas cell, has been evaluated for nonmodulated microwaves [7] and for modulated microwaves [8]. These experiments [7], [8] confirm that the observed characteristics of the light shift differ from the theoretical ones [5].

In this paper, by using the results of our investigations of its characteristics, a novel method is proposed to compensate for the effect of light shift in Rb^{87} atomic clocks pumped by a semiconductor laser. In Section II, the characteristics of light shift are studied.

The dependence of the optical microwave double resonance spectral lineshape on the transverse spatial distribution of laser beam intensity, laser frequency detuning, and modulation parameters are also investigated when the microwave frequency is modulated. In Section III, the principle of a self-tuning system, which utilized the experimental results on the double resonance spectral lineshapes deformation, is described. Experimental results of compensating the effect of light shift on the atomic clock frequency are also presented. The results are summarized in Section IV.

II. Measurements of Light Shift and Deformation of Spectral Lineshape

Fig. 1 shows the block diagram of a Rb^{87} atomic clock pumped by a semiconductor laser. The section surrounded by broken lines represents the atomic clock system. A cylindrical glass cell containing Rb^{87} vapor and buffer gases (total pressure 43 torr, $Ar/N_2 = 1.65$) was used. The temperature of the gas cell was kept at 48°C. The microwave frequency in the cavity was modulated by a low frequency signal (ω_m). The Rb^{87} atoms were excited by the linearly polarized light of a semiconductor laser (Hitachi, HL7802E, 780-nm wavelength). The temperature fluctuation of the laser was reduced to a value as low as 0.04 mK at room temperature by using two Peltier elements. A low noise current source whose bandwidth was 50 kHz was used to control the injection current of the laser. The current source was controlled by a 16-b personal computer. Explanation of the other parts of Fig. 1 will be given in Section III. The energy level diagram of Rb^{87} is shown in Fig. 2. Two hyperfine levels, (F =

Manuscript received February 9, 1989; revised December 9, 1989.

The authors are with the Graduate School at Nagatsuta, Tokyo Institute of Technology, Midori-ku, Yokohama 227 Japan.

IEEE Log Number 9034591.

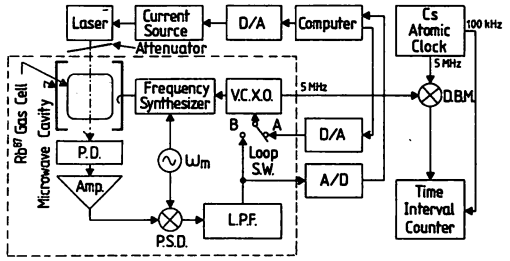

Fig. 1. Block diagram of a semiconductor laser pumped Rb^{87} atomic clock. A 16-b personal computer (NEC, PC9801VM) was used for this system. A Cs atomic clock (HP 5061B) was used as a frequency reference for measuring long-term frequency drift. The beat frequency from the DBM was measured by a time interval counter, which was built by the authors. A stable clock pulse (100 kHz) provided by the Cs atomic clock was used for measuring the period of the beat signal.

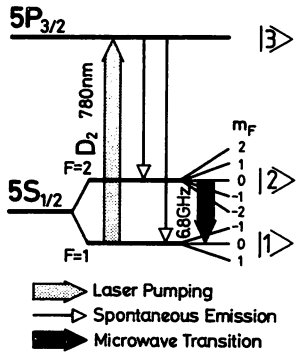

Fig. 2. Energy level diagram of the Rb^{87} atom.

1, $m_F = 0$) and ($F = 2$, $m_F = 0$) of the ground state ($5S_{1/2}$), and an excited state ($5P_{3/2}$) are relevant to the operation of the Rb^{87} atomic clock. They are labeled as $|1>$, $|2>$, and $|3>$, respectively. The Bohr frequency $\omega_{12}/2\pi$ between levels $|1>$ and $|2>$ is 6.8 GHz, while frequency $\omega_{13}/2\pi$ between levels $|1>$ and $|3>$ is 384 THz (780-nm wavelength).

The laser light transmitted through the Rb^{87} vapor was detected by a photodetector. Since the frequency of the microwave magnetic field in the cavity was modulated, the modulation signal was transferred from the microwaves to the laser light field due to the nonlinear complex polarizability of Rb^{87} atoms [9]. This modulation transfer effect in Rb^{87} vapor cell resonators was found by the authors [3]. A detailed analysis and characteristics of this effect has been published [8]. As a result of this analysis, the light intensity detected by the photodetector is given by

$$I_{\mathrm{DET}}(t) = \sum_{q=0}^{\infty} \left[C_q \cos(q\omega_m t) + S_q \sin(q\omega_m t) \right] \quad (1)$$

where

$$C_q = -I_0 \sum_{r=-\infty}^{\infty} \left(J_{r+q}(M) + J_{r-q}(M) \right) J_r(M) \delta_r \quad (2)$$

and

$$S_q = -I_0 \sum_{r=-\infty}^{\infty} \left(J_{r+q}(M) - J_{r-q}(M) \right) J_r(M) \phi_r. \quad (3)$$

In (1), $\omega_m/2\pi$ is the microwave modulation frequency, C_q and S_q are the in-phase and quadrature components of the qth order harmonic, respectively, I_0 is the laser light intensity incident upon the Rb^{87} gas cell, J_r is the Bessel function of the rth order, M is the microwave modulation index and δ_r and ϕ_r are the amplitude attenuation and the phase shift induced in the laser light by the microwave transition from level $|1>$ to $|2>$. The spectral lineshapes of C_q and S_q could, therefore, be measured separately by using a phase sensitive detection technique, and they coincided with the results obtained in FM spectroscopy [10]. Fig. 3 shows measured spectral lineshapes of C_q and S_q. These spectral lineshapes were mainly determined by the ratio ω_m/γ'_{21}, where γ'_{21} represents the transverse relaxation constant between levels $|1>$ and $|2>$ under the optical pumping condition. If $\omega_m/\gamma'_{21} \ll 1$, the spectral lineshapes of C_1 and S_1 can be approximated as the first derivative of the absorption and the second derivative of the dispersion, respectively [8], [10]. If $\omega_m/\gamma'_{21} \gg 1$, however, the modulation transfer effect can be clearly seen as shown in Fig. 3. To demonstrate this effect, the modulation frequency ($\omega_m/2\pi$) was fixed at 1 kHz in Fig. 3. As the spectral profiles of fundamental components (C_1, S_1) and third harmonic components (C_3, S_3) cross the abscissa at $\omega_{12}/2\pi$, they can be used as frequency discriminators for microwave frequency stabilization of the Rb^{87} atomic clock.

The microwave resonance frequency would be shifted by the optical Stark effect induced by the electric field of the pumping light. Therefore, the zero-crossing point of the discriminator would be also shifted if the laser frequency is detuned from the optical resonance frequency $\omega_{13}/2\pi$. A basic study of the hyperfine energy level shift of ground state has been given by Mathur *et al.* [5] for a nonmodulated microwave. However, it is necessary for the present study to investigate the light shift characteristics for a modulated microwave.

The light shift characteristics were evaluated by measuring the shift of the zero-crossing point of the spectral lineshapes of S_1. This was done because the slope of S_1 was the steepest among those of C_1, S_1, C_3, and S_3 when the modulation frequency $\omega_m/2\pi$ was 1 kHz. This steep slope gave very high resolution measurements. The signal-to-noise ratio of the measurement of spectral profile S_1 was about 65 dB, where the detection bandwidth was 1 Hz. Fig. 4 shows the measured relation between the shift of the zero-crossing point of S_1 and laser frequency detuning from the optical resonance frequency $\omega_{13}/2\pi$, with the laser light intensities fixed at several values. Fig. 5 shows the measured relation between the shift of the zero-crossing point of S_1 and the laser light intensity, with the laser frequency detuning $(\omega_L - \omega_{13})/2\pi$ fixed at several values. Conventional theories on light shift have claimed that the hyperfine energy level shift of the ground state was linearly proportional to the laser light intensity at fixed laser frequency detuning [5]. However, it can be clearly seen from Fig. 5 that the shift of the zero-crossing point of the frequency discriminator was not linearly pro-

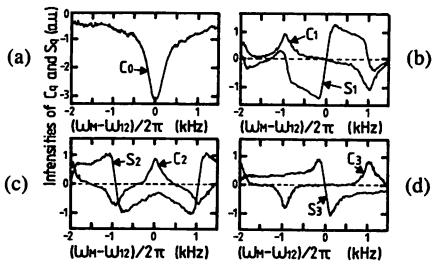

Fig. 3. Measured dependencies of in-phase component C_q and quadrature component S_q ($q = 0, 1, 2, 3$) on microwave frequency. The modulation frequency was $\omega_m/2\pi = 1$ kHz, and the laser light intensity was $I_0 = 144\ \mu W/cm^2$. The values of modulation index M were (a) 0.0, (b), (c) 1.2, and (d) 3.9.

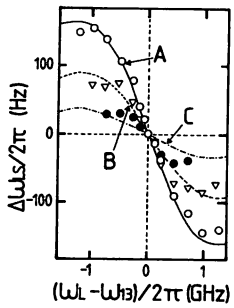

Fig. 4. Relation between light shift and laser frequency detuning. ω_L: Laser angular frequency. ω_{13}: Angular frequency of the optical resonance. $\Delta\omega_{LS}$: Shift of zero-crossing point of S_1. The curves represent theoretical results. The values of laser light intensity I_0 were 1008 $\mu W/cm^2$ (○, A), 360 $\mu W/cm^2$ (▽, B), and 144 $\mu W/cm^2$ (●, C). The values of the laser Rabi frequency $n_L/2\pi$ were 1800 kHz (solid curve, A), 900 kHz (dashed curve, B), and 500 kHz (dot-dashed curve, C). The modulation frequency and index were $\omega_m/2\pi = 1$ kHz and $M = 1.2$, respectively.

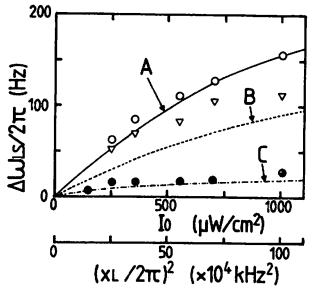

Fig. 5. Relation between light shift and laser light intensity. I_0: Laser light intensity. x_L: Laser Rabi angular frequency. $\Delta\omega_{LS}$: Shift of zero-crossing point of S_1. The curves represent theoretical results. The values of the laser frequency detuning $(\omega_L - \omega_{13})/2\pi$ were 1000 MHz (○, A), 500 MHz (▽, B), and 100 MHz (●, C). The modulation frequency and index were $\omega_m/2\pi = 1$ kHz and $M = 1.2$, respectively.

portional to the laser light intensity. As pointed out by Camparo *et al.* [7], this discrepancy is due to spatially inhomogeneous optical pumping, which depends on the profile of the transverse mode of the laser beam transmitted through the gas cell. Therefore, as schematically explained by Fig. 6, the transverse spatial integral should be carried out to estimate the light shift characteristics.

Calculated light shift characteristics are shown in Figs. 4 and 5; they correspond to the experimental results. These calculations were carried out by following the au-

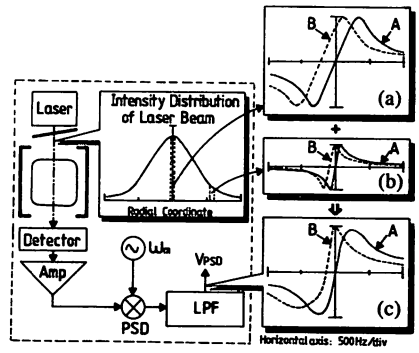

Fig. 6. Schematic explanation of the distortion of spectral lineshape. (a) Spectral lineshapes of double resonance of Rb^{87} atoms pumped around the center of the transverse spatial distribution of the laser beam intensity. (b) Spectral lineshapes of double resonance of Rb^{87} atoms pumped at the tail of the transverse spatial distribution of the laser beam intensity. (c) Superposition of (a) and (b). The dotted lines inside the transverse spatial distribution of the laser beam spectrum represent the center and tail of the transverse spatial distribution of laser beam intensity. The values of laser frequency detuning $(\omega_L - \omega_{13})/2\pi$ were A: 0 MHz, B: 750 MHz.

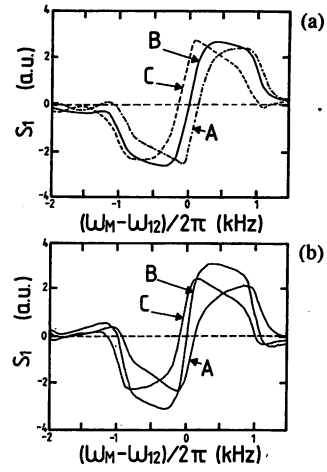

Fig. 7. Distorted spectral lineshapes of S_1. (a) Calculated lineshapes, where the laser Rabi frequency $x_L/2\pi$ was 1000 kHz. This calculation was carried out by following the theoretical analysis [8]. (b) Measured lineshapes, where the laser light intensity I_0 was 1008 $\mu W/cm^2$. The values of laser frequency detuning $(\omega_L - \omega_{13})/2\pi$ were A: 7500 MHz, B: 0 MHz, and C: −7500 MHz. The modulation frequency and index were $\omega_m/2\pi = 1$ kHz and $M = 1.2$, respectively.

thor's analysis [8], where Gaussian transverse intensity distribution of the laser beam was assumed. It can be claimed that good agreement was obtained between the experimental and the theoretical results in Figs. 4 and 5. The slight differences between the experimental and theoretical results in these figures are because the accuracy of the adiabatic approximation employed in analysis [8] was not high enough. Fig. 7(a) shows the spectral profiles S_1 calculated by assuming a Gaussian transverse intensity distribution of the laser beam. The spectral profile S_1 is the dependence of the spectral profile defined by (3) on microwave frequency. These profiles agree well with the experimental results shown by Fig. 7(b). From this agreement, it was confirmed that the spectral lineshapes would be distorted by the optical Stark effect and become asym-

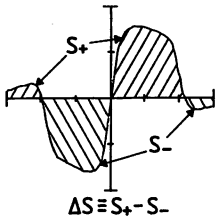

Fig. 8. Graphical depiction of the asymmetry factor ΔS.

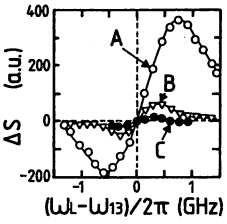

Fig. 9. Measured relation between the asymmetry factor ΔS and laser frequency detuning. ω_L: Laser angular frequency. ω_{13}: Angular frequency of optical resonance. ΔS: Asymmetric factor of S_1. The laser light intensities I_0 were 1008 $\mu W/cm^2$ (A), 360 $\mu W/cm^2$ (B), and 144 $\mu W/cm^2$ (C). The modulation frequency and index were $\omega_m/2\pi$ = 1 kHz and M = 1.2, respectively.

metric. To evaluate quantitatively the degree of asymmetry of a spectral lineshape, an asymmetric parameter ΔS was introduced,

$$\Delta S = S_+ - S_- \qquad (4)$$

where S_+ and S_- represent the values of areas defined by Fig. 8. The characteristics of distortion and asymmetry of the frequency discrimination were investigated by measuring the value of ΔS for the spectral profile S_1. A measured relation between the value of ΔS and the laser frequency detuning from the optical resonance frequency $(\omega_L - \omega_{13})/2\pi$ is shown in Fig. 9, where the laser light intensities were fixed at several values. It can be seen from this figure that $\Delta S = 0$ at $\omega_L = \omega_{13}$, and that ΔS decreased by decreasing the laser light intensity.

III. Performance of the System Developed to Compensate for the Effect of Light Shift

The microwave frequency drift caused by light shift can be reduced by controlling the laser frequency so as to keep the value of ΔS zero. In fact the slopes of the curves in Fig. 4 are proportional to those in Fig. 9 at $\omega_L \simeq \omega_{13}$. By using the computer-aided system in Fig. 1, the atomic clock could be controlled. This system, based on the results of distortion measurement of the frequency discriminator, can be used to compensate for the effect of the light shift. Since this system does not require any additional reference frequency source, it can be referred to as a self-tuning system. A similar system has been proposed for improving the frequency stability of a hydrogen maser [11]. In that case the asymmetry used would be that of the oscillation spectral profile. The performance of the self-tuning system described here was evaluated by using a highly stable Cs atomic clock (HP, 5061B) as a frequency reference. The sequence of the control procedure for the self-tuning system is enumerated as follows.

A) Initial setting of the laser injection current:

1) The laser injection current is fixed initially to an appropriate value by a 16-b A/D converter so as to keep the value of the light shift $\Delta\omega_{LS}/2\pi$ zero.

B) Recording of the spectral profile of frequency discriminator:

2) The loop switch is turned to position A in Fig. 1 by using a relay switch driven by a TTL level signal. In this way, the microwave frequency becomes free-running, and can be swept by the voltage applied to a voltage controlled crystal oscillator (VCXO).

3) To record the spectral lineshape of the frequency discriminator with the computer, the voltage applied to the VCXO is swept by the output voltage of a D/A converter. The swept voltage was divided by 7000 (not shown in this figure). The output voltage of a phase sensitive detector (PSD) followed by a low pass filter (LPF) is sampled by a 12-b A/D converter, and is stored into the computer memory. The time constant of the LPF is fixed to 10 ms to optimize the response of the PSD. The sampling and recording is carried out 5 times to improve the resolution of the measurements, and their averaged value is recorded.

C) Estimation of ΔS and injection current control:

4) When operation 3 is finished the switch is turned to position B. Then, the microwave frequency is determined by the output frequency of the VCXO, whose frequency is stabilized at the zero-crossing point of the frequency discriminator.

5) The asymmetry factor ΔS is calculated by using the spectral profile of the frequency discriminator recorded by the computer.

6) The laser injection current change necessary to make ΔS zero is calculated. This will compensate for the drift caused by light shift.

7) The feedback signal which corresponds to the value of this change is applied to the current source.

8) Return to step B).

It took 120s and 300s to carry out steps B) and C), respectively. This system is very simple because it can be built by adding a computer and several interfaces to an atomic clock. Though we used a personal computer for our experimental convenience, it can be replaced by a one chip microprocessor. Therefore, the portability of Rb standards is not lost by employing the self-tuning system. The beat signal between the output frequency (5 MHz) of this system and the output frequency (5 MHz) of the Cs atomic clock (HP, 5061B) was obtained by using a double balanced mixer (DBM), and the period of the beat signal (about 260 s) was measured by a time interval counter. A stable clock pulse (100 kHz) from the Cs clock was used for measuring the period of the beat signal.

Fig. 10 shows the results of drift measurements. These measurements were carried out continuously over 21000s. The results obtained by using the self-tuning

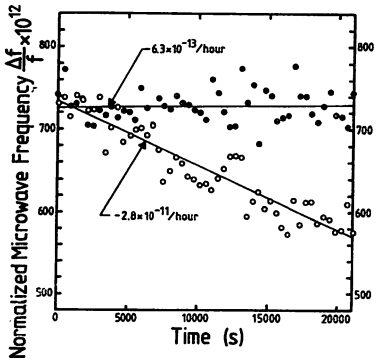

Fig. 10. Drift of the microwave frequency. ● and ○ represent the results obtained with and without the self-tuning technique, respectively. The value of laser light intensity I_0 was 1008 $\mu W/cm^2$. Least square fitting was applied to the results. The two straight lines represent the results of this fitting. The values of their slopes are 6.3×10^{-13}/h and -2.8×10^{-11}/h, respectively.

technique are given by the closed circles in this figure. The open circles represent the results obtained for the Rb^{87} atomic clock pumped by a semiconductor laser without using the self-tuning technique. Least square fitting was applied to the two sets of results. The two solid lines shown in Fig. 10 were obtained. The slopes of the lines for the results with and without using the self-tuning technique were 6.3×10^{-13}/h and -2.8×10^{-11}/h, respectively. These values can be considered a measure of the long-term microwave frequency stability. It was confirmed by comparing these two values that the microwave frequency drift was reduced by a factor of 45 by employing the self-tuning technique, i.e., the long-term frequency microwave stability was improved. Though the microwave frequency drift caused by light shift cannot be reduced in conventional Rb standards, it was first demonstrated that the microwave frequency drift caused by light shift can be reduced by using the self-tuning system. Furthermore, the drift of microwave frequency can be compensated perpetually by using this system. Therefore, it can be concluded that the long-term drift of 6.3×10^{-13}/hour obtained within 21 000s was a good result.

IV. Summary

The light shift in a rubidium atomic clock pumped by a semiconductor laser was precisely measured. Based on the experimental results of the distortion of the double resonance spectral lineshape, a self-tuning system was built to compensate for the effect of light shift. The laser frequency was controlled to make the value of the asymmetrical factor zero. As the results of this, a long-term microwave frequency drift of the Rb^{87} atomic clock pumped by a semiconductor laser was only 6.3×10^{-13}/h. This means that the drift was reduced by a factor of 45 from that obtained without the self-tuning technique.

Acknowledgment

The authors would like to express their gratitude to Messrs. Kasai, Gounji, and Chiba, Fujitsu Co. Ltd., Dr. Kano, Japan IBM Co. Ltd., Prof. Oura, and Dr. Kuramochi, Tokyo Institute of Technology, for their valuable discussions, and to Director Hayashi and Dr. Nakagiri, Standards and Measurements Division, Communications Research Lab., Ministry of Posts and Telecommunications for supplying a high performance Cs atomic clock.

References

[1] J. L. Picque, "Hyperfine optical pumping of a cesium atomic beam, and applications," *Metrologia*, vol. 13, pp. 115-119, 1977.
[2] L. L. Lewis and M. Feldman, "Optical pumping by lasers in atomic frequency standards," in *Proc. 35th Ann. Frequency Control Symp.*, Fort Monmouth, NJ, pp. 612-624, May 1981.
[3] M. Hashimoto and M. Ohtsu, "Experiments on a semiconductor laser pumped rubidium atomic clock," *IEEE J. Quantum Electron.*, vol. QE-23, pp. 446-451, 1987.
[4] M. Hashimoto, M. Ohtsu, and H. Furuta, "Ultra-sensitive frequency discrimination in a diode laser pumped Rb^{87} atomic clock," in *Proc. 41st Ann. Frequency Control Symp.*, Philadelphia, PA, pp. 25-35, May 1987.
[5] B. S. Mathur, H. Tang, and W. Happer, "Light shifts in the alkali atoms," *Phys. Rev.*, vol. 171, pp. 11-19, 1968.
[6] H. Hellwig, "Atomic frequency standards: A survey," in *Proc. 28th Ann. Frequency Control Symp.*, Fort Monmouth, NJ, pp. 612-624, May 1974.
[7] J. C. Camparo, R. P. Frueholz, and C. H. Volk, "Inhomogeneous light shift in alkali-metal atoms," *Phys. Rev.*, vol. 27, pp. 1914-1925, 1983.
[8] M. Hashimoto and M. Ohtsu, "Modulation transfer and optical Stark effect in rubidium atomic clock pumped by a semiconductor laser," *J. Opt. Soc. Amer. B*, vol. 6, pp. 1777-1789, 1989.
[9] M. Ducloy and D. Bloch, "Theory of degenerate four-wave mixing in resonant Doppler-broadened media. Doppler-free heterodyne spectroscopy via collinear four-wave mixing in two- and three-level systems," *J. Physique*, vol. 43, pp. 57-65, 1982.
[10] G. C. Bjorklund, "Frequency-modulation spectroscopy: a new method for measuring absorptions and dispersions," *Opt. Lett.*, vol. 5, pp. 15-17, 1980.
[11] T. W. Wang, "An oscillating compact hydrogen maser," in *Proc. 34th Ann. Frequency Control Symp.*, Fort Monmouth, NJ, pp. 364-369, May 1980.

DIODE LASER-PUMPED Rb-BEAM ATOMIC CLOCK AS A NOVEL PRIMARY FREQUENCY STANDARD

H. Furuta, K. Nakagawa, and M. Ohtsu
Graduate School at Nagatsuta, Tokyo Institute of Technology
4259 Nagatsuta, Midori-ku, Yokohama
Kanagawa 227, Japan

Abstract

Laser-pumped rubidium beam (Rb-beam) atomic clock is proposed to improve the accuracy of its microwave frequency, and to develop a novel primary frequency standard. In the preliminary experiments, we obtained ~1 kHz of linewidth in the derivative of microwave resonant signal. The potential of high accuracy was discussed.

Introduction

Highly precise and compact rubidium (^{87}Rb) atomic clocks have been required for various applications, e.g., the signal sources for GPS satellites. For the improvement of their performances, the ^{87}Rb atomic clock pumped by a diode laser have been investigated[1]-[3]. By using diode lasers, Hashimoto and Ohtsu demonstrated that both short- and long-time stabilities of the microwave frequency could drastically improved. These improvements are because a very sensitive discriminator for microwave frequency stabilization could be obtained due to the effect of modulation transfer in the optical-microwave double resonance (short-time stability)[4][5], and because the precise analysis and the compensation for the light shift (which is the microwave frequency shift caused by the detuning of the pumping light frequency) could be done (long-time stability)[6]. On the other hand, the accuracy of the frequency has been limited by the frequency shifts due to various origins. The principal shifts were the light shift and the buffer-gas-shift (which is the pressure shift of the microwave frequency caused by collisions between ^{87}Rb atoms and buffer gases). As mentioned above, the light shift has been compensated[6]. If the accuracy of the clock can be improved by eliminating the buffer-gas-shift, ^{87}Rb atomic clock can be used as a primary frequency standard.

We propose a highly accurate ^{87}Rb-beam atomic clock pumped by coherent diode lasers, in order to realize a novel primary frequency standard. In this system, we try to obtain both the high stability and the high accuracy of the clock, by using the optical-microwave double resonance[4]-[6] in the Rb atomic beam without using any buffer gases. In this paper, several results of the preliminary experiments for this system are shown.

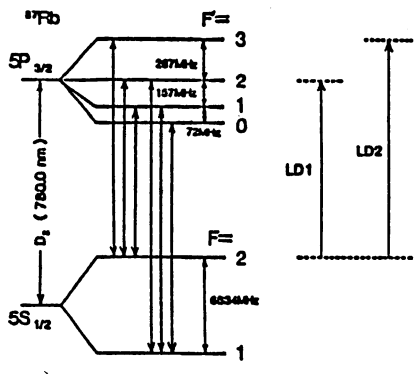

Fig. 1 Energy level diagram of ^{87}Rb D_2 resonance line.

CH2822-5/90/0000-0428 $01.00 © 1990 IEEE

Observation of Fluorescence Signal

Optical pumping with diode lasers at 780.0 nm is expected to improve the performances of Rb-beam atomic clocks. Optical pumping with a diode laser induces the population difference between the $|F=1, m_F=0\rangle$, $|F=2, m_F=0\rangle$ ground state hyperfine levels of ^{87}Rb. The microwave transition at 6,834 MHz in a microwave cavity is detected by observing the intensity variations of the fluorescence using the same (or another) laser in the downstream. The characteristics of the microwave resonant signal are important for frequency locking of the atomic clock.

Figure 1 shows the energy level diagram corresponding to the D_2 resonance line of ^{87}Rb at 780.0 nm.

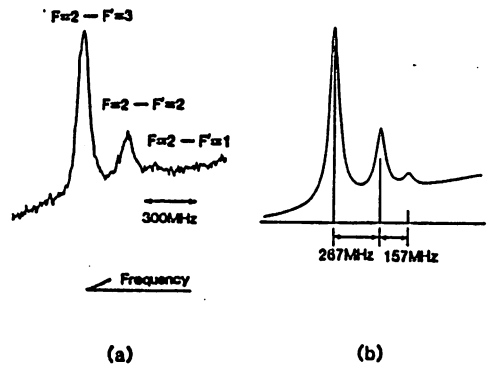

Fig. 2 The fluorescence signals from Rb-beam as a function of laser frequency. These are spectral shapes corresponding to the transitions $F=2$ in the ground state $F'=1$, 2, and 3 in the excited state. (a) Experimental result. The incident laser power was 10 μW. (b) Calculated result, based on ref. [2].

Six optical transitions are allowed between the ground state and the $P_{3/2}$ excited state. The transitions $F=1 - F'=1$ or 2 and $F=2 - F'=1$ or 2 are popularly used for optical pumping. And the recycling transitions $F=1 - F'=0$ and $F=2 - F'=3$ are used more appropriately for detection because a larger number of fluorescence photons can be generated from the atomic beam.

Figure 2(a) shows the observed fluorescence signal of optically pumped atomic beam as a function of the laser frequency, while fig. 2(b) illustrates the calculated profile based on ref. [2]. These figures show a good agreement between each other, and the hyperfine spectral lines were well resolved because the Doppler broadening was well reduced.

Figure 3 shows the population change by the optical pumping. This figure was obtained by using two diode lasers. One laser (probing laser) beam in the downstream of Rb-beam was chopped mechanically and the fluorescence was synchronously detected. The frequency of probing laser was fixed at the center of the transition between $F=2$ and $F'=3$. The other laser (pumping laser) frequency was swept during the measurement, and the population change was traced as a function of this frequency. Optical pumping on the recycling transition $F=2 - F'=3$ did not produce any population change, which agreed with the transition rule as shown in fig. 1.

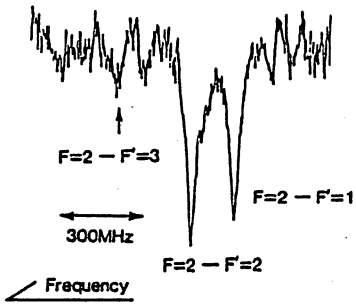

Fig. 3 The population change by the optical pumping, as a function of pumping laser frequency. This was obtained by using two diode lasers. One laser was used for pumping. The other laser (probing laser) beam was chopped mechanically and its frequency was fixed at the peak of the fluorescence signal of the transition between F=2 and F'=3. The incident laser power of pumping and detection lights were 0.2 mW and 75 μW, respectively.

Detection of Microwave Resonant Signal

Figure 4 shows an experimental setup, by which we have preliminarily detected the microwave resonant signal. The diode laser LD1 was used for optical pumping to produce the population difference between hyperfine levels of the ground state. The frequency of LD1 was locked to the transition F=2 — F'=2. The microwave field was applied by the cylindrical cavity. The cavity mode was TE_{012} and the cavity was set with the cylindrical axis perpendicular to the Rb-beam, in order to eliminate the Doppler shift. The diode laser LD2 was used for the detection of microwave resonant signal. The frequency of LD2 was locked on the transition F=2 — F'=3. Figure 5 shows the derivative of the microwave resonant signal detected as a function of the applied microwave frequency. This signal was obtained by phase sensitive detection with frequency modulation of microwave frequency. About 1 kHz of linewidth between peak-to-peak signal amplitude was obtained, and at the resonant frequency was measured as 6,834,682,600.Hz. Compared with a few hundreds Hz of linewidth of the Ramsey signal, detected by optically pumped cesium beam atomic clock, this can be quite satisfactory result in the preliminary stage. This narrow linewidth of the resonant signal was due to the Doppler-free components of the system, i.e. three axes of diode laser beams, cylindrical cavity and Rb-beam were perpendicular to each other. By using the double resonance, narrower linewidth can be expected. The improvement of accuracy of the resonant frequency can be expected because no buffer gases are contained in this system.

Summary

Laser-pumped rubidium beam (Rb-beam) atomic clock is proposed to improve the accuracy of its microwave frequency, and to develop a novel primary frequency standard. In this system, the clock is controlled by using the optical-microwave double resonant signal, based on the principles referred in ref. [4]-[6].

We have carried out several preliminary experiments. As the first step, we have observed the fluorescence signal of pumped atoms in Rb-beam, and confirmed the effect of optical pumping. As the second step, we obtained ~1 kHz of linewidth in the derivative of microwave resonant signal.

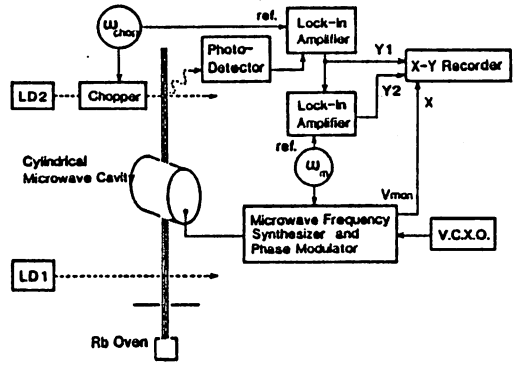

Fig. 4 The experimental setup for the detection of microwave resonant signal. This signal was obtained by modulating the microwave frequency and by phase-sensitive detection.

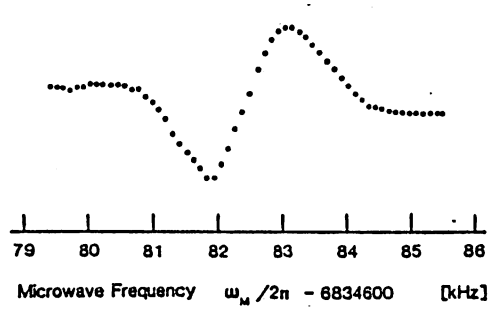

Fig. 5 The derivative of microwave resonant signal obtained by using the setup in fig. 4. Here, the modulation frequency $\omega_m/2\pi$ was 165 Hz and the modulation index M was 3.2.

References

[1] L. L. Lewis and M. Feldman, "Optical Pumping by Lasers in Atomic Frequency Standards," in Proceedings of 35th Annual Symposium on Frequency Control, Ft. Monmouth, NJ, May 1981, pp.612-624

[2] M. Feldman, J. C. Bergquist, L. L. Lewis, and F. L. Walls, "Preliminary Investigation of a New Optically Pumped Atomic Rubidium Standards," in Proceedings of 35th Annual Symposium on Frequency Control, Ft. Monmouth, NJ, May 1981, pp.625-636

[3] J. C. Camparo, R. P. Frueholz, and C. H. Volk, "Inhomogeneous light shift in alkali-metal atoms," Phys. Rev. Lett., Vol. 27, 1983, pp.1914-1925

[4] M. Hashimoto and M. Ohtsu, "Experiments on a Semiconductor Laser Pumped Rubidium Atomic Clock," IEEE J. Quantum Electron., Vol. QE-23, 1987, pp.446-451

[5] M. Hashimoto and M. Ohtsu, "Modulation Transfer and Optical Stark Effect in a Rubidium Atomic Clock Pumped by a Semiconductor Laser," J. Opt. Soc. Am. B, Series 2, Vol. 6, 1989, pp.1777-1789

[6] M. Hashimoto and M. Ohtsu, "A Novel Method to Compensate for the Effect of the Light Shift in Rubidium Atomic Clock Pumped by a Semiconductor Laser," submitted to IEEE Trans. Instrum. Meas.

Super-Resolution Photon Scanning Tunneling Microscope

M. Ohtsu, K. Nakagawa, S. Jiang, and N. Tomita

Graduate School at Nagatsuta, Tokyo Institute of Technology,
4259 Nagatsuta, Midori-ku, Yokohama 227, Japan

<ABSTRACT>

Transmission- and reflection-type photon STM's were proposed for super-resolution, non-contact, and non-destructive measurements. The estimated resolution of the reflection and resonant type is higher than 1 nm by a frequency shift measurement.

1. INTRODUCTION

A novel optical microscope, i.e., a photon scanning tunneling microscope (PSTM) is proposed for non-contact and non-destructive measurements of three-dimensional profiles of biomembranes, organic thin films, and micro-electronic devices with the super-resolution beyond the limit imposed by the optical diffraction. Although several systems of near field microscope (NFM) have been proposed[1-7], their resolutions and sensitivities have not yet been sufficiently improved. It is expected that the present system could improve drastically these performances.

2. TRANSMISSION PSTM USING A DIODE LASER[8]

As the diode laser light impinging onto the sample with the incident angle large enough to get the total reflection, the transmitted evanescent light field on the sample surface contains the informations of the sample surface topography and its power decreases exponentially with the sample-probe separation z. This evanescent light power is picked up by an optical fiber probe, whose tip is sharpened and metal film coated with a sub-micron sized aperture. It corresponds to the squeeze of the measurement error of the photon position at the small aperture. If the aperture diameter is smaller than the wavelength, super-resolution is, thus, realized along the lateral direction on the sample. Because the power decreases exponentially with z, a very high resolution normal to the sample surface can be also obtained. Figure 1 shows a calculated relation between z and the evanescent power density for a standard sample, i.e., a sinusoidal diffraction grating with the interval Λ and depth h_0.

Techniques for servo-control of the probe position and for image processing by a computer developed for the conventional STM can be commonly employed for the present system.

By using a diode laser with the 10 mW output power, the probed power is as low as the order of 10 pW. However, use of directly modulatable diode lasers can improve the measurement sensitivity by techniques such as phase-sensitive detection, heterodyne detection, and photon counting. In this case, the system can be considered as a miniature version of the coherent optical communication system. One of the outstanding advantages is that the local analytical spectroscopy can be carried out by easily wavelength tunable diode lasers with a wide bandwidth. Figure 2 shows an example of the optical fiber probe, of which fabricating procedure is as follows; The tip of the fiber is sharpened by a technique of selective chemical etching using a HF solution within the radius of curvature of 280nm, and then the sharpened fiber is Cr-coated. Finally, the aperture of several nm diameter can be made by the electro-etching [9].

3. REFLECTION AND RESONANT PSTM

The system proposed in section 2 may have two principal problems : (1) A biomembrane may be destroyed if it is irradiated by a high power laser beam because free-radicals can be generated in the membranes. In a strict meaning, the non-destructive measurements are not realized as long as the transmission PSTM is used. (2) Pick-upped power is low, which limits the sensitivity and the time constant of the measurements. The first problem can be solved by modifying the system to the reflection type. The second problem can be solved by realizing the impedance matching, in other words, by employing the resonant-type probe, and by measuring the frequency shift instead of measuring the power. Figure 3 shows the system. A fiber Fabry-Perot cavity (FFPC) is fabricated by polishing both ends of the fiber and then coating reflecting films. A sub-micron aperture is made on one end of the FFPC faced to the sample. When this end is located very close to the sample surface (<< optical wavelength), the complex reflectivity of this end could be perturbed with magnitude depending upon the sample surface topography because a very little amount of light, i.e., the evanescent wave, leaking out through the aperture, is reflected back by the sample surface. The resonance frequency shift of the FFPC resulting from the complex reflectivity perturbation can be measured by locking the diode laser frequency to this FFPC. As a simple method of this locking, resonant optical feedback by the FFPC can be employed, for which the auxiliary fiber is connected by a directional coupler with the FFPC. It has been confirmed that the laser frequency was pulled into the resonance frequency of this FFPC, by which the laser linewidth was reduced as narrow as 20 kHz, and a compact module of this highly coherent diode laser has been fabricated [10]. It has been also confirmed that the frequency shift Δf normalized to the optical frequency f_1 can be measured by using a heterodyne optical phase locked loop with the error as low as $6.3\ 10^{-17}\ \tau^{-1}$[11], where τ is the integration time of measurements. For example, the frequency shift as low as 0.1 mHz can be measured at τ=70s,which is about 10^7-10^9 times more sensitive than that obtained by the power measurement employed in section 2. Further advantageous property is that the theoretical analysis for estimating the resolution is simpler than that of the transmission PSTM. The estimated resolution is basically same as that of the system explained in the next section, which is shown by Figure 4.

4. REFLECTION AND ACTIVE RESONANT PSTM

Principal problems of the system in section 3 may be fluctuations of the resonant frequency of the FFPC due to ambient temperature fluctuations, acoustics and mechanical vibrations. Technical attentions should be paid to reduce these fluctuations by temperature control and using a shield case. To avoid these difficulties, we propose here an advanced system by using a diode laser itself as a probe, i.e., a sub-micron aperture is made on a laser facet after a high reflection film is coated. When this facet is placed very close to the sample surface, the complex reflectivity of the laser facet and the laser frequency are varied depending on the sample surface profile by the same reason as that described in section 2. Figure 4 shows an estimated relation between the lateral and normal resolutions Δx and Δz by using the normalized frequency shift $\Delta f/f_1$ as a parameter[12]. The resolutions higher than that of the conventional STM can be expected because the values of Δx or Δz can be lower than 1 nm for $\Delta f/f_1 = 1\ 10^{-18}$ as shown by Fig.4.

5. DISCUSSIONS AND OUTLOOK

The novel PSTM proposed here have several advantages as compared with the conventional STM. Although a non-contact and non-destructive atomic force STM has also been proposed, the present system is more attractive because of further additional performances, e.g., possibility of the local analytical spectroscopy, the sensitivity improvement by employing the fluorescence enhancement, and so on. Furthermore, a scanning range on the sample surface can be larger than that of the conventional STM.

Future problems to be solved could be development of the reliable and reproducible fabrication technology of a sub-micron sized aperture and establishment of a theory of near-field wave optics. Employment of the non-classical photon could improve the sensitivity, the lateral, and normal resolutions, i.e., a novel quantum microscope can be expected. Furthermore, it can be expected that the present system can be used as not only a super-resolution microscope but also an actuator in a novel research field of quantum optics, e.g., control and manipulation of the single-atom by the localized photon.

6. SUMMARY

Novel super-resolution microscopes, i.e., transmission- and reflection-type PSTM's, using diode lasers and optical fibers, were described to measure biomembrances in non-contact and non-destructive manners. It was claimed that the sensitivity of the reflection and resonant PSTM could improve drastically the sensitivity as compared with the conventional NFM, and the lateral or normal resolutions higher than 1 nm, can be expected. It was pointed out that the development of the aperture fabrication technology is indispensable for a practical application of these PSTM. Furthermore, a comment was given for the application of these PSTM's, as a quantum microscope, to the novel field of quantum optics.

REFERENCES

[1] E.K. Ash and G. Nichols : Nature, 237 (1972) 510
[2] U. Durig, et.al. : J. Appl. Phys., 59 (1986) 3318
[3] E. Betzig, et.al. : Appl. Phys. Lett., 51 (1987) 2088
[4] D.W. Pohl, et.al. : SPIE, vol.897, "Scanning Microscopy Technology and Applications", (1988) 84
[5] U.Ch. Fischer, et.al. : Appl. Phys. Lett., 249 (1988) 249
[6] R.C. Reddick, et.al. : Phys. Rev. B, 39 (1989) 767
[7] M. Fee, et.al. : Opt. Commun., 69 (1989) 219
[8] S.Jiang, et.al., : Proc. the 4th Meeting on Lightwave Sensing Technol., December,1989, (Osaka), LST4-9 (in Japanese)
[9] P.F. Marella and R.F. Pease : Appl. Phys. Lett., 55 (1989)
[10] C.H.Shin, et.al. : IEEE Photonics Technol. Lett., March issue,2 (1990) in press
[11] C.H. Shin and M. Ohtsu : IEEE Photonics Technol. Lett., April issue, 2 (1990) in press
[12] S. Jiang, et.al. : Submitted to OEC'90

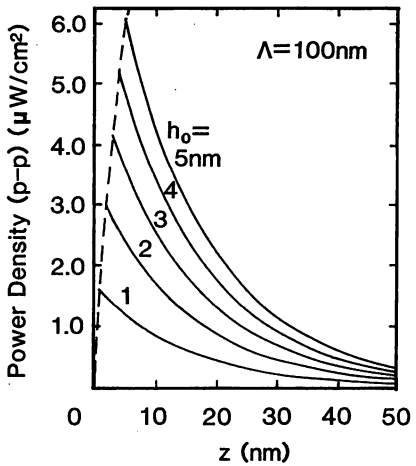

Fig.1 A calculated relation between the sample-probe separation z and the evanescent power density for a standard sample, i.e., a sinusoidal diffraction grating with the interval Λ and a depth h_0 [8].

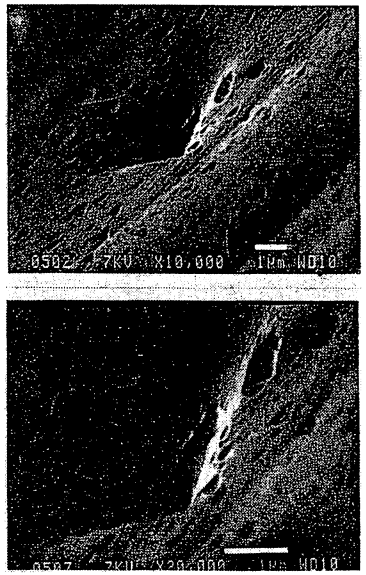

Fig.2 Photographs of a sharpened tip of a single mode fiber.

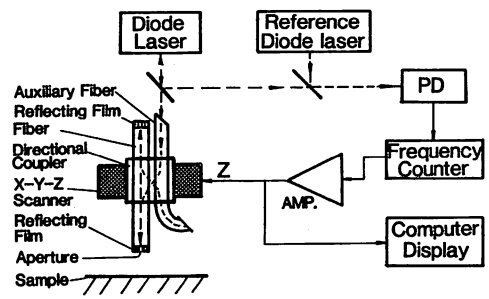

Fig.3 The schematic diagram of the reflection and resonant PSTM.

Fig.4 Calculated relation between the normal and lateral resolutions with the parameter of normalized frequency shift [12].

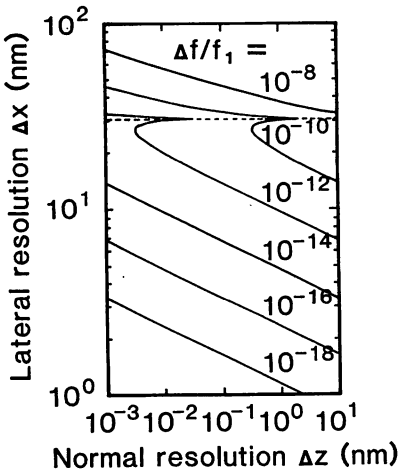

Fig.4

Proposal of super-sensitive reflection-mode phase-locked photon scanning tunneling microscope by diode lasers

S.Jiang, N.Tomita, K.Nakagawa, and M.Ohtsu

Graduate School at Nagatsuta, Tokyo Institute of Technology
4259 Nagatsuta, Midori-ku, Yokohama, Japan

<ABSTRACT>

A novel PSTM is proposed for the perfect non-destructive measurement of biomembrane. Estimated three-dimentional resolution is as high as 1nm. The scanning speed can be increased to 10^4 times that of the previous PSTM.

1. INTRODUCTION

The microscope of non-contact, non-destructive, and super-resolution is necessary to the industry of semiconductor manufacturing and the biological sciences. In recent years, several research groups have demonstrated the feasibility of circumventing the diffraction limit with the photon scanning tunnel microscope (PSTM, also named as near-field scanning optical microscope) which forces incident light through a submicron-sized aperture [1][2]. Unfortunately, even in the ideal case, it has been proved that the total flux transmitted by a small hole drops with the sixth power of the aperture radius [3]. As a result, a high power laser, sensitive photon counting, and very slow scanning speed had to be used, and improvements in resolution and sensitivity appear difficult. Similar problems are also encountered in another type of PSTM, in which, optical fiber with submicron-sized aperture at its end is used to pick up the power of the evanescent wave from the sample surface [4][5].

Another problem of the PSTM mentioned above is that the light has to be transmitted through the sample. Thus the photon-induced free-radicals can be generated in the cell, which makes the non-destructive measurement difficult for the organic samples.

In this paper, we propose a new type of PSTM, i.e., super-sensitive reflection-mode phase-locked PSTM to observe the biomembrane in a completely non-destructive manner. A diode laser is used as both a light source and a receiver. Also, because the topographical information about the sample surface is given by the laser frequency variation instead of the light intensity change which has been used in all of the conventional PSTM's, the sensitivity is improved greatly while maintaining the use of low power laser. Furthermore, because the sensitivity of frequency variation ($\Delta f/f$) measurement has been improved to as high as $6.3\times10^{-17}\times\tau^{-1}$ (where τ is an integration time) by the author's group [6], the three-dimensional resolution of 1 nm is possible by fixing τ = 63sec.

2. PRINCIPLE OF OPERATION

Figure.1 shows the setup of the presently proposed PSTM. A diode laser chip(LD1), whose one facet is covered with both the insulator film and the metal film containing a hole (aperture) is mounted on a sensitive xyz translator which is consisted of three piezoelectric elements. The LD1 works as both the light source and the receiver. A heterodyne-type optical phase looked loop (HOPLL) is formed between LD1 and an another frequency-stable diode laser (LD2). The frequency (f_1) of the LD1 is shifted with the roughness of the sample surface, while the HOPLL, however, is maintained by controlling its injection current. The control signal for the injection current of the LD1 is used to display three-dimensional topography of the sample surface. Because the direct FM response of diode laser is as high as 10^4 times that of the PZT voltage modulation, it is possible to realize the scanning speed as high as 10^4 times that of the other PSTM.

When the LD1 is located very close to the sample (<<the wavelength of the LD1), the presence of the sample will modulate the complex reflectivity of the laser facet because a very little amount of light (known as an evanescent wave) leaking out through the aperture is reflected by the sample surface. The laser frequency can be varied by the change of this complex reflectivity. The lateral resolution is limited by the diameter of the aperture on the metal film, and the normal resolution is limited by the sensitivity of the variation measurement of the laser frequency.

3. CALCULATED RESULTS AND DISCUSSIONS

Figure.2 shows a schematic model used for estimating the laser frequency variation induced by the roughness of the sample surface. LD1 is regarded as an active resonant cavity composed of two parallel reflecting surfaces whose reflectivities are r_1 and r_2, and the insulator film is assumed to have a quarter-wave optical thickness for simplicity. The metal film with an aperture and the sample surface are considered as a reflector with the complex reflectivity r_{eff}.

The plane wave approximation can be conventionally used to estimate the complex reflectivity r_{eff} when the sample-aperture separation z is smaller than the diameter of the aperture[7]. However, the light propagated through the aperture is diverge a little because of the slight diffraction phenomenon which will be included into the analysis as a correction factor.

For the aperture radius a, sample-aperture separation z, sample reflectivity r_s, and laser wavelength λ_1 respectively, r_{eff} is now expressed as

$$r_{eff} \simeq 1 - j\frac{64}{27\pi^2}k^4a^4r_s\left(\alpha\frac{1}{1+(2z/ka^2)^2}\right)^{1/2}\sin\frac{4\pi z}{\lambda_1} \qquad (1)$$

according to the Bethe's theory[3] and Kirchhoff-Huygens diffraction integral where the far field approximation was not employed. k is a wave number of the free-running laser LD1, i.e. the wave number without any perturbation from the sample. α is the ratio of the laser power through the aperture to the total power, and can be calculated from the electric field profile of the guided mode of the diode laser[8].

The frequency shift Δf from the free-running laser frequency f_1 is then given by

$$\Delta f = \frac{c}{4\pi n_{eff} l}\tan^{-1}\left(\mathrm{Im}\{r_{eff}\}\right) \qquad (2)$$

where c is the speed of the light in vacuum, l = 300μm and n_{eff} = 3.5 are the length of the diode laser cavity and the effective refractive index, respectively.

Figures.3(a),(b) shows the dependence of the frequency shift Δf normalized to the free-running laser frequency f_1 on the sample-aperture separation z and the aperture radius a, plotted in linear and logarithmic ordinates. From Fig.3(a), for a = 50 nm, the frequency shift is increased by increasing of z within z < 30nm, and then decreased exponentially to the separation z within 30nm < z < 100nm, respectively. This can be explained as that the frequency

shift is mainly varied with the phase change of complex reflectivity in the range of $z < 30$nm, and mainly varied with the amplitude change of complex reflectivity when $z > 30$nm.

When the aperture radius a is increased from 10nm to 50nm, as the result shown in Fig.3(b), the normalized frequency shift is changed within the order of $10^{-12} \sim 10^{-8}$. Also it is shown that the value of z at which the $\Delta f/f_1$ takes the maximum is approximately expressed as $0.6a$. Therefore, it is clear that the range which can be used to the measurement is divided into two parts, i.e., $z < 0.6a$ and $z > 0.6a$, and it is necessary to choose one of them for a designate aperture radius a.

In Fig.4, a relation between the lateral resolution and the normal resolution is shown for $z = 10$nm, where the normalized frequency shifts $\Delta f/f_1$ are set at several values. As shown in Fig.4, the lateral resolution ($\Delta x \simeq 2a$ [1]) is increased with decreasing the normal resolution or increasing the detection sensitivity of frequency shift except for the singular region $a \simeq z/0.6$.

According to Fig.4, the sensitivity of frequency shift detection 10^{-18} (which has been already realized in author's group [6]) is sufficient for resolving 1 nm in three-dimension if z is assumed to be 10nm. This kind of quantitative analyses for estimating the resolution was carried out by the present study for the first time, while it has not been carried out even for the conventional PSTM up to now.

Although the lateral resolution is theoretically depended on the sensitivity of frequency shift detection, the minimum of the aperture diameter is also limited from the aperture forming technology. The method of forming submicron-sized aperture on diode laser facet is proposed as follows: First, an insulator film is coated on the chip facet of a diode laser, and then a metal film ($d \simeq 10$nm $\sim$ 100nm)is coated on the insulator film for maintaining the reflectivity high enough. Lastly a hole, ($\simeq$ 2nm in diameter)is formed by electroetching using scanning tunneling microscope [9].

4. CONCLUSION

Super-sensitive reflection-mode phase-locked photon scanning tunneling microscope using diode lasers is proposed for the perfect non-destructive measurement of biomembrane. It is possible to improve the three-dimensional resolution to as high as 1nm. The scanning speed appeared to 10^4 times that of the all previous PSTM.

REFERENCES

[1] U.Durig, D.W.Pohl, and F.Rohner, J.Appl.Phys.,59,(1986) p.3381
[2] E.Betzig, M.Isaacson,and A.Lewis, Appl.Phys.Lett,51,(1987)p2088
[3] H.A.Bethe, Phys.Rev., 66,(1944), p163
[4] R.C.Reddik, R.J.Warmack,T.L.Ferrell, Am.Phys.Soc.,39,(1989),p767
[5] D.Courjon, K.Sarayeddine, M.Spajer, Opt.Com.,71,(1989),p.23
[6] C.H.Shin and M.Ohtsu, submitted to OEC'90
[7] H.C.Casey and M.B.Panish, Heterostructure Lasers (Academic Press, New York, 1978)Part A, Chapter 2.
[8] D.Marcuse, Light Transmission Optics (Van Nostrand Reinhold, New York, 1972) Chapter 2.
[9] P.F.Marella, and R.F.Pease, Appl.Phys.Lett,55,(1989)p2366

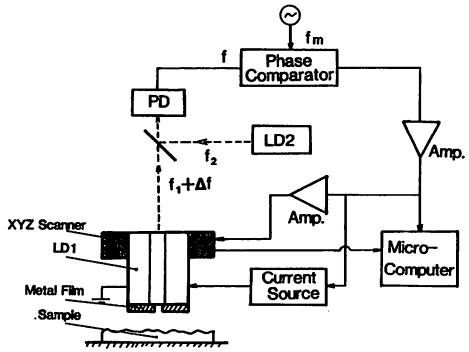

Fig.1 General arrangement of the proposed super-sensitive reflection-mode phase-locked PSTM by laser diodes.

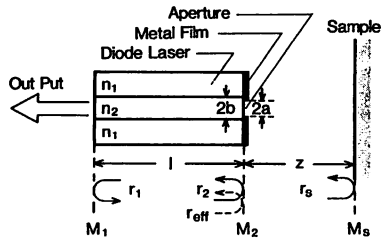

Fig.2 The model for the present calculation. a, z, and r_{eff} are the radius of the aperture, the separation between the aperture and the sample,and the effective complex reflectivity considering into the size of the aperture and reflectivities of M_2 and M_s.

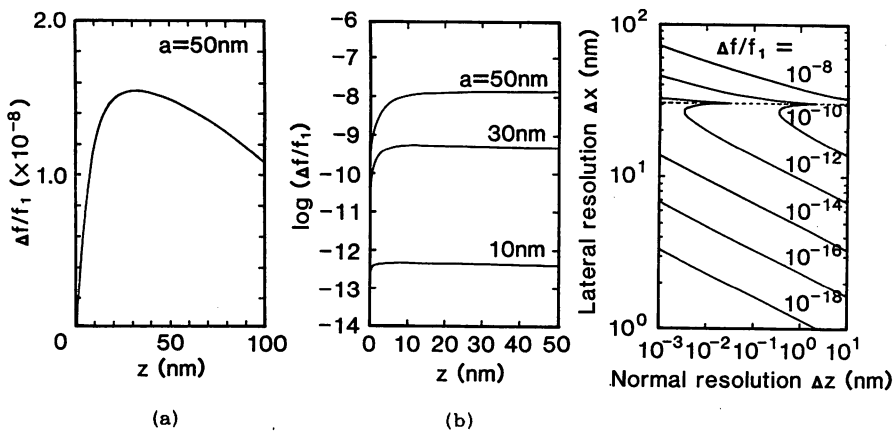

Fig.3 Calculated results of the relation between normalized frequency shifts and aperture-sample separations. The scales of (a) and (b) are linear and logarithmic, respectively. $r_s = 0.5$, $\lambda_1 = 800$nm.

Fig.4 Calculated results of the lateral resolution vs. the normal resolution with the parameter of normalized frequency shift, where $\Delta x = 2a$, $r_s = 0.5$, $\lambda_1 = 800$nm.